

Exploring Subsurface Water Storage Dynamics with Daily Satellite Gravimetry and Remotely Sensed Soil Moisture

Dissertation

zur Erlangung des akademischen Grades

Doktor-Ingenieur (Dr.-Ing.)

an der

HafenCity Universität Hamburg

vorgelegt von

Daniel Hendrik Blank

Hamburg, July 2026

Dissertation, HafenCity University Hamburg

Title: *Exploring Subsurface Water Storage Dynamics with Daily Satellite Gravimetry and Remotely Sensed Soil Moisture*

Author:	Daniel Hendrik Blank
Research Field:	Geodesy and Geoinformatics
Supervisors:	Prof. Dr.-Ing. Annette Eicker
	Prof. Dr. Andreas Güntner

Handed in:	2nd July 2026
Date of Defence:	25th September 2026

Imprint

HafenCity University Hamburg

Henning-Voscherau-Platz 1

20457 Hamburg

Publication date: December 2026

DOI: https://doi.org/10.34712/142.87

Copyright / Licence information



Except where otherwise noted, this work is licensed under the Creative Commons licence CC BY 4.0 www.creativecommons.org/licenses/by/4.0.

Acknowledgements

First and foremost, I would like to express my deepest gratitude to Annette Eicker. I am sincerely grateful that she gave me the opportunity to pursue this dissertation and for her continuous support throughout the many years of this journey. Her guidance and encouragement have been invaluable, and I deeply appreciate the role she has played in making this work possible.

I would also like to thank Andreas Güntner for his support in the preparation of all three papers. I greatly appreciate his advice and constructive feedback, which have been highly important throughout the development of this work.

My thanks also go to my co-authors of the individual studies that form this dissertation. I am grateful to Laura Jensen for her support in the first study and for initially bringing forward the idea that led to this doctoral project during my master's thesis. I would also like to thank John T. Reager for his input and ideas in shaping the storyline of the second study. Finally, I am grateful to Daniel Rasche for his support in implementing the ideas that formed the basis of the third study.

I would also like to thank my colleagues in the Geodesy department at HCU for creating a pleasant working environment. Special thanks go to Kuei-Hua Hsu, Klara Middendorf, and Viviana Roggendorf, with whom I had the pleasure of sharing an office throughout the years.

I am grateful to my parents Helga and Uwe, my sister Sarah, and my brother Simon for their continuous support, understanding, and for always being there throughout the years.

Finally, I would like to thank my wife Naiara for her constant support, patience, and understanding throughout this journey, and my son Hendrik for the joy he brought into our lives. Together, they gave me the chance to clear my mind after work and to focus on what matters most.

Abstract

Subsurface water storage dynamics control the temporal evolution of hydrological extremes, groundwater recharge, and land-atmosphere interactions. However, they remain difficult to observe consistently at large spatial scales. Satellite soil moisture observations provide global information on near-surface conditions, but are limited in their vertical sensitivity. GRACE and GRACE-FO satellite gravimetry, in contrast, observe vertically integrated changes in terrestrial water storage (TWS), including soil moisture, groundwater, surface water, and snow. This dissertation combines both observation types to investigate how water storage signals evolve from surface soil moisture towards deeper and more integrated storage compartments. Particular emphasis is placed on the added value of daily GRACE-based TWS for resolving short-term and depth-dependent storage dynamics.

The analyses show that satellite-derived soil moisture and GRACE-based TWS are systematically related at the global scale, but this relationship depends strongly on vertical representativeness, temporal scale, product characteristics, and regional hydroclimatic conditions. Products representing deeper soil layers generally show closer agreement and smaller temporal shifts with TWS than surface soil moisture products. This demonstrates that the link between soil moisture and TWS becomes stronger as the soil moisture signal becomes more representative of deeper storage dynamics. Daily GRACE solutions make it possible to examine the relationship beyond the dominant seasonal cycle. After removing the seasonal component, significant correlations between soil moisture and TWS remain in many regions at sub-monthly timescales. This indicates that daily satellite gravimetry also captures short-term storage changes that are hydrologically related to soil moisture dynamics.

Building on this relationship, the dissertation provides global observational evidence for a storage-based drought cascade in the subsurface. Water storage deficits develop first in near-surface soil moisture, take longer to build up in the root zone, and accumulate over time as storage anomalies in the TWS signal observed by GRACE. This progression is quantified by a distribution-based recovery-time analysis, which shows that storage deficit persistence increases systematically with storage depth as drought signals become more delayed and damped in deeper storage compartments.

Finally, daily GRACE observations are used as a constraint to calibrate an exponential

filter for estimating sub-seasonal subsurface storage dynamics from satellite-derived surface soil moisture. The GRACE-constrained filter improves the agreement between soil moisture and TWS and provides spatially varying time constants that reflect regional differences in storage behaviour. Overall, this dissertation demonstrates that daily satellite gravimetry, when combined with satellite soil moisture observations, provides a strong observational basis for analysing temporal and depth-dependent subsurface water storage dynamics at the global scale.

Zusammenfassung

Die Dynamik der Wasserspeicherung im Untergrund bestimmt die zeitliche Entwicklung hydrologischer Extremereignisse, die Grundwasserneubildung und die Wechselwirkungen zwischen Land und Atmosphäre. Sie lässt sich jedoch auf großen räumlichen Skalen nur schwer konsistent beobachten. Satellitenbasierte Bodenfeuchtebeobachtungen liefern globale Informationen über oberflächennahe Bedingungen, sind jedoch in ihrer vertikalen Sensitivität begrenzt. Die Satellitengravimetrie der GRACE- und GRACE-FO-Missionen beobachtet dagegen vertikal integrierte Änderungen des terrestrischen Wasserspeichers (TWS), einschließlich Bodenfeuchte, Grundwasser, Oberflächengewässer und Schnee. Diese Dissertation kombiniert beide Beobachtungstypen, um zu untersuchen, wie sich Wasserspeichersignale von der Oberflächenbodenfeuchte hin zu tieferen und stärker integrierten Speicherkompartimenten entwickeln. Ein besonderer Schwerpunkt liegt auf dem Mehrwert täglicher GRACE-basierter TWS-Daten für die Erfassung kurzfristiger und tiefenabhängiger Speicherdynamiken.

Die Analysen zeigen, dass satellitenbasierte Bodenfeuchte und GRACE-basierter TWS auf globaler Skala systematisch miteinander verbunden sind, diese Beziehung jedoch stark von der vertikalen Repräsentativität, der zeitlichen Skala, den Eigenschaften der Bodenfeuchteprodukte und den regionalen hydroklimatischen Bedingungen abhängt. Produkte, die tiefere Bodenschichten repräsentieren, zeigen im Allgemeinen eine engere Übereinstimmung und kleinere zeitliche Verschiebungen mit TWS als Produkte der Oberflächenbodenfeuchte. Dies zeigt, dass die Verbindung zwischen Bodenfeuchte und TWS stärker wird, je besser das Bodenfeuchtesignal tiefere Speicherdynamiken repräsentiert. Tägliche GRACE-Lösungen zeigen zudem, dass diese Beziehung nicht auf den dominanten saisonalen Zyklus beschränkt ist. Auf submonatlichen Zeitskalen bleibt in zahlreichen Regionen eine signifikante Übereinstimmung zwischen Bodenfeuchte und TWS nachweisbar, was darauf hinweist, dass die tägliche Satellitengravimetrie hydrologisch relevante kurzfristige Speicheränderungen erfasst.

Aufbauend auf dieser Beziehung liefert die Dissertation globale Beobachtungsevidenz für eine speicherbasierte Dürrekaskade im Untergrund. Wasserspeicherdefizite entstehen rasch in der oberflächennahen Bodenfeuchte, werden in der Wurzelzone persistenter und manifestieren sich schließlich als kumulative Speicheranomalien im von GRACE beobach-

teten TWS-Signal. Diese Entwicklung wird durch eine verteilungsbasierte Analyse der Erholungszeiten quantifiziert. Sie zeigt, dass die Persistenz von Wasserspeicherdefiziten systematisch mit der Speichertiefe zunimmt, da Dürresignale in tieferen Speicherkompartimenten zunehmend verzögert und gedämpft werden.

Schließlich werden tägliche GRACE-Beobachtungen als Kalibrierungsgrundlage verwendet, um einen exponentiellen Filter zur Abschätzung sub-saisonaler unterirdischer Speicherdynamiken aus satellitenbasierter Oberflächenbodenfeuchte zu kalibrieren. Der so bestimmte Filter verbessert die Übereinstimmung zwischen Bodenfeuchte und TWS und liefert räumlich variierende Zeitkonstanten, die regionale Unterschiede im Speicherverhalten widerspiegeln. Insgesamt zeigt diese Dissertation, dass tägliche Satellitengravimetrie in Kombination mit satellitenbasierten Bodenfeuchtebeobachtungen eine starke beobachtungsbasierte Grundlage für die Analyse zeitlicher und tiefenabhängiger Dynamiken unterirdischer Wasserspeicher auf globaler Skala bietet.

Contents

Abstract **vii**

1. Introduction **1**
1.1. Motivation and background 1
1.2. State-of-the-art and research gap 2
1.3. Outline 4
1.4. Publication overview 4

2. Soil Moisture **7**
2.1. Definition and role in the Earth system 7
2.2. Observing soil moisture 9
2.2.1. In-situ soil moisture 9
2.2.2. Soil moisture by remote sensing 11
2.3. Soil moisture representation in hydrological models 14
2.4. Conceptual representation of subsurface soil moisture 15
2.4.1. Exponential filtering approach for subsurface soil moisture estimation 16
2.5. Soil moisture data products 17
2.5.1. Soil moisture products from SMOS 17
2.5.2. Soil moisture products from SMAP 19
2.5.3. Soil moisture products from ESA CCI 20
2.5.4. Supplementary soil moisture data sets 21
2.5.5. Spatial comparison of soil moisture products 22

3. Terrestrial Water Storage **27**
3.1. Definition and role in the Earth system 27
3.2. Observing TWS 28
3.2.1. Satellite gravimetry 29
3.2.2. TWS from GRACE and GRACE-FO 31
3.2.3. Data processing from GRACE and GRACE-FO 32

4. Research Objectives **35**
4.1. Comparability of remotely sensed soil moisture and GRACE/GRACE-FO TWS observations . . . 35
4.2. Relationship between soil moisture and GRACE-based TWS . . . 36
4.3. Propagation of water storage deficits in the subsurface . . . 37
4.4. Using GRACE as a constraint to derive subsurface storage dynamics from satellite soil moisture . . . 39

5. Results and Conclusion **41**
5.1. Comparability of remotely sensed soil moisture and GRACE/GRACE-FO TWS observations . . . 41
5.2. Relationship between soil moisture and GRACE-based TWS . . . 55
5.3. Propagation of water storage deficits in the subsurface . . . 61
5.4. Using GRACE as a constraint to derive subsurface storage dynamics from satellite soil moisture . . . 66

6. Summary and Outlook **73**
6.1. Summary . . . 73
6.2. Outlook . . . 75

References **79**

List of Figures **99**

List of Tables **102**

List of Acronyms **104**

A. Peer-reviewed publications **107**
A.1. A global analysis of water storage variations from remotely sensed soil moisture and daily satellite gravimetry . . . 107
A.2. Revisiting Sub-Surface Drought Cascades With Daily Satellite Observations of Soil Moisture and Terrestrial Water Storage . . . 133
A.3. Assessing sub-seasonal subsurface water storage dynamics using exponential filtering of ESA CCI soil moisture and daily GRACE terrestrial water storage data . . . 168

1. Introduction

1.1. Motivation and background

Soil moisture is a key variable in the terrestrial water cycle. Its role in linking atmospheric effects to processes occurring on and below the surface is essential. The distribution of incoming water into runoff, groundwater recharge, and evapotranspiration, for instance, is controlled by soil moisture conditions. Therefore, soil moisture affects both the hydrologic response over the short term and water availability for extended time frames (Seneviratne et al., 2010). Although it represents only a small fraction of global freshwater supplies, soil moisture has a major influence on the coupling between the land and the atmosphere (Seneviratne et al., 2010). Soil moisture dynamics range from rapid fluctuations at the surface to more persistent signals in deeper soil layers.

Observing these dynamics at larger spatial scales is not straightforward. While in-situ measurements provide detailed data at a particular location, satellite-based observations of soil moisture have been the primary tool for measuring soil moisture at large scales (regional/global). However, satellite-based observations mainly capture soil moisture variations in the upper few centimetres of the soil and thus generally reflect near-surface conditions (Cosh et al., 2004), where variability is strongest and response times are shortest. Therefore, they provide little to no information about deeper subsurface storage.

Terrestrial water storage (TWS) represents the full water column on and below the land surface. This includes soil moisture, groundwater, surface water, and snow (Syed et al., 2008). Satellite gravity data from the Gravity Recovery and Climate Experiment (GRACE) and GRACE Follow-On (GRACE-FO) missions enable the observation of global changes in TWS. These changes are measured by variations in the Earth's gravity field over time (Tapley et al., 2004; Landerer et al., 2020). Due to this integrative nature, GRACE observations are sensitive to water mass changes. However, they do not provide direct information on individual storage compartments or their vertical distribution (Scanlon et al., 2016).

The combined features of satellite-derived surface soil moisture (SSM) and GRACE-based TWS measurements provide an opportunity to improve our understanding of subsurface water storage processes. While SSM reflects surface conditions that typically

change rapidly, TWS integrates signals from all other storage compartments, including both shallow soil moisture and deeper storage components. Therefore, the linkage between these two data types will contain information on how water storage signals evolve with depth, including damping, changes in variability, and time-domain persistence.

Recent developments in processing GRACE data enable the estimation of TWS at daily temporal resolution (Kvas et al., 2019). This provides an opportunity to analyse water storage dynamics at a higher temporal resolution than has been possible with the traditional monthly scale. In particular, this will enhance the analysis of processes at sub-monthly timescales, which are more directly related to soil moisture fluctuations. The current understanding of how SSM observations relate to TWS and to its integrated nature remains limited, especially at daily timescales. To fill this gap, a joint analysis of both parameters that clearly considers the differences in integration depth and time characteristics is needed.

1.2. State-of-the-art and research gap

Continental GRACE and GRACE-FO observations provide an integrated measure of mass redistribution based on changes in the Earth's gravity field over time. The dominant contribution to these signals originates from TWS. Because all mass contributions are superimposed in the gravity signal, GRACE data alone do not allow for a separation of individual hydrological components. Because of this combination of multiple storage compartments, validating GRACE-based TWS is still a major challenge (Scanlon et al., 2016). While in-situ observations of individual hydrological variables can be used for comparison, they usually reflect just an isolated component across a different spatial and temporal scale. Observations such as groundwater levels, lake levels, river discharge, or soil water storage cannot be easily combined into a mass estimate comparable to the GRACE signal (Jiao et al., 2022).

Hydrological and land surface models offer a useful alternative reference for evaluations. However, these models have uncertainties based on the model structure and the input data (Beck et al., 2017). Discrepancies between model-based trends in water storage and GRACE observations have also been reported (Scanlon et al., 2018). Therefore, model-based TWS estimates should not be regarded as an absolute standard, but rather as a tool for interpreting storage variations derived from GRACE.

Despite this, GRACE-derived TWS observations provide globally consistent information on TWS variability that other observing systems cannot provide. Many studies have shown their value for examining regional and global water storage changes (e.g., Syed et al., 2008; Scanlon et al., 2019; Vishwakarma et al., 2021). Additionally, GRACE

data have been widely used to explore extreme events like droughts and floods (e.g., Reager and Famiglietti, 2009; Houborg et al., 2012; Thomas et al., 2014; Sun et al., 2017). Using GRACE, groundwater storage changes were estimated and regions affected by groundwater depletion were identified (e.g., Chen et al., 2016; Güntner et al., 2026; Rodell et al., 2009; Famiglietti et al., 2011), and ice mass loss was quantified (e.g., Ramillien et al., 2006; Velicogna, 2009). Furthermore, GRACE observations have been assimilated into hydrological models to improve simulations of water storage dynamics (e.g., Zaitchik et al., 2008; Werth et al., 2009; Eicker et al., 2014; Tangdamrongsub et al., 2017).

While most of the studies mentioned above are based on conventional monthly GRACE solutions, an increasing number of investigations have explored the potential of daily GRACE TWS solutions to capture rapid changes in water mass. These daily solutions are also used in this thesis. Daily gravity fields have been applied to analyse storage variations associated with extreme precipitation events, for example, in the Greater Horn of Africa (Omondi et al., 2014), as well as to investigate major flood events (Gouweleeuw et al., 2018), high-frequency atmospheric mass fluxes (Eicker et al., 2020), and to analyse hydrological extremes using drought and flood indices (Xiong et al., 2022). Additionally, daily GRACE(-FO)-based TWS estimates have only rarely been combined with hydrological models (Zhao and Yang, 2018; Retegui-Schiettekatte et al., 2025).

A complementary strategy for interpreting GRACE signals is to relate the TWS signal to a specific hydrological compartment in a region that is expected to dominate the signal there. In glacier regions, long-term trends in TWS are often mostly due to changes in ice mass. In semi-arid areas, groundwater depletion may play a major role. In large river basins and lake systems, variations in surface water storage can affect the TWS signal. As a result, many studies have compared GRACE-derived storage changes to link observed TWS variations to specific hydrological compartments.

Within the framework of this cumulative thesis, we focus on the interaction between TWS and soil moisture. Many studies have examined TWS and soil moisture separately, but comprehensive joint analyses of both at the global scale remain rare. Swenson et al. (2008b) compared GRACE TWS with soil moisture data from the Oklahoma Mesonet. The first comparisons between satellite-based soil moisture products and GRACE TWS were conducted by Abelen and Seitz (2013), Abelen et al. (2015), and Abelen (2016). They focused on monthly timescales using soil moisture data from the Advanced Scatterometer (ASCAT) and the Advanced Microwave Scanning Radiometer for EOS (AMSR-E) missions. More recently, Szabó and Osińska-Skotak (2023) provided a global comparison of GRACE TWS and AMSR-E soil moisture. Additionally, several studies have explored methods connecting the two variables. They suggest that satellite-

derived soil moisture can be used to downscale GRACE-based TWS estimates (Crow et al., 2017), or conversely, GRACE-derived storage variations can be used to retrieve global soil moisture (Sadeghi et al., 2020).

However, the joint analysis of TWS and soil moisture at sub-monthly or daily time scales has so far remained largely unexplored. Because soil moisture has a relatively short residence time and considerable temporal variability, it is likely to have an important influence on changes in TWS on relatively short timescales. The analyses in this thesis will explore the relationship between changes in TWS, as determined by gravity measurements, and changes in soil moisture across varying timescales.

1.3. Outline

This doctoral thesis is organised as a cumulative work comprising three peer-reviewed articles (see Appendix A) and one framework text. This framework text establishes the scientific basis for the work, outlines the research setting, and integrates the key conclusions from the included papers. Chapter 2 describes soil moisture as a component of the terrestrial water cycle. It defines its function in the Earth System and outlines the observational techniques. Additionally, conceptual frameworks for relating surface to subsurface soil moisture are discussed, along with an overview of common data products used to assess soil moisture. Chapter 3 focuses on TWS and how it can be observed using satellite gravimetry. Following this, Chapter 4 articulates the primary research objectives of this dissertation. Chapter 5 then presents and examines the primary findings of the dissertation. The findings from each of the three articles are organised around the research questions and integrated to explain the relationships between soil moisture and TWS across various temporal and spatial scales. Lastly, Chapter 6 synthesises the most important conclusions of the dissertation and outlines possible directions for future research.

1.4. Publication overview

The three scientific papers in this thesis explore different aspects of subsurface water storage dynamics using daily satellite-based observations of soil moisture and TWS from GRACE and GRACE-FO. Figure 1.1 illustrates their conceptual relationship and thematic structure. Together, they create a unified and organised research framework. This framework moves from observational analysis through a process-based application to the development of new methods. Each paper consistently uses combined soil moisture and TWS data to improve the understanding of subsurface water storage dynamics at various

depths. Below is a brief overview of the research focus of each publication and how they relate to one another:

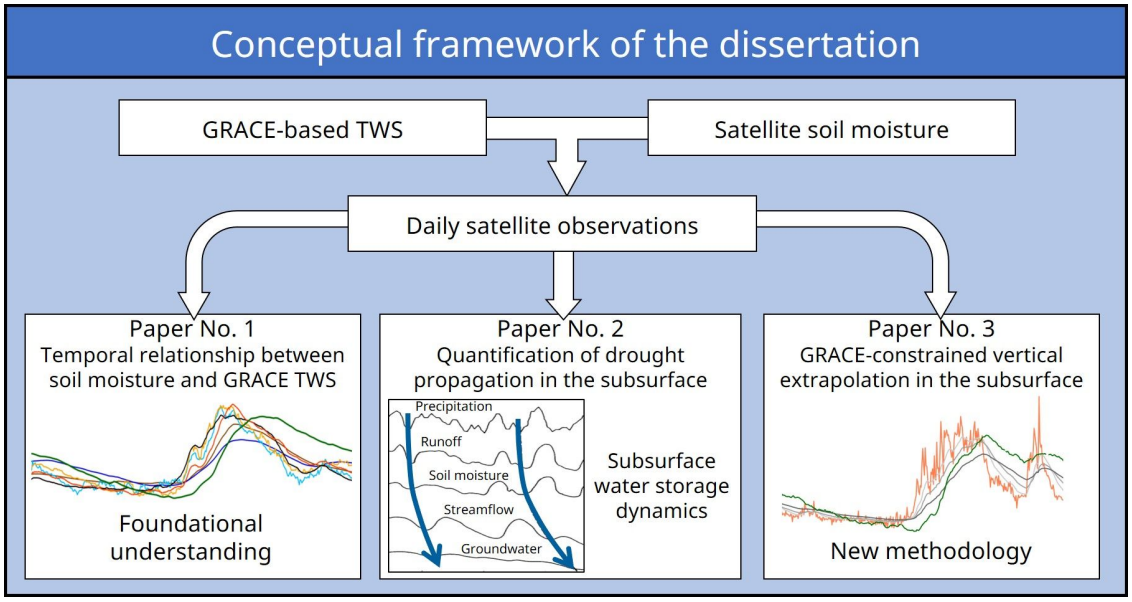

Figure 1.1.: Conceptual framework of the dissertation. The three panels correspond to the three papers included in this thesis. The schematic in the middle panel is adapted from Changnon (1987).

Paper 1 – Relationship between soil moisture and GRACE-based TWS

The first paper (Blank et al., 2023) develops the theoretical framework for this dissertation by comparing satellite-based soil moisture data with GRACE-derived TWS. This study investigates how surface- and root-zone soil moisture signals relate to TWS at seasonal and sub-monthly scales. By investigating correlation and temporal lags among these data sets, this study provides new insights into how water storage dynamics change with depth and their timing. In addition, it identifies areas where GRACE-derived TWS represents sub-monthly changes in soil moisture, highlighting the potential of daily GRACE solutions for analysing high-frequency subsurface processes. Therefore, the results of this study provide the basis for the methodological developments and process-oriented analyses.

Paper 2 – Drought propagation in subsurface water storage

Building on the findings of the first paper, the second paper (Blank et al., 2025) examines how drought-related water storage deficits propagate and recover within the subsurface. Using daily satellite observations of soil moisture and TWS, it analyses how deficit signals evolve from the surface through the root zone towards deeper storage compartments. The daily temporal resolution allows drying and recovery dynamics to be followed more

continuously and makes it possible to assess how the timing and persistence of deficits change with storage depth. In this way, Paper 2 shows that daily GRACE observations can capture short-term variations in water storage deficits and contribute to a better understanding of drought cascades in the subsurface on a global scale.

Paper 3 – GRACE-constrained estimation of subsurface storage dynamics

The third paper (Blank et al., 2026) develops a method to estimate subsurface water storage dynamics from satellite-based SSM observations. It calibrates an exponential filter against daily GRACE-based TWS, using GRACE as an integrated observational reference. This calibration provides spatially varying time constants that describe how SSM needs to be smoothed and delayed to better represent deeper storage dynamics. The resulting patterns are coherent across regions and can be related to hydrological conditions. In several regions, the GRACE-calibrated filter performs similarly to, or better than, conventional uniformly calibrated or in-situ calibrated filter settings. Paper 3 therefore extends the previous analyses by using GRACE not only to compare storage signals, but also to constrain the estimation of subsurface storage dynamics from SSM.

2. Soil Moisture

Satellite-based observations of soil moisture form the observational basis of this thesis. This chapter introduces soil moisture as a key component of the terrestrial water cycle and provides the conceptual and observational background required for the analyses presented in the following chapters. It outlines its role within the land–atmosphere system and the terrestrial water cycle, discusses how soil moisture can be observed using in-situ measurements and satellite remote sensing, and summarises the main limitations associated with each observation technique. The chapter further introduces conceptual approaches to link SSM observations to subsurface conditions. It provides an overview of the satellite-based soil moisture data products used in this thesis.

2.1. Definition and role in the Earth system

Soil moisture is a key environmental variable and an essential climate variable (ECV) of the global water cycle (Dorigo et al., 2021), impacting land–atmosphere interactions and hydrological processes. Soil moisture refers to the water stored in the unsaturated soil zone, also known as the vadose zone (Hillel, 2004). Figure 2.1 illustrates the position of the unsaturated zone, which is located above the groundwater table and, in contrast to the saturated soil zone, is not fully saturated with water but contains a porous soil matrix in which pore spaces are filled with water and air (Grotzinger and Jordan, 2017). This zone is characterised, on the one hand, by water loss through evapotranspiration, including evaporation from the soil surface and transpiration by vegetation, which results in an upward-directed water flux. On the other hand, precipitation replenishes soil water storage and induces a downward percolation of water toward the groundwater (Fredlund et al., 2012). Although soil moisture makes up only a very small fraction of global freshwater resources, about 0.05% (Shiklomanov, 1993), soil moisture plays an important role in regulating hydrological and climatic processes at the land surface.

In practice, soil moisture must be considered with respect to a specific volume of soil. One of the most common representations of soil moisture is volumetric soil moisture θ, expressed as the ratio of the volume of water V_w to the total soil volume V within a control volume (Seneviratne et al., 2010):

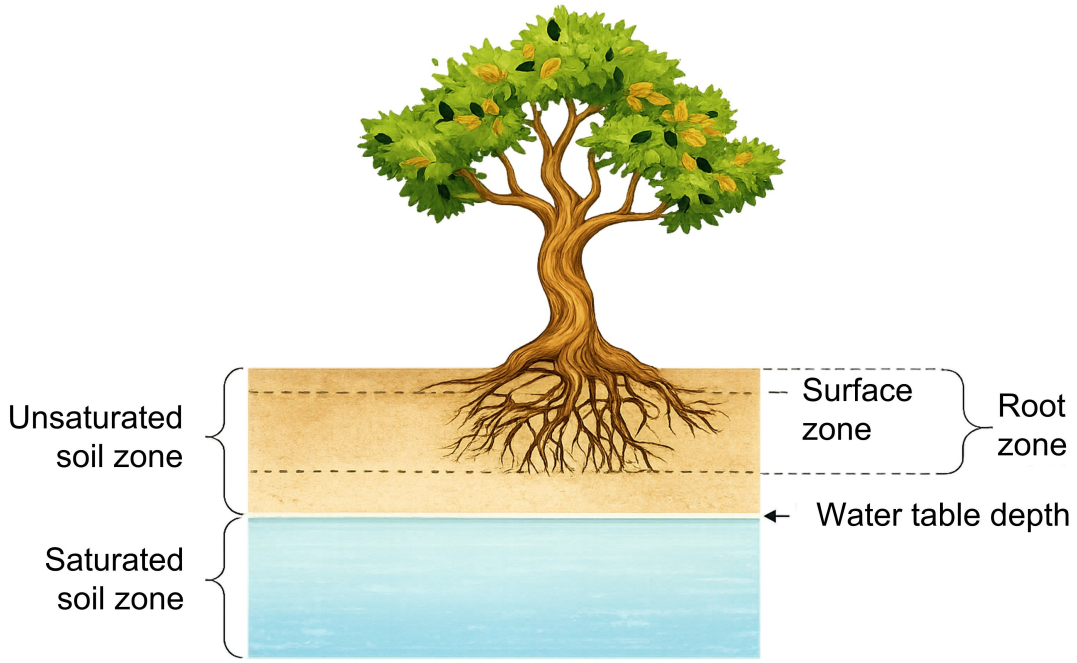

Figure 2.1.: Division of the soil into saturated and unsaturated soil zones and the depth of the surface zone and root zone in the unsaturated soil zone (figure generated using AI (OpenAI, 2026) inspired by Seneviratne et al. (2010))

$$\theta = \frac{V_w}{V} \tag{2.1}$$

Volumetric soil moisture is a dimensionless quantity and is commonly reported either as a fraction (e.g. $m^3\,m^{-3}$) or as a percentage.

The measurable fraction of soil moisture strongly depends on the applied technique and measurement method. In-situ soil moisture sensors, for example, can measure soil moisture at depths ranging from a few centimetres down to approximately 2 m below the land surface (Wu et al., 2015). In contrast, satellite-based remote sensing using microwave sensors allows for the observation of soil moisture only in the uppermost soil layer, typically within the top few centimetres (up to 5 cm) of the soil, referred to as the surface zone (Cosh et al., 2004). The most reliable retrievals are generally achieved for depths of up to about 2 cm (Escorihuela et al., 2010).

For many climate-related applications, the so-called root zone (see Figure 2.1) is of particular importance (Seneviratne et al., 2010). The root zone represents the soil layer occupied by plant roots and thus the primary zone of water uptake by vegetation (Fredlund et al., 2012). However, this zone cannot be defined by a fixed depth, as its vertical extent varies spatially and temporally depending on vegetation type, soil properties, and environmental conditions (Seneviratne et al., 2010).

2.2. Observing soil moisture

Soil moisture can be observed using a variety of measurement techniques that differ in spatial coverage, temporal resolution, and measurement depth. These techniques can be broadly divided into in-situ measurements and remote sensing approaches.

2.2.1. In-situ soil moisture

In-situ observations provide direct measurements of soil moisture at specific locations and depths and are therefore well suited for process studies as well as for the calibration and validation of indirect measurement techniques. Although such observations are not used directly in the papers of this thesis, they have been considered in supporting analyses and provide an important reference for satellite-based soil moisture measurements and their uncertainties. In addition, they help to facilitate the understanding of the physical principles underlying satellite retrievals, as many in-situ measurement techniques rely on the dielectric properties of the soil, similar to satellite observations. Since measurements are point-based, their spatial representativeness is limited. Many measurement methods have been created over time.

The thermo-gravimetric approach directly measures soil moisture. The soil sample is taken from the field and afterwards oven-dried. By weighing the soil sample before and after drying, its water content can be quantified (Walker et al., 2004). However, this method is very time-consuming and destructive, as the soil sample is irreversibly altered during drying, preventing repeated measurements at the same location. Nevertheless, this method is widely used as a reference for calibrating and validating other soil moisture measurement techniques (Walker et al., 2004).

More recent soil moisture measurement techniques measure soil moisture indirectly by relying on the electrical properties of the soil, such as dielectric permittivity, capacitance, or electrical resistance (Lekshmi et al., 2014). Among the most widely used in-situ soil moisture measurement techniques are Time Domain Reflectometry (TDR) and Frequency Domain Reflectometry (FDR) (Bogena et al., 2007; Lekshmi et al., 2014). Both methods employ electromagnetic principles to infer soil moisture from the dielectric permittivity of the soil, which describes how strongly the soil responds to an electric field (World Meteorological Organization, 2024). This is commonly described by the dielectric constant, which is about 20 times higher for liquid water than for average dry soil (Wagner, 1998; World Meteorological Organization, 2024).

In the TDR method, the dielectric constant is derived from the travel time of an electromagnetic pulse along metal rods inserted into the soil. The velocity of the pulse depends on the soil water content through its dielectric properties, allowing changes in soil

moisture to be detected (World Meteorological Organization, 2024). The FDR approach operates on a similar principle, but instead of measuring travel time, it detects changes in operational frequency between sensor electrodes caused by soil moisture variations (Lekshmi et al., 2014).

The in-situ measurement methods described above are usually invasive, although they provide very precise measurements of soil moisture at specific locations. Global Navigation Satellite System-Reflectometry (GNSS-R) is a non-invasive geodetic method to observe soil moisture. In conventional GNSS positioning, multipath signal reception is a major source of error, whereas GNSS-R intentionally exploits these reflected signals to observe environmental parameters such as soil moisture, snow depth, and vegetation density (Larson et al., 2014). In GNSS-R, both the direct signal and a surface-reflected signal are received by a ground-based antenna, leading to characteristic interference patterns that can be identified through variations in the signal-to-noise ratio (SNR) (Larson et al., 2008). Soil moisture affects the penetration depth and dielectric properties of the soil, which in turn modifies the amplitude and frequency of the SNR signal. As a result, soil moisture variations within the upper 1–6 cm of the soil can be inferred (Larson et al., 2010). Although GNSS-R observations are point-based, the reflected signals originate from the surrounding area, resulting in an effective horizontal footprint of approximately 1000 m^2 (Larson et al., 2010). Several studies have demonstrated the potential of GNSS-R (Larson et al., 2008; Rodriguez-Alvarez et al., 2009; Vey et al., 2016).

Another non-invasive approach for observing soil moisture is Cosmic-Ray Neutron Sensing (CRNS) (Zreda et al., 2008). This in-situ technique exploits naturally occurring neutrons generated by cosmic radiation, with the neutron count near the land surface being inversely related to soil water content. By counting reflected neutrons above the ground surface, CRNS provides area-integrated soil moisture estimates of several meters and sensing depths of up to several decimetres, making it particularly suitable for the validation of satellite-based soil moisture products (Schrön et al., 2017; Montzka et al., 2017; Köhli et al., 2021; Schmidt et al., 2024).

Many in-situ soil moisture networks are available worldwide, ranging from local experimental sites to regional meteorological networks. These networks provide soil moisture measurements several times per day. Nevertheless, soil moisture exhibits strong spatial and temporal variability. Representing this variability globally with in-situ measurements would require a very dense and large network of stations, which is not feasible due to high costs and the limited accessibility of certain regions (Gruber et al., 2013). In-situ observations remain essential for determining soil moisture at the local scale and for validating satellite soil moisture products (Albergel et al., 2012).

2.2.2. Soil moisture by remote sensing

Unlike in-situ observations, satellite-based remote sensing allows for the observation of soil moisture over larger areas, making it especially useful for analysis on a regional to global scale. Although satellites have provided soil moisture information since the 1970s, the first dedicated soil moisture mission was launched only in 2009 with the Soil Moisture and Ocean Salinity (SMOS) mission (Ochsner et al., 2013). Satellite-based microwave sensors are capable of observing soil moisture in the surface layer (up to 5 cm) because they are sensitive to the dielectric permittivity of the soil, which becomes larger as the soil water content increases (Ulaby et al., 1982). This makes microwave remote sensing, especially at frequencies between 1 and 10 GHz, well suited for observing soil moisture.

The three major frequency bands used in extracting soil moisture information are the L-band with frequencies of $f = 1$–$2\,\text{GHz}$ and corresponding wavelengths of $\lambda = 30$–$15\,\text{cm}$, the C-band with frequencies of $f = 4$–$8\,\text{GHz}$ and wavelengths of $\lambda = 7.5$–$3.8\,\text{cm}$, and the X-band with frequencies of $f = 8$–$12\,\text{GHz}$ and wavelengths of $\lambda = 3.8$–$2.5\,\text{cm}$ (Wagner et al., 2007). Cloud cover, rainfall, and vegetation affect microwave observations less strongly at longer wavelengths. For wavelengths above approximately 4 cm, the influence of rain and clouds is usually small. Longer wavelengths also penetrate deeper into the soil, increasing the sensitivity to subsurface soil moisture variations (Ulaby et al., 1982). However, they require larger antennas, which makes satellite sensor design more complex and expensive (Kerr et al., 2010).

In microwave remote sensing, soil moisture can be observed using either active or passive techniques. The basic principles of both approaches are shown in Figure 2.2. Active microwave sensors, often referred to as radar systems, emit an electromagnetic pulse and observe the part of the signal that is backscattered from the Earth's surface (Robinson et al., 2008). The measured signal depends on sensor characteristics, observation geometry, and surface properties (Ulaby et al., 1982). The strength of the received signal mainly depends on how strongly the surface reflects or scatters the emitted radiation back towards the sensor (Joseph, 2005). This scattering behaviour is strongly dependent on the ground's reflectivity, which is influenced by the dielectric properties of the soil surface and increases with soil water content (Abelen, 2016). Therefore, variations in soil moisture can be inferred from changes in the backscattered radar signal.

Passive microwave sensors, also referred to as radiometers, observe microwave radiation emitted by the Earth's surface (Robinson et al., 2008). This signal is expressed as brightness temperature and includes radiation from the surface, atmospheric effects, and cosmic background radiation. For the microwave frequencies used in soil moisture retrieval, the atmospheric and cosmic contributions can largely be corrected using auxiliary information. The remaining signal is mainly controlled by surface temperature and surface

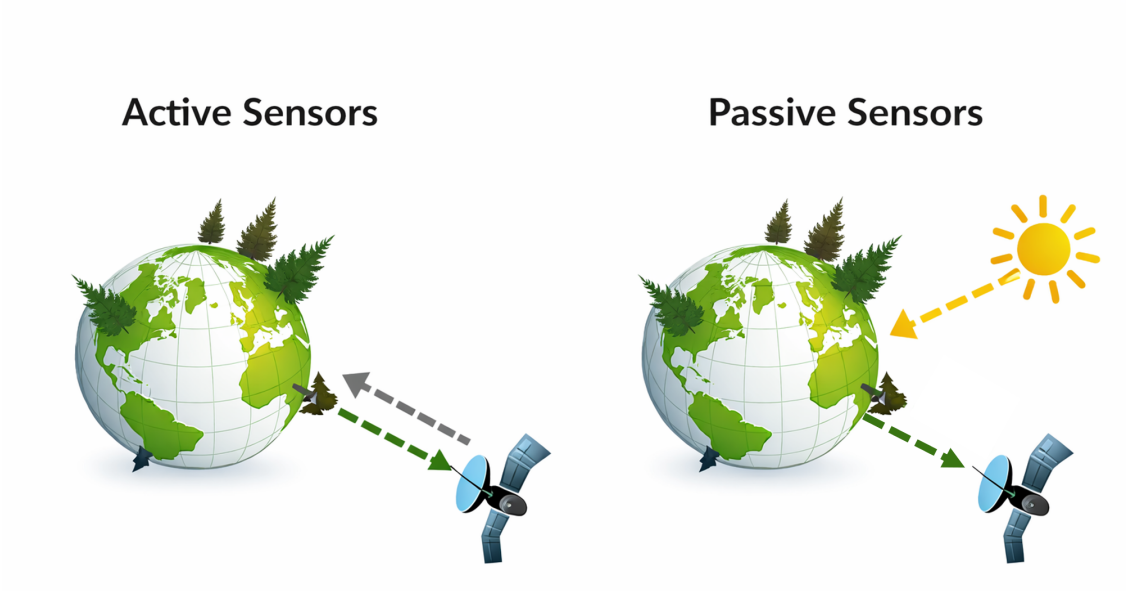

Figure 2.2.: Principle and difference between active and passive microwave sensors (figure generated using AI (OpenAI, 2026) inspired by Aberle and Bill (2026))

emissivity (Abelen, 2016).

Soil moisture can be estimated from brightness temperature because surface emissivity is closely linked to soil reflectivity and its dielectric properties. If the physical surface temperature is known, either from model-based estimates or independent satellite observations, the emissivity component of the measured signal can be isolated. Since soil emissivity decreases with increasing water content, changes in emissivity can be related to changes in soil moisture (Abelen, 2016). The accuracy of passive microwave soil moisture retrievals strongly depends on the quality of the surface temperature estimates (Parinussa et al., 2011).

Since 1978, satellite instruments have provided global passive microwave observations to estimate soil moisture (World Meteorological Organization, 2024), beginning with the Scanning Multichannel Microwave Radiometer (SMMR). This was followed by missions such as the Special Sensor Microwave/Imager (SSM/I), the Tropical Rainfall Measuring Mission Microwave Imager (TRMM-TMI), the Advanced Microwave Scanning Radiometer for EOS (AMSR-E), and WindSat aboard the Coriolis satellite. Since the 2010s, satellite-based soil moisture observations have become more widely available through dedicated and multi-purpose missions, including Soil Moisture and Ocean Salinity (SMOS), the Chinese FengYun-3 (FY-3B/C/D) series, Advanced Microwave Scanning Radiometer 2 (AMSR-2), the Global Precipitation Measurement (GPM) mission, and Soil Moisture Active Passive (SMAP). Active microwave soil moisture observations have been available since 1991 from the European Remote Sensing satellites ERS-1 and ERS-2 and have continued with the Advanced Scatterometer (ASCAT-A/B/C) instruments. Among these

missions, SMOS and SMAP provide dedicated L-band soil moisture observations (World Meteorological Organization, 2024). SMAP was originally designed to combine both active radar and passive radiometer measurements. However, the active radar instrument failed only a few months after launch, and since then, soil moisture retrievals have relied exclusively on passive radiometer observations (Cole and Buis, 2015).

In addition, GNSS-R can be used as a remote sensing technique to observe soil moisture using a geodetic method. Since 2018, the Cyclone Global Navigation Satellite System (CYGNSS) mission has provided near-global soil moisture observations using this technique (Chew and Small, 2018). Although CYGNSS was originally designed to study tropical cyclones (Ruf et al., 2016), its measurements have proven valuable for soil moisture monitoring. Based on GNSS-R technology, ESA launched the HydroGNSS mission, a microsatellite mission, in late 2025. It seeks to provide global coverage of GNSS-R measurements for soil moisture applications (Unwin et al., 2021).

Remote sensing techniques enable reliable, large-scale soil moisture observations and allow measurements in remote and inaccessible regions (Kerr et al., 2010; Ochsner et al., 2013). However, soil moisture retrieval from microwave remote sensing is strongly affected by land cover characteristics. Vegetation, in particular, influences the observed signal through the absorption and scattering of soil-emitted radiation as well as through its own emission (Jackson and Schmugge, 1991). All microwave frequency bands are sensitive to vegetation effects, with higher frequencies being more strongly affected, making vegetation-related corrections an essential component of soil moisture retrieval algorithms (World Meteorological Organization, 2024).

In regions with very dense vegetation, such as tropical rainforests, soil moisture observation becomes impractical because soil emission is largely masked, and the measured signal is dominated by vegetation contributions (Owe et al., 2001). In contrast, desert regions present distinct challenges, in which the low dielectric permittivity of dry soils reduces sensitivity to soil moisture variations (De Jeu et al., 2008). Additional complications arise in areas covered by snow or frozen ground, where the dielectric properties of ice differ substantially from those of liquid water, further limiting the reliability of soil moisture retrievals (Wagner, 1998). Surface or standing water introduces another challenge (Ye et al., 2015; Tong et al., 2025), as its presence within the observed footprint can lead to mixed signals that need to be accounted for in the retrieval algorithm.

Radio Frequency Interference (RFI) poses a challenge to passive microwave soil moisture observations by contaminating measurement frequencies with radio emissions from anthropogenic sources, such as communication systems or GPS jammers operating within or near the observed bands (Wagner et al., 2007; De Jeu et al., 2008). Although the L-band frequencies between 1.400 and 1.427 GHz are formally protected for passive

applications, they can still be affected by RFI (Kunkee, 2005), which can significantly impair soil moisture retrieval and, in some cases, make it impossible (Wagner et al., 2007).

2.3. Soil moisture representation in hydrological models

Although this thesis does not focus on hydrological modelling, model-based soil moisture representations provide important context for interpreting satellite observations. Hydrological and land surface models represent water partitioning and dynamics in the terrestrial system and are used to estimate and assess soil moisture processes and applications. In addition, some of the satellite-based data sets used in this thesis rely on model components, such as the SMAP Level-4 product, which uses data assimilation. Furthermore, model-based data are used in Paper 2 for validation purposes. A brief overview is therefore given to help understand soil moisture modelling frameworks.

Hydrological models approximate the behaviour of the terrestrial water cycle and its components, by representing the interactions between climate forcing, land surface characteristics, soil properties, and water fluxes (Lundin et al., 2000). These models use meteorological variables like precipitation and temperature to simulate hydrological processes, with soil moisture playing a central role in controlling evapotranspiration, runoff generation, and land–atmosphere interactions (Hingray et al., 2014). Due to their broad range of applications in water resources management, agriculture, and climate research, hydrological models form an important interdisciplinary research field. Central elements of hydrological models include external forcing data, simplified model equations describing water fluxes and storage processes, parameter sets controlling soil and land-surface behaviour, and simulated output variables, such as soil moisture, that are used for further analysis (Lundin et al., 2000).

Land surface models (LSM) and water balance models are often used to get global information on soil moisture content. LSMs focus on land–atmosphere interactions and simulate near-surface processes, producing output variables such as SSM or soil moisture in deeper layers (Overgaard et al., 2006). A prominent example is the Global Land Data Assimilation System (GLDAS; Rodell et al., 2004), which provides spatially and temporally consistent soil moisture estimates at the global scale.

In addition to LSMs, global water balance models also simulate soil moisture as an integral component of the terrestrial water cycle. These models represent soil moisture as part of overall storage dynamics and estimate its temporal variability using water balance principles. The WaterGAP Global Hydrology Model (WGHM; Döll et al., 2003; Müller

Schmied et al., 2024), simulates soil moisture alongside other hydrological components of the terrestrial water cycle such as groundwater, snow, and surface waters. Therefore, water balance models provide valuable large-scale estimates of soil moisture dynamics and serve as important reference frameworks for interpreting observation-based soil moisture products.

In recent years, satellite observations have gained increasing importance in hydrological and land surface modelling frameworks. Satellite-based soil moisture products and TWS observations provide spatially continuous information and help constrain model simulations at regional to global scales. These observations are increasingly incorporated into models through data assimilation techniques, which optimally combine model predictions with satellite-derived soil moisture to better represent soil moisture and other components of the terrestrial water cycle (Li et al., 2019; Tangdamrongsub et al., 2020; Tian et al., 2021; Springer et al., 2026).

2.4. Conceptual representation of subsurface soil moisture

Satellite-based soil moisture products provide spatially continuous information across large areas but only cover the top few centimetres of soil. On the other hand, many hydrological applications for drought assessment or water resource management require soil moisture data in deeper layers. In-situ measurements can provide soil moisture observations at multiple depths with high temporal resolution, but their spatial coverage is sparse. As a result, a gap exists between the depth represented by satellite observations and the subsurface soil moisture information needed at regional to global scales.

There are various methods to estimate subsurface soil moisture from SSM observations (Tian et al., 2020), and previous studies have shown that SSM contains information on subsurface soil moisture (Mahmood and Hubbard, 2007; Wang et al., 2017). Data assimilation techniques integrate remotely sensed soil moisture into land surface or hydrological models to improve soil moisture profiles (Han et al., 2013). Physically based approaches explicitly represent soil moisture transport processes but strongly depend on detailed input data and parametrisation, which makes them challenging to apply over large spatial domains (Manfreda et al., 2014; Rasche et al., 2024). Statistical methods aim to exploit empirical relationships between SSM and subsurface soil moisture without explicitly resolving the underlying physical processes, such as cumulative distribution function (CDF) matching (Han et al., 2012; Gao et al., 2018). In addition, machine-learning approaches such as artificial neural networks can be used to derive subsurface soil moisture information from surface observations (e.g. Kornelsen and Coulibaly, 2014;

Pan et al., 2017; Lamichhane et al., 2025).

Among the available approaches, the exponential filter proposed by Wagner et al. (1999) represents a particularly conceptually simple method for estimating subsurface soil moisture from surface observations and is explained in detail in Section 2.4.1. The approach uses the characteristic time constant T to control the smoothing and delay of the SSM signal. This parameter reflects the effective response of the subsurface system and is influenced by soil texture, vegetation, and climate conditions (Ceballos et al., 2005; Albergel et al., 2008). The exponential filter has been applied and evaluated in numerous studies. It has been shown to perform robustly, demonstrating considerable potential for estimating subsurface soil moisture despite its conceptual simplicity (e.g. Brocca et al., 2010; Ford et al., 2014; Paulik et al., 2014; Bouaziz et al., 2020; Pasik et al., 2023).

2.4.1. Exponential filtering approach for subsurface soil moisture estimation

The estimation of subsurface or root-zone soil moisture (RZSM) from satellite-derived SSM is a central methodological component of this thesis and forms the basis of the third paper. For completeness and conceptual clarity, the exponential filtering approach is therefore described in detail in this section.

The exponential filter method is based on a simplified two-layer soil water balance concept. The soil column consists of a surface layer and an underlying subsurface reservoir, and the only exchange process considered between the two layers is vertical infiltration. The method assumes that water flux from the surface to deeper layers is driven by the difference in soil moisture between the surface and deeper layers. As a result, subsurface soil moisture can be approximated as a temporally filtered version of SSM (Wagner et al., 1999; Albergel et al., 2008).

In this study, the recursive formulation of the exponential filter is employed following Albergel et al. (2008), with abbreviations used from Pasik et al. (2023):

$$RZSM(t_n) = RZSM(t_{n-1}) + K_n \left(SSM(t_n) - RZSM(t_{n-1}) \right), \tag{2.2}$$

$$K_n = \frac{K_{n-1}}{K_{n-1} + \mathrm{e}^{-\frac{t_n - t_{n-1}}{T}}}. \tag{2.3}$$

In this formulation, subsurface soil moisture at a given point in time is calculated as a weighted combination of the current SSM observation and the previous RZSM estimate. The parameters t_n and t_{n-1} denote the current and previous timestamp, and K_t (which ranges from 0 to 1) is the gain term. The parameter T in Eq. 2.3 is the only unknown

parameter and controls the smoothing and delaying of the signal. Larger values of T result in smaller gain factors K_t, leading to stronger smoothing and an increased temporal lag in the subsurface response, while smaller values of T imply weaker smoothing and a closer correspondence between subsurface and SSM. At the first step, when no previous estimate is available, the filter is initialised with $K_0 = 1$ and $RZSM_{t_0} = SSM_{t_0}$. (Wagner et al., 1999; Albergel et al., 2008)

The time constant T controls how much memory is introduced into the filtered soil moisture signal. Small T-values keep the filtered signal close to the original SSM observations, whereas larger T-values produce a smoother and more delayed signal. The choice of T is therefore central when SSM is used to approximate storage dynamics below the surface. In many applications, T is calibrated against in-situ soil moisture measurements at a given depth. Different T-values, for example between 1 and 100 days, are tested, and the T-value that gives the closest agreement with the reference time series is selected. This agreement can be measured by using correlation, the Nash-Sutcliffe efficiency, or the root mean square error. In Paper 3, the same principle is applied, but the reference is no longer an in-situ soil moisture profile. Instead, daily GRACE-based TWS is used as an integrated storage constraint for optimising T.

Subsurface soil moisture variability is smaller than at the surface due to smoothing effects in deeper soil layers. As a result, the characteristic time constant T generally increases with soil depth to smooth the SSM signal more strongly (Wagner et al., 1999; Paulik et al., 2014). The optimal value of T can vary between regions and depends on factors such as sensor characteristics, temporal sampling, and land surface conditions (Albergel et al., 2008; Brocca et al., 2010; Bouaziz et al., 2020). In this sense, T is not a direct physical parameter, but an effective response time that describes how quickly the surface signal is translated into a slower subsurface storage signal.

2.5. Soil moisture data products

This section introduces the satellite soil moisture data sets used in this thesis and summarises their main characteristics.

2.5.1. Soil moisture products from SMOS

SMOS is an ESA Earth Explorer mission dedicated to global observations of soil moisture and sea surface salinity. It was launched in November 2009 and remains operational. A detailed description of the mission and its measurement principle is given by Kerr et al. (2010).

SMOS flies in a sun-synchronous orbit at an altitude of about 760 km. It crosses the

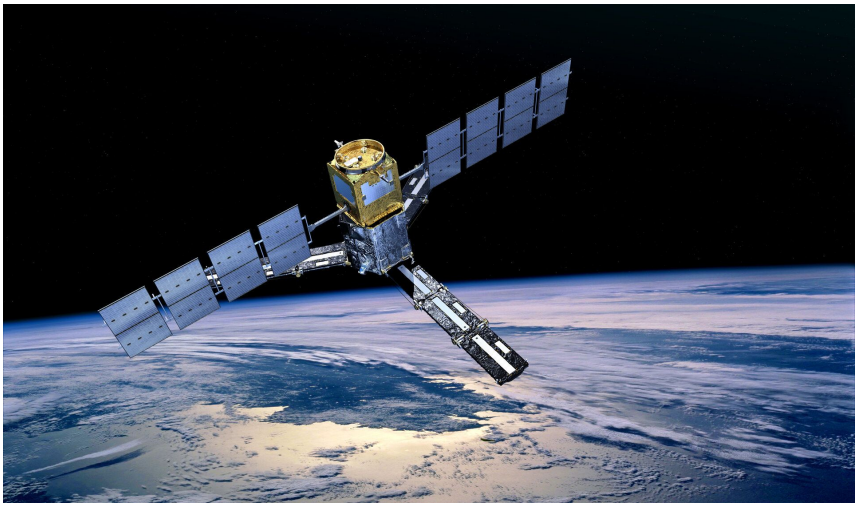

Figure 2.3.: Illustration of the SMOS satellite in space. Image credit: © ESA / AOES Medialab

equator at around 06:00 local time on the ascending orbit and around 18:00 local time on the descending orbit. With an orbital period of about 100 minutes, SMOS provides a revisit time of less than three days. Soil moisture is retrieved from passive L-band microwave observations between 1.400 and 1.427 GHz, which are mainly sensitive to the upper few centimetres of the soil. The effective spatial resolution is about 40–50 km, with most of the signal originating from within roughly 25 km of the observation point (Al Bitar et al., 2012).

SMOS data products are distributed at different processing levels. Level 1 (L1) products consist of raw satellite observations, such as brightness temperature measurements. Soil moisture estimates are first included in Level 2 (L2) products, which are provided as swath-based data for individual satellite overpasses (Al Bitar et al., 2017). To facilitate large-scale analyses, Level 3 (L3) soil moisture products have been processed into globally gridded data sets. These L3 products are provided, for example, by the Centre Aval de Traitement des Données SMOS (CATDS), which performs the additional processing. The L3 data consist of daily global SSM maps, with additional temporally aggregated products available.

It is important to note that these L3 products are treated as observation-based data sets, but they are not purely observational, since the raw measurements from passive radiometers are brightness temperature. L3 soil moisture products are generated from satellite observations, but their estimation also uses additional information, such as vegetation indices or land surface temperature.

CATDS also provides Level 4 (L4) soil moisture products, which include estimates of RZSM for the 0-100 cm layer. The L4 RZSM products are derived from L3 SSM data in combination with auxiliary data sets and are generated using a two-layer hydrological bucket model representing soil layers of 0–40 cm and 40–100 cm, which are estimated

using the exponential filter (see 2.4.1). The estimation of the T parameter for the exponential filter is based on soil properties from models, meaning that the L4 product is not purely observational but combines satellite observations with model-based information. A detailed description of the L4 processing approach is given by Al Bitar and Mahmoodi (2020).

In this thesis, SMOS L3 SSM (CATDS, 2022b) and L4 RZSM (CATDS, 2022a) products from CATDS are used in the first and second papers. These data sets enable research on soil moisture variability across vertical compartments and temporal scales.

2.5.2. Soil moisture products from SMAP

Additional soil moisture products are provided by the SMAP satellite mission, which was developed by the National Aeronautics and Space Administration (NASA). Technical details are described in Entekhabi et al. (2010) and Entekhabi et al. (2014). The mission was launched in January 2015 and is currently operational.

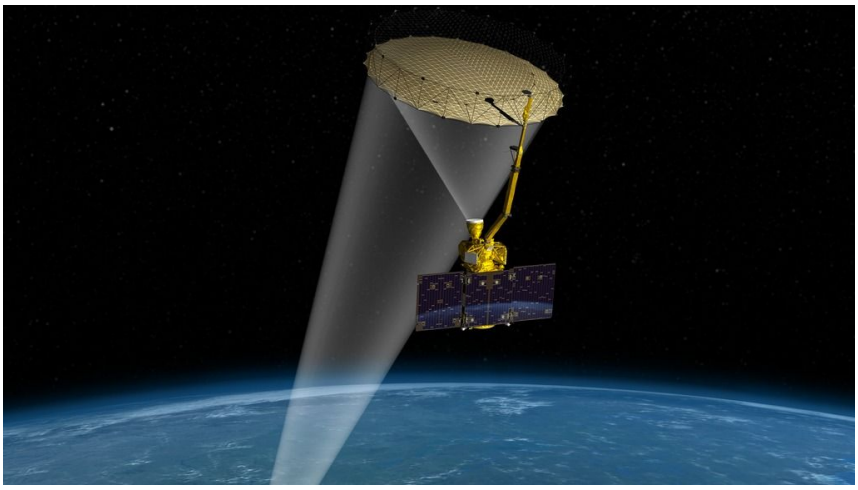

Figure 2.4.: Illustration of the SMAP satellite in space. Image credit: NASA / Scientific Visualization Studio

SMAP operates in a sun-synchronous orbit at an altitude of approximately 680 km. In contrast to SMOS, the equator crossing times are reversed, with the ascending orbit occurring at around 18:00 local time and the descending orbit at approximately 06:00 local time. The orbital period is about 98 minutes. The mission is equipped with an L-band active radar and a passive radiometer to retrieve SSM with a revisit time of 2-3 days. The radar has a 3 km spatial resolution at 1.2 GHz, while the radiometer has a 40 km resolution at 1.41 GHz. A combined active–passive product was intended to achieve a spatial resolution of approximately 10 km. However, the active radar instrument failed in July 2015 and could not be restored. As a result, SMAP soil moisture observations

since mid-2015 are based exclusively on measurements from the passive radiometer, and radar-based products are only available for the period from April 2015 to July 2015 (Cole and Buis, 2015).

SMAP data products are distributed by the National Snow and Ice Data Center (NSIDC) and are available at processing levels L1 to L4. Similar to SMOS, the L1 products consist of raw instrument measurements, L2 products provide soil moisture estimates for individual satellite overpasses, and L3 products contain spatially gridded daily soil moisture composites. The further processed L4 products provide global estimates of SSM and RZSM.

In this thesis, daily L3 radiometer-based SSM products (O'Neill et al., 2023) as well as daily L4 products for SSM and RZSM are used (Reichle et al., 2022). The L3 SSM data are provided on a regular grid with a spatial resolution of approximately 36 km $\times$ 36 km and distinguish between ascending and descending satellite overpasses. Similar to the SMOS L3 product, these data are commonly treated as observation-based, but they are not purely observational, as they are derived from brightness temperature measurements using retrieval algorithms that also rely on ancillary data. The L4 products provide three-hourly estimates of SSM (0–5 cm) and RZSM (0–100 cm) on a 9 km $\times$ 9 km grid. The L4 soil moisture estimates are generated within a data assimilation framework that combines SMAP observations with simulations from the GEOS-5 LSM, which incorporates meteorological forcing, e.g., precipitation. This method generates spatially continuous soil moisture estimates with enhanced temporal and spatial resolution (Entekhabi et al., 2014), but cannot be regarded as a pure satellite-based product due to the data assimilation approach and should instead be interpreted as observation-informed.

2.5.3. Soil moisture products from ESA CCI

The ESA Climate Change Initiative (CCI) SSM data set is provided as part of the CCI and represents a harmonised multi-mission record of satellite-based SSM observations (Dorigo et al., 2017; Gruber et al., 2019; Preimesberger et al., 2021). A consistent long-term climate data set is created by merging and intercalibrating soil moisture retrievals from multiple active and passive microwave satellite missions. ESA CCI provides three SSM products: an active microwave product, a passive microwave product, and a combined active-passive product. This thesis uses the combined active-passive SSM product, with different versions applied in the three papers: v7.1 in Paper 1, v8.1 in Paper 2, and v9.1 in Paper 3. Figure 2.5 illustrates the satellite missions contributing to the different ESA CCI products, including both active and passive sensors, covering nearly all missions introduced in Section 2.2.2. The combined product provides daily global SSM observations on a 0.25° grid and covers the period from 1978 to the present.

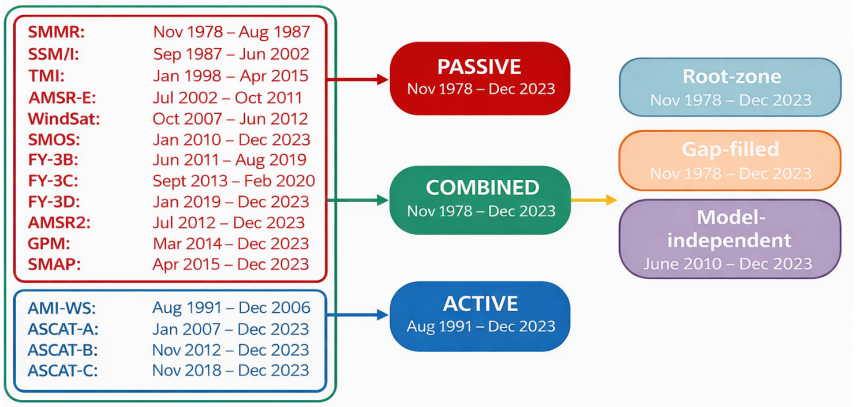

Figure 2.5.: Overview of the time periods and satellite inputs used to generate ESA CCI data set. Image credit: Dorigo et al. (2024).

Before merging, satellite retrievals are rescaled to a common climatology to ensure consistency across sensors with different characteristics and sensing geometries. Harmonisation is performed separately for active and passive sensors, and then combined using GLDAS climatology as a reference (Gruber et al., 2019). The ESA CCI SSM product includes quality flags and masking procedures to exclude regions and conditions where reliable soil moisture retrievals are not possible. In particular, dense tropical rainforest regions are masked due to strong vegetation scattering effects in microwave observations (see Sec. 2.2.2). In addition, retrievals are excluded for days when soil temperature is below 0°C and snow water equivalent (SWE) is greater than 0 mm, which represent frozen soil and snow-covered conditions. These conditions would lead to unreliable microwave-based soil moisture estimates (Gruber et al., 2019).

This thesis also uses the ESA CCI RZSM product (v9.1; Stradiotti and Preimesberger, 2025), which is exponentially filtered from the combined SSM data set on a 0.25° grid. The exponential filter temporally smooths SSM observations to estimate subsurface soil moisture. To optimise the globally uniform T parameter, a large global set of in-situ soil moisture data is used (Pasik et al., 2023). The ESA CCI RZSM product provides soil moisture estimates for three subsurface layers (0–10 cm, 10–40 cm, 40–100 cm). One global, depth-specific T value was applied to generate each discrete depth layer. Pasik et al. (2023) also describes the generation of a 100-200 cm soil moisture layer, which was adopted in this study. Soil moisture for integrated depths of 0–10, 0–40, 0–100, and 0–200 cm is computed as thickness-weighted averages.

2.5.4. Supplementary soil moisture data sets

Beyond the satellite-based soil moisture products that form the primary data basis of this thesis, other data sets were used to support interpretation and provide independent

reference information. These data sets were used selectively to evaluate the consistency and plausibility of soil moisture patterns.

In-situ soil moisture observations from the International Soil Moisture Network (ISMN; Dorigo et al., 2011) were used as an independent reference for selected regions. The ISMN has created a global data set based on in-situ soil moisture data collected at a large number of locations across the world, including a variety of climate regimes, soil types, and soil depths. This data was used to qualitatively compare satellite-derived surface and subsurface signals.

Satellite products were additionally compared with model-based soil moisture estimates from GLDAS (Rodell et al., 2004), serving as a complementary model-based reference. GLDAS is derived using LSM and meteorological forcing data. One of its outputs is global soil moisture data for multiple soil layers (0-10, 10-40, 40-100, 100-200 cm). Model-based estimates have uncertainties associated with the structure and parameters. However, GLDAS offers a physically consistent framework for understanding the large-scale patterns observed in satellite products.

These additional data sets helped to clarify the results in this thesis. They offer different views on soil moisture variability, while the main analyses still rely entirely on satellite observations.

2.5.5. Spatial comparison of soil moisture products

This section presents a qualitative global map comparison of the soil moisture data sets used in this thesis to highlight their spatial similarities and differences. This comparison provides a first visual assessment of how consistently large-scale patterns are represented across products and helps to identify differences in data coverage. Instead of evaluating the products quantitatively, the focus is on their spatial patterns. Two representative days, characterised by contrasting large-scale hydrological conditions, are selected to highlight seasonal differences.

Figures 2.6 and 2.7 show global SSM and RZSM maps derived from SMOS, SMAP, and ESA CCI products for two different points in time as volumetric soil moisture (from 0 to 0.6 $m^3 m^{-3}$). While absolute soil moisture levels vary regionally, all products consistently capture large-scale wet and dry regions, as well as persistently dry desert areas.

At the same time, data sets differ significantly. The L3 SSM products from SMOS and SMAP exhibit swath-like striping patterns related to the satellites' orbits and overpasses. These patterns are consistent across both figures. SMOS's ascending orbit, in which the satellite travels from south to north, produces east–west swaths. SMAP's descending orbit produces west-to-east swaths as the satellite moves from north to south. For the analyses

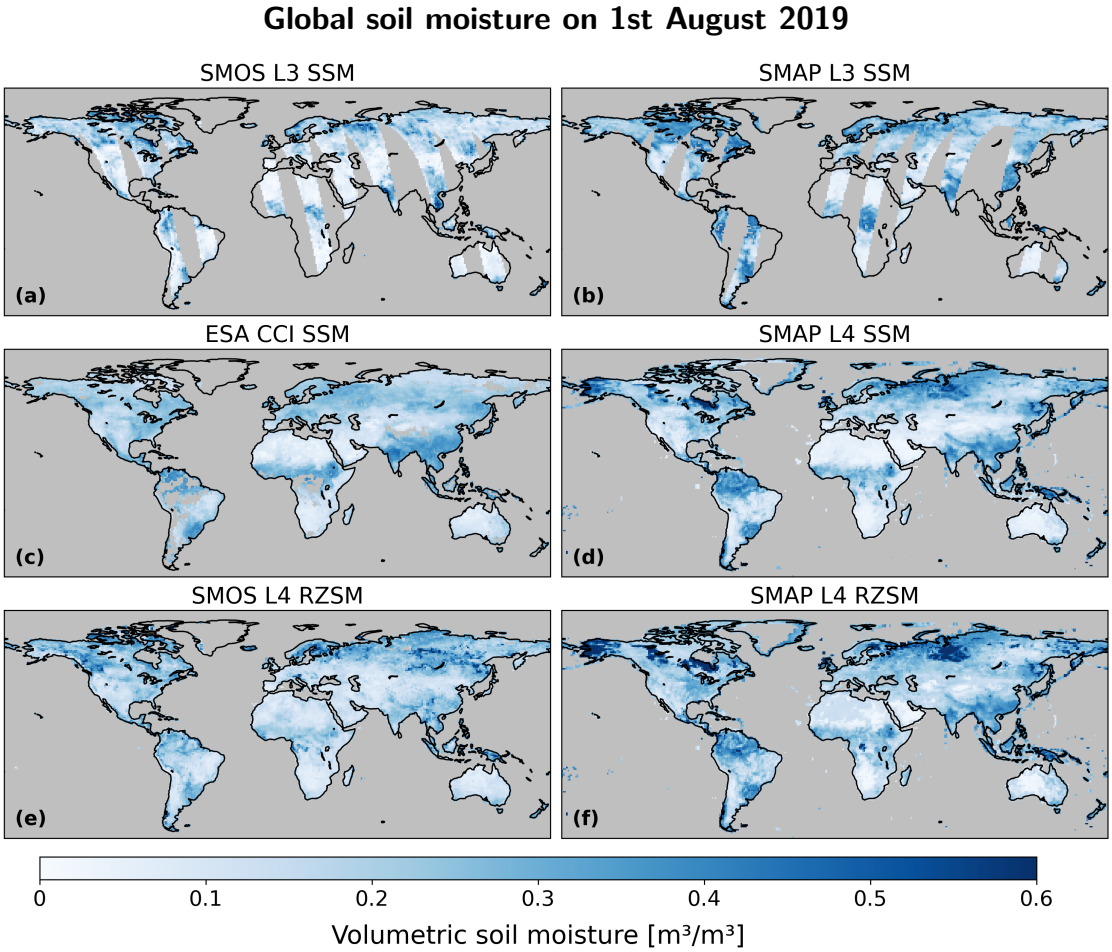

Figure 2.6.: Global soil moisture maps on 1st August 2019 for the soil moisture products used in this thesis. Panels (a–d) show SSM from SMOS L3, SMAP L3, ESA CCI, and SMAP L4. Panels (e–f) show RZSM from the SMOS and SMAP L4 products.

presented in this thesis, the SMOS descending orbit and the SMAP ascending orbit products are used (as shown in the figures), since both correspond to an early-morning overpass at approximately 06:00 local solar time. The alternative configurations, namely the SMOS ascending and SMAP descending orbits, represent evening overpasses around 18:00 local solar time.

The early-morning overpass is generally preferred for passive microwave soil moisture retrievals because thermal differences between the soil surface and the vegetation canopy are reduced during the nighttime and early-morning hours. In addition, temperature differences among land cover types within a pixel are typically smaller in the morning and at night. These conditions reduce thermal heterogeneity effects and lead to more reliable soil moisture estimates with lower retrieval uncertainty (Entekhabi et al., 2014; Lei et al., 2015).

In contrast, the ESA CCI product provides more spatially complete coverage, reflecting its multi-sensor merging approach that combines observations from multiple satellite

missions. Although global coverage is not entirely complete on a daily basis, data gaps have become increasingly rare in recent years. The remaining gaps are partly due to regions not observed daily by all contributing sensors. In addition, deliberately masked regions are visible, most notably over tropical rainforest areas in South America, Africa, and Southeast Asia. These regions are excluded because dense vegetation strongly attenuates the microwave signal, leading to unreliable soil moisture retrievals (see Section 2.2.2).

L4 products from SMAP have nearly complete continental coverage, which result from the data assimilation framework into an LSM. In contrast, the SMOS L4 product achieves improved coverage primarily through the temporal aggregation of multiple SMOS L3 observations.

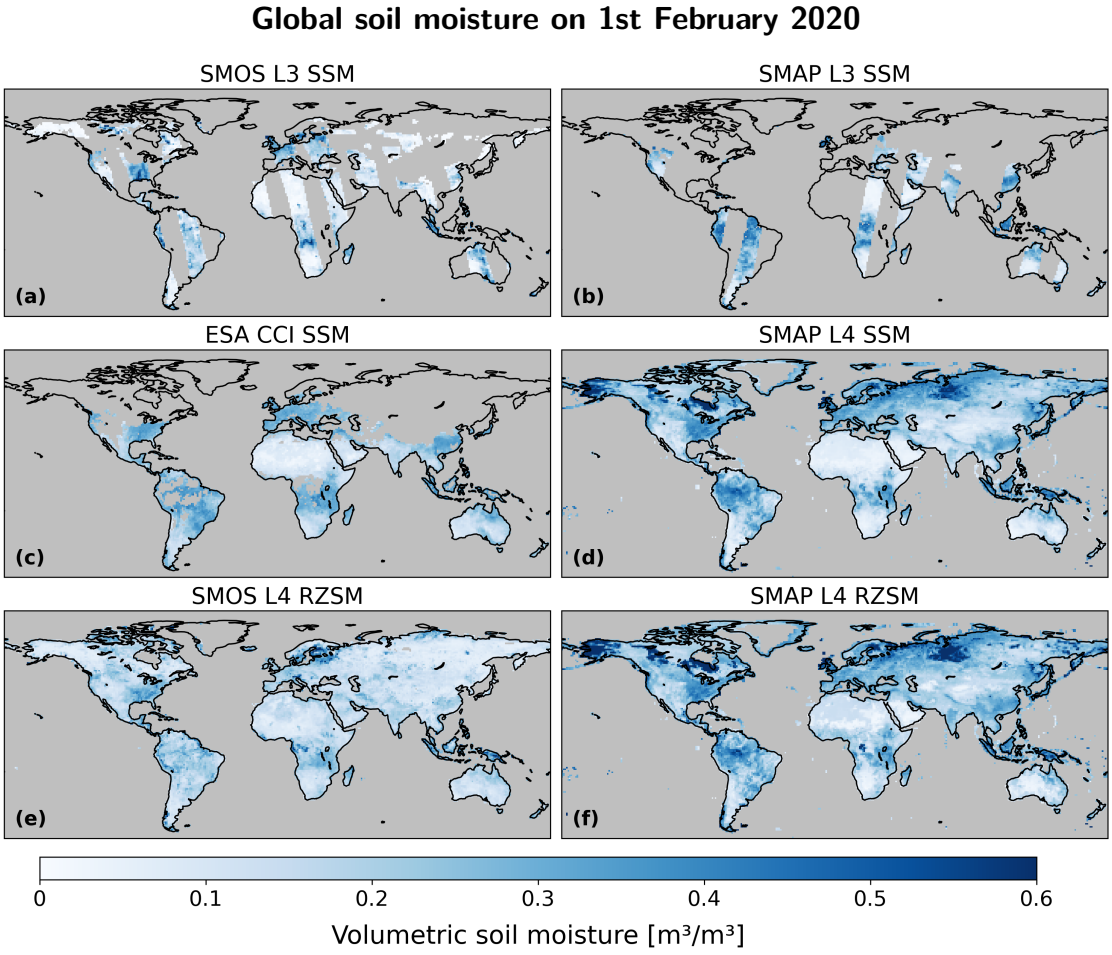

Figure 2.7.: Global soil moisture maps on 1st February 2020 for the soil moisture products used in this thesis. Panels (a–d) show SSM from SMOS L3, SMAP L3, ESA CCI, and SMAP L4. Panels (e–f) show RZSM from the SMOS and SMAP L4 products.

A comparison of the two figures, with particular focus on the maps from February 2020 in Fig. 2.7, reveals an increased occurrence of data gaps, especially in the Northern Hemisphere during cold-season conditions. These gaps are most pronounced in the ESA

CCI product and the L3 soil moisture products from SMOS and SMAP, whereas the L4 products retain a spatially complete coverage. The observed data gaps are primarily caused by frozen soil and snow cover, as discussed in Section 2.2.2.

In the ESA CCI product, grid cells affected by snow or frozen ground are excluded from the soil moisture estimates (see Section 2.5.3). In contrast, the SMOS and SMAP L3 products still contain soil moisture values in some of these regions because their respective retrieval algorithms do not apply masking. As a result, soil moisture estimates in these areas may be associated with increased uncertainty and should be interpreted with caution.

Beyond these qualitative differences, the soil moisture products also differ in their temporal variability. These aspects may influence the quantitative comparability of the products and their relationship to TWS. It can therefore be expected that differences in retrieval algorithms, vertical representativeness, spatial coverage, and post-processing will affect the strength of correlations with GRACE-based TWS signals, and this is primarily the topic of Paper 1.

3. Terrestrial Water Storage

Gravity-based observation of TWS provides the second observational basis for this thesis. This chapter introduces the definition of TWS and its relation to the terrestrial water balance. Furthermore, it describes satellite gravimetry as the primary observing system for global TWS variations and outlines how TWS is derived from GRACE and GRACE-FO observations.

3.1. Definition and role in the Earth system

TWS includes all water components located on and beneath the Earth's surface, including soil moisture, groundwater, surface water, and water stored in snow and ice (Syed et al., 2008). Since 2022, TWS has been listed as a new ECV (World Meteorological Organization, 2022). According to Shiklomanov (1993), approximately 97.5% of the Earth's total water resources are saline water, mostly found in the oceans. Only about 2.5% of freshwater resources are important for terrestrial hydrology and water supply. Nearly 99% of this freshwater is stored in ice masses and groundwater, while only about 0.05% is found in soil moisture.

Soil moisture, although a small part of total freshwater storage, is important for driving temporal variations in TWS (Güntner et al., 2007), as it exhibits much stronger variability on short timescales than deeper or frozen water storage components. Groundwater and frozen water stores can retain water over very long periods, often from hundreds to thousands of years. Soil moisture, in contrast, is renewed much more quickly, typically within about two weeks to one year (UNEP, 2002). As a result, soil moisture is a dominant contributor to short-term and seasonal changes in TWS, even though it makes up only a small part of the overall storage volume (Abelen, 2016).

Changes in TWS can be described by the terrestrial water balance. In its simplified form, the storage change results from the difference between the incoming water from precipitation P and outgoing water through evapotranspiration E and runoff R:

$$\frac{\partial \mathrm{TWS}}{\partial \mathrm{t}} = P - E - R. \tag{3.1}$$

From a storage perspective, the same TWS change represents the combined response of the individual water compartments:

$$\Delta\text{TWS} = \Delta\text{SM} + \Delta\text{GW} + \Delta\text{SW} + \Delta\text{SWE} + \Delta\text{GL}. \tag{3.2}$$

Here, ΔSM denotes changes in soil moisture, ΔGW changes in groundwater storage, ΔSW changes in surface water storage (e.g., lakes and rivers), ΔSWE changes in snow water equivalent, and ΔGL changes in glacier storage. Consequently, ΔTWS provides an integrated view of water storage changes across the entire water column.

The storage components that dominate TWS changes differ between regions and timescales. In regions with limited recharge, groundwater often shows only slow natural variations, but much larger changes can occur where irrigation or depletion affect the storage system (Rodell et al., 2018). The dominant contributors to TWS therefore depend on regional hydrological conditions and land use. Moreover, the relative importance of individual storage components varies with temporal scale and is heavily influenced by seasonal processes in many regions (Girotto and Rodell, 2019).

3.2. Observing TWS

For a long time, the lack of spatially consistent observations has limited the direct monitoring of TWS at regional to global scales. While changes in TWS can be observed from in-situ gravimetric measurements, such observations are sparse, making them unsuitable for mapping TWS variations at global scales (Crossley et al., 2012). Alternatively, TWS can be estimated by adding up the individual storage components. At the global scale, in-situ measurements do not provide continuous coverage of all major water storage components, especially groundwater (Seneviratne et al., 2004; Famiglietti et al., 2015; Abelen, 2016).

Remote sensing products provide valuable information on individual water storage components, such as soil moisture, snow, or surface water. However, they generally do not capture the entire water column and, for example, soil moisture observations are limited in their effective sensing depth (see Sec. 2.2.2). In addition, data quality varies from region to region. These heterogeneities lead to uncertainties when trying to reconstruct TWS from individual components, and the lack of direct groundwater observations is a major limitation. As a result, large-scale assessments of TWS mainly depend on hydrological models, as discussed in Section 2.3, and on satellite gravimetry.

3.2.1. Satellite gravimetry

Satellite gravimetry observes the Earth's gravity field from space and detects how it changes over time. These changes occur when mass is redistributed within the Earth system. They can be caused by processes inside the Earth, by changes in ocean mass, or by variations in water storage on land (Rummel, 2004).

The notation used in the following equations follows Springer (2019). Determining the Earth's gravitational potential V is the main goal of satellite gravimetry. In the exterior of the Earth, the gravitational potential fulfils Laplace's equation $\Delta V = 0$. It can therefore be expressed as an infinite sum of spherical harmonic functions (Heiskanen and Moritz, 1967):

$$V(\lambda, \theta, r) = \frac{GM}{R} \sum_{n=0}^{\infty} \left(\frac{R}{r}\right)^{n+1} \sum_{m=-n}^{n} c_{nm} \Upsilon_{nm}(\lambda, \theta). \tag{3.3}$$

Here, r, θ, λ denote the spherical polar coordinates, with r representing the distance of the satellite from the Earth's centre. G is the gravitational constant, M is the Earth's mass, and R is the Earth's radius. The coefficients c_{nm} are the Stokes coefficients, and $\Upsilon_{nm}(\lambda, \theta)$ are the surface spherical harmonic functions defined as:

$$\Upsilon(\lambda, \theta) = P_{n|m|}(\cos\theta) \begin{cases} \cos|m|\,\lambda & \text{for } m \geq 0 \\ \sin|m|\,\lambda & \text{for } m < 0 \end{cases} \tag{3.4}$$

Here, $P_{n|m|}$ denotes the fully normalised Legendre function of degree n and order $|m|$.

Higher spherical harmonic degrees describe smaller spatial features of the gravity field. In practice, however, the maximum degree that can be resolved is limited by the accuracy of the satellite observations. The term $(R/r)^{n+1}$ describes the upward attenuation of the gravity signal. It is equal to one at the Earth's surface and decreases with increasing satellite altitude. As a result, gravity signals are progressively smoothed in satellite observations (Barthelmes, 2013).

Variations in gravitational potential are caused by the redistribution of mass within the Earth system. However, deriving the underlying mass redistribution from observed gravity changes represents a non-unique inverse problem, since different mass distributions can produce the same gravitational potential. This ambiguity is commonly reduced by assuming that mass changes are concentrated in a thin layer at the Earth's surface. Under this assumption, the mass redistribution is described by surface density changes $\Delta\kappa(\lambda, \theta)$. These are defined by Wahr et al. (1998) as the radial integral of density variations within this layer. The surface density changes can then be linked to changes in gravitational potential through a spherical harmonic expansion using the Stokes coefficient changes

Δc_{nm} by:

$$\Delta\kappa(\theta,\lambda) = \frac{M}{4\pi R^2}\sum_{n=0}^{\infty}\sum_{m=-n}^{n}\left(\frac{2n+1}{1+k'_n}\right)\Delta c_{nm}\,\Upsilon_{nm}(\lambda,\theta). \tag{3.5}$$

Surface mass redistribution leads to the elastic deformation of the solid Earth due to the effects of loading, which results in additional secondary gravity changes. These effects are accounted for using the Load Love numbers k'_n (Farrell, 1972; Lambeck, 1988). By dividing gravity-derived surface density changes by the density of water $\rho_w = 1000\frac{kg}{m^3}$, it is possible to obtain TWS variations expressed as equivalent water heights (EWH) (Wahr et al., 1998):

$$EWH(\lambda,\theta) = \frac{M}{4\pi R^2\rho_w}\sum_{n=0}^{\infty}\sum_{m=-n}^{n}\left(\frac{2n+1}{1+k'_n}\right)\Delta c_{nm}\,\Upsilon_{nm}(\lambda,\theta). \tag{3.6}$$

TWS estimates from satellite gravimetry rely on the fact that gravity variations over land are largely driven by changes in terrestrial water mass (Ramillien et al., 2008). To isolate the hydrological signal, gravity contributions from non-hydrological sources must be removed, including effects from ocean tides and atmospheric mass variability (Dobslaw et al., 2017). Among these non-hydrological influences are solid Earth processes such as glacial isostatic adjustment (GIA; Steffen et al., 2009; A et al., 2013), which refers to the ongoing vertical land motion caused by the melting of large ice masses since the last glacial period. In addition, major earthquakes can also induce detectable gravity changes that must be considered in the analysis (Rummel, 2004). Satellite gravimetry provides observations of TWS as relative changes to a reference state and not as absolute storage values. Gravity observations alone are unable to distinguish between mass changes of individual hydrological components without additional data (Abelen, 2016).

Two main techniques are used to observe the Earth's gravity field with satellites: Satellite-to-Satellite Tracking (SST) and Satellite Gravity Gradiometry (SGG), and are described in detail by Rummel et al. (2002) and Xu et al. (2007). SST exploits orbit disturbances caused by mass anomalies and is applied to low Earth orbit (LEO) satellites. It can be implemented as high–low SST (SST-hl), where satellite orbits are tracked using GPS observations combined with onboard accelerometer measurements, or as low–low SST (SST-ll), where the relative distance between two satellites flying in the same orbit is observed with high precision.

In the SST-ll configuration, mass anomalies cause changes in the inter-satellite distance when the leading and trailing satellites sequentially pass over the anomaly, allowing the gravity field to be inferred from these distance variations. The SST-hl and SST-ll configurations can be used together. In SST-hl, the position and velocity

of the satellite are determined through continuous tracking by GPS satellites. These measurements then enable an accurate determination of the satellite's orbit. Additionally, a three-dimensional accelerometer is placed onboard, which enables the measurement of non-gravitational forces.

SGG measures gravity field gradients directly with pairs of highly sensitive accelerometers mounted on orthogonal axes close to the satellite's centre of mass. By comparing the accelerations recorded by each sensor pair, non-gravitational forces are largely eliminated. As such, it is possible to isolate the gravity-induced signals (Seeber, 2003).

Among recent satellite gravimetry missions, the Challenging Minisatellite Payload (CHAMP) mission measured the gravity field of the Earth from 2000 to 2010 using SST-hl. The GRACE mission employed SST-ll with two twin satellites operating from 2002 to 2017, followed by its successor GRACE-FO, which was launched in May 2018 and is still operational. The Gravity Field and Steady-State Ocean Circulation Explorer (GOCE) mission measured the gravity field using SGG between 2009 and 2013. While CHAMP and GOCE primarily target the static components of the Earth's gravity field, GRACE and GRACE-FO are specifically designed to detect temporal gravity variations and are therefore suitable for observing TWS variations.

3.2.2. TWS from GRACE and GRACE-FO

The GRACE mission (Tapley et al., 2004) was a joint satellite mission between NASA and the German Aerospace Center (DLR), launched in March 2002 and operated until June 2017 to observe temporal gravity changes. These observations are being continued by GRACE-FO (Landerer et al., 2020), launched in May 2018 and jointly operated by NASA and the German Research Centre for Geosciences (GFZ). Together, the two missions provide a long-term record of temporal variations in the Earth's gravity field, with the primary objective of monitoring mass redistribution processes within the Earth system.

Both missions are based on the SST concept, in which two nearly identical satellites fly in the same LEO at an initial altitude of approximately 500 km, separated by a distance of about 220–250 km. The distance between the two satellites is continuously measured with high accuracy using a K-band microwave ranging system, achieving relative accuracies on the order of 10^{-12}. Spatial and temporal variations in gravity slightly change the distance between the two satellites. When the satellite pair moves towards a region of increased mass, the leading satellite experiences the stronger gravitational attraction first. This difference in acceleration temporarily increases the separation between the two satellites. These distance differences are measured as range-rate measurements and relate directly to gravity anomalies.

By observing these gravity anomalies frequently over the span of a month, GRACE

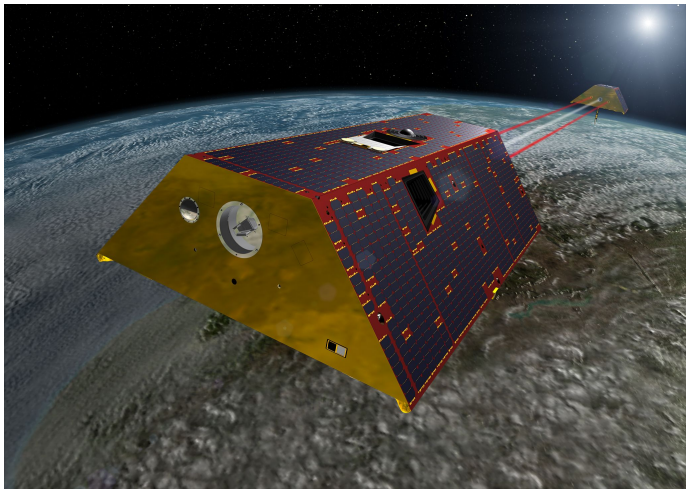

Figure 3.1.: Illustration of the GRACE-FO satellites in space. Image credit: NASA / JPL-Caltech

and GRACE-FO observations make it possible to estimate temporal mass changes that are related to changes in water storage. Standard gravity field solutions are typically derived from about 30 days of data and therefore have a spatial resolution of a few hundred kilometres. In contrast to GRACE, GRACE-FO also carries a laser ranging interferometer (LRI), which improves ranging accuracy between the two satellites compared to the microwave system alone (Abich et al., 2019). To ensure accurate gravity field recovery, each satellite carries a three-axis accelerometer that measures non-gravitational forces such as atmospheric drag and solar radiation pressure. Additionally, star cameras are used to determine satellite attitude, while GNSS receivers provide precise observations of the satellites' orbits.

GRACE and GRACE-FO detect temporal gravity variations that primarily reflect large-scale mass redistribution processes. These variations are dominated by changes in TWS on the continents, but other contributions arise from ocean dynamics, atmospheric mass transport, ice mass changes, and solid Earth processes such as GIA and seismic events. The combined GRACE and GRACE-FO record provides direct observations of global mass gain and loss and offers a unique look at large-scale water storage changes. It has become a vital resource for hydrological and climate research (Tapley et al., 2019). The hydrological relevance of the GRACE and GRACE-FO data sets was already discussed in Section 1.2.

3.2.3. Data processing from GRACE and GRACE-FO

Gravity field solutions are computed from the GRACE and GRACE-FO intersatellite ranging observations (Level 1B) by several analysis centres, including the GFZ, the Center for Space Research at the University of Texas (CSR), and the Jet Propulsion

Laboratory (JPL). In addition, other scientific institutes, such as the Institute of Geodesy at Graz University of Technology (ITSG), provide pre-processed GRACE data. Combined products based on solutions from multiple analysis centres are further distributed by the Combination Service for Time-variable Gravity Fields (COST-G).

GRACE gravity fields are traditionally estimated as monthly averaged spherical harmonic coefficients of the gravitational potential. These monthly coefficient sets are commonly referred to as GRACE L2 products. To avoid temporal aliasing, faster sub-monthly mass variations are approximated by geophysical background models and removed during processing. These de-aliasing corrections consider astronomical tides and both tidal and non-tidal mass variations in the atmosphere and oceans (Dobslaw et al., 2017; Kvas et al., 2019).

In contrast to these classical monthly L2 products, this thesis makes use of daily GRACE and GRACE-FO gravity field solutions provided by ITSG-Grace2018 (Kvas et al., 2019), which represent the current processing version. The daily solutions are specifically designed to resolve sub-monthly mass variability and are therefore particularly useful for evaluating short-term TWS changes.

Kalman smoothing is used in the processing of the daily solutions since GRACE does not collect enough data within a day to fully estimate independent daily gravity field solutions. This method follows an approach similar to that described by Kurtenbach et al. (2012). The Kalman smoother incorporates information about the expected temporal variation of the gravity field through a stochastic process model derived from geophysical background information. Importantly, only the stochastic behaviour of the model is used rather than the exact model values themselves. As a consequence, the resulting daily gravity field solutions are temporally correlated and should not be interpreted as independent daily estimates. As for monthly products, de-aliasing corrections are applied so that the daily GRACE signal primarily contains hydrological, cryospheric, and glacial isostatic adjustment (GIA) signals. The daily gravity field solutions are provided as L2 spherical harmonic coefficients of the gravitational potential up to degree $n = 40$, corresponding to an effective spatial resolution of approximately 500 km.

Before surface mass changes can be derived, the GRACE gravity fields require several standard corrections. Degree-1 spherical harmonic coefficients are added to account for geocenter motion, using estimates from Sun et al. (2016) based on the approach of Swenson et al. (2008a). The c_{20} coefficient is then replaced by satellite laser ranging data (Cheng and Ries, 2017), and lastly the influence of glacial isostatic adjustment is removed using the ICE6G-D model of Peltier et al. (2018).

Standard monthly GRACE gravity field solutions typically require spatial filtering. Satellite observations from 400–500 km heights amplify small-scale noise during downward

continuation. Additionally, undersampling of short-term changes in atmospheric and oceanic mass leads to temporal aliasing in monthly solutions. Due to the orbital geometry and the along-track distance measurement principle, noticeable north-south striping is visible in the data. Spatial filtering is therefore applied to suppress correlated noise and extract the geophysical signal. For the daily data, no further spatial filtering is applied, as the Kalman smoothing approach used for the daily ITSG-Grace2018 solutions already effectively reduces spatially correlated noise during the estimation process. After these steps, the resulting gravity field solutions are assumed to primarily reflect water mass changes on the continents and are converted into EWH on a global grid.

4. Research Objectives

This chapter introduces the research questions that guide this thesis. Section 4.1 presents the overarching questions concerning the general potential and methodological framework for comparing GRACE-based TWS with soil moisture. More detailed questions are stated in Sections 4.2, 4.3, and 4.4, each corresponding to the focus and research questions of the three individual papers included in this cumulative thesis.

The three parts of this thesis build upon each other conceptually. Paper 1 establishes the statistical relationship between soil moisture and TWS across depths and timescales. Paper 2 extends this relationship to the dynamic behaviour of water storage deficits and their depth-dependent propagation as a process-based analysis. Paper 3 uses GRACE-based TWS data as a constraint to obtain subsurface storage dynamics with the help of vertically extrapolating SSM.

4.1. Comparability of remotely sensed soil moisture and GRACE/GRACE-FO TWS observations

In Chapter 2, particularly in Section 2.2.2, the limitations of remotely sensed soil moisture observations are discussed. Limitations also apply to the observation of TWS by GRACE. Moreover, the two quantities are not directly comparable, which requires an appropriate methodological framework to relate and quantify them consistently. In addition, a spatial mismatch exists between the two observation types that must be addressed in the analysis. Since multiple remotely sensed soil moisture data sets are used in this thesis, their quantitative differences (see Section 2.5.5 for qualitative differences) in spatial and temporal characteristics are also investigated. This includes assessing how these differences affect their comparability with GRACE-based TWS. Figure 4.1 provides an overview of the analysis framework adopted in this thesis, illustrating the integration of soil moisture observations and GRACE-based TWS, as well as the main challenges associated with their joint analysis. These overarching questions are also addressed collectively and appear throughout the three papers of this dissertation.

1. What can the combined analysis of soil moisture and GRACE TWS reveal about

subsurface storage dynamics?

2. How do differences in spatial, temporal and depth characteristics of satellite soil moisture products influence their comparability with GRACE-based TWS?

3. Which methods enable a consistent and harmonised comparison between satellite soil moisture and GRACE-based TWS?

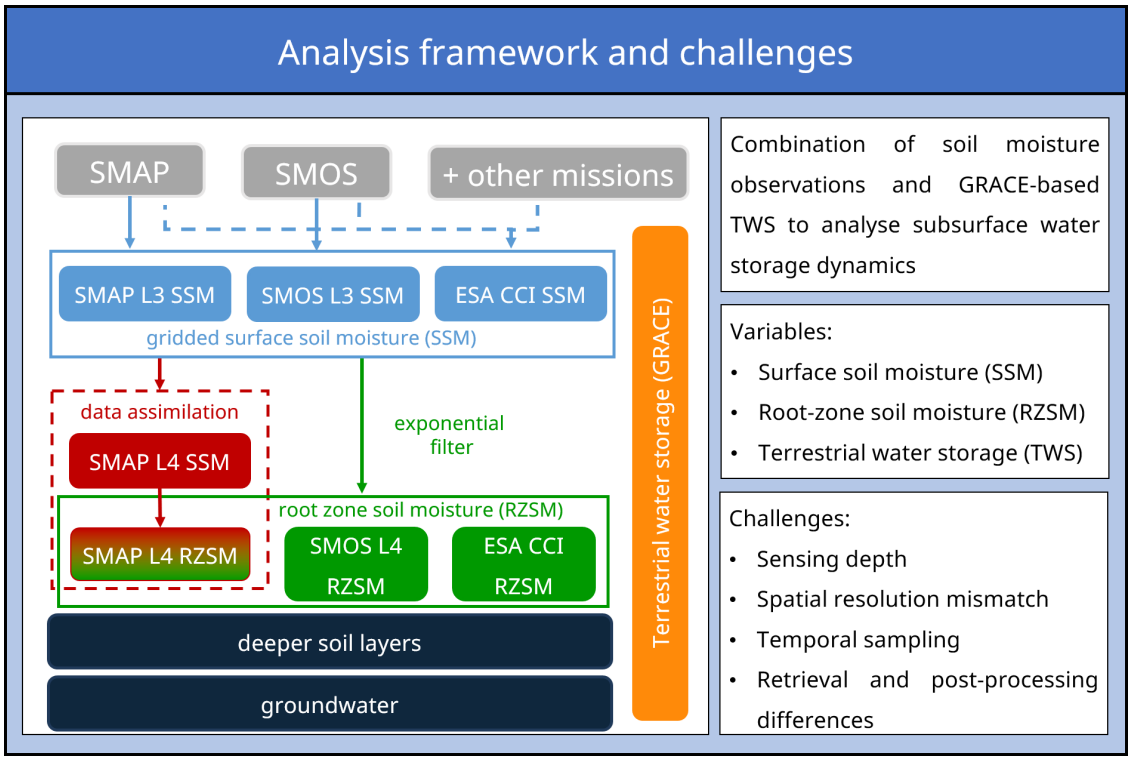

Figure 4.1.: Schematic illustration of the analysis framework used in this thesis, showing the integration of satellite-based soil moisture observations and GRACE-derived TWS. The main challenges are summarised on the right-hand side.

4.2. Relationship between soil moisture and GRACE-based TWS

The relationship between soil moisture and TWS is analysed in this section, which is also the main focus of Paper 1. The goal is to identify connections between the two variables in various regions and at different timescales. Figure 4.2 shows the conceptual difference in depth representativeness between satellite-based soil moisture and TWS. This difference represents a major challenge for their direct comparison. Correlation and cross-correlation analyses are performed to quantify the strength of agreement and to identify temporal shifts between soil moisture and TWS. In addition, the sub-monthly signal component is

derived to assess whether daily GRACE solutions capture high-frequency TWS variability associated with soil moisture dynamics. The following research questions are addressed, particularly in the context of Paper 1:

1. How well does the temporal variability of soil moisture (SSM and RZSM) agree with GRACE-based TWS?
2. How do temporal shifts between soil moisture and TWS vary with integration depth, and what do they reveal about subsurface water redistribution?
3. Can daily GRACE data detect high-frequency variations in soil moisture and are the observed variations statistically significant?

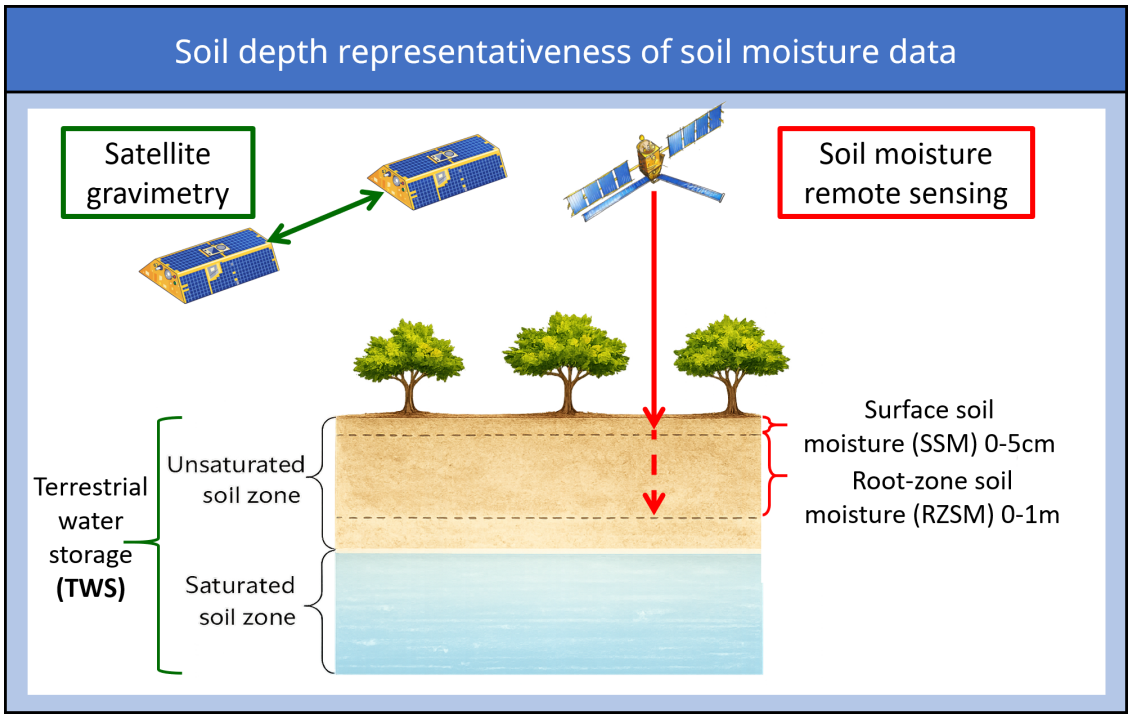

Figure 4.2.: Schematic illustration of the depth representativeness in the soil of satellite-based soil moisture observations compared to GRACE-based TWS. The figure was created by the author using AI tools (OpenAI, 2026). The illustration of the unsaturated and saturated soil zones is inspired by Seneviratne et al. (2010), and satellite pictures are based on publicly available images from NASA (GRACE) and ESA (SMOS).

4.3. Propagation of water storage deficits in the subsurface

This section focuses on how subsurface water storage behaves during deficits and how drought signals persist with increasing storage depth, and is mainly part of Paper 2. The

drought cascade concept of Changnon (1987) suggests that drought signals become delayed, damped, and more persistent with depth. Figure 4.3 illustrates this concept by linking deficits in precipitation to responses in soil moisture, streamflow, and groundwater. In addition, the cascade describes the progression from meteorological drought to agricultural and eventually hydrological drought. In this study, this concept is revisited with a focus on subsurface storage using satellite observations. While the previous section focused on total and sub-monthly signal components, this section instead analyses the de-seasonalised (seasonal residual) signal. The term *drought* is typically defined relative to a long-term climatology of at least 30 years. However, as this study is based on a shorter period of approximately 7 years, the term *water storage deficit* is used to describe negative anomalies in water storage. The following research questions are addressed in the context of Paper 2:

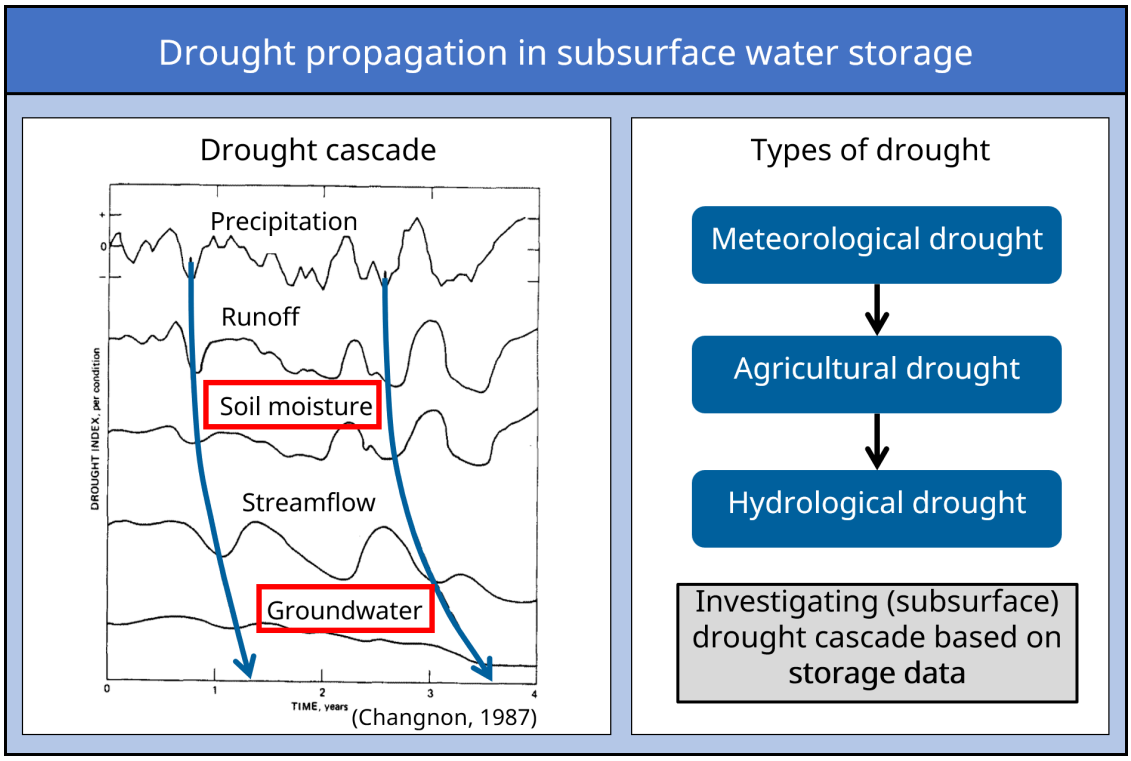

Figure 4.3.: Schematic illustration of drought propagation across the terrestrial water cycle. The left panel shows the conceptual drought cascade adapted from Changnon (1987) with a focus on the variables outlined in red. The right panel summarises different types of drought and highlights the focus of this study on subsurface drought dynamics based on water storage compartments.

1. How do de-seasonalised water storage deficits propagate across increasing integration depth, from SSM to integrated TWS?
2. How can drought propagation be quantified beyond conventional event-based comparisons of drought onset and end?

3. How do drying and recovery rates of subsurface water storage deficits vary across different regions?

4.4. Using GRACE as a constraint to derive subsurface storage dynamics from satellite soil moisture

This section focuses on a methodological approach to derive subsurface storage dynamics from SSM observations. It builds on the concept of the exponential filter for the vertical extrapolation of SSM. The main objective is to investigate whether GRACE-based TWS can be used as an independent, spatially varying global constraint to optimise the T parameter of this filter, which is commonly assumed to be uniform or calibrated using in-situ observations. In addition, it is analysed whether the optimised T parameters show physically interpretable spatial patterns. The framework of this approach is illustrated in Figure 4.4, where SSM and multiple RZSM input layers are linked to depth-integrated TWS using the exponential filter. The role of the T parameter is also shown, as it controls the smoothing and temporal delay of the signal. The main research questions addressed in this part of the thesis and in the context of Paper 3 are:

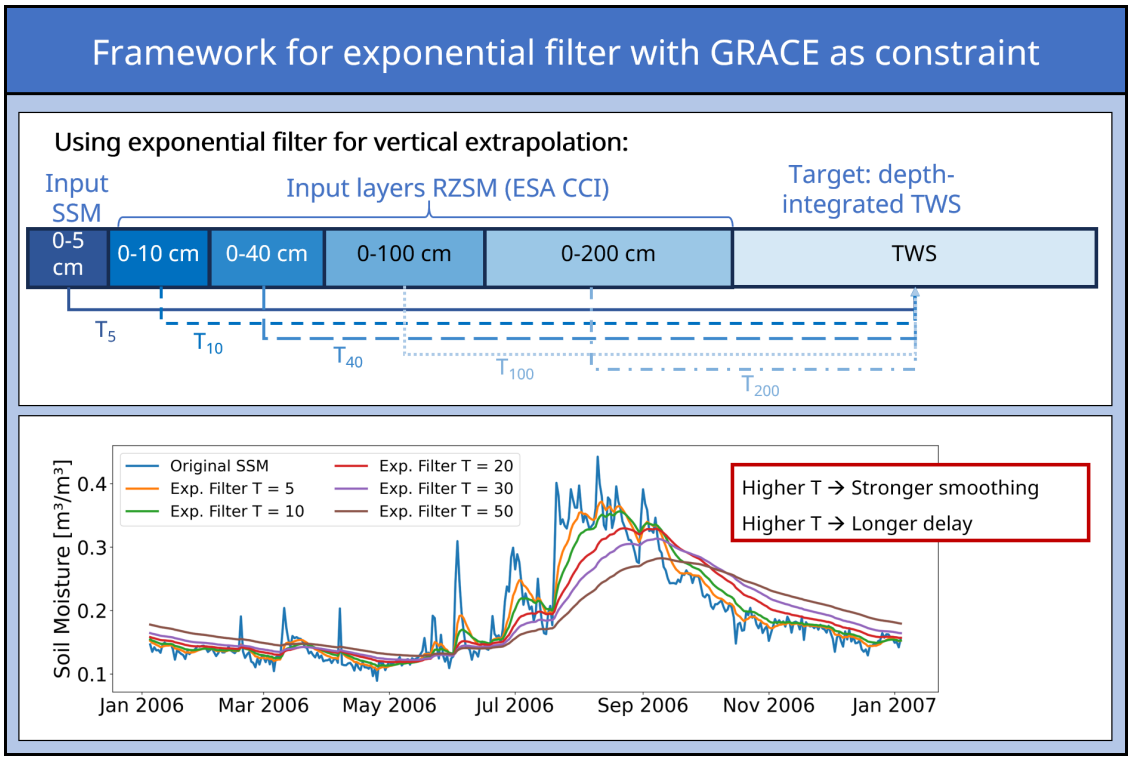

Figure 4.4.: Schematic illustration of the exponential filtering framework used in this thesis. The upper panel shows the conceptual setup, and the lower panel illustrates the effect of different filter time constants T on the temporal dynamics of soil moisture.

1. Can daily GRACE TWS be used as a constraint to estimate sub-seasonal subsurface storage variability from satellite SSM?
2. Does spatial calibration outperform a uniform exponential filter parametrisation?
3. What is the benefit of regionally adapted GRACE-optimised filter time constants for interpreting underlying controls on subsurface storage dynamics?
4. How does the optimised T-value vary across soil moisture products with different soil depths?

5. Results and Conclusion

This chapter revisits and addresses the research questions formulated in Chapter 4. For consistency, the questions are answered in the same order in which they were introduced in the previous chapter and are numbered from Q1 to Q13. The aim is to summarise the key results and highlight their broader scientific implications, while referring to the detailed methodology and analyses presented in the three peer-reviewed papers, which are reprinted in Appendix A. It is important to understand the characteristics of the data sets used in this thesis before addressing the main research questions. This thesis focuses on an observation-driven framework and is limited to satellite-based data sets. Extending the model-based data sets would be possible, but it would be beyond the scope of the present work.

5.1. Comparability of remotely sensed soil moisture and GRACE/GRACE-FO TWS observations

Q1: What can the combined analysis of soil moisture and GRACE TWS reveal about subsurface storage dynamics?

The combined analysis of satellite soil moisture products and daily GRACE-based TWS provides an observation-driven basis for studying subsurface storage dynamics. Soil moisture observations represent different parts of the upper soil column, whereas GRACE observes vertically integrated changes in TWS. Comparing both data types therefore makes it possible to investigate how storage signals change from the near surface towards deeper and more integrated storage compartments.

Vertical propagation of storage signals:
The joint analysis can be used to investigate how water storage signals change with depth. Since soil moisture represents shallow layers and GRACE integrates the full water column, differences in variability between both data sets make it possible to infer how signals are damped and delayed as they propagate into deeper storage compartments.

Time lags and vertical redistribution:
This approach enables the quantification of time lags between shallow and deeper storage. Such time shifts can be interpreted as indicators of infiltration and vertical redistribution processes. By comparing soil moisture products with different sensing depths, it is possible to assess how closely they represent depth-integrated storage dynamics.

Evaluation and depth representativeness of soil moisture products:
The combined analysis helps to compare how well different soil moisture products represent storage changes below the surface. Products that agree more closely with GRACE-based TWS are likely more sensitive to deeper storage dynamics. This makes it possible to distinguish products that mainly reflect near-surface variability from those that are more consistent with the integrated storage changes observed by GRACE. Deviations between soil moisture and GRACE-based TWS can also indicate storage contributions below the commonly represented soil depths.

Storage variability across temporal scales:
The use of daily GRACE data allows the comparison to be carried out not only at seasonal timescales, but also at shorter timescales of days to weeks. This makes it possible to analyse whether short-term soil moisture variations are reflected in TWS, or whether they remain mainly confined to the near-surface soil layer.

Observational basis for further analyses:
The combined analysis offers an observational basis for interpreting subsurface storage dynamics. This supports the following analyses of drought propagation, recovery behaviour, and GRACE-constrained estimation of subsurface storage dynamics. It also allows regional differences in storage timing and variability to be related to possible physical controls, such as climate or soil properties.

In summary, analysing soil moisture alongside GRACE-based TWS reveals important insights into how storage signals change with depth, how they experience delays and damping over time, and how consistently different soil moisture products represent deeper storage dynamics. Thus, it provides the observational basis for the analysis of depth-dependent subsurface water storage dynamics for the following research questions.

Q2: How do differences in spatial, temporal, and depth characteristics of satellite soil moisture products influence their comparability with GRACE-based TWS?

The soil moisture products analysed in this thesis reveal distinct differences between them in terms of spatial and temporal characteristics, as well as regarding their effective sensing depth. The differences arise because these satellite soil moisture products are produced and processed differently in their retrieval methodologies and may also be post-processed, for example, by integrating multiple sensors or assimilating model data into the final product.

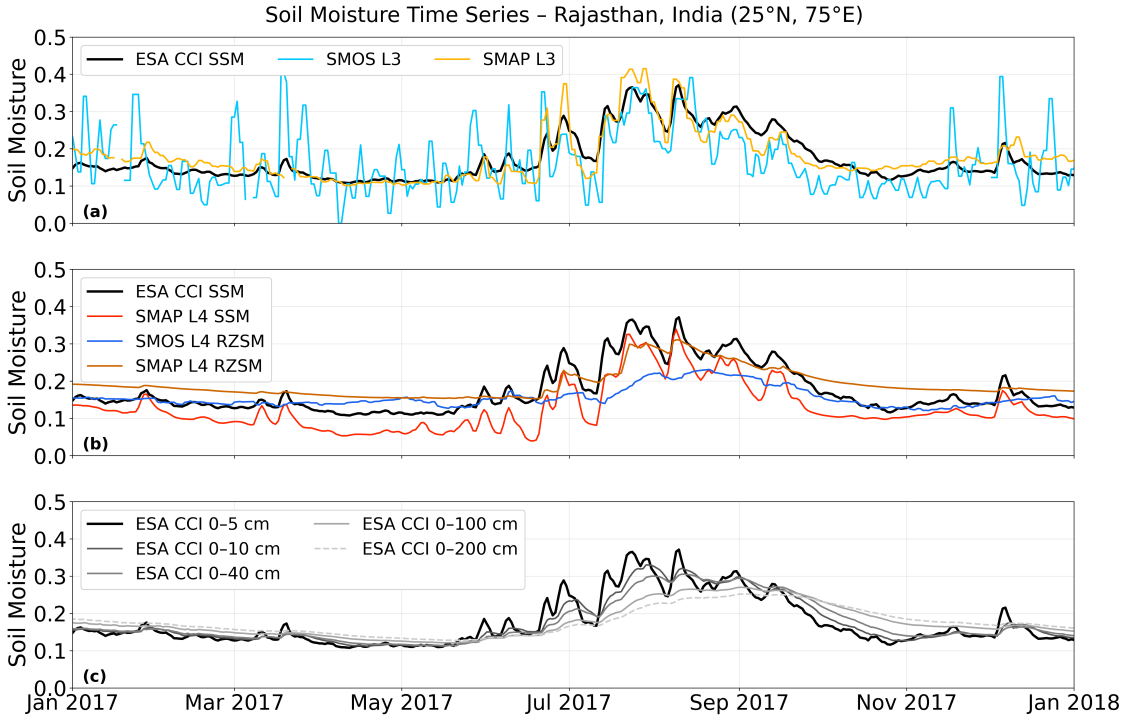

Figure 5.1.: Time series of satellite soil moisture products in Rajasthan, India (25°N, 75°E). (a) shows SSM from SMOS L3, SMAP L3 and ESA CCI. (b) shows L4 products for SSM and RZSM. (c) shows ESA CCI soil moisture profiles across increasing depths. In all panels, ESA CCI SSM is shown in black as a reference. All time series are smoothed using a 3-day moving average for improved visualisation. Soil moisture is expressed as volumetric water content (m^3/m^3)

Figure 5.1 visualises all soil moisture data products used in this thesis for an exemplary 1-year time series, highlighting the temporal characteristics of the different data sets and what can generally be expected from them. ESA CCI SSM is shown in black as a reference throughout the figure. Panel (a) additionally shows the SSM products from SMOS L3 and SMAP L3. Higher variability is observed in the SMOS L3 signal, while the overall signal behaviour remains similar to the other two products. This is also consistent with previous studies reporting higher noise levels in SMOS L3 (Montzka et al., 2017; Cui et al., 2017; Xu and Frey, 2021). In Panel (b), the signals from ESA CCI and SMAP L4 SSM show a comparable variability. However, during the dry months, especially from October onwards, the SMAP L4 SSM appears smoother than the ESA CCI, likely

because model assimilation suppresses observational noise. Both RZSM time series from SMOS and SMAP L4 are even more smoothed and delayed compared to the SSM signal, reflecting their larger integration depth and associated slower dynamics. Lastly, Panel (c) shows the ESA CCI data set across all depth layers from 0–5 cm to 0–200 cm. It is clearly visible that with increasing depth integration, the signal becomes progressively smoother and more delayed.

When we compare depth representations, SSM products typically represent the top few centimetres of soil, whereas RZSM products provide a deeper representation of water storage due to either an exponential filter or model-based extrapolation. This vertical integration results in smoother temporal behaviour compared to SSM data, since it represents a deeper soil zone and variations are slower compared to the surface layer. Because TWS has an integrated water column, which includes deeper unsaturated and groundwater storage, products like RZSM, which show deeper soil representation, should generally match TWS better. Therefore, the difference in the depth sampled by SSM retrievals and TWS is a major limitation for directly comparing these two types of observations. However, this difference also provides an opportunity to extract physical insights from their contrasting dynamics and is further explored in the following research questions.

As shown in Figures 2.6 and 2.7, L3 products exhibit sampling patterns unique to their orbital swath, as well as regional limitations due to gaps in data coverage, especially for grid cells affected by snow or frozen soil. In contrast, L4 and multi-satellite products result in more continuous grids through assimilation frameworks, merging algorithms, or temporal aggregation. However, the increase in spatial continuity is coupled with a much greater dependence on modelled or auxiliary data. The structural differences in spatial continuity will affect the comparison with GRACE-based TWS, which has a significantly coarser spatial resolution and represents spatially averaged mass variations.

Observational limitations further influence product comparability and are presented side by side in Table 5.1 (limitations are mentioned as well in Chapters 2 and 3). For example, the quality of soil moisture retrieval decreases under dense vegetation or when affected by RFI. Snow cover, frozen soil conditions, and surface water can lead to spatial masking or increased retrieval uncertainty. In contrast, GRACE is not directly affected by these conditions, but it cannot distinguish between different storage compartments when multiple components contribute to the signal. Furthermore, GRACE-based TWS observations are affected by signal leakage, as they represent spatially averaged gravity changes over larger areas. This can lead to signal mixing, where, for example, ocean mass changes can leak into coastal land areas or vice versa. This effect does not affect passive radiometer-based soil moisture retrievals. Very dry regions introduce further

challenges that affect both measurement approaches. As this study mainly focuses on water storage changes, the signal variability is often very low under such conditions, and the observed signals are therefore often dominated by noise in both data sets. Overall, these observational limitations affect both data types individually and need to be considered when analysing how well soil moisture and TWS agree across different regions.

Table 5.1.: Overview of observational constraints affecting satellite soil moisture and GRACE-based TWS observations.

Constraint	**Satellite soil moisture**	**GRACE-based TWS**
Dry regions	Low variability leading to weak signals and low SNR	Low variability leading to weak signals and low SNR
Snow and frozen soil	Retrieval not possible or increased uncertainty, leading to data gaps	Combined signal of snow and subsurface storage, no separation possible
Dense vegetation	Soil contribution masked and increased retrieval uncertainty	No direct impact
Signal leakage	Not affected	Signal mixing (e.g. ocean-land leakage)
Surface water	Mixed signal and increased retrieval uncertainty	Combined signal of surface water and subsurface storage, no separation possible
RFI	Affecting passive radiometers, leading to increased uncertainty	No impact

To identify regions mainly affected by these observational limitations, a spatial mask was created to provide context and identify the specific grid cells (Figure 5.2). These include regions of dense vegetation, areas with persistent snow cover and frozen soil, and regions with low soil moisture variability (e.g., deserts). For dense vegetation, the ESA CCI mask is used. Grid cells mainly influenced by snow/frozen soil conditions are identified using GLDAS soil temperature ($<0°C$) and SWE ($>0mm$), and grid cells where more than 40% of all observations are affected by these conditions are included in the mask. Dry regions are classified based on low soil moisture variability using the root mean square of daily soil moisture time series derived from SMOS L3 (with other data sets showing similar results) and a reference value in the Sahara desert, where

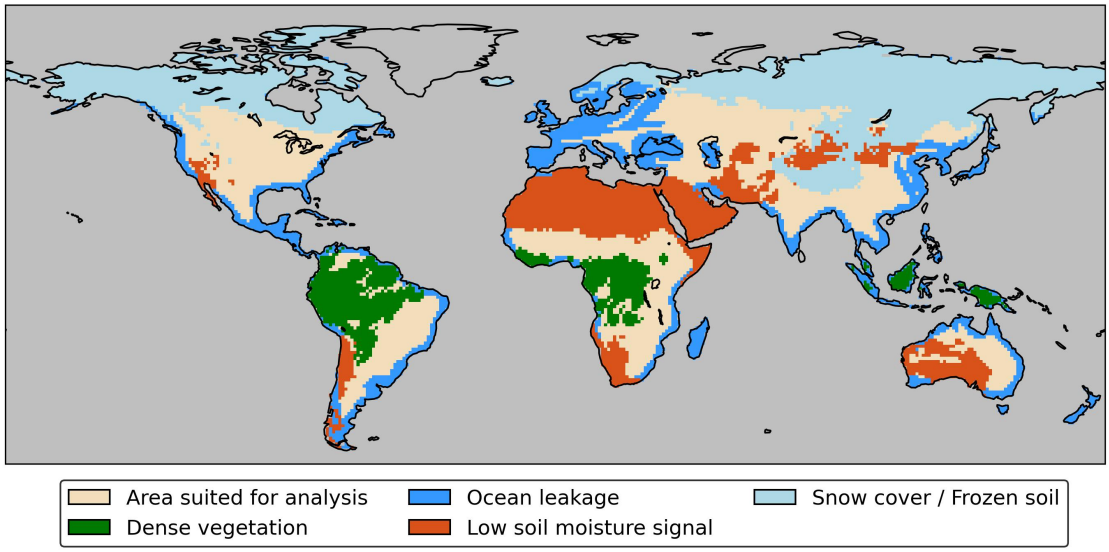

Figure 5.2.: Spatial masks to identify regions with low soil moisture variability (orange), dense vegetation (green), snow cover/frozen soil (light blue) and ocean leakage (dark blue). Other areas (beige) are considered to be suited for analysis.

variability is very low. The GRACE-based TWS estimates are affected by signal leakage, which leads to non-independence between neighbouring grid cells, particularly in coastal regions. To account for this, we use the leakage mask provided by Eicker et al. (2020) (Fig. S4 in Supporting Information) to identify areas strongly influenced by ocean leakage. GRACE TWS further includes storage variations such as surface water bodies, which are not separated in the GRACE signal. To locate such regions, we use the analysis by Jensen et al. (2020) (Fig. S2 in Supporting Information) to identify areas where these contributions are dominant, such as the Great Lakes, Lake Victoria, or the Caspian Sea. RFI is not explicitly considered in this study. It mainly affects SMOS L3 observations, while SMAP is less impacted due to its improved RFI mitigation approaches (Entekhabi et al., 2014).

While the remaining areas are generally suitable for analysis, regions with low soil moisture variability, such as deserts, are excluded from all analyses, as no meaningful variability in either soil moisture or TWS can be expected. Dense vegetation in tropical rainforest regions is masked only for the ESA CCI data set, as this masking is already applied in the provided data. The other regions are retained in the analysis or treated individually across the individual papers. For example, leakage-affected areas are only excluded in Paper 2, where the day-to-day variability is more important, and leakage would limit the analysis. Another example is snow cover, which leads to temporal masking and is further discussed in Section 5.2.

In general, how well soil moisture products and GRACE-based TWS compare depends on (i) the product selected and how effectively it represents depth, (ii) the temporal characteristics, in particular whether the signal is smoothed due to model input or due to

the deeper soil representation, and (iii) observational limitations that are specific to each region. These differences need to be taken into account to enable a meaningful joint analysis of soil moisture and TWS dynamics.

Q3: Which methods enable a consistent and harmonised comparison between satellite soil moisture and GRACE-based TWS?

In order to compare daily satellite soil moisture with TWS estimates derived from GRACE, a framework has to be developed which harmonises the data sets and considers (i) scale mismatch, (ii) differences in temporal sampling, (iii) signal processing, and (iv) suitable methods to quantify the comparison. This comparability is established through a set of spatial, temporal, and spectral processing steps that bring all data sets into a common analytical framework, while at the same time preserving as much of the natural variability of each data set as possible.

Spatial harmonisation and consistency:
Soil moisture products and GRACE-derived TWS are brought onto a common global grid of $1^\circ \times 1^\circ$. The soil moisture products, which have a higher native spatial resolution, are aggregated to the $1^\circ \times 1^\circ$ grid using a conservative remapping approach to preserve spatially integrated values and avoid artificial biases introduced by interpolation. This option offers a practical balance between the finer resolution of soil moisture retrievals and the coarser effective resolution of daily GRACE solutions (truncated spherical harmonics, degree $n = 40$; $\sim$500 km). As a result, GRACE TWS grid cells are not independent of neighbouring grid cells. These effects are regarded as observational constraints.

Converting soil moisture products into spherical harmonic coefficients truncated at degree $n = 40$ would be an alternative way to achieve full spatial consistency with GRACE. However, this approach would introduce additional smoothing and reduce the native spatial information content of the soil moisture data. An experiment described in the Supporting Information of Paper 2 compares this spatial harmonisation with the native 1° grid representation, indicating that the spatial harmonisation does not significantly affect the overall conclusions, although it influences the magnitude of the resulting values due to smoothing effects.

Maintaining the soil moisture data on the 1° grid preserves spatial variability that would otherwise be smoothed when applying a spherical harmonic solution. This would impose GRACE-like smoothing on the soil moisture data and redistribute local signals across neighbouring regions. Keeping the data on the 1° grid, therefore, makes it easier to identify where the underlying hydrological signals originate. This is also illustrated

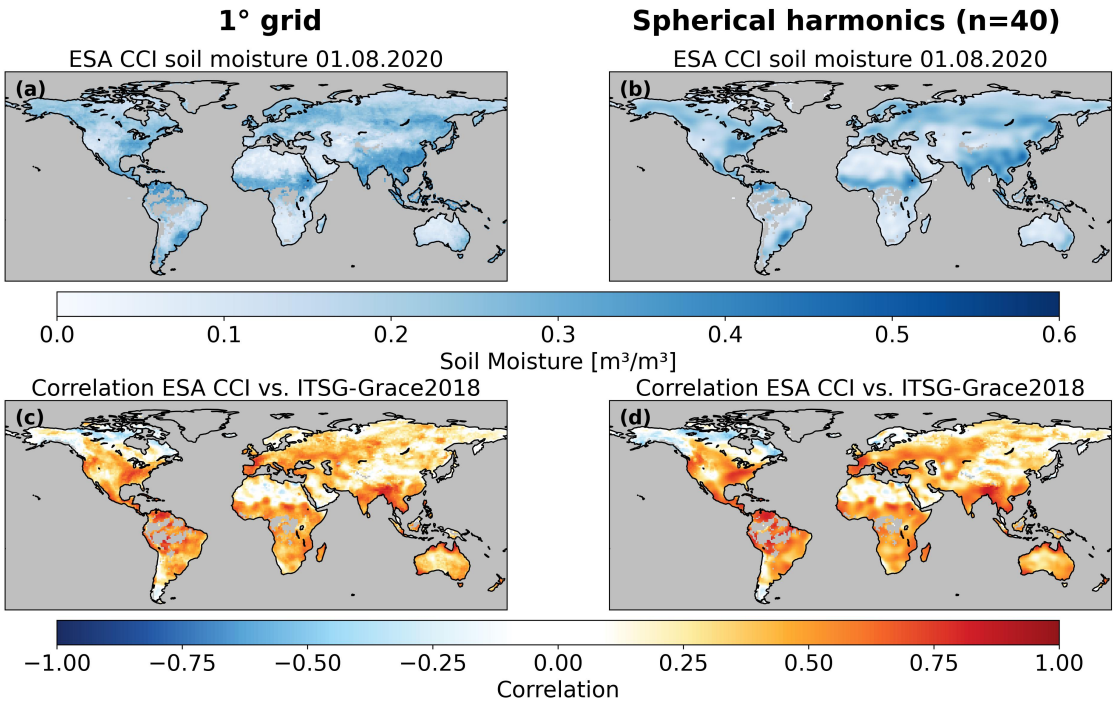

Figure 5.3.: Spatial comparison of ESA CCI soil moisture on a 1° grid and in spherical harmonic representation (n = 40). (a–b) show soil moisture grids, while (c–d) show their correlation with GRACE-based TWS from ITSG-Grace2018.

in Figure 5.3, where the soil moisture data on the 1° grid show more local variability compared to the smoother patterns in the spherical harmonic representation. The same behaviour is reflected in the correlation patterns with daily ITSG-Grace2018, where more localised structures are identifiable on the native grid. If the soil moisture data were represented in spherical harmonics, this localised signal would be smeared across neighbouring grid cells in a similar manner to the GRACE signal. Overall, large-scale patterns remain similar across both spatial representations.

Temporal alignment and quality control:

Time series are temporally aligned over a common analysis period and synchronised to the daily sampling of the GRACE solutions. In general, Paper 1 uses a period from 01.04.2015 to 31.12.2021, while Paper 2 extends this period to 31.12.2022. This choice is mainly driven by the launch of the SMAP mission in 2015, allowing for a common analysis period across all data sets. For a consistent comparison, it is essential that all data sets cover the same time period, even though it would be possible to include longer records, for example, using SMOS data from 2010 or ESA CCI data starting in 2002, along with the start of the GRACE mission. In contrast, Paper 3 focuses on the long-term record from ESA CCI only and therefore uses an extended period from 01.01.2003 to 31.12.2022.

The quality control of the daily ITSG-Grace2018 solutions is mainly based on the

observation count, which is provided with the data set. This is important because daily GRACE estimates can become dominated by the process model when observation coverage is low. Based on this observation count, a threshold of fewer than 10,000 observations per day is used to exclude these days. As low observation counts often occur for longer periods, this filtering typically removes whole months, especially during the well-known gaps in the GRACE record. This ensures that the resulting daily TWS time series remains predominantly observation-driven. The temporal gap between the GRACE and GRACE-FO missions (06.2017 to 05.2018) is excluded because no GRACE data are available during this period. For consistency, the same period is also excluded from the soil moisture data sets. In addition, days removed from the GRACE time series due to low observation counts are consistently masked in the soil moisture data sets to ensure a comparable temporal sampling.

While no quality control for the soil moisture products was applied in Paper 1, a temporal mask is introduced in the subsequent analysis to account for retrieval conditions under snow cover and frozen soil. Specifically, a temporal mask consistent with the ESA CCI soil moisture product is applied, where days with SWE greater than 0 mm and soil temperatures below 0 °C are excluded. The introduction of this temporal mask improves the correlation between soil moisture and TWS signals by reducing soil moisture retrieval artefacts in snow-affected regions. More details on this topic are provided in Section 5.2.

Additionally, due to the orbital sampling patterns of the SMOS and SMAP satellites, the L3 products contain short temporal gaps. These gaps are treated consistently across the analysis using limited linear interpolation for gaps of up to five consecutive days. This is done for all data sets, while SMOS and SMAP L3 are the most affected. ESA CCI has fewer gaps, and the L4 products have none. Sensitivity tests show that this interpolation has a negligible effect on the calculated correlations or time shifts. However, it can slightly influence day-to-day variability, which is relevant for the analyses in Paper 2 and is shown in the Supporting Information of Paper 2.

Signal decomposition:

To compare different dynamics across temporal scales between TWS and soil moisture, the harmonised time series are decomposed into components that isolate distinct frequency bands. The decomposition has to be applied consistently to both data sets. The individual steps are illustrated for an exemplary grid cell using the TWS signal in Figure 5.4, but the same procedure is applied to all soil moisture products as well. In general, the decomposition starts by estimating the long-term trend (Fig. 5.4a) and removing it from the full signal, resulting in a de-trended time series (Fig. 5.4b). In addition to the trend,

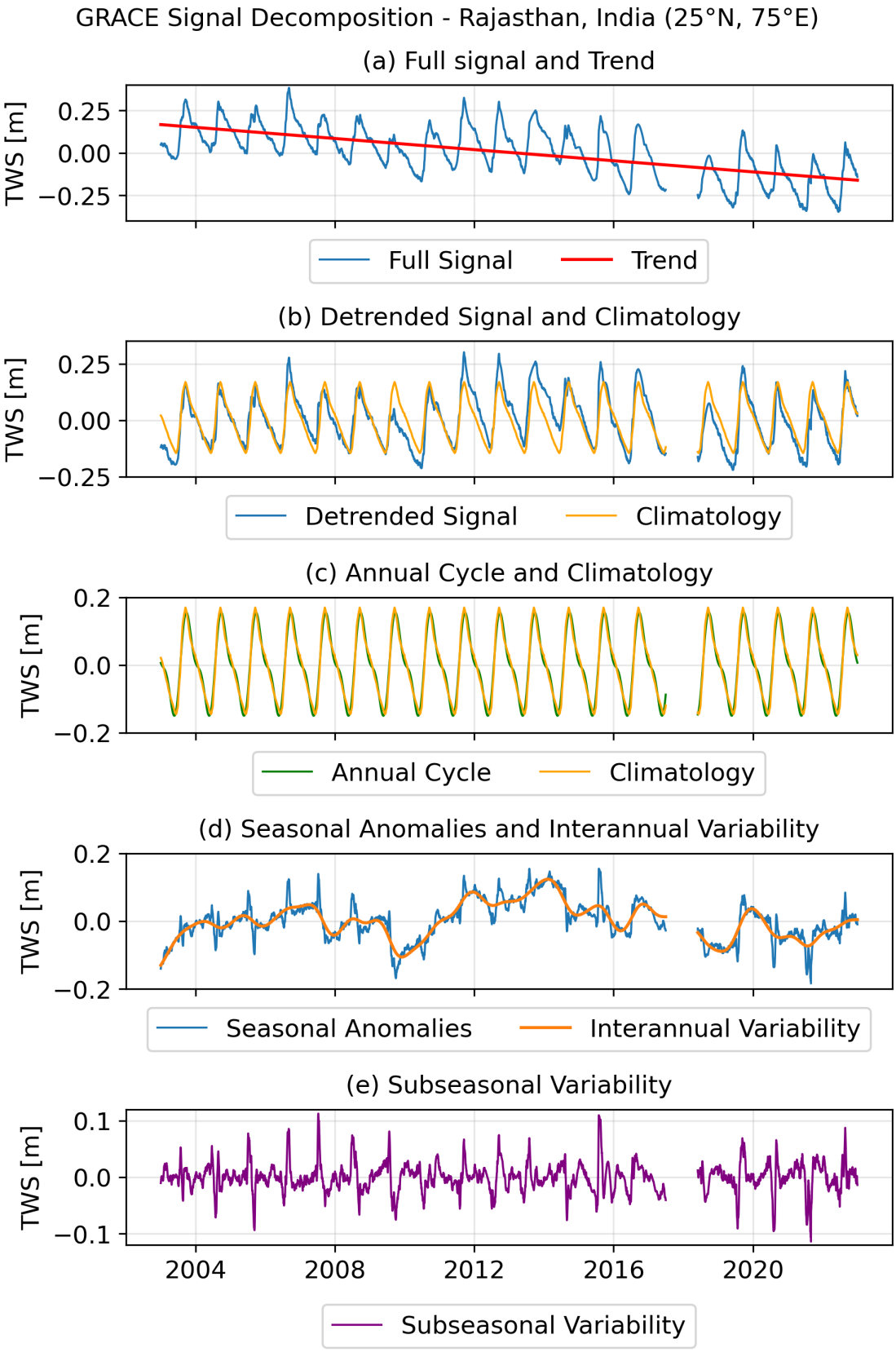

Figure 5.4.: GRACE TWS signal decomposition for an exemplary grid cell in Rajasthan, India (25°N, 75°E). (a) Full TWS anomaly signal with trend, (b) de-trended signal with climatology, (c) annual cycle compared to climatology, (d) seasonal anomalies and interannual variability, and (e) sub-seasonal variability.

the mean (bias) of the time series is also removed. This is important, as the soil moisture products are biased relative to each other (see Fig. 5.1).

Next, the seasonal cycle is estimated from the de-trended signal. Two approaches are used: (i) a climatology, defined as the mean value for each day of the year over the full period, and (ii) parameters of a harmonic function are estimated based on least-squares fitting of a sinusoidal function (in this function, parameters represent the annual and semi-annual components of the signal; see Eq. 2 in Paper 2). As shown in Figure 5.4c, both approaches lead to similar results, with small differences in amplitude and timing. For longer time periods, the climatology approach is preferred as it better represents the observed variability, but for shorter periods (as in Paper 1 and Paper 2), the harmonic approach is more stable and less sensitive to data gaps. After removing the seasonal component from the de-trended time series, the remaining signal represents seasonal anomalies (de-seasonalised signal), which are used in Paper 2.

Depending on the research question, additional filtering is applied to further separate the signal. For example, an interannual component is derived (see Fig. 5.4d) and the sub-seasonal component (Fig. 5.4e), which forms the basis for the analysis in Paper 3. In addition, sub-monthly variability is analysed using a Butterworth high-pass filter with a cut-off frequency of 30 days (Fig. 5.5), which is investigated in Paper 1. Overall, using a consistent spectral framework ensures that soil moisture and TWS are compared at the same temporal scales.

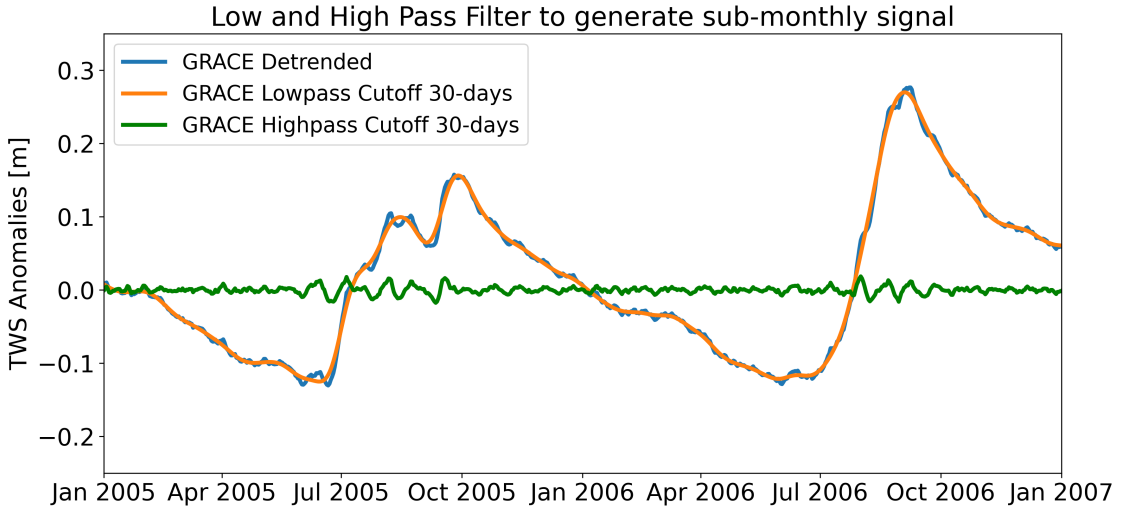

Figure 5.5.: Low- and high-pass filtering of de-trended GRACE TWS anomalies for an exemplary grid cell in Rajasthan, India (25°N, 75°E). The high-pass filter isolates sub-monthly variability.

Accounting for non-soil moisture storage compartments in GRACE TWS:
In Paper 3, when using GRACE to investigate subsurface storage compartments, and in particular when using it as a constraint for estimating subsurface storage dynamics, it is important to account for non-soil moisture storage. GRACE-based TWS captures all changes in TWS, including contributions from snow and surface water. To mitigate these influences, these compartments must be removed when possible and if available (e.g., by subtracting estimates of snow and surface water storage from GRACE). This will ensure that the remaining GRACE-based TWS signal is primarily driven by storage changes associated with subsurface water dynamics.

Methods for quantifying the comparison:
To quantify the relationship between soil moisture and GRACE-based TWS, different metrics are applied depending on the temporal scale and the specific research question. In general, the comparison in this thesis focuses on the agreement in variability rather than absolute values, as both data sets differ in depth representation, physical meaning, and units. Because of this, a direct comparison of absolute values or amplitudes is not meaningful. Therefore, magnitude-based metrics such as the root mean squared deviation are not suitable for this analysis. Even if the time series are normalised or standardised, the differences remain. Instead, the analysis mainly relies on calculating the Pearson correlation coefficient between soil moisture and TWS across temporal scales. To identify possible time shifts between data sets, cross-correlation is applied. The maximum correlation indicates the temporal shift at which both signals have the strongest agreement. An example of this approach is shown in Figure 5.6 for the ESA CCI and GRACE data set in Rajasthan, India (25°N, 75°E). The scatter plot before time shift (lag) correction shows a correlation coefficient of $\rho = 0.54$ between both data sets. The cross-correlation reveals a clear time shift of -36 days. In this case, negative time shift values indicate that soil moisture leads the GRACE signal. After applying this lag correction, the agreement between both time series improves to $\rho = 0.79$, which is also visible in the scatter plot. The time series comparison further illustrates that the shifted GRACE signal aligns better with the soil moisture time series. These correlation-based methods are applied throughout all three papers.

In Paper 2, the de-seasonalised signals are additionally standardised, resulting in a z-score time series. To obtain and analyse the day-to-day variability, the time derivative of these z-score time series is calculated by the backward difference method. Based on this, empirical CDFs are computed and used to compare the statistical behaviour of both data sets in the context of drying and recovery dynamics.

As an additional method, Principal Component Analysis (Preisendorfer and Mobley,

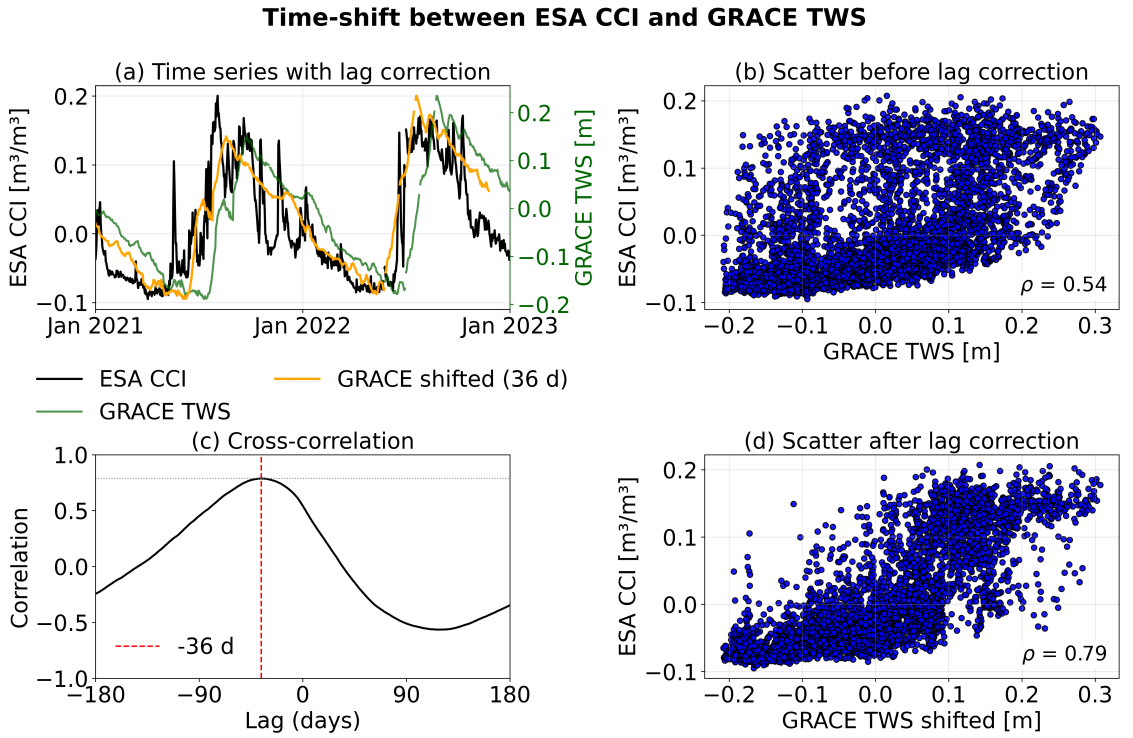

Figure 5.6.: Time-shift analysis between ESA CCI soil moisture and GRACE-based TWS. (a) Time series with lag correction, (b) scatter plot before correction, (c) cross-correlation, (d) scatter plot after correction. Time series are based on an exemplary grid cell in Rajasthan, India (25°N, 75°E).

1988) could be used to identify the primary modes of variability within the soil moisture and GRACE-based TWS data sets. This approach decomposes the data into dominant spatial patterns and their associated temporal evolution, allowing for a direct comparison of large-scale variability between both data sets. However, this approach is not used in this thesis's analysis.

Similarly, Wavelet Coherence Analysis (WCA, Torrence and Compo, 1998) could be used to investigate time-dependent relationships between soil moisture and GRACE-based TWS across different temporal scales and is presented here as an additional analysis, although it is not part of the main results of the individual papers. In contrast to correlation-based methods, this approach allows both the time and frequency domains to be analysed simultaneously. Therefore, it shows when and at which frequencies the two data sets behave similarly. The results are displayed in Figure 5.7c (illustration based on Rahmati, 2024) for the same exemplary grid cell in Rajasthan, India (25°N, 75°E) seen before. High coherence indicates strong agreement in variability. In addition, the phase information of the WCA can be converted into a time delay, which describes the timing between both signals (not shown in the figure). Positive delays indicate that soil moisture leads TWS, while negative delays indicate that TWS responds earlier. The cone of influence marks regions where edge effects become important, and results are less

reliable. Therefore, the interpretation focuses on areas within this region. In addition, significance can be estimated, and in this plot, significant coherence is outlined in black.

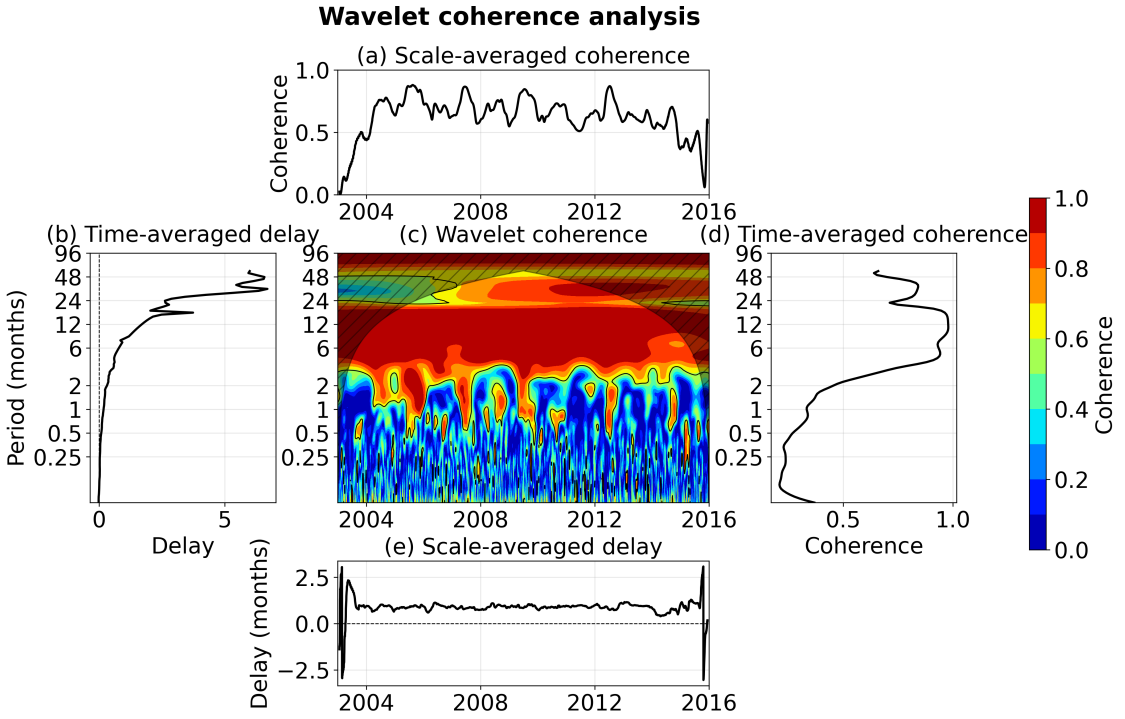

Figure 5.7.: WCA between soil moisture and GRACE-based TWS. (c) Wavelet coherence, (a, e) scale-averaged coherence and delay, and (b, d) time-averaged delay and coherence. Results are based on an exemplary grid cell in Rajasthan, India (25°N, 75°E)

To simplify the interpretation, scale-averaged coherence and delay are calculated over selected periods (Figure 5.7a and 5.7e). These results show that delays increase towards higher frequencies, while at lower frequencies the delay is smaller. At the same time, coherence is strongest at seasonal time scales (around 6–12 months), whereas shorter sub-monthly frequencies show weaker agreement. Time-averaged values represent the dominant coherence or delay across all time steps (Figure 5.7b and 5.7d). Coherence remains relatively high over time, with some variability between years. On average, coherence is around 0.60, and the scale-averaged delay is close to one month, indicating that soil moisture generally leads GRACE-based TWS.

WCA provides a consistent framework to analyse both the strength and timing of the relationship between soil moisture and TWS. Although this method offers insights into non-stationary signals, it is used here only as a complementary analysis, as it is mainly applicable to individual time series and not transferable to global-scale analyses. However, it would be well suited for larger regions such as river basins.

Overall, the developed framework enables a consistent comparison between soil moisture and GRACE-based TWS despite their differences. By combining (i) spatial harmonisa-

tion, (ii) temporal alignment, and (iii) signal decomposition, the data sets are brought onto a common basis while preserving their variability. Correlation-based methods and time-shift analysis enable robust quantification of their relationship globally, while additional methodologies can be applied at the grid-cell level. Together, these approaches provide a reliable foundation for analysing the relationship between soil moisture and TWS.

5.2. Relationship between soil moisture and GRACE-based TWS

Q4: How well does the temporal variability of soil moisture (SSM and RZSM) agree with GRACE-based TWS?

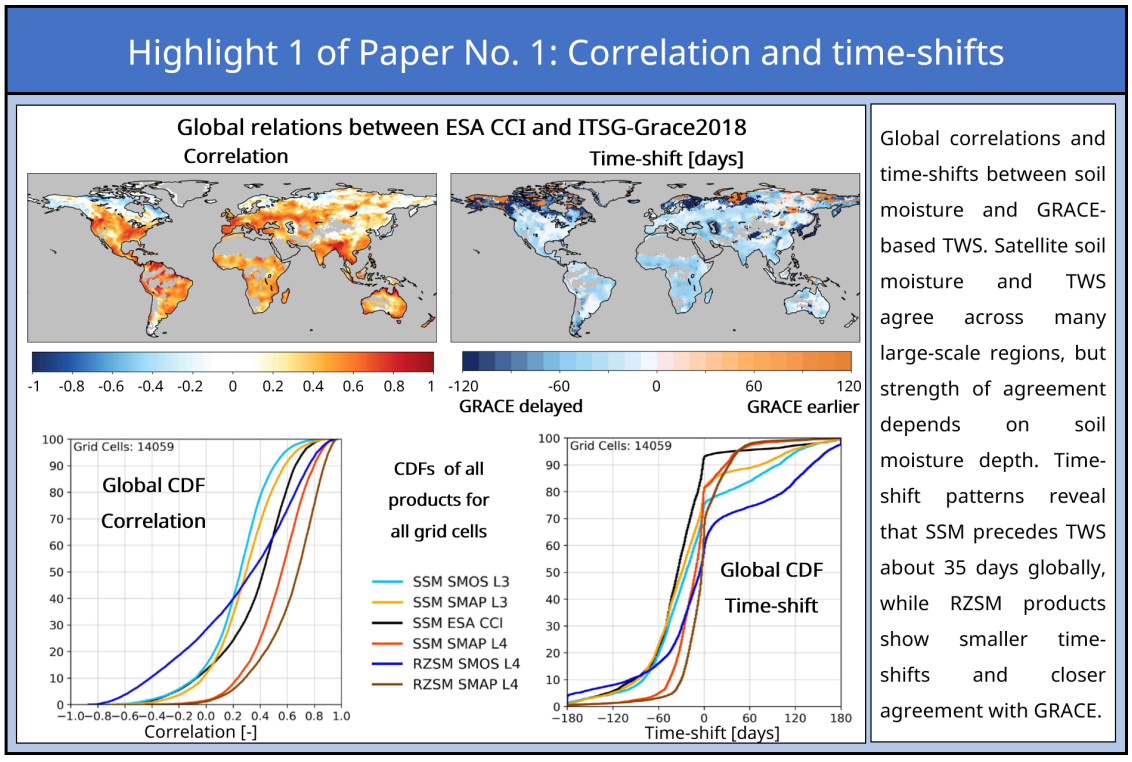

Figure 5.8.: Overview of the main results from Paper 1, showing global patterns of correlation and temporal shifts between soil moisture and GRACE-based TWS. The maps illustrate the example of ESA CCI SSM, while the CDFs summarise the results across all analysed soil moisture products. SSM generally precedes TWS, whereas RZSM products show smaller time shifts and closer agreement with GRACE-based TWS.

The results of Paper 1 show that satellite-derived soil moisture and GRACE TWS exhibit a similar relationship at the global scale, although the strength of agreement systematically depends on vertical representativeness, product characteristics, and the

level of processing of the soil moisture products. These correlations are calculated without correcting for temporal shifts between the signals. Therefore, they describe the direct temporal agreement between soil moisture and TWS, while possible lagged relationships are examined separately in Q5. For the full signal, which is largely dominated by seasonal and interannual variability, all soil moisture products capture the dominant large-scale spatial patterns of TWS variability across major hydroclimatic regions, although with varying correlation strengths.

Particularly high correlations occur in humid climate zones and in regions characterised by pronounced wet–dry cycles. Examples include parts of tropical South America, Southeast Asia, the south-eastern USA, northern Australia, and the outer tropics in Africa. In these regions, storage dynamics are primarily influenced by coherent hydroclimatic forcing, which is consistently captured by soil moisture retrievals and GRACE observations. In contrast, arid and semi-arid regions have weaker correlations, owing to low signal variability and increased noise during dry periods, which reduces the detectability of coupled storage dynamics.

The correlation values vary across the different soil moisture products and are also reflected in the global correlation distributions shown as a CDF in Figure 5.8 (lower-left panel). Surface L3 retrievals generally show lower correlations with GRACE-based TWS. Among the single-mission data sets, SMAP L3 show slightly higher agreement than SMOS L3, likely due to higher noise levels in the SMOS product. In contrast, the multi-sensor product ESA CCI shows stronger spatial agreement with GRACE-based TWS, indicating the stabilising effect of merging and harmonisation procedures. As such, when combining multiple data sets, the ensemble product reduces spurious contributions from individual sensors, leading to a more stable representation of large-scale soil moisture variability. L4 products derived through data assimilation show higher correlations overall. In particular, the SMAP L4 RZSM product shows the strongest agreement with GRACE TWS. The SMOS-based RZSM data generated using an exponential filter show slightly weaker agreement than the SMAP L4 RZSM, but are more closely related to GRACE-based TWS than the original SMOS L3 SSM data set. Additionally, soil moisture products that incorporate model information, such as SMAP L4 SSM, typically exhibit smoother temporal variability than direct surface retrievals, resulting in a closer correspondence with GRACE-based TWS.

In Paper 1, regional differences were also examined by distinguishing between areas generally well suited for the analysis and those affected by snow cover or dense vegetation. The results show that correlation values in densely vegetated regions do not differ substantially from those in other suitable regions. In contrast, correlations in regions affected by snow cover and frozen soils are generally lower and often become negative.

This indicates that soil moisture and GRACE-based TWS are not consistently linked throughout the year. In winter, GRACE observes an increase in TWS due to snow accumulation, while soil moisture content is usually unchanged or may decrease due to snow cover. As a result, the two signals can evolve in opposite directions during these periods, resulting in negative or low correlations. Subsequent analyses demonstrated that temporally masking these periods in the soil moisture time series improved correlations in snow-affected regions. As this masking was not applied in Paper 1, it was implemented as an additional pre-processing step in the subsequent analyses to ensure a more consistent comparison between soil moisture observations and GRACE-derived TWS.

Most of the strong correlations between soil moisture and GRACE TWS are driven by the seasonal cycle. Consequently, correlation values decrease when the seasonal component is removed, and the analysis is performed on a de-seasonalised signal. Although this analysis was not part of Paper 1, it was conducted subsequently and is presented in the Supporting Information of Paper 2. While the residual signal has lower correlations compared to those computed from the full seasonal signals (for example, the global median correlation value for SMAP L4 RZSM decreased from about 0.7 to 0.5 and for the ESA CCI from about 0.5 to 0.3), there are still several regions with strong correlations present across multiple regions (e.g., the southeastern US, Paraná Basin in South America, or the southeastern regions of Asia) with maximum correlation values reaching 0.6 in these regions.

At sub-monthly time scales, the agreement decreases compared to the full signal because higher-frequency variability is associated with a higher noise level. As this aspect primarily concerns short-term dynamics, it is discussed in more detail in Q6.

In summary, the strength of the soil moisture – TWS relationship increases with vertical representativeness and the degree of post-processing. While SSM retrievals capture rapid fluctuations near the land surface, deeper and assimilation-based products are more consistent with the integrated storage signal observed by GRACE. At the same time, the relationship weakens at higher temporal frequencies, with the strongest agreement for the full signal dominated by seasonal variability, and lower agreement for de-seasonalised and sub-monthly components.

Q5: How do temporal shifts between soil moisture and TWS vary with integration depth, and what do they reveal about subsurface water redistribution?

While Q4 focused on the strength of agreement between soil moisture and TWS, this research question examines their temporal lag. Cross-correlation analyses reveal systematic temporal shifts between soil moisture retrievals and TWS, suggesting that

soil moisture and TWS respond to hydrometeorological forcing on different time scales. These time shifts provide insight into the redistribution of water within the subsurface.

In most regions not strongly influenced by persistent snow cover, variations in SSM precede changes in GRACE-based TWS, particularly at seasonal time scales. This temporal shift reflects the typical sequence of hydrological processes. Precipitation first influences SSM, while changes in deeper storage components occur more gradually as water infiltrates and moves through the subsurface before contributing to the integrated TWS signal.

The magnitude of the temporal shift decreases with increasing effective soil depth of the soil moisture product. SSM retrievals generally exhibit the largest lags relative to TWS, whereas RZSM products show considerably smaller delays. This systematic reduction in phase shift from shallow to deeper soil layers indicates that increasing vertical integration yields a closer temporal correspondence to the integrated storage signal observed by GRACE.

SSM products such as ESA CCI, SMAP L3, and SMOS L3 generate the largest time shifts, with global median values of about -35 days, while local lags can reach -60 to -90 days. SMAP L4 SSM shows smaller lags, with a median of approximately -17 days. The smallest delays are found for the RZSM products, with global median values of about -5 days for SMAP L4 RZSM and -13 days for SMOS L4 RZSM. In some humid regions with strong vertical coupling, RZSM and TWS approach near phase alignment. The corresponding global distributions are shown as CDF in Figure 5.8.

This highlights the advantage of daily GRACE solutions, as they allow for a more precise characterisation of the temporal relationship between soil moisture and TWS. Using monthly data alone would considerably limit the temporal resolution and prevent the identification of lags occurring within a single month.

In snow-dominated regions, the temporal relationship between soil moisture and GRACE-based TWS often differs from that observed elsewhere, with soil moisture frequently lagging behind TWS. These regions also exhibit lower and often negative correlations. As discussed in Q4, this behaviour is likely related to snow accumulation, which increases TWS while satellite soil moisture retrievals under snow-covered or frozen-soil conditions are often unreliable or do not provide realistic values. The ESA CCI product performs differently as it shows time shifts, which are more similar to those found in regions not affected by persistent snow cover. This behaviour is likely related to the temporal masking of snow-covered and frozen soil conditions applied in the ESA CCI product. The comparison suggests that excluding these periods results in a more consistent representation of the relationship between soil moisture and TWS, particularly during the snow-free months in the Northern Hemisphere.

The largest temporal shifts are primarily associated with the seasonal signal and its large amplitude. After removing the seasonal component, the estimated lags become considerably smaller. This de-seasonalised perspective also forms the basis for the analysis in Paper 2, where temporal shifts are examined in the context of water storage deficits. Temporal shifts are further reduced at sub-monthly time scales, suggesting a closer temporal correspondence between short-term variations in soil moisture and TWS. This aspect is discussed in more detail in Q6.

In general, analysing temporal shifts complements the correlation analysis by providing insight into the temporal structure of storage variations across different depths. The observed depth-dependent lag pattern supports the interpretation of TWS as an integrated and temporally smoothed response to surface forcing. Moreover, it suggests that water storage signals propagate gradually from the surface towards deeper storage compartments. Larger lags between SSM and TWS are consistent with the time scales associated with infiltration and redistribution processes, whereas the smaller lags observed for RZSM reflect its closer connection to the integrated storage dynamics represented by TWS. It is important to note, however, that these lags represent statistical timing differences between the signals and should not be interpreted as measures of physical flow velocities. Nevertheless, their systematic dependence on soil depth provides indirect observational evidence of the downward propagation and redistribution of water within the subsurface.

Q6: Can daily GRACE data detect high-frequency variations in soil moisture and are the observed variations statistically significant?

The findings suggest that daily GRACE solutions can capture hydrologically meaningful high-frequency variability beyond the dominant seasonal cycle. After removing the seasonal component and applying a Butterworth filter to isolate sub-monthly anomalies, statistically significant positive correlations between soil moisture and GRACE-based TWS remain detectable in numerous regions.

These regions include parts of the southeastern United States, large areas of southeastern South America, the Ganges–Brahmaputra basin, eastern China, and northern Australia. In these regions, correlations between high-pass filtered soil moisture and GRACE-based TWS remain positive, reaching up to approximately 0.6 for the SMAP L4 RZSM product. SSM products generally exhibit lower correlations and a more limited spatial extent of significant agreement, likely because shallow retrievals capture deeper storage dynamics less effectively and contain higher noise levels.

Despite the generally lower magnitudes of the correlations in the high-pass filtered

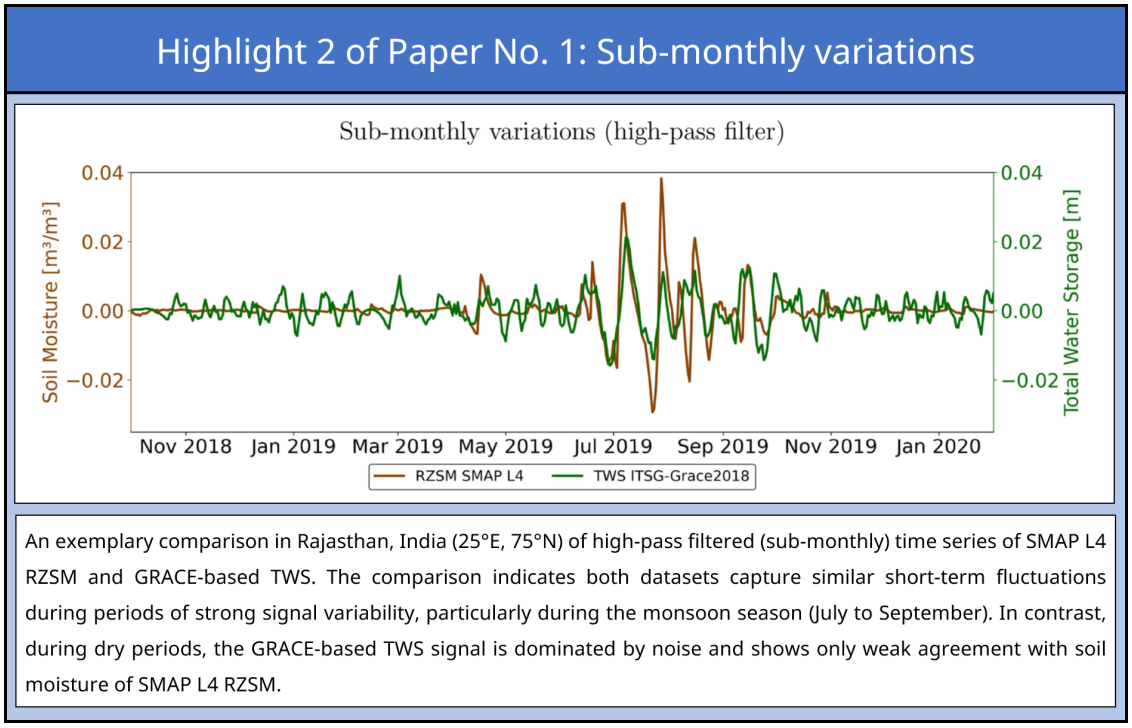

Figure 5.9.: Exemplary comparison of sub-monthly variations for SMAP L4 RZSM and GRACE-based TWS in Rajasthan, India from Paper 1.

signals, they remain predominantly positive and statistically significant across large parts of the continents. Statistical significance is assessed at the $\alpha = 0.05$ significance level using Student's t-distribution. For example, significantly positive correlations are found in approximately 43% of land areas for SMAP L3 SSM and increase to 58% for ESA CCI. The agreement is even more pronounced for root-zone products, where SMAP L4 RZSM shows significant positive correlations across roughly 77% of the analysed land areas. The widespread sub-monthly agreement indicates that the daily GRACE solutions are sensitive to short-term mass redistribution processes, which are also reflected in the soil moisture observations.

In Paper 1, the idea of masking the analysis to precipitation events was only briefly illustrated for a representative grid cell and also described in Figure 5.9. Additional analyses conducted afterward applied this event-based masking more systematically. In this approach, only days with precipitation and a few days before and after the event were retained, while all other days were excluded from the time series. The results showed that applying this mask generally increased the global median correlations across all soil moisture products by about 5% on average. Locally, the increase reached up to approximately 10%, especially in regions of India, southeastern South America, East Africa, and the southeastern United States. This suggests that the relationship between soil moisture and GRACE-based TWS is strongest during periods directly influenced by precipitation, when both variables respond more coherently to the same

hydrometeorological forcing.

The time-shift analysis of the high-pass filtered signals demonstrates that we obtain smaller temporal lags compared to the full seasonal signal. On average, the estimated shifts remain negative, indicating that GRACE-based TWS slightly lags behind soil moisture variations also on short time scales. For the SSM products, time shifts reach values of up to -3 days. For the root-zone products, the magnitude of the shifts becomes smaller and often approaches zero, particularly for SMAP L4 RZSM. This indicates that including deeper soil layers reduces the time difference between soil moisture and the integrated storage signal seen by GRACE. On the other hand, SMOS L4 RZSM often shows slightly positive time shifts. This is less consistent with the expected propagation from SSM towards integrated storage and may point to limitations in the product's depth-scaling approach, for example an overly slow representation of infiltration or vertical redistribution processes.

Overall, the results demonstrate that daily GRACE observations capture sub-monthly water storage variability comparable to short-term variations in soil moisture that cannot be resolved with conventional monthly gravity field products. In particular, precipitation events lead to similar sub-monthly dynamics in SSM and RZSM that are subsequently reflected in the integrated TWS signal observed by GRACE, typically with delays of only a few days. Although the strength and spatial extent of this high-frequency agreement vary across regions and soil moisture products, the results show that daily GRACE observations provide meaningful information on short-term TWS dynamics in regions with sufficiently strong hydrometeorological variability.

5.3. Propagation of water storage deficits in the subsurface

Q7: How do de-seasonalised water storage deficits propagate across increasing integration depth, from SSM to integrated TWS?

Paper 2 investigates how deficit signals evolve across subsurface storage layers, from SSM to RZSM and further to vertically integrated TWS, using observation-driven data sets on a global scale. The analysis builds on the conceptual framework described by Changnon (1987), who showed that drought characteristics change systematically across different components of the hydrological cycle. This idea is often referred to as the drought cascade. While drought conditions in the atmosphere and near-surface soil tend to be short-lived and highly variable, drought signals generally become more delayed, damped, and persistent as they propagate through deeper water storage compartments. Building

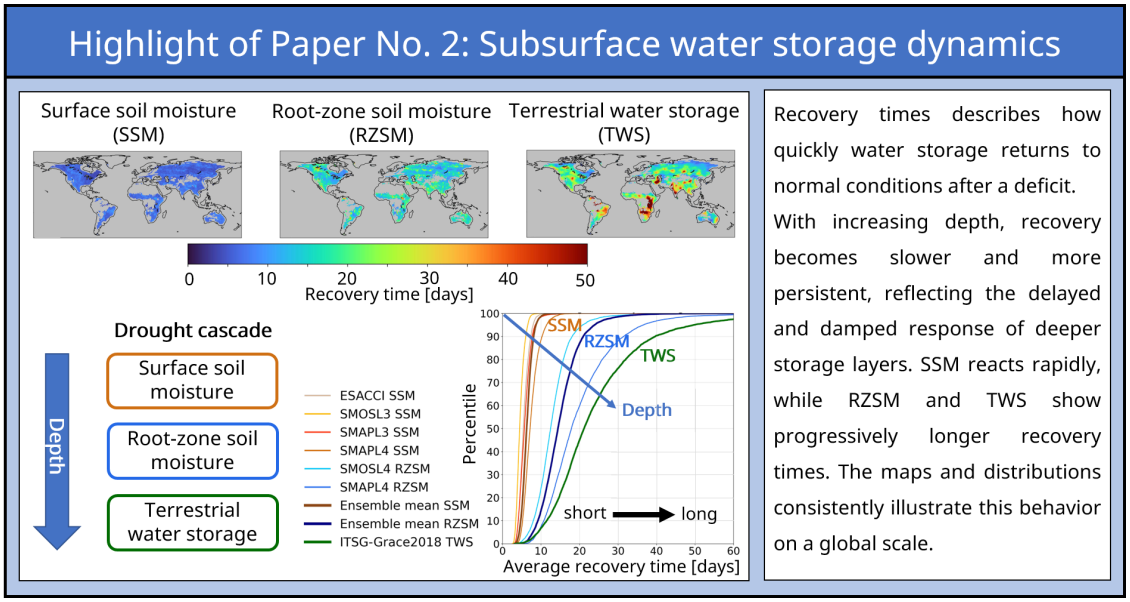

Figure 5.10.: Highlights from Paper 2. Recovery times derived from soil moisture and GRACE-based TWS demonstrate that water storage deficits become increasingly persistent with storage depth, reflecting the propagation of storage anomalies through the subsurface.

on this concept, Paper 2 examines whether global satellite observations can provide observational evidence of such a storage-based drought cascade within the subsurface, from shallow soil moisture to deeper and vertically integrated storage compartments. This is a central step beyond earlier work, because it tests the drought cascade concept directly with satellite observations and applies it consistently at the global scale.

Previous investigations of the drought cascade have primarily relied on in-situ observations, limiting the analysis to specific locations. At larger spatial scales, studies have often depended on model-based data sets, while observation-driven approaches have commonly used monthly GRACE observations as a proxy for TWS or as a constraint for deeper storage components such as groundwater. Paper 2 goes beyond these studies in two ways. First, it analyses the storage-based drought cascade globally using daily satellite observations. Second, it quantifies drying and recovery behaviour statistically, based on CDFs and daily rates of change, instead of defining individual drought events by fixed start and end dates.

The findings of Paper 2 demonstrate that de-seasonalised water storage deficits propagate systematically with increasing integration depth. To enable a consistent comparison across storage compartments, deficit periods are identified from anomalies after removing the dominant seasonal cycle. Deficits typically emerge first in the near-surface soil layer, which responds rapidly to precipitation anomalies. With increasing depth, the deficit signals become progressively smoother and more persistent. As a result, RZSM exhibits a more gradual and temporally smoothed response than SSM, reflecting the integration of water fluxes across a larger soil volume. This behaviour

becomes even more pronounced in GRACE-based TWS, which integrates storage changes across the entire terrestrial water column and therefore represents the most aggregated response within the storage cascade. Consequently, water storage deficit signals propagate downward through the subsurface in an increasingly damped form, and TWS deficits may persist even after SSM has largely recovered. This behaviour reflects the influence of deeper storage compartments, including the unsaturated zone and groundwater, which respond on longer timescales and therefore prolong the overall storage deficit signal. This increasing persistence is shown in Figure 5.10 and quantified in Q9.

These patterns are consistently observed at the global scale and demonstrate that the drought cascade can be identified using observation-driven storage data sets, including daily GRACE-based TWS. The key finding is therefore not only that deficits become more persistent with depth, but that this behaviour can be observed globally from satellite data. In addition, daily GRACE observations reveal temporal differences between storage compartments that are largely unresolved in conventional monthly GRACE products, highlighting the added value of daily gravity field solutions for analysing subsurface deficit dynamics.

Q8: How can drought propagation be quantified beyond conventional event-based comparisons of drought onset and end?

Paper 2 introduces a distribution-based statistical framework that allows drought propagation to be analysed using daily, de-seasonalised storage anomalies without explicitly defining drought onset and end dates. The approach extends the concept of Thomas et al. (2014) by applying it to multiple storage compartments and evaluating deficit behaviour over the full time series rather than for selected individual drought events. This addresses a key limitation of conventional event-based analyses, where the identification of drought onset and recovery depends on the selected threshold. Such definitions can lead to inconsistent estimates of drought propagation when comparing storage compartments with different persistence and variability characteristics, such as SSM, RZSM, and TWS.

The analysis is only applied within deficit periods. For this purpose, the time series are first de-seasonalised, and deficits are defined as all days with negative anomalies. This means that no additional drought threshold has to be selected, and the method does not require fixed onset or recovery dates. All time series are then transformed into z-scores, so that SSM, RZSM, and TWS can be compared despite their different units and amplitudes. To describe how deficits develop and recover, the daily change of the z-score time series is calculated for each deficit day, where negative changes indicate a further intensification of the deficit, whereas positive changes indicate recovery. The distributions

of these daily changes are summarised with CDFs. These CDFs show whether a storage compartment typically loses or regains storage. The positive values (storage recovery) of the distribution are used to compare recovery rates across SSM, RZSM, and TWS.

The expected recovery time is calculated by relating the magnitude of a storage deficit to the median observed recovery rate described by the CDF. Specifically, the deficit magnitude is divided by the 50th percentile of the positive rate-of-change CDF. The result describes the time that would be needed to recover from a given deficit under typical recovery conditions. It should therefore be interpreted as a statistical estimate of persistence, rather than as the observed duration of an individual drought event. This approach avoids defining fixed drought onset and end dates. Instead, it uses all daily negative storage anomalies to compare deficit behaviour across SSM, RZSM, and TWS. This allows the delay and increasing persistence of deficit signals with storage depth to be analysed consistently. Daily observations are useful in this context because they resolve short-term changes in deficit development and recovery that are partly lost in monthly data sets. The same method could also be extended to snow or surface water storage to assess how these components contribute to TWS deficit dynamics.

Q9: How do drying and recovery rates of subsurface water storage deficits vary across different regions?

The rate-of-change analysis, together with the derived recovery-time metric, provides a quantitative way to describe how quickly storage deficits intensify and recover as integration depth increases. While Q7 of this section focused on the propagation of deficits across storage compartments in general, this research question investigates how drying and recovery rates vary across different environmental settings and regions.

Across most regions, a clear depth-dependent pattern emerges. SSM exhibits the largest day-to-day changes and the shortest recovery times. In the root zone, changes become smaller, and recovery takes longer. For integrated TWS, daily variations are further reduced, while recovery times are the longest. The increase in recovery time from SSM to TWS often amounts to several times the surface recovery duration, reflecting the increasing influence of deeper storage compartments and their longer persistence.

The comparison of recovery times shows that the temporal evolution of deficit signals is strongly controlled by storage depth. The reported recovery times should be interpreted as statistical estimates rather than observed durations of individual drought events. They are derived from the rate-of-change distributions over the full time series, using the 50% level of the recovery-rate distributions and assuming a linear recovery from a given storage deficit. On a global scale, SSM shows the shortest recovery times, with an

ensemble mean median of about 6 days. RZSM shows a longer median recovery time of around 14 days, while TWS responds most slowly, with a median recovery time of approximately 21 days. These patterns are also illustrated in Figure 5.10. Although the absolute values depend on the chosen percentile and the linear recovery assumption, the relative differences between storage depths remain robust.

In addition to the global differences between storage depths, the results also show clear regional differences. These differences suggest that storage deficits are not controlled by depth alone, but also by local environmental conditions such as topography, land cover, and climate. Topography appears to have an influence. Recovery times are generally shorter in lowland regions than in higher-elevation areas, especially for TWS and RZSM. One possible explanation is that water can accumulate more easily in low-lying regions through lateral flow, which may help replenish storage more quickly. However, the underlying processes cannot be fully resolved here. Land cover also seems to affect drying and recovery. Grassland regions generally show longer recovery times, whereas savanna regions tend to recover more quickly. This may be related to differences in vegetation and soil structure. In savannas, deeper roots and more porous soils may support faster vertical water movement, allowing storage deficits to recover more rapidly after dry periods. Recovery behaviour also differs between climate zones. Deficits in equatorial regions tend to recover more slowly, while deficits in warm temperate regions recover faster. This suggests that large-scale climate conditions affect how long storage deficits persist. Soil texture shows a similar pattern. Regions with more clay generally have longer recovery times, likely because clay-rich soils slow down infiltration and vertical water movement.

These regional patterns should be interpreted as broad tendencies, not as strict relationships. Many factors, such as climate, soil properties, land cover, or groundwater depth, can act at the same time. Therefore, the effect of one single factor cannot be clearly separated in this analysis. A more detailed analysis would be needed to show how these factors interact and how they influence subsurface storage and recovery together.

Overall, the results show that storage deficits change with depth and are also affected by regional conditions. With increasing depth, the deficits become smoother and tend to last longer. At the same time, climate, topography, land cover, and soil properties influence how quickly storage recovers in different regions.

5.4. Using GRACE as a constraint to derive subsurface storage dynamics from satellite soil moisture

Q10: Can daily GRACE TWS be used as a constraint to estimate sub-seasonal subsurface storage variability from satellite SSM?

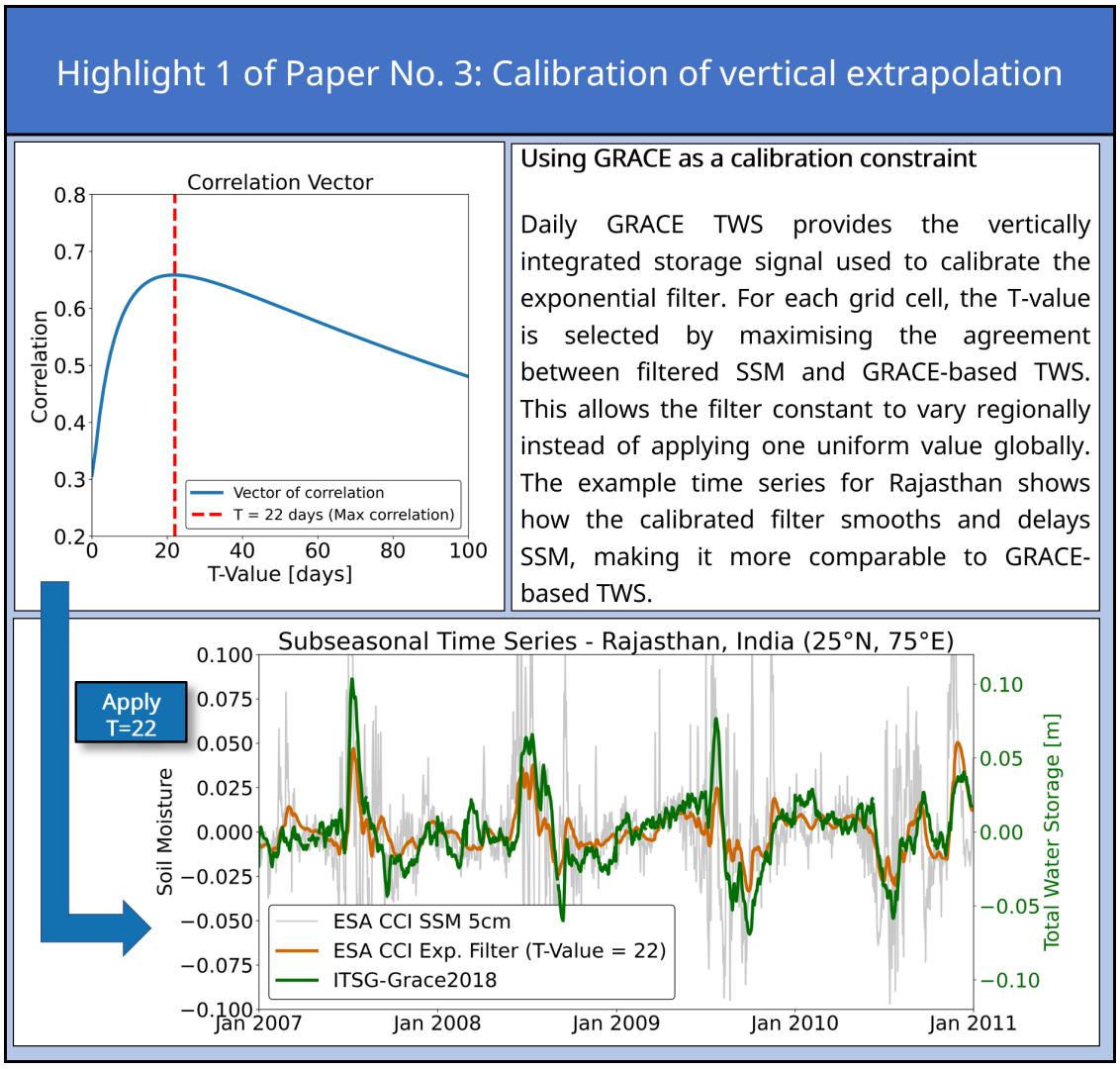

Figure 5.11.: Conceptual illustration of the GRACE-constrained exponential filter approach used in Paper 3. For each grid cell, an optimal time constant T is calibrated against GRACE-based TWS and subsequently applied to SSM to estimate subsurface storage dynamics. The shown time series illustrates the approach for an exemplary grid cell, while the calibration itself is applied globally.

The results of Paper 3 demonstrate that satellite-derived SSM can be used to estimate sub-seasonal variability in subsurface water storage when constrained by daily GRACE-based TWS. Calibrating an exponential filter against GRACE observations enables SSM observations to be translated into estimates of subsurface storage changes. A key

advantage of using GRACE as a constraint is that the filter parameter can be estimated spatially for each grid cell, instead of applying a single globally uniform time constant. This allows the calibrated T-values to reflect regional differences in storage behaviour and provides a more locally adapted representation of subsurface storage dynamics.

To isolate subsurface storage dynamics, non-soil moisture contributions contained in the GRACE signal, such as snow and surface water storage, were removed prior to the calibration. To assess the added value of GRACE constraints for short-term storage dynamics, the analysis focused on sub-seasonal variability since retaining the dominant seasonal cycle would cause the calibration to be dominated by low-frequency variability. Figure 5.11 illustrates the calibration procedure. For each grid cell, the exponential filter parameter T is determined by maximising the agreement between filtered soil moisture and GRACE-based TWS. The calibrated T-value is subsequently applied to transform SSM into an estimate of subsurface storage variability.

Before applying the calibrated exponential filter, the agreement between sub-seasonal ESA CCI SSM and GRACE-based TWS is generally weak. This reflects the fundamental difference in vertical representativeness. The global area-weighted mean correlation between the original ESA CCI signal and GRACE TWS is approximately 0.19. After calibration, the global mean correlation increases to approximately 0.39, while maximum correlations reach values of up to 0.80. This represents a substantial improvement in the agreement between SSM and GRACE-based TWS. This improvement indicates that the filtered soil moisture signal captures temporal variability that is more consistent with the integrated storage dynamics represented by GRACE.

The optimised filter smooths the SSM signal and introduces a temporal delay, making it more representative of deeper storage dynamics. Consequently, the filtered signal shows substantially improved agreement with GRACE-based TWS, particularly in regions where TWS is closely linked to processes in the unsaturated zone.

The performance of the GRACE-constrained exponential filter varies across regions. The strongest improvements are found in humid regions. The filter effect is less pronounced in arid regions and in areas affected by snow, where GRACE captures storage components that are only weakly represented by SSM. These limitations indicate that TWS integrates multiple hydrological storages and cannot be fully reconstructed from soil moisture observations alone. Overall, the results demonstrate that a GRACE-constrained exponential filter provides a simple framework for estimating sub-seasonal subsurface storage dynamics from satellite-derived SSM. Although the method does not reproduce the complete TWS signal, it captures a substantial fraction of the depth-integrated variability represented by GRACE and therefore provides a practical approach for inferring subsurface storage dynamics from widely available soil moisture observations.

Q11: Does spatial calibration outperform a uniform exponential filter parametrisation?

A major advantage of GRACE-derived filter time constants is the spatial calibration, i.e. the possibility to adapt T individually for each grid cell. The results show that spatial calibration of the exponential filter parameter improves the representation of sub-seasonal TWS variability compared to a uniform parametrisation. However, the benefits are not uniform across all regions and depend on the soil moisture depth used as input layer (see Figure 4.4). Although all input depths achieve similar global mean correlations of approximately 0.39 after optimisation, the regions in which they perform best differ considerably (see Figure 5 of Paper 3). This indicates that global summary statistics alone mask substantial regional differences in the optimal parametrisation. Therefore, the results show that no single input depth yields optimal performance globally. Instead, the optimal input depth for the filter parametrisation varies across regions.

The benefits of spatial calibration are most evident in regions where shallow soil moisture input layers lead to the highest agreement with GRACE. In these regions, locally optimised T-values appear to better capture regional differences in storage dynamics than a globally uniform parametrisation. This behaviour is particularly visible in parts of the high northern latitudes. In contrast, regions where deeper soil moisture input layers perform best generally show smaller gains from spatial optimisation. This is likely because these products are not independent surface observations, but have already been extrapolated towards deeper soil layers using depth-dependent filter settings. Part of the smoothing and delay needed to approximate the GRACE-based storage signal is therefore already contained in the input data. In such cases, an additional spatial optimisation of T has a smaller effect than for shallow SSM inputs, where the full adjustment from surface variability towards integrated storage dynamics has to be introduced by the GRACE-calibrated filter.

Overall, the results indicate that spatial calibration does not necessarily lead to a substantially higher global mean agreement. Still, it provides a more regionally adaptive representation of subsurface storage dynamics than a globally uniform parametrisation. This leads to an improved representation of subsurface dynamics in various regions. The findings therefore support the use of GRACE as a large-scale observational constraint for estimating spatially varying filter parameters and highlight the importance of accounting for regional differences in subsurface storage behaviour.

Q12: What is the benefit of regionally adapted GRACE-optimised filter time constants for interpreting underlying controls on subsurface storage dynamics?

As shown in the previous research question, using gridded GRACE data as a reference allows the estimation of regionally optimised time constants T of the exponential filter. This means that the calibrated T-values are not fixed globally, but can vary between regions. This spatial variability is useful because it allows the T-values themselves to be analysed. The results show that the spatial distribution of T is not random but follows coherent regional patterns. These patterns suggest that the estimated time constants reflect large-scale climatic, soil and subsurface controls on storage dynamics.

As one of the physical controls, the mean SSM from the ESA CCI data set is used. It represents the long-term average over the 20-year period and serves as a proxy to distinguish between wetter and drier regions. Wetter regions generally exhibit shorter time constants, indicating a relatively rapid adjustment of integrated storage to surface forcing. In contrast, dry regions tend to exhibit longer time constants, suggesting slower responses and longer integration of anomalies within the subsurface. This is plausible because in drier regions, less water is available to reach deeper layers, so the connection between SSM and integrated storage is weaker and slower. This interpretation is consistent with the findings of Paper 2, where storage deficits in drier regions also tended to show longer recovery times.

Soil texture also influences the estimated time constants. Regions with low clay content generally exhibit shorter time constants, whereas soils with a higher clay content tend to show larger values. Higher clay content is typically associated with slower water movement and reduced vertical transport. As a result, variations in water storage tend to be integrated over longer periods, leading to larger values of T. This is also consistent with the results from Paper 2.

Water table depth shows a similar relationship. Regions with shallow groundwater tables generally exhibit shorter time constants, whereas deeper groundwater systems tend to have larger values. This suggests that thicker unsaturated zones increase the delay between surface forcing and the resulting integrated storage response. However, in regions with strong groundwater flow or human influences, the estimated time constants may reflect additional processes not directly attributable to soil moisture dynamics.

Overall, the optimised time constants exhibit coherent large-scale spatial patterns and appear to reflect the combined influence of climate, soil properties, and subsurface structure on storage dynamics. Although they should not be interpreted as direct physical parameters, they provide observation-based indicators of the effective response time of subsurface storage systems at sub-seasonal timescales. The observed relationships

represent general tendencies rather than strict causal links, as multiple environmental controls interact simultaneously within the hydrological system.

Q13: How does the optimised T-value vary across soil moisture products with different soil depths?

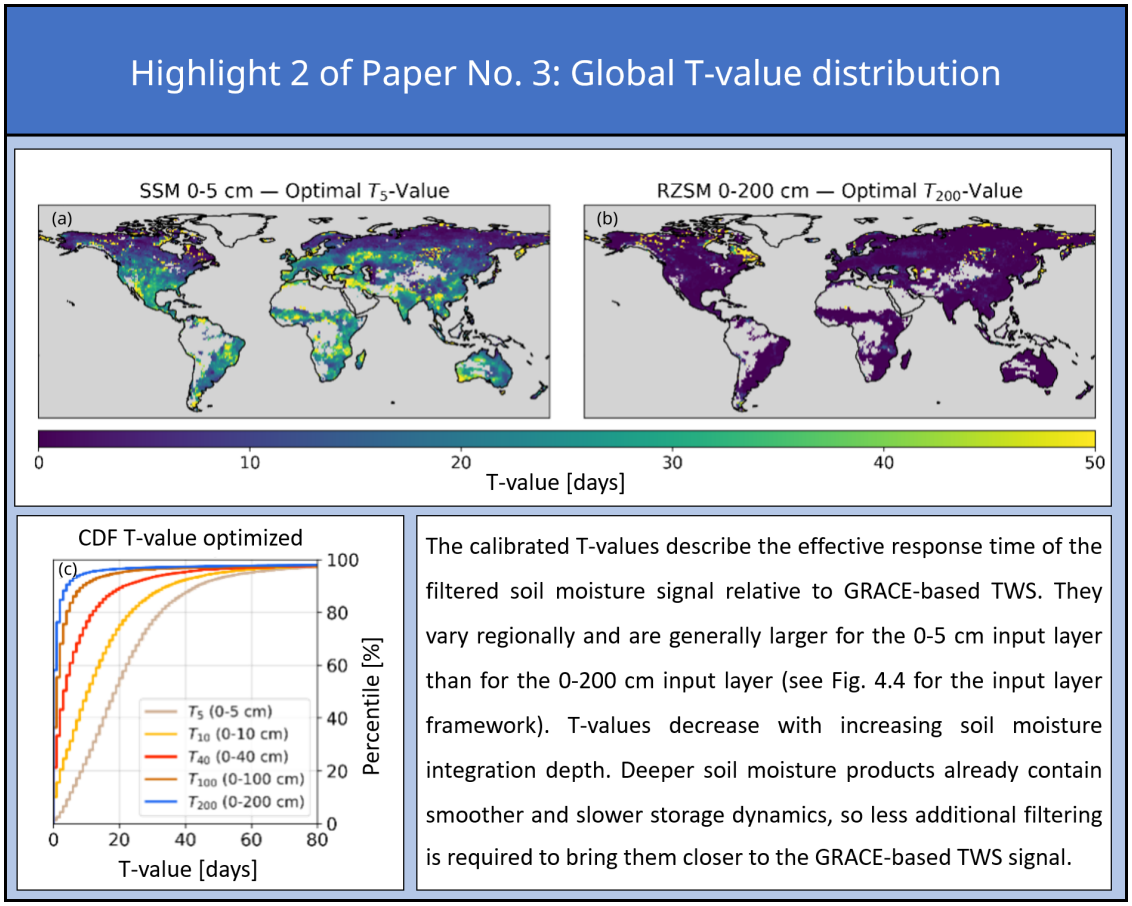

Figure 5.12.: Global distribution of GRACE-optimised exponential filter time constants for different soil moisture integration depths, based on Paper 3.

As expected, the results of Paper 3 show a clear dependence of the optimised T-value on the integration depth of the input soil moisture data. Larger T-values are obtained for shallow SSM products, whereas T decreases systematically as deeper soil layers are included. For SSM (0–5 cm), the global mean T is approximately 24 days (median: 16 days). In contrast, the ESA CCI RZSM product (0–200 cm) exhibits a mean T of about 5 days and a median close to 0 days.

Deeper soil moisture products already capture a larger fraction of the sub-seasonal variability represented by GRACE. Shallow surface measurements require stronger temporal smoothing and larger temporal shifts to represent subsurface storage dynamics inferred from GRACE. This is demonstrated by the decreasing T-values as the depth of the

analysed layer increases. The global average of T-values is approximately 17 days for the 0-10 cm layer, 11 days for the 0-40 cm layer, and 7 days for the 0-100 cm layer. The CDF shown in Figure 5.12 further demonstrates this behaviour, revealing a systematic shift towards smaller T-values as the integration depth increases.

Overall, the systematic decrease in T with increasing integration depth indicates that part of the temporal smoothing needed to match GRACE-based TWS is already captured by deeper soil moisture products. This supports the interpretation that increasing soil depth leads to storage dynamics that are more similar to the vertically integrated behaviour observed by GRACE. This finding is consistent with the results of Papers 1 and 2, which showed increasing agreement between soil moisture and GRACE TWS as integration depth increased.

6. Summary and Outlook

6.1. Summary

This dissertation examined how water storage signals change from SSM towards deeper and vertically integrated storage observed by GRACE. It uses daily satellite soil moisture observations and daily GRACE-based TWS to analyse both the timing and the depth-dependence of subsurface storage variability at the global scale. Satellite soil moisture products provide information on the near-surface, but their direct sensitivity is limited to the upper few centimetres of the soil. In contrast, GRACE and GRACE-FO observe vertically integrated changes in TWS but cannot distinguish between individual storage compartments. Combining both observation types helps to examine how short-term SSM variations are reflected in deeper and more integrated storage changes observed by GRACE.

The results of this thesis demonstrate that soil moisture and GRACE-based TWS are systematically related. This relationship is stronger and closer in time for deeper soil moisture products, depends on whether seasonal or short-term variability is analysed, and is further shaped by product-specific processing and regional hydrological conditions. Paper 1 established the observational basis for this interpretation by comparing several satellite-derived SSM and RZSM products with daily GRACE-based TWS. The analysis shows that correlations generally increase with the depth represented by the soil moisture product. Shallow SSM products capture rapid near-surface fluctuations, whereas root-zone and assimilation-based products show stronger agreement with GRACE-based TWS because they better represent deeper and temporally integrated storage dynamics. The time-shift analysis revealed that SSM often precedes TWS changes by 1 to 2 months, with global median lags of about -35 days for surface products, while RZSM products exhibit shorter lags and closer temporal alignment with GRACE, thereby further supporting this interpretation. In Paper 1, the high-pass filtered analysis showed that significant correlations between soil moisture and GRACE-based TWS remain in numerous regions. This indicates that daily GRACE solutions capture storage variations on timescales of days to weeks, which would be difficult to resolve using conventional monthly GRACE products.

Building on this observational relationship, Paper 2 investigated how de-seasonalised water storage deficits propagate through subsurface storage compartments. The results show a systematic storage-based drought cascade, where deficits emerge rapidly in SSM, become smoother and more persistent in the root zone, and accumulate over time as storage anomalies in the TWS signal observed by GRACE. The rate-of-change and recovery-time analyses provide a statistical alternative to conventional onset–end based drought-event comparisons and quantify this behaviour by demonstrating longer recovery times from SSM to RZSM and TWS.

Paper 3 translated these findings into a methodological framework that uses daily GRACE-based TWS as a constraint for estimating sub-seasonal subsurface storage dynamics from satellite-derived SSM. Calibrating an exponential filter against GRACE substantially improved the agreement between ESA CCI SSM and TWS. The global area-weighted mean correlation increased from approximately 0.19 to 0.39, while local maximum correlations reached values of up to 0.80. The calibrated T-values show coherent regional patterns. They are largest for SSM and decrease for deeper soil moisture layers. This suggests that deeper products already include slower storage dynamics and therefore require less additional filtering to become consistent with the integrated TWS signal observed by GRACE.

All three papers demonstrate the added value of daily satellite gravimetry for analysing subsurface water storage dynamics beyond the temporal resolution of conventional monthly GRACE products. In Paper 1, the daily solutions enabled the comparison of soil moisture and TWS not only at seasonal scales but also at sub-monthly timescales, where short-term storage variations can still be detected in regions with sufficiently strong hydrological signals. The daily temporal resolution also enabled more precise analysis of temporal shifts between soil moisture and TWS, including lags occurring within a single month. In Paper 2, the daily temporal resolution enabled the drying and recovery processes of water storage deficits to be analysed more continuously, avoiding the restriction to monthly drought data. It also enabled the investigation of short-term deficits, which would be difficult to characterise with monthly observations alone. In Paper 3, daily GRACE observations provided the temporal information needed to constrain sub-seasonal storage dynamics from satellite-derived SSM using an exponential filter. This approach would not be feasible in the same way with monthly data. Across all three studies, daily GRACE therefore acted not only as an integrated storage observation but also as a temporal constraint for investigating short-term subsurface storage processes at the global scale.

The main contribution of this dissertation is therefore the development of an integrated observational framework for analysing subsurface water storage dynamics using daily GRACE and satellite soil moisture observations. The work shows that daily GRACE data

can extend the analysis of TWS beyond conventional monthly variations and provide information on sub-monthly to sub-seasonal hydrological processes. At the same time, the thesis highlights the limitations of such analyses. GRACE-based TWS remains an integrated signal that includes multiple storage compartments and has limited spatial resolution. Nevertheless, by combining both observation types in a consistent spatial, temporal, and spectral framework, this thesis demonstrates that satellite observations can provide new insight into the temporal and depth-dependent dynamics of subsurface water storage at the global scale.

6.2. Outlook

The results of this dissertation open several directions for future research. A first important direction concerns the further exploitation of daily and high-frequency satellite gravimetry. This thesis has shown that daily GRACE solutions contain hydrologically meaningful information at sub-monthly scales. However, the interpretation of these signals remains challenging because daily gravity fields are noisier than monthly products and have an even coarser spatial resolution. Future improvements in GRACE and GRACE-FO processing could therefore enhance the detectability of short-term TWS variations. In addition, upcoming satellite gravity missions and multi-pair constellation concepts are expected to provide improved spatial and temporal resolution (Daras et al., 2024; Kusche et al., 2025). Such developments would directly benefit the type of analyses presented in this thesis, because they could allow short-term storage dynamics to be studied in greater regional detail and with reduced noise. This would be particularly relevant for analysing rapid hydrological responses to precipitation extremes, floods, and drought recovery processes. Technical improvements in satellite soil moisture retrievals would provide an additional benefit, especially if future products offer more reliable information on root-zone or vertically integrated soil moisture dynamics. In addition, emerging geodetic observation techniques such as GNSS-R, including the HydroGNSS mission, could provide complementary information on SSM dynamics. Together with satellite gravimetry, this would further expand the geodetic observational basis of this dissertation and enable the investigation of water storage dynamics using independent yet complementary geodetic measurements.

Another important challenge is the improved separation of individual storage compartments within GRACE-based TWS. Throughout this thesis, GRACE has been used as an integrated measure of TWS, with soil moisture interpreted as one important component of this signal. However, TWS also includes groundwater, surface water, snow, and ice. These components can dominate the GRACE signal in certain regions and seasons,

thereby complicating the interpretation of the soil moisture–TWS relationship. Paper 3 already addressed this issue by removing snow and surface-water storage where suitable data were available, but this remains an approximation. Future work should further combine GRACE observations with independent global data sets at a daily temporal resolution of snow water equivalent, surface-water storage, groundwater, and glacier or ice mass change. This would help to more accurately isolate subsurface storage variability and improve the physical interpretation of the relationship between satellite soil moisture and TWS.

A further step would be to move beyond a single-parameter link between SSM and deeper storage. The exponential filter used in Paper 3 is useful because it translates SSM variations into a smoother and delayed storage signal. However, it assumes one effective response time for the whole subsurface system. This is a simplification, because water moving through the unsaturated zone may respond on different timescales. Future approaches could, therefore, include multi-parameter formulations that better represent different response times within the unsaturated zone and groundwater. These developments could also be integrated into hydrological modelling frameworks, where daily GRACE and soil moisture observations may provide useful constraints for evaluating modelled soil moisture profiles, drought propagation, storage recovery, and subsurface storage memory.

The drought cascade analysis could also be extended to broader applications and additional storage compartments. Paper 2 focused on soil moisture and TWS, but the framework could be expanded to include indicators related to snow, surface water, groundwater, and vegetation. This would allow drought propagation to be examined more comprehensively across the terrestrial water cycle, from precipitation deficits to ecosystem impacts and hydrological storage deficits. The framework developed in Paper 2 also offers opportunities for broader applications. While the analysis focused mainly on the recovery of water storage deficits, the same rate-of-change approach could also be applied to positive storage anomalies. This would allow the investigation of water storage surplus and antecedent wetness conditions before flood events. Such an extension could help assess how rapidly different storage compartments accumulate water and how this accumulation contributes to flood susceptibility.

Finally, future studies should investigate the regional dependencies identified in this thesis in more detail. Many results show strong spatial variability, including soil moisture and TWS correlations, temporal shifts, recovery times, and optimised filter parameters. These patterns are likely controlled by interacting factors such as climate, soil texture, vegetation, topography, groundwater depth, and human water management. A more detailed multi-factorial analysis could help separate the influence of individual controls.

However, such an analysis would benefit strongly from observations with finer spatial resolution, as the coarse resolution of current GRACE-based TWS products limits the interpretation of regional-scale processes and mainly allows broad, large-scale tendencies to be assessed.

Overall, the results of this dissertation show that daily satellite gravimetry and satellite soil moisture observations provide complementary information on subsurface water storage dynamics. Future research should build on this complementarity by improving the separation of storage components, refining the physical interpretation of depth-dependent response times, developing more flexible modelling approaches, and exploiting improved gravity missions. These developments would strengthen the role of satellite observations in monitoring TWS and enhance our understanding of subsurface hydrological processes.

References

A, Geruo, John Wahr, and Shijie Zhong (2013). 'Computations of the viscoelastic response of a 3-D compressible Earth to surface loading: an application to Glacial Isostatic Adjustment in Antarctica and Canada'. en. In: *Geophysical Journal International* 192.2, pp. 557–572. ISSN: 0956-540X, 1365-246X. DOI: 10.1093/gji/ggs030.

Abelen, Sarah (2016). 'Signals of Weather Extremes in Soil Moisture and Terrestrial Water Storage from Multi-Sensor Earth Observations and Hydrological Modeling'. en. PhD Thesis. Technische Universität München.

Abelen, Sarah and Florian Seitz (2013). 'Relating satellite gravimetry data to global soil moisture products via data harmonization and correlation analysis'. en. In: *Remote Sensing of Environment* 136, pp. 89–98. ISSN: 00344257. DOI: 10.1016/j.rse.2013.04.012.

Abelen, Sarah, Florian Seitz, Rodrigo Abarca-del Rio, and Andreas Güntner (2015). 'Droughts and Floods in the La Plata Basin in Soil Moisture Data and GRACE'. en. In: *Remote Sensing* 7.6, pp. 7324–7349. ISSN: 2072-4292. DOI: 10.3390/rs70607324.

Aberle, Helmut and Ralf Bill (2026). *Sensoren und Atmosphäre*. URL: https://learn.opengeoedu.de/fernerkundung/vorlesung/Fernerkundung/grundlagen/teil_201 (accessed 02/05/2026).

Abich, Klaus, Alexander Abramovici, Bengie Amparan, Andreas Baatzsch, Brian Bachman Okihiro, David C. Barr, Maxime P. Bize, Christina Bogan, Claus Braxmaier, Michael J. Burke, Ken C. Clark, Christian Dahl, Katrin Dahl, Karsten Danzmann, Mike A. Davis, Glenn De Vine, Jeffrey A. Dickson, Serge Dubovitsky, Andreas Eckardt, Thomas Ester, Germán Fernández Barranco, Reinhold Flatscher, Frank Flechtner, William M. Folkner, Samuel Francis, Martin S. Gilbert, Frank Gilles, Martin Gohlke, Nicolas Grossard, Burghardt Guenther, Philipp Hager, Jerome Hauden, Frank Heine, Gerhard Heinzel, Mark Herding, Martin Hinz, James Howell, Mark Katsumura, Marina Kaufer, William Klipstein, Alexander Koch, Micah Kruger, Kameron Larsen, Anton Lebeda, Arnold Lebeda, Thomas Leikert, Carl Christian Liebe, Jehhal Liu, Lynette Lobmeyer, Christoph Mahrdt, Thomas Mangoldt, Kirk McKenzie, Malte Misfeldt, Phillip R. Morton, Vitali Müller, Alexander T. Murray, Don J. Nguyen, Kolja Nicklaus, Robert Pierce, Joshua A. Ravich, Gretchen Reavis, Jens Reiche, Josep Sanjuan, Daniel Schütze, Christoph Seiter,

Daniel Shaddock, Benjamin Sheard, Michael Sileo, Robert Spero, Gary Spiers, Gunnar Stede, Michelle Stephens, Andrew Sutton, Joseph Trinh, Kai Voss, Duo Wang, Rabi T. Wang, Brent Ware, Henry Wegener, Steve Windisch, Christopher Woodruff, Bernd Zender, and Marcus Zimmermann (2019). 'In-Orbit Performance of the GRACE Follow-on Laser Ranging Interferometer'. en. In: *Physical Review Letters* 123.3, p. 031101. ISSN: 0031-9007, 1079-7114. DOI: 10.1103/PhysRevLett.123.031101.

Al Bitar, Ahmad, Delphine Leroux, Yann H. Kerr, Olivier Merlin, Philippe Richaume, Alok Sahoo, and Eric F. Wood (2012). 'Evaluation of SMOS Soil Moisture Products Over Continental U.S. Using the SCAN/SNOTEL Network'. In: *IEEE Transactions on Geoscience and Remote Sensing* 50.5, pp. 1572–1586. ISSN: 0196-2892, 1558-0644. DOI: 10.1109/TGRS.2012.2186581.

Al Bitar, Ahmad and Ali Mahmoodi (2020). *Algorithm Theoretical Basis Document (ATBD) for the SMOS Level 4 Root Zone Soil Moisture*. en. Tech. rep. Version Number: v30_01. Zenodo. DOI: 10.5281/ZENODO.4298572.

Al Bitar, Ahmad, Arnaud Mialon, Yann H. Kerr, François Cabot, Philippe Richaume, Elsa Jacquette, Arnaud Quesney, Ali Mahmoodi, Stéphane Tarot, Marie Parrens, Amen Al-Yaari, Thierry Pellarin, Nemesio Rodriguez-Fernandez, and Jean-Pierre Wigneron (2017). 'The global SMOS Level 3 daily soil moisture and brightness temperature maps'. en. In: *Earth System Science Data* 9.1, pp. 293–315. ISSN: 1866-3516. DOI: 10.5194/essd-9-293-2017.

Albergel, C., C. Rüdiger, T. Pellarin, J.-C. Calvet, N. Fritz, F. Froissard, D. Suquia, A. Petitpa, B. Piguet, and E. Martin (2008). 'From near-surface to root-zone soil moisture using an exponential filter: an assessment of the method based on in-situ observations and model simulations'. en. In: *Hydrology and Earth System Sciences* 12.6, pp. 1323–1337. ISSN: 1607-7938. DOI: 10.5194/hess-12-1323-2008.

Albergel, Clement, Patricia De Rosnay, Claire Gruhier, Joaquin Muñoz-Sabater, Stefan Hasenauer, Lars Isaksen, Yann Kerr, and Wolfgang Wagner (2012). 'Evaluation of remotely sensed and modelled soil moisture products using global ground-based in situ observations'. en. In: *Remote Sensing of Environment* 118, pp. 215–226. ISSN: 00344257. DOI: 10.1016/j.rse.2011.11.017.

Barthelmes, Franz (2013). 'Definition of functionals of the geopotential and their calculation from spherical harmonic models: theory and formulas used by the calculation service of the International Centre for Global Earth Models (ICGEM); http://icgem.gfz-potsdam.de/ICGEM/ ; revised edition'. en. In: *Scientific Technical Report; 09/02; ISSN 1610-0956*. DOI: 10.2312/GFZ.B103-0902-26.

Beck, Hylke E., Albert I. J. M. Van Dijk, Ad De Roo, Emanuel Dutra, Gabriel Fink, Rene Orth, and Jaap Schellekens (2017). 'Global evaluation of runoff from 10 state-

of-the-art hydrological models'. en. In: *Hydrology and Earth System Sciences* 21.6, pp. 2881–2903. ISSN: 1607-7938. DOI: 10.5194/hess-21-2881-2017.

Blank, Daniel, Annette Eicker, Laura Jensen, and Andreas Güntner (2023). 'A global analysis of water storage variations from remotely sensed soil moisture and daily satellite gravimetry'. en. In: *Hydrology and Earth System Sciences* 27.13, pp. 2413–2435. ISSN: 1607-7938. DOI: 10.5194/hess-27-2413-2023.

Blank, Daniel, Annette Eicker, John T. Reager, and Andreas Güntner (2025). 'Revisiting Sub-Surface Drought Cascades With Daily Satellite Observations of Soil Moisture and Terrestrial Water Storage'. en. In: *Water Resources Research* 61.8, e2024WR039321. ISSN: 0043-1397, 1944-7973. DOI: 10.1029/2024WR039321.

Blank, Daniel, Daniel Rasche, Andreas Güntner, and Annette Eicker (2026). 'Assessing Sub-seasonal Subsurface Water Storage Dynamics Using Exponential Filtering of ESA CCI Soil Moisture and Daily GRACE Terrestrial Water Storage Data'. In: Series Title: International Association of Geodesy Symposia. Berlin, Heidelberg: Springer Berlin Heidelberg. DOI: 10.1007/1345_2026_357.

Bogena, H.R., J.A. Huisman, C. Oberdörster, and H. Vereecken (2007). 'Evaluation of a low-cost soil water content sensor for wireless network applications'. en. In: *Journal of Hydrology* 344.1-2, pp. 32–42. ISSN: 00221694. DOI: 10.1016/j.jhydrol.2007.06.032.

Bouaziz, Laurène J. E., Susan C. Steele-Dunne, Jaap Schellekens, Albrecht H. Weerts, Jasper Stam, Eric Sprokkereef, Hessel H. C. Winsemius, Hubert H. G. Savenije, and Markus Hrachowitz (2020). 'Improved Understanding of the Link Between Catchment-Scale Vegetation Accessible Storage and Satellite-Derived Soil Water Index'. en. In: *Water Resources Research* 56.3, e2019WR026365. ISSN: 0043-1397, 1944-7973. DOI: 10.1029/2019WR026365.

Brocca, L., F. Melone, T. Moramarco, W. Wagner, and S. Hasenauer (2010). 'ASCAT soil wetness index validation through in situ and modeled soil moisture data in central Italy'. en. In: *Remote Sensing of Environment* 114.11, pp. 2745–2755. ISSN: 00344257. DOI: 10.1016/j.rse.2010.06.009.

CATDS (2022a). *RZSM CATDS L4SM - 1 day global map of root zone soil moisture values from SMOS satellite*. DOI: 10.12770/316E77AF-CB72-4312-96A3-3011CC5068D4.

CATDS (2022b). *SSM CATDS L3SM Filtered - 1 day global map of soil moisture values from SMOS satellite*. en. DOI: 10.12770/9CEF422F-ED3F-4090-9556-B2E895BA2CA8.

Ceballos, Antonio, Klaus Scipal, Wolfgang Wagner, and José Martínez-Fernández (2005). 'Validation of ERS scatterometer-derived soil moisture data in the central part of

the Duero Basin, Spain'. en. In: *Hydrological Processes* 19.8, pp. 1549–1566. ISSN: 0885-6087, 1099-1085. DOI: 10.1002/hyp.5585.

Changnon, Stanley A. (1987). *Detecting Drought Conditions in Illinois*. Circular 169. Champaign, IL, USA: Illinois State Water Survey.

Chen, Jianli, James S. Famiglietti, Bridget R. Scanlon, and Matthew Rodell (2016). 'Groundwater Storage Changes: Present Status from GRACE Observations'. en. In: *Surveys in Geophysics* 37.2, pp. 397–417. ISSN: 0169-3298, 1573-0956. DOI: 10.1007/s10712-015-9332-4.

Cheng, Minkang and John Ries (2017). 'The unexpected signal in GRACE estimates of C_{20}'. en. In: *Journal of Geodesy* 91.8, pp. 897–914. ISSN: 0949-7714, 1432-1394. DOI: 10.1007/s00190-016-0995-5.

Chew, C. C. and E. E. Small (2018). 'Soil Moisture Sensing Using Spaceborne GNSS Reflections: Comparison of CYGNSS Reflectivity to SMAP Soil Moisture'. en. In: *Geophysical Research Letters* 45.9, pp. 4049–4057. ISSN: 0094-8276, 1944-8007. DOI: 10.1029/2018GL077905.

Cole, Steve and Alan Buis (2015). *NASA Soil Moisture Radar Ends Operations, Mission Science Continues*.

Cosh, Michael H., Thomas J. Jackson, Rajat Bindlish, and John H. Prueger (2004). 'Watershed scale temporal and spatial stability of soil moisture and its role in validating satellite estimates'. In: *Remote Sensing of Environment* 92.4. 2002 Soil Moisture Experiment (SMEX02), pp. 427–435. ISSN: 0034-4257. DOI: https://doi.org/10.1016/j.rse.2004.02.016.

Crossley, David, Caroline De Linage, Jacques Hinderer, Jean-Paul Boy, and James Famiglietti (2012). 'A comparison of the gravity field over Central Europe from superconducting gravimeters, GRACE and global hydrological models, using EOF analysis: Ground-satellite gravity comparisons in Europe'. en. In: *Geophysical Journal International* 189.2, pp. 877–897. ISSN: 0956540X. DOI: 10.1111/j.1365-246X.2012.05404.x.

Crow, Wade T., Eunjin Han, Dongryeol Ryu, Christopher R. Hain, and Martha C. Anderson (2017). 'Estimating annual water storage variations in medium-scale (2000–10 000 km^2) basins using microwave-based soil moisture retrievals'. en. In: *Hydrology and Earth System Sciences* 21.3, pp. 1849–1862. ISSN: 1607-7938. DOI: 10.5194/hess-21-1849-2017.

Cui, Chenyang, Jia Xu, Jiangyuan Zeng, Kun-Shan Chen, Xiaojing Bai, Hui Lu, Quan Chen, and Tianjie Zhao (2017). 'Soil Moisture Mapping from Satellites: An Intercomparison of SMAP, SMOS, FY3B, AMSR2, and ESA CCI over Two Dense Network Regions at

Different Spatial Scales'. en. In: *Remote Sensing* 10.1, p. 33. ISSN: 2072-4292. DOI: 10.3390/rs10010033.

Daras, I, G March, R Pail, C W Hughes, C Braitenberg, A Güntner, A Eicker, B Wouters, B Heller-Kaikov, T Pivetta, and A Pastorutti (2024). 'Mass-change And Geosciences International Constellation (MAGIC) expected impact on science and applications'. en. In: *Geophysical Journal International* 236.3, pp. 1288–1308. ISSN: 0956-540X, 1365-246X. DOI: 10.1093/gji/ggad472.

De Jeu, R. A. M., W. Wagner, T. R. H. Holmes, A. J. Dolman, N. C. Van De Giesen, and J. Friesen (2008). 'Global Soil Moisture Patterns Observed by Space Borne Microwave Radiometers and Scatterometers'. en. In: *Surveys in Geophysics* 29.4-5, pp. 399–420. ISSN: 0169-3298, 1573-0956. DOI: 10.1007/s10712-008-9044-0.

Dobslaw, H., I. Bergmann-Wolf, R. Dill, L. Poropat, M. Thomas, C. Dahle, S. Esselborn, R. König, and F. Flechtner (2017). 'A new high-resolution model of non-tidal atmosphere and ocean mass variability for de-aliasing of satellite gravity observations: AOD1B RL06'. en. In: *Geophysical Journal International* 211.1, pp. 263–269. ISSN: 0956-540X, 1365-246X. DOI: 10.1093/gji/ggx302.

Dorigo, W. A., W. Wagner, R. Hohensinn, S. Hahn, C. Paulik, A. Xaver, A. Gruber, M. Drusch, S. Mecklenburg, P. Van Oevelen, A. Robock, and T. Jackson (2011). 'The International Soil Moisture Network: a data hosting facility for global in situ soil moisture measurements'. en. In: *Hydrology and Earth System Sciences* 15.5, pp. 1675–1698. ISSN: 1607-7938. DOI: 10.5194/hess-15-1675-2011.

Dorigo, Wouter, Stephan Dietrich, Filipe Aires, Luca Brocca, Sarah Carter, Jean-François Cretaux, David Dunkerley, Hiroyuki Enomoto, René Forsberg, Andreas Güntner, Michaela I. Hegglin, Rainer Hollmann, Dale F. Hurst, Johnny A. Johannessen, Christian Kummerow, Tong Lee, Kari Luojus, Ulrich Looser, Diego G. Miralles, Victor Pellet, Thomas Recknagel, Claudia Ruz Vargas, Udo Schneider, Philippe Schoeneich, Marc Schröder, Nigel Tapper, Valery Vuglinsky, Wolfgang Wagner, Lisan Yu, Luca Zappa, Michael Zemp, and Valentin Aich (2021). 'Closing the Water Cycle from Observations across Scales: Where Do We Stand?' In: *Bulletin of the American Meteorological Society* 102.10, E1897–E1935. ISSN: 0003-0007, 1520-0477. DOI: 10.1175/BAMS-D-19-0316.1.

Dorigo, Wouter, pietro stradiotti, Wolfgang Preimesberger, Richard Kidd, Robin van der Schalie, Thomas Frederikse, Nemesio Rodriguez-Fernandez, and nicolas baghdadi (2024). 'ESA Climate Change Initiative Plus - Soil Moisture Algorithm Theoretical Baseline Document (ATBD) Supporting Product Version 09.0'. In: DOI: 10.5281/ZENODO.13860922.

Dorigo, Wouter, Wolfgang Wagner, Clement Albergel, Franziska Albrecht, Gianpaolo Balsamo, Luca Brocca, Daniel Chung, Martin Ertl, Matthias Forkel, Alexander Gruber, Eva Haas, Paul D. Hamer, Martin Hirschi, Jaakko Ikonen, Richard De Jeu, Richard Kidd, William Lahoz, Yi Y. Liu, Diego Miralles, Thomas Mistelbauer, Nadine Nicolai-Shaw, Robert Parinussa, Chiara Pratola, Christoph Reimer, Robin Van Der Schalie, Sonia I. Seneviratne, Tuomo Smolander, and Pascal Lecomte (2017). 'ESA CCI Soil Moisture for improved Earth system understanding: State-of-the art and future directions'. en. In: *Remote Sensing of Environment* 203, pp. 185–215. ISSN: 00344257. DOI: 10.1016/j.rse.2017.07.001.

Döll, Petra, Frank Kaspar, and Bernhard Lehner (2003). 'A global hydrological model for deriving water availability indicators: model tuning and validation'. en. In: *Journal of Hydrology* 270.1-2, pp. 105–134. ISSN: 00221694. DOI: 10.1016/S0022-1694(02)00283-4.

Eicker, Annette, Laura Jensen, Viviana Wöhnke, Henryk Dobslaw, Andreas Kvas, Torsten Mayer-Gürr, and Robert Dill (2020). 'Daily GRACE satellite data evaluate short-term hydro-meteorological fluxes from global atmospheric reanalyses'. en. In: *Scientific Reports* 10.1, p. 4504. ISSN: 2045-2322. DOI: 10.1038/s41598-020-61166-0.

Eicker, Annette, Maike Schumacher, Jürgen Kusche, Petra Döll, and Hannes Müller Schmied (2014). 'Calibration/Data Assimilation Approach for Integrating GRACE Data into the WaterGAP Global Hydrology Model (WGHM) Using an Ensemble Kalman Filter: First Results'. en. In: *Surveys in Geophysics* 35.6, pp. 1285–1309. ISSN: 0169-3298, 1573-0956. DOI: 10.1007/s10712-014-9309-8.

Entekhabi, Dara, Eni G. Njoku, Peggy E. O'Neill, Kent H. Kellogg, Wade T. Crow, Wendy N. Edelstein, Jared K. Entin, Shawn D. Goodman, Thomas J. Jackson, Joel Johnson, John Kimball, Jeffrey R. Piepmeier, Randal D. Koster, Neil Martin, Kyle C. McDonald, Mahta Moghaddam, Susan Moran, Rolf Reichle, J. C. Shi, Michael W. Spencer, Samuel W. Thurman, Leung Tsang, and Jakob Van Zyl (2010). 'The Soil Moisture Active Passive (SMAP) Mission'. In: *Proceedings of the IEEE* 98.5, pp. 704–716. ISSN: 0018-9219, 1558-2256. DOI: 10.1109/JPROC.2010.2043918.

Entekhabi, Dara, Simon Yueh, Peggy E. O'Neill, Kenneth H. Kellogg, Alexander Allen, Rajat Bindlish, Molly Brown, Shih-Yu Chan, Andreas Colliander, Wade T. Crow, Narendra Das, Gabrielle De Lannoy, R. Scott Dunbar, William N. Edelstein, Jared K. Entin, Victor Escobar, Shawn D. Goodman, Thomas J. Jackson, Bhaskar Jai, Joel Johnson, Edward Kim, Sungmin Kim, John Kimball, Randal D. Koster, Alejandro Leon, Kyle C. McDonald, Mahta Moghaddam, Parinaz Mohammed, Susan Moran, Eni G. Njoku, Jeffrey R. Piepmeier, Rolf Reichle, Frederic Rogez, Jiancheng Shi, Mark W. Spencer, Samuel W. Thurman, Leung Tsang, Jakob Van Zyl, Brian Weiss, and Robert

West (2014). *SMAP Handbook: Soil Moisture Active Passive: Mapping Soil Moisture and Freeze/Thaw from Space*. Pasadena, CA, USA: NASA Jet Propulsion Laboratory.

Escorihuela, M.J., A. Chanzy, J.P. Wigneron, and Y.H. Kerr (2010). 'Effective soil moisture sampling depth of L-band radiometry: A case study'. en. In: *Remote Sensing of Environment* 114.5, pp. 995–1001. ISSN: 00344257. DOI: 10.1016/j.rse.2009.12.011.

Famiglietti, J. S., A. Cazenave, A. Eicker, J. T. Reager, M. Rodell, and I. Velicogna (2015). 'Satellites provide the big picture'. en. In: *Science* 349.6249, pp. 684–685. ISSN: 0036-8075, 1095-9203. DOI: 10.1126/science.aac9238.

Famiglietti, J. S., M. Lo, S. L. Ho, J. Bethune, K. J. Anderson, T. H. Syed, S. C. Swenson, C. R. De Linage, and M. Rodell (2011). 'Satellites measure recent rates of groundwater depletion in California's Central Valley'. en. In: *Geophysical Research Letters* 38.3, 2010GL046442. ISSN: 0094-8276, 1944-8007. DOI: 10.1029/2010GL046442.

Farrell, W. E. (1972). 'Deformation of the Earth by surface loads'. en. In: *Reviews of Geophysics* 10.3, pp. 761–797. ISSN: 8755-1209, 1944-9208. DOI: 10.1029/RG010i003p00761.

Ford, T. W., E. Harris, and S. M. Quiring (2014). 'Estimating root zone soil moisture using near-surface observations from SMOS'. en. In: *Hydrology and Earth System Sciences* 18.1, pp. 139–154. ISSN: 1607-7938. DOI: 10.5194/hess-18-139-2014.

Fredlund, Delwyn G., Harianto Rahardjo, and Murray D. Fredlund (2012). *Unsaturated soil mechanics in engineering practice*. eng. Hoboken, N.J: John Wiley & Sons. ISBN: 978-1-118-28049-2.

Gao, Xiaodong, Xining Zhao, Luca Brocca, Daili Pan, and Pute Wu (2018). 'Testing of observation operators designed to estimate profile soil moisture from surface measurements'. en. In: *Hydrological Processes* 33.4, pp. 575–584. ISSN: 0885-6087, 1099-1085. DOI: 10.1002/hyp.13344.

Girotto, Manuela and Matthew Rodell (2019). 'Terrestrial water storage'. en. In: *Extreme Hydroclimatic Events and Multivariate Hazards in a Changing Environment*. Elsevier, pp. 41–64. ISBN: 978-0-12-814899-0. DOI: 10.1016/B978-0-12-814899-0.00002-X.

Gouweleeuw, Ben T., Andreas Kvas, Christian Gruber, Animesh K. Gain, Thorsten Mayer-Gürr, Frank Flechtner, and Andreas Güntner (2018). 'Daily GRACE gravity field solutions track major flood events in the Ganges–Brahmaputra Delta'. en. In: *Hydrology and Earth System Sciences* 22.5, pp. 2867–2880. ISSN: 1607-7938. DOI: 10.5194/hess-22-2867-2018.

Grotzinger, John and Thomas Jordan (2017). *Press/Siever Allgemeine Geologie*. de. Berlin, Heidelberg: Springer Berlin Heidelberg. ISBN: 978-3-662-48341-1 978-3-662-48342-8. DOI: 10.1007/978-3-662-48342-8.

Gruber, A., W.A. Dorigo, S. Zwieback, A. Xaver, and W. Wagner (2013). 'Characterizing Coarse-Scale Representativeness of in situ Soil Moisture Measurements from the International Soil Moisture Network'. en. In: *Vadose Zone Journal* 12.2, pp. 1–16. ISSN: 1539-1663, 1539-1663. DOI: 10.2136/vzj2012.0170.

Gruber, Alexander, Tracy Scanlon, Robin Van Der Schalie, Wolfgang Wagner, and Wouter Dorigo (2019). 'Evolution of the ESA CCI Soil Moisture climate data records and their underlying merging methodology'. en. In: *Earth System Science Data* 11.2, pp. 717–739. ISSN: 1866-3516. DOI: 10.5194/essd-11-717-2019.

Güntner, Andreas, Ehsan Sharifi, Julian Haas, Eva Boergens, Feifei Cao, Christoph Dahle, Neda Darbeheshti, Henryk Dobslaw, Inés Dussaillant, Wouter Dorigo, Frank Flechtner, Adrian Jäggi, Miriam Kosmale, Martin Lasser, Kari Luojus, Ulrich Meyer, Adam Pasik, Wolfgang Preimersberger, Claudia Ruz Vargas, and Michael Zemp (2026). *The Global Gravity-based Groundwater Product (G3P)*. DOI: 10.5194/essd-2025-797.

Güntner, Andreas, Jochen Stuck, Susanna Werth, Petra Döll, Kerstin Verzano, and Bruno Merz (2007). 'A global analysis of temporal and spatial variations in continental water storage'. en. In: *Water Resources Research* 43.5, 2006WR005247. ISSN: 0043-1397, 1944-7973. DOI: 10.1029/2006WR005247.

Han, Eunjin, Gary C. Heathman, Venkatesh Merwade, and Michael H. Cosh (2012). 'Application of observation operators for field scale soil moisture averages and variances in agricultural landscapes'. en. In: *Journal of Hydrology* 444-445, pp. 34–50. ISSN: 00221694. DOI: 10.1016/j.jhydrol.2012.03.035.

Han, Xujun, Harrie-Jan Hendricks Franssen, Xin Li, Yanlin Zhang, Carsten Montzka, and Harry Vereecken (2013). 'Joint Assimilation of Surface Temperature and L-Band Microwave Brightness Temperature in Land Data Assimilation'. en. In: *Vadose Zone Journal* 12.3, pp. 1–16. ISSN: 1539-1663, 1539-1663. DOI: 10.2136/vzj2012.0072.

Heiskanen, Weikko A. and Helmut Moritz (1967). *Physical Geodesy*. San Francisco, CA, USA: W. H. Freeman and Company.

Hillel, Daniel (2004). *Introduction to environmental soil physics*. eng. Amsterdam Boston: Elsevier Academic Press. ISBN: 978-0-12-348655-4 978-0-08-049577-4.

Hingray, Benoît, Cécile Picouet, and André Musy (2014). *Hydrology: a science for engineers*. eng. Elektronische Ressource. Boca Raton, Fla.: CRC Press. ISBN: 978-1-4665-9059-5 978-1-4665-9060-1. DOI: 10.1201/b17169.

Houborg, Rasmus, Matthew Rodell, Bailing Li, Rolf Reichle, and Benjamin F. Zaitchik (2012). 'Drought indicators based on model-assimilated Gravity Recovery and

Climate Experiment (GRACE) terrestrial water storage observations'. en. In: *Water Resources Research* 48.7, 2011WR011291. ISSN: 0043-1397, 1944-7973. DOI: 10.1029/2011WR011291.

Jackson, T.J. and T.J. Schmugge (1991). 'Vegetation effects on the microwave emission of soils'. en. In: *Remote Sensing of Environment* 36.3, pp. 203–212. ISSN: 00344257. DOI: 10.1016/0034-4257(91)90057-D.

Jensen, Laura, Annette Eicker, Tobias Stacke, and Henryk Dobslaw (2020). 'Predictive Skill Assessment for Land Water Storage in CMIP5 Decadal Hindcasts by a Global Reconstruction of GRACE Satellite Data'. In: *Journal of Climate* 33.21, pp. 9497–9509. ISSN: 0894-8755, 1520-0442. DOI: 10.1175/JCLI-D-20-0042.1.

Jiao, Jiashuang, Yuanjin Pan, Mirjam Bilker-Koivula, Markku Poutanen, and Hao Ding (2022). 'Basin Mass Changes in Finland From GRACE: Validation and Explanation'. en. In: *Journal of Geophysical Research: Solid Earth* 127.6, e2021JB023489. ISSN: 2169-9313, 2169-9356. DOI: 10.1029/2021JB023489.

Joseph, George (2005). *Fundamentals of remote sensing*. eng. 2. ed. Hyderabad: Universities Press. ISBN: 978-81-7371-535-8.

Kerr, Yann H, Philippe Waldteufel, Jean-Pierre Wigneron, Steven Delwart, François Cabot, Jacqueline Boutin, Maria-José Escorihuela, Jordi Font, Nicolas Reul, Claire Gruhier, Silvia Enache Juglea, Mark R Drinkwater, Achim Hahne, Manuel Martín-Neira, and Susanne Mecklenburg (2010). 'The SMOS Mission: New Tool for Monitoring Key Elements ofthe Global Water Cycle'. In: *Proceedings of the IEEE* 98.5, pp. 666–687. ISSN: 0018-9219, 1558-2256. DOI: 10.1109/JPROC.2010.2043032.

Kornelsen, Kurt C. and Paulin Coulibaly (2014). 'Root-zone soil moisture estimation using data-driven methods'. en. In: *Water Resources Research* 50.4, pp. 2946–2962. ISSN: 0043-1397, 1944-7973. DOI: 10.1002/2013WR014127.

Kunkee, David (2005). 'Frequency Management for Remote Sensing'. In: *IEEE Geoscience and Remote Sensing Society Newsletter* 135, pp. 18–19.

Kurtenbach, E., A. Eicker, T. Mayer-Gürr, M. Holschneider, M. Hayn, M. Fuhrmann, and J. Kusche (2012). 'Improved daily GRACE gravity field solutions using a Kalman smoother'. en. In: *Journal of Geodynamics* 59-60, pp. 39–48. ISSN: 02643707. DOI: 10.1016/j.jog.2012.02.006.

Kusche, Jürgen, Christina Strohmenger, Helena Gerdener, Bernd Uebbing, Anne Springer, Yorck Ewerdwalbesloh, Annette Eicker, Carla Braitenberg, Alberto Pastorutti, Roland Pail, Philipp Zingerle, Marius Schlaak, Mirko Reguzzoni, Lorenzo Rossi, Federica Migliaccio, and Ilias Daras (2025). 'Benefit of MAGIC and multipair quantum satellite gravity missions in Earth science applications'. en. In: *Geophysical Journal International* 242.2, ggaf195. ISSN: 0956-540X, 1365-246X. DOI: 10.1093/gji/ggaf195.

Kvas, Andreas, Saniya Behzadpour, Matthias Ellmer, Beate Klinger, Sebastian Strasser, Norbert Zehentner, and Torsten Mayer-Gürr (2019). 'ITSG-Grace2018: Overview and Evaluation of a New GRACE-Only Gravity Field Time Series'. en. In: *Journal of Geophysical Research: Solid Earth* 124.8, pp. 9332–9344. ISSN: 2169-9313, 2169-9356. DOI: 10.1029/2019JB017415.

Köhli, Markus, Jannis Weimar, Martin Schrön, Roland Baatz, and Ulrich Schmidt (2021). 'Soil Moisture and Air Humidity Dependence of the Above-Ground Cosmic-Ray Neutron Intensity'. In: *Frontiers in Water* 2, p. 544847. ISSN: 2624-9375. DOI: 10.3389/frwa.2020.544847.

Lambeck, Kurt (1988). *Geophysical geodesy - The slow deformations of the earth*. Publication Title: Research supported by CNES and Universite de Paris VI. Oxford and New York ADS Bibcode: 1988oxny.book.....L.

Lamichhane, Manoj, Sushant Mehan, and Kyle R. Mankin (2025). 'Soil Moisture Prediction Using Remote Sensing and Machine Learning Algorithms: A Review on Progress, Challenges, and Opportunities'. en. In: *Remote Sensing* 17.14, p. 2397. ISSN: 2072-4292. DOI: 10.3390/rs17142397.

Landerer, Felix W., Frank M. Flechtner, Himanshu Save, Frank H. Webb, Tamara Bandikova, William I. Bertiger, Srinivas V. Bettadpur, Sung Hun Byun, Christoph Dahle, Henryk Dobslaw, Eugene Fahnestock, Nate Harvey, Zhigui Kang, Gerhard L. H. Kruizinga, Bryant D. Loomis, Christopher McCullough, Michael Murböck, Peter Nagel, Meegyeong Paik, Nadege Pie, Steve Poole, Dmitry Strekalov, Mark E. Tamisiea, Furun Wang, Michael M. Watkins, Hui-Ying Wen, David N. Wiese, and Dah-Ning Yuan (2020). 'Extending the Global Mass Change Data Record: GRACE Follow-On Instrument and Science Data Performance'. en. In: *Geophysical Research Letters* 47.12, e2020GL088306. ISSN: 0094-8276, 1944-8007. DOI: 10.1029/2020GL088306.

Larson, Kristine M., John J. Braun, Eric E. Small, Valery U. Zavorotny, Ethan D. Gutmann, and Andria L. Bilich (2010). 'GPS Multipath and Its Relation to Near-Surface Soil Moisture Content'. In: *IEEE Journal of Selected Topics in Applied Earth Observations and Remote Sensing* 3.1, pp. 91–99. ISSN: 1939-1404, 2151-1535. DOI: 10.1109/JSTARS.2009.2033612.

Larson, Kristine M., Eric E. Small, J. Braun, and Vladimir Zavorotny (2014). 'Environmental Sensing: A Revolution in GNSS Applications'. In: *Inside GNSS* 9.4, pp. 36–46.

Larson, Kristine M., Eric E. Small, Ethan Gutmann, Andria Bilich, Penina Axelrad, and John Braun (2008). 'Using GPS multipath to measure soil moisture fluctuations: initial results'. en. In: *GPS Solutions* 12.3, pp. 173–177. ISSN: 1080-5370, 1521-1886. DOI: 10.1007/s10291-007-0076-6.

Lei, Fangni, Wade Crow, Huanfeng Shen, Robert Parinussa, and Thomas Holmes (2015). 'The Impact of Local Acquisition Time on the Accuracy of Microwave Surface Soil Moisture Retrievals over the Contiguous United States'. en. In: *Remote Sensing* 7.10, pp. 13448–13465. ISSN: 2072-4292. DOI: 10.3390/rs71013448.

Lekshmi, S.U., D.N. Singh, and Maryam Shojaei Baghini (2014). 'A critical review of soil moisture measurement'. en. In: *Measurement* 54, pp. 92–105. ISSN: 02632241. DOI: 10.1016/j.measurement.2014.04.007.

Li, Bailing, Matthew Rodell, Sujay Kumar, Hiroko Kato Beaudoing, Augusto Getirana, Benjamin F. Zaitchik, Luis Gustavo De Goncalves, Camila Cossetin, Soumendra Bhanja, Abhijit Mukherjee, Siyuan Tian, Natthachet Tangdamrongsub, Di Long, Jamiat Nanteza, Jejung Lee, Frederick Policelli, Ibrahim B. Goni, Djoret Daira, Mohammed Bila, Gabriëlle De Lannoy, David Mocko, Susan C. Steele-Dunne, Himanshu Save, and Srinivas Bettadpur (2019). 'Global GRACE Data Assimilation for Groundwater and Drought Monitoring: Advances and Challenges'. en. In: *Water Resources Research* 55.9, pp. 7564–7586. ISSN: 0043-1397, 1944-7973. DOI: 10.1029/2018WR024618.

Lundin, Lars-Christer, Sten Bergström, Erik Eriksson, and Jan Seibert (2000). 'Hydrological Models and Modelling: The Waterscape'. In: *Sustainable Water Management in the Baltic Sea Basin*. 2nd ed. Vol. 1. Uppsala, Sweden: Uppsala University.

Mahmood, Rezaul and Kenneth G. Hubbard (2007). 'Relationship between soil moisture of near surface and multiple depths of the root zone under heterogeneous land uses and varying hydroclimatic conditions'. en. In: *Hydrological Processes* 21.25, pp. 3449–3462. ISSN: 0885-6087, 1099-1085. DOI: 10.1002/hyp.6578.

Manfreda, S., L. Brocca, T. Moramarco, F. Melone, and J. Sheffield (2014). 'A physically based approach for the estimation of root-zone soil moisture from surface measurements'. en. In: *Hydrology and Earth System Sciences* 18.3, pp. 1199–1212. ISSN: 1607-7938. DOI: 10.5194/hess-18-1199-2014.

Montzka, Carsten, Heye Bogena, Marek Zreda, Alessandra Monerris, Ross Morrison, Sekhar Muddu, and Harry Vereecken (2017). 'Validation of Spaceborne and Modelled Surface Soil Moisture Products with Cosmic-Ray Neutron Probes'. en. In: *Remote Sensing* 9.2, p. 103. ISSN: 2072-4292. DOI: 10.3390/rs9020103.

Müller Schmied, Hannes, Tim Trautmann, Sebastian Ackermann, Denise Cáceres, Martina Flörke, Helena Gerdener, Ellen Kynast, Thedini Asali Peiris, Leonie Schiebener, Maike Schumacher, and Petra Döll (2024). 'The global water resources and use model WaterGAP v2.2e: description and evaluation of modifications and new features'. en. In: *Geoscientific Model Development* 17.23, pp. 8817–8852. ISSN: 1991-9603. DOI: 10.5194/gmd-17-8817-2024.

Ochsner, Tyson E., Michael H. Cosh, Richard H. Cuenca, Wouter A. Dorigo, Clara S. Draper, Yutaka Hagimoto, Yann H. Kerr, Kristine M. Larson, Eni G. Njoku, Eric E. Small, and Marek Zreda (2013). 'State of the Art in Large-Scale Soil Moisture Monitoring'. en. In: *Soil Science Society of America Journal* 77.6, pp. 1888–1919. ISSN: 03615995. DOI: 10.2136/sssaj2013.03.0093.

Omondi, Philip Aming'o, Joseph L. Awange, Ehsan Forootan, Laban Ayieko Ogallo, Ruben Barakiza, Gezahegn Bogale Girmaw, Isaac Fesseha, Venerabilis Kululetera, Caroline Kilembe, Mathieu Mugunga Mbati, Mary Kilavi, Stephen Mutua King'uyu, Peter Adek Omeny, Andrew Njogu, Eldin Mamoun Badr, Tibin Adam Musa, Peris Muchiri, Deus Bamanya, and Everline Komutunga (2014). 'Changes in temperature and precipitation extremes over the Greater Horn of Africa region from 1961 to 2010'. en. In: *International Journal of Climatology* 34.4, pp. 1262–1277. ISSN: 0899-8418, 1097-0088. DOI: 10.1002/joc.3763.

O'Neill, Peggy, Steven Chan, Eni Njoku, Thomas Jackson, Rajat Bindlish, and Julian Chaubell (2023). *SMAP L3 Radiometer Global Daily 36 km EASE-Grid Soil Moisture, Version 9*. DOI: 10.5067/4XXOGXOOOW1S.

OpenAI (2026). *Generative AI outputs (ChatGPT v5.2, DALL · E v4)*.

Overgaard, J., D. Rosbjerg, and M. B. Butts (2006). 'Land-surface modelling in hydrological perspective – a review'. en. In: *Biogeosciences* 3.2, pp. 229–241. ISSN: 1726-4189. DOI: 10.5194/bg-3-229-2006.

Owe, M., R. De Jeu, and J. Walker (2001). 'A methodology for surface soil moisture and vegetation optical depth retrieval using the microwave polarization difference index'. In: *IEEE Transactions on Geoscience and Remote Sensing* 39.8, pp. 1643–1654. ISSN: 01962892. DOI: 10.1109/36.942542.

Pan, Xiaojun, Kurt C. Kornelsen, and Paulin Coulibaly (2017). 'Estimating Root Zone Soil Moisture at Continental Scale Using Neural Networks'. en. In: *JAWRA Journal of the American Water Resources Association* 53.1, pp. 220–237. ISSN: 1093-474X, 1752-1688. DOI: 10.1111/1752-1688.12491.

Parinussa, R. M., T. R. H. Holmes, M. T. Yilmaz, and W. T. Crow (2011). 'The impact of land surface temperature on soil moisture anomaly detection from passive microwave observations'. en. In: *Hydrology and Earth System Sciences* 15.10, pp. 3135–3151. ISSN: 1607-7938. DOI: 10.5194/hess-15-3135-2011.

Pasik, Adam, Alexander Gruber, Wolfgang Preimesberger, Domenico De Santis, and Wouter Dorigo (2023). 'Uncertainty estimation for a new exponential-filter-based long-term root-zone soil moisture dataset from Copernicus Climate Change Service (C3S) surface observations'. en. In: *Geoscientific Model Development* 16.17, pp. 4957–4976. ISSN: 1991-9603. DOI: 10.5194/gmd-16-4957-2023.

Paulik, Christoph, Wouter Dorigo, Wolgang Wagner, and Richard Kidd (2014). 'Validation of the ASCAT Soil Water Index using in situ data from the International Soil Moisture Network'. en. In: *International Journal of Applied Earth Observation and Geoinformation* 30, pp. 1–8. ISSN: 15698432. DOI: 10.1016/j.jag.2014.01.007.

Peltier, Richard, Donald F. Argus, and Rosemarie Drummond (2018). 'Comment on "An Assessment of the ICE-6G_C (VM5a) Glacial Isostatic Adjustment Model" by Purcell et al.' en. In: *Journal of Geophysical Research: Solid Earth* 123.2, pp. 2019–2028. ISSN: 2169-9313, 2169-9356. DOI: 10.1002/2016JB013844.

Preimesberger, Wolfgang, Tracy Scanlon, Chun-Hsu Su, Alexander Gruber, and Wouter Dorigo (2021). 'Homogenization of Structural Breaks in the Global ESA CCI Soil Moisture Multisatellite Climate Data Record'. In: *IEEE Transactions on Geoscience and Remote Sensing* 59.4, pp. 2845–2862. ISSN: 0196-2892, 1558-0644. DOI: 10.1109/TGRS.2020.3012896.

Preisendorfer, Rudolph W. and Curtis D. Mobley (1988). *Principal component analysis in meteorology and oceanography*. Developments in atmospheric science 17. Amsterdam ; New York : New York, NY, U.S.A: Elsevier ; Distributors for the U.S. and Canada, Elsevier Science Pub. Co. ISBN: 978-0-444-43014-4.

Rahmati, Mehdi (2024). *mehdirmti/Coherence-delay map plotter*. DOI: 10.5281/ZENODO.13992031.

Ramillien, G., J. S. Famiglietti, and J. Wahr (2008). 'Detection of Continental Hydrology and Glaciology Signals from GRACE: A Review'. en. In: *Surveys in Geophysics* 29.4-5, pp. 361–374. ISSN: 0169-3298, 1573-0956. DOI: 10.1007/s10712-008-9048-9.

Ramillien, G., A. Lombard, A. Cazenave, E.R. Ivins, M. Llubes, F. Remy, and R. Biancale (2006). 'Interannual variations of the mass balance of the Antarctica and Greenland ice sheets from GRACE'. en. In: *Global and Planetary Change* 53.3, pp. 198–208. ISSN: 09218181. DOI: 10.1016/j.gloplacha.2006.06.003.

Rasche, Daniel, Theresa Blume, and Andreas Güntner (2024). *Depth-extrapolation of field-scale soil moisture time series derived with cosmic-ray neutron sensing using the SMAR model*. DOI: 10.5194/egusphere-2024-170.

Reager, J. T. and J. S. Famiglietti (2009). 'Global terrestrial water storage capacity and flood potential using GRACE'. en. In: *Geophysical Research Letters* 36.23, 2009GL040826. ISSN: 0094-8276, 1944-8007. DOI: 10.1029/2009GL040826.

Reichle, Rolf, Gabrielle De Lannoy, Randal Koster, Wade Crow, John Kimball, Qing Liu, and Michel Bechtold (2022). *SMAP L4 Global 3-hourly 9 km EASE-Grid Surface and Root Zone Soil Moisture Geophysical Data, Version 7*. DOI: 10.5067/EVKPQZ4AFC4D.

Retegui-Schiettekatte, Leire, Maike Schumacher, Henrik Madsen, and Ehsan Forootan (2025). 'Assessing daily GRACE Data Assimilation during flood events of the Brahma-

putra River Basin'. en. In: *Science of The Total Environment* 975, p. 179181. ISSN: 00489697. DOI: 10.1016/j.scitotenv.2025.179181.

Robinson, D. A., C. S. Campbell, J. W. Hopmans, B. K. Hornbuckle, S. B. Jones, R. Knight, F. Ogden, J. Selker, and O. Wendroth (2008). 'Soil Moisture Measurement for Ecological and Hydrological Watershed-Scale Observatories: A Review'. en. In: *Vadose Zone Journal* 7.1, pp. 358–389. ISSN: 1539-1663, 1539-1663. DOI: 10.2136/vzj2007.0143.

Rodell, M., J. S. Famiglietti, D. N. Wiese, J. T. Reager, H. K. Beaudoing, F. W. Landerer, and M.-H. Lo (2018). 'Emerging trends in global freshwater availability'. en. In: *Nature* 557.7707, pp. 651–659. ISSN: 0028-0836, 1476-4687. DOI: 10.1038/s41586-018-0123-1.

Rodell, M., P. R. Houser, U. Jambor, J. Gottschalck, K. Mitchell, C.-J. Meng, K. Arsenault, B. Cosgrove, J. Radakovich, M. Bosilovich, J. K. Entin, J. P. Walker, D. Lohmann, and D. Toll (2004). 'The Global Land Data Assimilation System'. en. In: *Bulletin of the American Meteorological Society* 85.3, pp. 381–394. ISSN: 0003-0007, 1520-0477. DOI: 10.1175/BAMS-85-3-381.

Rodell, Matthew, Isabella Velicogna, and James S. Famiglietti (2009). 'Satellite-based estimates of groundwater depletion in India'. en. In: *Nature* 460.7258, pp. 999–1002. ISSN: 0028-0836, 1476-4687. DOI: 10.1038/nature08238.

Rodriguez-Alvarez, N., X. Bosch-Lluis, A. Camps, M. Vall-llossera, E. Valencia, J.F. Marchan-Hernandez, and I. Ramos-Perez (2009). 'Soil Moisture Retrieval Using GNSS-R Techniques: Experimental Results Over a Bare Soil Field'. In: *IEEE Transactions on Geoscience and Remote Sensing* 47.11, pp. 3616–3624. ISSN: 0196-2892, 1558-0644. DOI: 10.1109/TGRS.2009.2030672.

Ruf, Christopher S., Robert Atlas, Paul S. Chang, Maria Paola Clarizia, James L. Garrison, Scott Gleason, Stephen J. Katzberg, Zorana Jelenak, Joel T. Johnson, Sharanya J. Majumdar, Andrew O'brien, Derek J. Posselt, Aaron J. Ridley, Randall J. Rose, and Valery U. Zavorotny (2016). 'New Ocean Winds Satellite Mission to Probe Hurricanes and Tropical Convection'. en. In: *Bulletin of the American Meteorological Society* 97.3, pp. 385–395. ISSN: 0003-0007, 1520-0477. DOI: 10.1175/BAMS-D-14-00218.1.

Rummel, R. (2004). 'Geoid and Gravity in Earth Sciences – An Overview'. en. In: *Earth, Moon, and Planets* 94.1-2, pp. 3–11. ISSN: 0167-9295, 1573-0794. DOI: 10.1007/s11038-005-3755-8.

Rummel, R., G. Balmino, J. Johannessen, P. Visser, and P. Woodworth (2002). 'Dedicated gravity field missions—principles and aims'. en. In: *Journal of Geodynamics* 33.1-2, pp. 3–20. ISSN: 02643707. DOI: 10.1016/S0264-3707(01)00050-3.

Sadeghi, Morteza, Lun Gao, Ardeshir Ebtehaj, Jean-Pierre Wigneron, Wade T. Crow, John T. Reager, and Arthur W. Warrick (2020). 'Retrieving global surface soil moisture from GRACE satellite gravity data'. en. In: *Journal of Hydrology* 584, p. 124717. ISSN: 00221694. DOI: 10.1016/j.jhydrol.2020.124717.

Scanlon, B. R., Z. Zhang, A. Rateb, A. Sun, D. Wiese, H. Save, H. Beaudoing, M. H. Lo, H. Müller-Schmied, P. Döll, R. Van Beek, S. Swenson, D. Lawrence, M. Croteau, and R. C. Reedy (2019). 'Tracking Seasonal Fluctuations in Land Water Storage Using Global Models and GRACE Satellites'. en. In: *Geophysical Research Letters* 46.10, pp. 5254–5264. ISSN: 0094-8276, 1944-8007. DOI: 10.1029/2018GL081836.

Scanlon, Bridget R., Zizhan Zhang, Himanshu Save, Alexander Y. Sun, Hannes Müller Schmied, Ludovicus P. H. Van Beek, David N. Wiese, Yoshihide Wada, Di Long, Robert C. Reedy, Laurent Longuevergne, Petra Döll, and Marc F. P. Bierkens (2018). 'Global models underestimate large decadal declining and rising water storage trends relative to GRACE satellite data'. en. In: *Proceedings of the National Academy of Sciences* 115.6. ISSN: 0027-8424, 1091-6490. DOI: 10.1073/pnas.1704665115.

Scanlon, Bridget R., Zizhan Zhang, Himanshu Save, David N. Wiese, Felix W. Landerer, Di Long, Laurent Longuevergne, and Jianli Chen (2016). 'Global evaluation of new GRACE mascon products for hydrologic applications'. en. In: *Water Resources Research* 52.12, pp. 9412–9429. ISSN: 0043-1397, 1944-7973. DOI: 10.1002/2016WR019494.

Schmidt, Toni, Martin Schrön, Zhan Li, Till Francke, Steffen Zacharias, Anke Hildebrandt, and Jian Peng (2024). 'Comprehensive quality assessment of satellite- and model-based soil moisture products against the COSMOS network in Germany'. en. In: *Remote Sensing of Environment* 301, p. 113930. ISSN: 00344257. DOI: 10.1016/j.rse.2023.113930.

Schrön, Martin, Markus Köhli, Lena Scheiffele, Joost Iwema, Heye R. Bogena, Ling Lv, Edoardo Martini, Gabriele Baroni, Rafael Rosolem, Jannis Weimar, Juliane Mai, Matthias Cuntz, Corinna Rebmann, Sascha E. Oswald, Peter Dietrich, Ulrich Schmidt, and Steffen Zacharias (2017). 'Improving calibration and validation of cosmic-ray neutron sensors in the light of spatial sensitivity'. en. In: *Hydrology and Earth System Sciences* 21.10, pp. 5009–5030. ISSN: 1607-7938. DOI: 10.5194/hess-21-5009-2017.

Seeber, Günter (2003). *Satellite Geodesy*. Walter de Gruyter. ISBN: 978-3-11-017549-3. DOI: 10.1515/9783110200089.

Seneviratne, Sonia I., Thierry Corti, Edouard L. Davin, Martin Hirschi, Eric B. Jaeger, Irene Lehner, Boris Orlowsky, and Adriaan J. Teuling (2010). 'Investigating soil moisture–climate interactions in a changing climate: A review'. en. In: *Earth-Science Reviews* 99.3-4, pp. 125–161. ISSN: 00128252. DOI: 10.1016/j.earscirev.2010.02.004.

Seneviratne, Sonia I., Pedro Viterbo, Daniel Lüthi, and Christoph Schär (2004). 'Inferring Changes in Terrestrial Water Storage Using ERA-40 Reanalysis Data: The Mississippi River Basin'. en. In: *Journal of Climate* 17.11, pp. 2039–2057. ISSN: 0894-8755, 1520-0442. DOI: 10.1175/1520-0442(2004)017<2039:ICITWS>2.0.CO;2.

Shiklomanov, Igor A. (1993). 'World Fresh Water Resources'. In: *Water in Crisis: A Guide to the World's Fresh Water Resources*. Ed. by Peter H. Gleick. New York, USA: Oxford University Press. ISBN: 978-0-19-507628-8.

Springer, Anne (2019). 'A water storage reanalysis over the European continent: assimilation of GRACE data into a high-resolution hydrological model and validation'. PhD thesis. Rheinische Friedrich-Wilhelms-Universität Bonn.

Springer, Anne, Gabriëlle De Lannoy, Matthew Rodell, Yorck Ewerdwalbesloh, Helena Gerdener, Mehdi Khaki, Bailing Li, Fupeng Li, Maike Schumacher, Natthachet Tangdamrongsub, Mohammad J. Tourian, Wanshu Nie, and Jürgen Kusche (2026). 'A review of current best practices and future directions in assimilating GRACE/-FO terrestrial water storage data into numerical models'. en. In: *Hydrology and Earth System Sciences* 30.4, pp. 985–1022. ISSN: 1607-7938. DOI: 10.5194/hess-30-985-2026.

Steffen, Holger, Svetozar Petrovic, Jürgen Müller, Roland Schmidt, Johann Wünsch, Franz Barthelmes, and Jürgen Kusche (2009). 'Significance of secular trends of mass variations determined from GRACE solutions'. en. In: *Journal of Geodynamics* 48.3-5, pp. 157–165. ISSN: 02643707. DOI: 10.1016/j.jog.2009.09.029.

Stradiotti, Pietro and Wolfgang Preimesberger (2025). *ESA CCI SM RZSM Long-term Climate Data Record of Root-Zone Soil Moisture from merged multi-satellite observations*. DOI: 10.48436/V8CWJ-JK556.

Sun, Alexander, Bridget Scanlon, Amir AghaKouchak, and Zizhan Zhang (2017). 'Using GRACE Satellite Gravimetry for Assessing Large-Scale Hydrologic Extremes'. en. In: *Remote Sensing* 9.12, p. 1287. ISSN: 2072-4292. DOI: 10.3390/rs9121287.

Sun, Yu, Riccardo Riva, and Pavel Ditmar (2016). 'Optimizing estimates of annual variations and trends in geocenter motion and J_2 from a combination of GRACE data and geophysical models'. en. In: *Journal of Geophysical Research: Solid Earth* 121.11, pp. 8352–8370. ISSN: 2169-9313, 2169-9356. DOI: 10.1002/2016JB013073.

Swenson, Sean, Don Chambers, and John Wahr (2008a). 'Estimating geocenter variations from a combination of GRACE and ocean model output'. en. In: *Journal of Geophysical Research: Solid Earth* 113.B8, 2007JB005338. ISSN: 0148-0227. DOI: 10.1029/2007JB005338.

Swenson, Sean, James Famiglietti, Jeffrey Basara, and John Wahr (2008b). 'Estimating profile soil moisture and groundwater variations using GRACE and Oklahoma Mesonet

soil moisture data'. en. In: *Water Resources Research* 44.1, 2007WR006057. ISSN: 0043-1397, 1944-7973. DOI: 10.1029/2007WR006057.

Syed, Tajdarul H., James S. Famiglietti, Matthew Rodell, Jianli Chen, and Clark R. Wilson (2008). 'Analysis of terrestrial water storage changes from GRACE and GLDAS'. en. In: *Water Resources Research* 44.2, 2006WR005779. ISSN: 0043-1397, 1944-7973. DOI: 10.1029/2006WR005779.

Szabó, Viktor and Katarzyna Osińska-Skotak (2023). 'Similarities and Differences in the Earth's Water Variations Signal Provided by Grace and AMSR-E Observations Using Maximum Covariance Analysis at Various Land Cover Data Backgrounds'. en. In: *Artificial Satellites* 58.2, pp. 63–87. ISSN: 2083-6104. DOI: 10.2478/arsa-2023-0006.

Tangdamrongsub, Natthachet, Shin-Chan Han, In-Young Yeo, Jianzhi Dong, Susan C. Steele-Dunne, Garry Willgoose, and Jeffrey P. Walker (2020). 'Multivariate data assimilation of GRACE, SMOS, SMAP measurements for improved regional soil moisture and groundwater storage estimates'. en. In: *Advances in Water Resources* 135, p. 103477. ISSN: 03091708. DOI: 10.1016/j.advwatres.2019.103477.

Tangdamrongsub, Natthachet, Susan C. Steele-Dunne, Brian C. Gunter, Pavel G. Ditmar, Edwin H. Sutanudjaja, Yu Sun, Ting Xia, and Zhongjing Wang (2017). 'Improving estimates of water resources in a semi-arid region by assimilating GRACE data into the PCR-GLOBWB hydrological model'. en. In: *Hydrology and Earth System Sciences* 21.4, pp. 2053–2074. ISSN: 1607-7938. DOI: 10.5194/hess-21-2053-2017.

Tapley, B. D., S. Bettadpur, M. Watkins, and C. Reigber (2004). 'The gravity recovery and climate experiment: Mission overview and early results'. en. In: *Geophysical Research Letters* 31.9, 2004GL019920. ISSN: 0094-8276, 1944-8007. DOI: 10.1029/2004GL019920.

Tapley, Byron D., Michael M. Watkins, Frank Flechtner, Christoph Reigber, Srinivas Bettadpur, Matthew Rodell, Ingo Sasgen, James S. Famiglietti, Felix W. Landerer, Don P. Chambers, John T. Reager, Alex S. Gardner, Himanshu Save, Erik R. Ivins, Sean C. Swenson, Carmen Boening, Christoph Dahle, David N. Wiese, Henryk Dobslaw, Mark E. Tamisiea, and Isabella Velicogna (2019). 'Contributions of GRACE to understanding climate change'. en. In: *Nature Climate Change* 9.5, pp. 358–369. ISSN: 1758-678X, 1758-6798. DOI: 10.1038/s41558-019-0456-2.

Thomas, Alys C., John T. Reager, James S. Famiglietti, and Matthew Rodell (2014). 'A GRACE-based water storage deficit approach for hydrological drought characterization'. en. In: *Geophysical Research Letters* 41.5, pp. 1537–1545. ISSN: 0094-8276, 1944-8007. DOI: 10.1002/2014GL059323.

Tian, Jie, Zhibo Han, Heye Reemt Bogena, Johan Alexander Huisman, Carsten Montzka, Baoqing Zhang, and Chansheng He (2020). 'Estimation of subsurface soil moisture from surface soil moisture in cold mountainous areas'. en. In: *Hydrology and Earth System Sciences* 24.9, pp. 4659–4674. ISSN: 1607-7938. DOI: 10.5194/hess-24-4659-2020.

Tian, Siyuan, Luigi J. Renzullo, Robert C. Pipunic, Julien Lerat, Wendy Sharples, and Chantal Donnelly (2021). 'Satellite soil moisture data assimilation for improved operational continental water balance prediction'. en. In: *Hydrology and Earth System Sciences* 25.8, pp. 4567–4584. ISSN: 1607-7938. DOI: 10.5194/hess-25-4567-2021.

Tong, Cheng, Xiaodong Deng, Yulin Shangguan, Baiyu Dong, Yurun Chen, Chenhao Huang, Luyao Zhu, Sinan Li, Yang Ye, and Hongquan Wang (2025). 'The passive microwave remote sensing in soil moisture retrieval: Products, models, applications and challenges'. en. In: *International Soil and Water Conservation Research* 13.4, pp. 843–859. ISSN: 20956339. DOI: 10.1016/j.iswcr.2025.06.006.

Torrence, Christopher and Gilbert P. Compo (1998). 'A Practical Guide to Wavelet Analysis'. en. In: *Bulletin of the American Meteorological Society* 79.1, pp. 61–78. ISSN: 0003-0007, 1520-0477. DOI: 10.1175/1520-0477(1998)079<0061:APGTWA>2.0.CO;2.

Ulaby, F. T., R. K. Moore, and A. K. Fung (1982). 'Microwave remote sensing: Active and passive. Volume 2 - Radar remote sensing and surface scattering and emission theory'. In: *Microwave remote sensing: Active and passive. Volume 2 - Radar remote sensing and surface scattering and emission theory by Ulaby*. Vol. 2. ADS Bibcode: 1982ntrs.book32822U, p. 32822.

UNEP, ed. (2002). *Vital water graphics: an overview of the state of the world's fresh and marine waters*. eng. Nairobi: United Nations Environment Programme. ISBN: 978-92-807-2236-9.

Unwin, Martin J., Nazzareno Pierdicca, Estel Cardellach, Kimmo Rautiainen, Giuseppe Foti, Paul Blunt, Leila Guerriero, Emanuele Santi, and Michel Tossaint (2021). 'An Introduction to the HydroGNSS GNSS Reflectometry Remote Sensing Mission'. In: *IEEE Journal of Selected Topics in Applied Earth Observations and Remote Sensing* 14, pp. 6987–6999. ISSN: 1939-1404, 2151-1535. DOI: 10.1109/JSTARS.2021.3089550.

Velicogna, I. (2009). 'Increasing rates of ice mass loss from the Greenland and Antarctic ice sheets revealed by GRACE'. en. In: *Geophysical Research Letters* 36.19, 2009GL040222. ISSN: 0094-8276, 1944-8007. DOI: 10.1029/2009GL040222.

Vey, Sibylle, Andreas Güntner, Jens Wickert, Theresa Blume, and Markus Ramatschi (2016). 'Long-term soil moisture dynamics derived from GNSS interferometric reflectometry: a case study for Sutherland, South Africa'. en. In: *GPS Solutions* 20.4, pp. 641–654. ISSN: 1080-5370, 1521-1886. DOI: 10.1007/s10291-015-0474-0.

Vishwakarma, B D, P Bates, N Sneeuw, R M Westaway, and J L Bamber (2021). 'Reassessing global water storage trends from GRACE time series'. In: *Environmental Research Letters* 16.3, p. 034005. ISSN: 1748-9326. DOI: 10.1088/1748-9326/abd4a9.

Wagner, Wolfgang (1998). *Soil moisture retrieval from ERS scatterometer data*. eng. OCLC: 43946363. Wien: Veröffentlichung des Instituts für Photogrammetrie und Fernerkundung. ISBN: 978-3-9500791-1-1.

Wagner, Wolfgang, Günter Blöschl, Paolo Pampaloni, Jean-Christophe Calvet, Bizzarro Bizzarri, Jean-Pierre Wigneron, and Yann Kerr (2007). 'Operational readiness of microwave remote sensing of soil moisture for hydrologic applications'. en. In: *Hydrology Research* 38.1, pp. 1–20. ISSN: 0029-1277, 2224-7955. DOI: 10.2166/nh.2007.029.

Wagner, Wolfgang, Guido Lemoine, and Helmut Rott (1999). 'A Method for Estimating Soil Moisture from ERS Scatterometer and Soil Data'. en. In: *Remote Sensing of Environment* 70.2, pp. 191–207. ISSN: 00344257. DOI: 10.1016/S0034-4257(99)00036-X.

Wahr, John, Mery Molenaar, and Frank Bryan (1998). 'Time variability of the Earth's gravity field: Hydrological and oceanic effects and their possible detection using GRACE'. en. In: *Journal of Geophysical Research: Solid Earth* 103.B12, pp. 30205–30229. ISSN: 0148-0227. DOI: 10.1029/98JB02844.

Walker, Jeffrey P, Garry R Willgoose, and Jetse D Kalma (2004). 'In situ measurement of soil moisture: a comparison of techniques'. en. In: *Journal of Hydrology* 293.1-4, pp. 85–99. ISSN: 00221694. DOI: 10.1016/j.jhydrol.2004.01.008.

Wang, Tiejun, Trenton E. Franz, Jinsheng You, Martha D. Shulski, and Chittaranjan Ray (2017). 'Evaluating controls of soil properties and climatic conditions on the use of an exponential filter for converting near surface to root zone soil moisture contents'. en. In: *Journal of Hydrology* 548, pp. 683–696. ISSN: 00221694. DOI: 10.1016/j.jhydrol.2017.03.055.

Werth, S., A. Güntner, S. Petrovic, and R. Schmidt (2009). 'Integration of GRACE mass variations into a global hydrological model'. en. In: *Earth and Planetary Science Letters* 277.1-2, pp. 166–173. ISSN: 0012821X. DOI: 10.1016/j.epsl.2008.10.021.

World Meteorological Organization (2022). *The 2022 GCOS Implementation Plan: GCOS-244*. Tech. rep. GCOS-244. Geneva, Switzerland: Global Climate Observing System (GCOS).

World Meteorological Organization (2024). *Guide to Instruments and Methods of Observation (WMO-No. 8), Volume I – Measurement of Meteorological Variables*. Tech. rep. Edition: 2024. World Meteorological Organization (WMO). DOI: 10.59327/WMO/CIMO/1.

Wu, Xiaopei, Qingsi Wang, and Mingyan Liu (2015). 'In-situ Soil Moisture Sensing: Measurement Scheduling and Estimation Using Sparse Sampling'. en. In: *ACM Transactions on Sensor Networks* 11.2, pp. 1–29. ISSN: 1550-4859, 1550-4867. DOI: 10.1145/2629439.

Xiong, Jinghua, Shenglian Guo, Abhishek, Jun Li, and Jiabo Yin (2022). 'A Novel Standardized Drought and Flood Potential Index Based on Reconstructed Daily GRACE Data'. In: *Journal of Hydrometeorology* 23.9, pp. 1419–1438. ISSN: 1525-755X, 1525-7541. DOI: 10.1175/JHM-D-22-0011.1.

Xu, Chen, Matthias Weigelt, Michael G Sideris, and Nico Sneeuw (2007). 'Spaceborne gravimetry and gravity field recovery'. en. In: *Canadian Aeronautics and Space Journal* 53.3/4, pp. 65–75. ISSN: 1712-7998, 1712-7998. DOI: 10.5589/q07-008.

Xu, Xiaoyong and Steven Frey (2021). 'Validation of SMOS, SMAP, and ESA CCI Soil Moisture Over a Humid Region'. In: *IEEE Journal of Selected Topics in Applied Earth Observations and Remote Sensing* 14, pp. 10784–10793. ISSN: 1939-1404, 2151-1535. DOI: 10.1109/JSTARS.2021.3122068.

Ye, N., J.P. Walker, J. Guerschman, D. Ryu, and R.J. Gurney (2015). 'Standing water effect on soil moisture retrieval from L-band passive microwave observations'. en. In: *Remote Sensing of Environment* 169, pp. 232–242. ISSN: 00344257. DOI: 10.1016/j.rse.2015.08.013.

Zaitchik, Benjamin F., Matthew Rodell, and Rolf H. Reichle (2008). 'Assimilation of GRACE Terrestrial Water Storage Data into a Land Surface Model: Results for the Mississippi River Basin'. en. In: *Journal of Hydrometeorology* 9.3, pp. 535–548. ISSN: 1525-7541, 1525-755X. DOI: 10.1175/2007JHM951.1.

Zhao, Long and Zong-Liang Yang (2018). 'Multi-sensor land data assimilation: Toward a robust global soil moisture and snow estimation'. en. In: *Remote Sensing of Environment* 216, pp. 13–27. ISSN: 00344257. DOI: 10.1016/j.rse.2018.06.033.

Zreda, Marek, Darin Desilets, T. P. A. Ferré, and Russell L. Scott (2008). 'Measuring soil moisture content non-invasively at intermediate spatial scale using cosmic-ray neutrons'. en. In: *Geophysical Research Letters* 35.21, 2008GL035655. ISSN: 0094-8276, 1944-8007. DOI: 10.1029/2008GL035655.

List of Figures

1.1. Conceptual framework of the dissertation. The three panels correspond to the three papers included in this thesis. The schematic in the middle panel is adapted from Changnon (1987). 5

2.1. Division of the soil into saturated and unsaturated soil zones and the depth of the surface zone and root zone in the unsaturated soil zone (figure generated using AI (OpenAI, 2026) inspired by Seneviratne et al. (2010)) 8

2.2. Principle and difference between active and passive microwave sensors (figure generated using AI (OpenAI, 2026) inspired by Aberle and Bill (2026)) 12

2.3. Illustration of the SMOS satellite in space. Image credit: © ESA / AOES Medialab 18

2.4. Illustration of the SMAP satellite in space. Image credit: NASA / Scientific Visualization Studio 19

2.5. Overview of the time periods and satellite inputs used to generate ESA CCI data set. Image credit: Dorigo et al. (2024). 21

2.6. Global soil moisture maps on 1st August 2019 for the soil moisture products used in this thesis. Panels (a–d) show SSM from SMOS L3, SMAP L3, ESA CCI, and SMAP L4. Panels (e–f) show RZSM from the SMOS and SMAP L4 products. 23

2.7. Global soil moisture maps on 1st February 2020 for the soil moisture products used in this thesis. Panels (a–d) show SSM from SMOS L3, SMAP L3, ESA CCI, and SMAP L4. Panels (e–f) show RZSM from the SMOS and SMAP L4 products. 24

3.1. Illustration of the GRACE-FO satellites in space. Image credit: NASA / JPL-Caltech 32

4.1. Schematic illustration of the analysis framework used in this thesis, showing the integration of satellite-based soil moisture observations and GRACE-derived TWS. The main challenges are summarised on the right-hand side. 36

4.2. Schematic illustration of the depth representativeness in the soil of satellite-based soil moisture observations compared to GRACE-based TWS. The figure was created by the author using AI tools (OpenAI, 2026). The illustration of the unsaturated and saturated soil zones is inspired by Seneviratne et al. (2010), and satellite pictures are based on publicly available images from NASA (GRACE) and ESA (SMOS). . . . 37

4.3. Schematic illustration of drought propagation across the terrestrial water cycle. The left panel shows the conceptual drought cascade adapted from Changnon (1987) with a focus on the variables outlined in red. The right panel summarises different types of drought and highlights the focus of this study on subsurface drought dynamics based on water storage compartments. 38

4.4. Schematic illustration of the exponential filtering framework used in this thesis. The upper panel shows the conceptual setup, and the lower panel illustrates the effect of different filter time constants T on the temporal dynamics of soil moisture. 39

5.1. Time series of satellite soil moisture products in Rajasthan, India (25°N, 75°E). (a) shows SSM from SMOS L3, SMAP L3 and ESA CCI. (b) shows L4 products for SSM and RZSM. (c) shows ESA CCI soil moisture profiles across increasing depths. In all panels, ESA CCI SSM is shown in black as a reference. All time series are smoothed using a 3-day moving average for improved visualisation. Soil moisture is expressed as volumetric water content (m^3/m^3) 43

5.2. Spatial masks to identify regions with low soil moisture variability (orange), dense vegetation (green), snow cover/frozen soil (light blue) and ocean leakage (dark blue). Other areas (beige) are considered to be suited for analysis. 46

5.3. Spatial comparison of ESA CCI soil moisture on a 1° grid and in spherical harmonic representation (n = 40). (a–b) show soil moisture grids, while (c–d) show their correlation with GRACE-based TWS from ITSG-Grace2018. 48

5.4. GRACE TWS signal decomposition for an exemplary grid cell in Rajasthan, India (25°N, 75°E). (a) Full TWS anomaly signal with trend, (b) de-trended signal with climatology, (c) annual cycle compared to climatology, (d) seasonal anomalies and interannual variability, and (e) sub-seasonal variability. 50
5.5. Low- and high-pass filtering of de-trended GRACE TWS anomalies for an exemplary grid cell in Rajasthan, India (25°N, 75°E). The high-pass filter isolates sub-monthly variability. 51
5.6. Time-shift analysis between ESA CCI soil moisture and GRACE-based TWS. (a) Time series with lag correction, (b) scatter plot before correction, (c) cross-correlation, (d) scatter plot after correction. Time series are based on an exemplary grid cell in Rajasthan, India (25°N, 75°E). . . 53
5.7. WCA between soil moisture and GRACE-based TWS. (c) Wavelet coherence, (a, e) scale-averaged coherence and delay, and (b, d) time-averaged delay and coherence. Results are based on an exemplary grid cell in Rajasthan, India (25°N, 75°E) 54
5.8. Overview of the main results from Paper 1, showing global patterns of correlation and temporal shifts between soil moisture and GRACE-based TWS. The maps illustrate the example of ESA CCI SSM, while the CDFs summarise the results across all analysed soil moisture products. SSM generally precedes TWS, whereas RZSM products show smaller time shifts and closer agreement with GRACE-based TWS. 55
5.9. Exemplary comparison of sub-monthly variations for SMAP L4 RZSM and GRACE-based TWS in Rajasthan, India from Paper 1. 60
5.10. Highlights from Paper 2. Recovery times derived from soil moisture and GRACE-based TWS demonstrate that water storage deficits become increasingly persistent with storage depth, reflecting the propagation of storage anomalies through the subsurface. 62
5.11. Conceptual illustration of the GRACE-constrained exponential filter approach used in Paper 3. For each grid cell, an optimal time constant T is calibrated against GRACE-based TWS and subsequently applied to SSM to estimate subsurface storage dynamics. The shown time series illustrates the approach for an exemplary grid cell, while the calibration itself is applied globally. 66
5.12. Global distribution of GRACE-optimised exponential filter time constants for different soil moisture integration depths, based on Paper 3. 70

List of Tables

5.1. Overview of observational constraints affecting satellite soil moisture and GRACE-based TWS observations. 45

List of Acronyms

AMSR-2 Advanced Microwave Scanning Radiometer 2

AMSR-E Advanced Microwave Scanning Radiometer for EOS

ASCAT Advanced Scatterometer

CATDS Centre Aval de Traitement des Données SMOS

CCI Climate Change Initiative

CDF Cumulative Distribution Function

CHAMP Challenging Minisatellite Payload

COST-G Combination Service for Time-variable Gravity Fields

CRNS Cosmic-Ray Neutron Sensing

CSR Centre for Space Research

DLR German Aerospace Center

ECV Essential Climate Variable

ERS European Remote Sensing Satellite

ESA European Space Agency

EWH Equivalent Water Heights

FDR Frequency Domain Reflectometry

FY-3B/C/D FengYun-3B/C/D

GFZ German Research Centre for Geosciences

GIA Glacial Isostatic Adjustment

GL Glacier Storage

GLDAS Global Land Data Assimilation System

GNSS Global Navigation Satellite System

GNSS-R Global Navigation Satellite System-Reflectometry

GOCE Gravity Field and Steady-State Ocean Circulation Explorer

GPM Global Precipitation Measurement

GPS Global Positioning System

GRACE Gravity Recovery and Climate Experiment

GRACE-FO Gravity Recovery and Climate Experiment Follow-On

GW Groundwater

ISMN International Soil Moisture Network

ITSG Institute of Geodesy at Graz University of Technology

JPL Jet Propulsion Laboratory

L-1 Level-1

L-2 Level-2

L-3 Level-3

L-4 Level-4

LEO Low Earth Orbit

LRI Laser Ranging Interferometer

LSM Land Surface Model

NASA National Aeronautics and Space Administration

NSIDC National Snow and Ice Data Center

RFI Radio Frequency Interference

RZSM Root-zone soil moisture

SGG Satellite Gravity Gradiometry

SM Soil Moisture

SMAP Soil Moisture Active Passive

SMMR Scanning Multichannel Microwave Radiometer

SMOS Soil Moisture and Ocean Salinity

SNR signal-to-noise ratio

SSM Surface soil moisture

SSM/I Special Sensor Microwave/Imager

SST Satellite-to-Satellite Tracking

SST-hl High-low Satellite-to-Satellite Tracking

SST-ll Low-low Satellite-to-Satellite Tracking

SW Surface Water

SWE Snow Water Equivalent

TDR Time Domain Reflectometry

TRMM-TMI Tropical Rainfall Measuring Mission Microwave Imager

TWS Terrestrial Water Storage

WCA Wavelet Coherence Analysis

WGHM WaterGap Global Hydrology Model

A. Peer-reviewed publications

A.1. A global analysis of water storage variations from remotely sensed soil moisture and daily satellite gravimetry

Reference

Blank, D., Eicker, A., Jensen, L., and Güntner, A.: A global analysis of water storage variations from remotely sensed soil moisture and daily satellite gravimetry, Hydrol. Earth Syst. Sci., 27, 2413–2435, https://doi.org/10.5194/hess-27-2413-2023, 2023.

Abstract

Water storage changes in the soil can be observed on a global scale with different types of satellite remote sensing. While active or passive microwave sensors are limited to the upper few centimeters of the soil, satellite gravimetry can detect changes in the terrestrial water storage (TWS) in an integrative way, but it cannot distinguish between storage variations in different compartments or soil depths. Jointly analyzing both data types promises novel insights into the dynamics of subsurface water storage and of related hydrological processes. In this study, we investigate the global relationship of (1) several satellite soil moisture products and (2) non-standard daily TWS data from the Gravity Recovery and Climate Experiment/Follow-On (GRACE/GRACE-FO) satellite gravimetry missions on different timescales. The six soil moisture products analyzed in this study differ in the post-processing and the considered soil depth. Level 3 surface soil moisture data sets of the Soil Moisture Active Passive (SMAP) and Soil Moisture and Ocean Salinity (SMOS) missions are compared to post-processed Level 4 data products (surface and root zone soil moisture) and the European Space Agency Climate Change Initiative (ESA CCI) multi-satellite product. On a common global 1° grid, we decompose all TWS and soil moisture data into seasonal to sub-monthly signal components and compare their spatial patterns and temporal variability. We find larger correlations between TWS and soil moisture for soil moisture products with deeper integration depths (root zone

vs. surface layer) and for Level 4 data products. Even for high-pass filtered sub-monthly variations, significant correlations of up to 0.6 can be found in regions with a large, high-frequency storage variability. A time shift analysis of TWS versus soil moisture data reveals the differences in water storage dynamics with integration depth.

Declaration of own contribution

Table 1: Contribution to Paper No. 1.

Involved in	**Estimated contribution**
Ideas and conceptual design	85%
Computation and results	100%
Analysis and interpretation	85%
Manuscript, figures and tables	90%
Total	90%

Confirmation of Co-Authors

I hereby confirm the correctness of the declaration of the contribution of **Daniel Blank** for Paper No. 1 in Table 1:

Annette Eicker	Date
Laura Jensen	Date
Andreas Güntner	Date

Hydrol. Earth Syst. Sci., 27, 2413–2435, 2023
https://doi.org/10.5194/hess-27-2413-2023
© Author(s) 2023. This work is distributed under
the Creative Commons Attribution 4.0 License.

Hydrology and Earth System Sciences
Open Access
EGU

A global analysis of water storage variations from remotely sensed soil moisture and daily satellite gravimetry

Daniel Blank[1], **Annette Eicker**[1], **Laura Jensen**[1], **and Andreas Güntner**[2,3]

[1]Geodesy and Geoinformatics, HafenCity University Hamburg, Hamburg, Germany
[2]GFZ German Research Centre for Geosciences, Helmholtz Centre Potsdam, Potsdam, Germany
[3]Institute of Environmental Sciences and Geography, University of Potsdam, Potsdam, Germany

Correspondence: Daniel Blank (daniel.blank@hcu-hamburg.de)

Received: 28 November 2022 – Discussion started: 2 December 2022
Revised: 5 May 2023 – Accepted: 31 May 2023 – Published: 4 July 2023

Abstract. Water storage changes in the soil can be observed on a global scale with different types of satellite remote sensing. While active or passive microwave sensors are limited to the upper few centimeters of the soil, satellite gravimetry can detect changes in the terrestrial water storage (TWS) in an integrative way, but it cannot distinguish between storage variations in different compartments or soil depths. Jointly analyzing both data types promises novel insights into the dynamics of subsurface water storage and of related hydrological processes. In this study, we investigate the global relationship of (1) several satellite soil moisture products and (2) non-standard daily TWS data from the Gravity Recovery and Climate Experiment/Follow-On (GRACE/GRACE-FO) satellite gravimetry missions on different timescales. The six soil moisture products analyzed in this study differ in the post-processing and the considered soil depth. Level 3 surface soil moisture data sets of the Soil Moisture Active Passive (SMAP) and Soil Moisture and Ocean Salinity (SMOS) missions are compared to post-processed Level 4 data products (surface and root zone soil moisture) and the European Space Agency Climate Change Initiative (ESA CCI) multi-satellite product. On a common global 1° grid, we decompose all TWS and soil moisture data into seasonal to sub-monthly signal components and compare their spatial patterns and temporal variability. We find larger correlations between TWS and soil moisture for soil moisture products with deeper integration depths (root zone vs. surface layer) and for Level 4 data products. Even for high-pass filtered sub-monthly variations, significant correlations of up to 0.6 can be found in regions with a large, high-frequency storage variability. A time shift analysis of TWS versus soil moisture data reveals the differences in water storage dynamics with integration depth.

1 Introduction

Freshwater stored on the continents sustains life on Earth and is a key variable in the global cycles of water, energy, and matter. Among the different continental storage compartments that make up terrestrial (or total) water storage (TWS), such as glaciers and ice caps, surface waterbodies, and groundwater, soil moisture (SM) plays a particularly important role at the soil–vegetation–atmosphere interface. Recognizing its important control of numerous processes in the climate system, SM and TWS have been declared as essential climate variables (Dorigo et al., 2021a). SM is defined as the water contained in the unsaturated soil zone (i.e., the zone above the groundwater table that is not completely filled with water). Even though SM only accounts for 0.05 % of the total freshwater resources on Earth (Shiklomanov, 1993), SM is fundamental for providing the water supply for the Earth's vegetation cover and for ecosystems in the critical zone. In spite of its small absolute volume, SM can make a large contribution to TWS variations (e.g., Güntner et al., 2007). SM is directly influenced by water fluxes at the land surface, such as precipitation, snowmelt, and evapotranspiration, and plays a decisive role in how the water input is distributed among root water uptake and groundwater recharge or runoff, for instance (i.e., how water fluxes are partitioned between different storage compartments). While near-surface SM usually exhibits high fluctuations on short

timescales due to its direct exposure to the hydrometeorological forcing, temporal SM variations tend to be smoother and delayed with increasing soil depth (e.g., Xu et al., 2021b), while the degree of coupling between near-surface, deeper, or depth-integrated water storage may vary considerably with the site conditions (e.g., Carranza et al., 2018). Overall, jointly analyzing both SM and TWS data sets may reveal better insights into the hydrological dynamics and the processes that govern water storage changes in the subsurface. Monitoring SM and TWS is thus crucial for understanding the variations and changes in the global water cycle. In spite of considerable efforts in collecting in situ SM observations at the global scale (Dorigo et al., 2021b), a global coverage that includes even remote regions of the globe is only possible by means of satellites. Moreover, for TWS monitoring, only very few in situ observations exist (e.g., Güntner et al., 2017), while large-scale and global coverage can be achieved by remote sensing. Two different types of satellite observations are sensitive to changes in the water in the subsurface. (1) Active or passive microwave remote sensing can observe SM in the top few centimeters of the soil, exploiting the fact that the dielectric constant of the soil changes with varying soil water content. Several dedicated instruments are currently in operation on different satellite missions (e.g., Soil Moisture and Ocean Salinity (SMOS), Soil Moisture Active Passive (SMAP), Advanced SCATterometer (ASCAT), or Advanced Microwave Scanning Radiometer 2 (AMSR2)). Also, the first results were obtained based on reflected signals of navigation satellite systems received in space (e.g., Camps et al., 2016; Chew and Small, 2018; Kim and Lakshmi, 2018). For estimating soil moisture with higher spatial and temporal resolution, optical approaches are used (e.g., Sadeghi et al., 2017). (2) Due to the fact that any redistribution of water mass on or above the Earth's surface leads to variations in the Earth's gravity field, satellite gravimetry can relate the changes in the gravitational acceleration that are acting on a satellite to variations in TWS, which includes SM. The twin satellite missions of Gravity Recovery and Climate Experiment (GRACE; Tapley et al., 2004) and its successor mission GRACE Follow-On (GRACE-FO; Landerer et al., 2020) have been observing gravity field changes since 2002.

The two types of satellite observations (remotely sensed surface soil moisture (SSM) and TWS from satellite gravimetry) both have their individual advantages and drawbacks. Satellite gravimetry is sensitive to all parts of TWS on and underneath the Earth's surface but cannot distinguish between water mass changes in individual water compartments (e.g., snow cover, groundwater, SM, and surface water). The separation of the integrative signal for studying individual compartments, e.g., SM variations, is challenging (Schmeer et al., 2012). Furthermore, the low spatial resolution of the GRACE data of a few 100 km makes the analysis of local phenomena difficult. SM remote sensing provides a much higher spatial resolution (20–40 km) but observes SM only in the top few centimeters (~ 2 cm) of the soil (Escorihuela et al., 2010). Also, measuring SM with microwave satellites is problematic in regions such as tropical rainforests due to dense vegetation or in Arctic regions because of snow cover or frozen ground (Karthikeyan et al., 2017). How (and if) the satellite-based surface SM can best be used to empirically extrapolate the wetness conditions into deeper soil layers and thus give evidence of large-scale contributions to the global water cycle is still under investigation (De Lannoy and Reichle, 2016). Approaches for estimating root zone SM from satellite surface SM data have been exploited by the operational Copernicus Global Land Service, which provides soil water index values (Bauer-Marschallinger et al., 2018), and by the EUMETSAT H SAF root zone SM products (H SAF, 2020). However, existing vertical extrapolation or depth-scaling algorithms exhibit large discrepancies, and their validation is difficult (Zhang et al., 2017). The comparison of the extrapolated root zone soil moisture (RZSM) dynamics against the integrative observations of TWS variations can be a valuable means of evaluating the depth-scaling approaches, in particular in areas where TWS is dominated by water storage variations in the unsaturated zone.

However, the temporal resolution of the standard GRACE data of 1 month is too low to record any fast water mass changes in the upper soil layers. Recent developments in GRACE data processing (Kvas et al., 2019) have enabled the computation of daily gravity fields with increased accuracy. Such daily gravity data were successfully used to study high-frequency, wind-driven sea level changes (Bonin and Chambers, 2011), short-term transport variations in the Antarctic Circumpolar Current (Bergmann and Dobslaw, 2012), the characteristics of major flood events (Gouweleeuw et al., 2018), high-frequency atmospheric fluxes (Eicker et al., 2020), and to analyze the development and propagation of water extremes by using a standardized drought and flood potential index (SDFPI; Xiong et al., 2022). Furthermore, the daily gravity-based TWS data appear particularly promising for capturing SM variations at short timescales but have not been used for this purpose yet.

While a large number of studies have examined TWS and SM individually, joint (global) analyses of the two observation types are largely missing. Only Abelen et al. (2015) and Abelen (2016) have provided the first comparisons between two satellite SM products and TWS but only on monthly and not on daily timescales. Besides the direct data comparison, the joint assimilation of both observables into hydrological models is currently an emerging field (e.g., Tian et al., 2019; Tangdamrongsub et al., 2020).

Given the potential value of combining SM and TWS observations for understanding water cycle dynamics as outlined above, the aim of this study is to investigate the global relationship between (1) non-standard daily TWS data from GRACE(-FO) and (2) several satellite SM products on different timescales to derive novel information content on Earth system dynamics. An overview of the data sets and their

characteristics is shown in Fig. 1. The six SM products analyzed in this study can be categorized based on their degree of post-processing and their integration depth into the soil. Original Level 3 (L3) surface SM data sets of SMAP (Entekhabi et al., 2010) and SMOS (Kerr et al., 2010) are compared to post-processed Level 4 (L4) data products (SSM and RZSM) and a multi-satellite product provided by the European Space Agency Climate Change Initiative (ESA CCI; Gruber et al., 2019; Dorigo et al., 2017). While strong correlations of the two data types in the dominant seasonal cycle are to be expected, finding such correlations on shorter (down to sub-monthly and daily) timescales would be first-time evidence that satellite gravimetry can indeed observe such fast-changing SM signals, opening new opportunities of applications of this observation technology.

The paper is organized as follows: in Sect. 2, we describe the satellite data products used for the comparison of the different data sets (SM and TWS), followed by information on the applied data processing in Sect. 3. The results are presented in Sect. 4, first for the full signal and afterwards for sub-monthly timescales isolated by high-pass filtering. In both cases, we first illustrate signal characteristics using an exemplary time series for a specific grid cell, followed by global maps of correlation coefficients and relative time shifts to show the (dis)agreement between the data types.

2 Data sets

2.1 GRACE and GRACE-FO data

To investigate fast temporal water storage changes, we use the daily gravity field solutions of the ITSG-Grace2018 model (Kvas et al., 2019) converted to a global time series of daily TWS anomalies. Compared to the standard monthly solutions, the limited satellite ground track coverage during 1 d does not allow for a stable global gravity field inversion; thus, additional information has to be introduced. The processing of the daily solutions is therefore carried out using a Kalman smoothing approach (similar to Kurtenbach et al., 2012), which introduces statistical information on the expected evolution of the gravity field over time in its process model. As a tradeoff, the resulting daily gravity field data are not fully independent daily solutions but exhibit some degree of correlation with previous time steps.

Daily gravity field data are given in the form of spherical harmonic coefficients (so-called Level 2 products) of the gravitational potential up to a degree of $n = 40$, corresponding to a spatial resolution of 500 km. During the data processing, temporally high-frequency mass variations caused by tides (ocean, Earth, and pole tides), in addition to non-tidal atmospheric and ocean mass variations, are removed by subtracting the output of the geophysical background models from the observations (dealiasing; Dobslaw et al., 2017). Post-processing steps account for the effect of geocenter motion (adding the degree 1 harmonic coefficients given by Sun et al., 2016, on the basis of Swenson et al., 2008), replace the c_{20} coefficient based on a time series from satellite laser ranging (Cheng and Ries, 2017), and subtract the influence of glacial isostatic adjustment (GIA), using the ICE6G-D model (Peltier et al., 2017). No extra spatial filtering is needed because the Kalman smoother effectively suppresses spatially correlated noise. After these processing steps, the resulting gravity field models are assumed to primarily contain water mass changes above and below the Earth's surface and can be converted to equivalent water heights on a global geographical grid of $1^\circ \times 1^\circ$, according to the following:

$$\mathrm{TWS}(\lambda, \vartheta) = \frac{M}{4\pi R^2 \rho_\mathrm{w}} \sum_{n=1}^{n_\mathrm{max}} \sum_{m=-n}^{n} \frac{(2n+1)}{\left(1+k'_n\right)} c_{nm} \Upsilon(\lambda, \vartheta), \quad (1)$$

where λ and ϑ symbolize the spherical coordinates, M and R are the mass and the radius of the Earth, ρ_w is the density of water $\left(\frac{1000\,\mathrm{kg}}{\mathrm{m}^3}\right)$, k'_n denote the load love numbers (Lambeck, 1988), c_{nm} are the spherical harmonic coefficients of the gravitational potential, and $\Upsilon(\lambda, \vartheta)$ are the surface spherical harmonic functions. The degree and order of the spherical harmonic functions are denoted by n and m. For a reasonable overlap with all satellite-based SM products, we used the time period from April 2015 to December 2021 for our study, excluding the time span between the end of the mission GRACE (August 2017) and the start of the successor mission GRACE-FO (July 2018). Even though the Kalman smoother output provides a continuous daily time series without data gaps for the mission time periods, all days with insufficient GRACE observations were excluded from our analysis (i.e., days with an observation count of less than 10 000 observations per day as given on the website of the ITSG-Grace2018 product). On these days, the daily solutions are mainly informed by the process model of the Kalman filter and thus tend towards an a priori mean trend and annual signal. Calculation of the GRACE TWS data was done using the Gravity Recovery Object Oriented Programming System (GROOPS; Mayer-Gürr et al., 2021).

Limitations of the GRACE TWS data that are relevant for this study relate to the limited spatial resolution (i.e., 500 km for daily data, as stated above), which results in the TWS grid cell values not being independent from neighboring grid cells. This can lead to leakage effects (Longuevergne et al., 2013) of spatially localized mass variations that are small in their spatial extent but strong in magnitude, such as surface water storage change in lakes or reservoirs. Coastal areas should also be regarded with care because the limited spatial resolution prevents a strict separation between land and ocean signals in the GRACE data sets. While a mere dampening of the continental signal caused by a much lower mass variability on the ocean does not influence the correlations between the TWS and SM discussed in the present study, the so-called "leakage in" (Baur et al., 2009; i.e., spurious high-frequency ocean signal being leaked onto land areas)

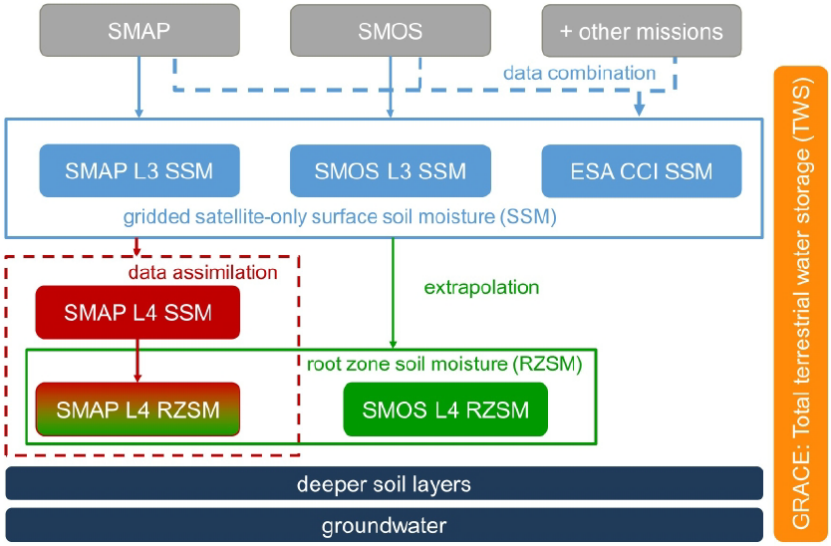

Figure 1. An overview of the soil moisture data sets used and their characteristics.

might have an influence on the comparison of TWS and SM in coastal areas. A more detailed discussion on this and a map (with areas that should be regarded with caution) is shown in Eicker et al. (2020, see Fig. 4 in their Supplement). Another issue that needs to be kept in mind when comparing TWS with SM data is the fact that the GRACE TWS observations represent the fully integrated vertical water column, which includes SM but is not limited to it. On the one hand, this is a challenge, as the two quantities (TWS and SM) are not directly comparable. One the other hand, it is the particular strength of the TWS observations to be sensitive to water storage dynamics that otherwise are not observable by remote sensing, such as those in deep soil layers down to the groundwater. To explore what we might learn from such differences (TWS versus SM), regarding hydrological process dynamics in the subsurface, is one motivation for this study.

2.2 Soil moisture data sets

Active or passive microwave remote sensing can observe SM in the top few centimeters of the soil, exploiting the fact that the dielectric constant of the soil changes with varying soil water content. Several dedicated instruments are currently in operation on different satellite missions. Active microwave sensors (radars) transmit an electromagnetic pulse to the Earth and measure the pulse's backscattered energy from the surface of the Earth, whereas passive microwave sensors (radiometers) observe the radiation naturally emitted by the Earth's soil, which is expressed as the brightness temperature (Robinson et al., 2008). The observed parameters (backscattered energy and brightness temperature) of both techniques depend on the dielectric constant of the soil, which allows the measurement of SM.

In our study, we use satellite-derived SSM products from the missions SMOS, SMAP, and from the combination data product ESA CCI, as well as RZSM products from SMOS and SMAP. Both SMOS and SMAP provide so-called Level 3 (L3) and Level 4 (L4) data, with L3 referring to the original satellite observations acquired over a 24 h period given as a multi-orbit global map of retrieved soil moisture (L3 data do not have complete global coverage), while L4 relates to post-processed data products. The way of post-processing differs between the two satellite missions and will be detailed below. The overlapping time span of all missions between April 2015 (start of the SMAP mission) and December 2021 was selected. In addition, it should be mentioned that the orbit direction (ascending/descending orbit) differs across the L3 products and therefore also the overpass time. In this study, the early morning overpass is chosen for the L3 satellite SM products. This is suggested for passive measurement methods, as the temperature difference between the soil surface and the vegetation canopy in the morning and night, in addition to the thermal difference between various types of land cover, within a pixel is reduced; this results in a minimization of SM retrieval errors and better reliability (Owe et al., 2008; Entekhabi et al., 2014; Lei et al., 2015; Montzka et al., 2017).

2.2.1 SMOS

The Soil Moisture and Ocean Salinity (SMOS; Kerr et al., 2010) satellite was implemented by ESA as part of the Earth Explorer missions and launched in November 2009. The satellite operates in a sun-synchronous orbit, and the ascending orbit overpasses the Equator at 6:00 local time. SM is observed by using an L-band radiometer, which receives the radiation emitted by the Earth's surface and measures the

brightness temperature. This technique allows observations in the first few centimeters of soil (SSM). SMOS needs less than 3 d to revisit the same area, with a maximum spatial resolution of around 40–50 km.

In this study, we use the daily L3 (v3.0) SSM product of the Centre Aval de Traitement des Données SMOS (CATDS), operated by the Centre National d'Etudes Spatiales (CNES). The L3 data contain all of the collected SM data for each day on a global grid, with a spatial resolution of 25 km × 25 km (Al Bitar et al., 2017). Additionally, the CATDS L4 RZSM product is used, which propagates the L3 SSM data set (0–5 cm) into the underlying soil (5–40 cm), using an exponential filter. Then, from the 40 cm layer to the root zone layer (up to 1 m soil depth), a budget model based on a linearized Richards equation formulation is adopted to compute the water content (Al Bitar et al., 2013). The RZSM is a weighted average of the two layers (expressed in $m^3\,m^{-3}$). Starting in February 2020, the SMOS L4 data set has been processed using a new algorithm. The method uses the SSM product from SMOS to calculate the SM of the root zone (1 m depth), based on a modified formulation of a recursive exponential filter, while considering soil properties and an optional implementation of transpiration (Al Bitar and Mahmoodi, 2020). As the data from 2015 to 2020 have not yet been reprocessed using the new algorithm, we decided to concatenate the two time series in order to adhere to the general comparison period of April 2015 to December 2021. An offset between the two differently processed time spans was calculated from the 14 d overlap period from 31 January to 13 February 2020 and removed from the February 2020 to December 2021 data to achieve a seamless transition with the previous data (April 2015 to January 2020). The L4 RZSM data set is provided in a global grid, with a spatial resolution of 25 km × 25 km.

2.2.2 SMAP

The Soil Moisture Active Passive (SMAP; Entekhabi et al., 2010) satellite was launched in January 2015 by the National Aeronautics and Space Administration (NASA) to observe SSM with an L-band active radar and passive radiometer. After a few months, the active system failed and since then only the passive system has been operational; it observes the brightness temperature of the Earth. Like the SMOS satellite, SMAP operates in a sun-synchronous orbit, but in contrast to SMOS, the overpass of the Equator at 06:00 local time occurs on the descending orbit. SMAP needs a maximum of 3 d to revisit the same area and measures the brightness temperature with a spatial resolution of around 40 km.

In this study, the L3 and L4 products from SMAP are used. The daily L3 data (v8.0; O'Neill et al., 2021) contain all SSM retrievals for an entire day mapped to a global grid with a spatial resolution of 36 km. In contrast, the L4 products are derived by assimilating SMAP surface brightness temperature observations into the Goddard Earth Observing Model System version 5 (GEOS-5) catchment land surface model. The land surface model is driven by observation-based surface meteorological forcing data, including precipitation, and represents essential land surface processes, such as the vertical movement of water in the soil between the surface and the root zone. Therefore, it should be pointed out that the resulting L4 data products cannot be regarded as purely being based on satellite soil moisture observations but have to be interpreted as a modeled data set that is heavily influenced by data assimilation and thus by the climate data used as input for the land surface model and by its model structure. Finally, the assimilation system interpolates and extrapolates SMAP observations in time and space using the land model, which gives estimates for the SSM (5 cm depth) and the RZSM (up to 1 m depth), which is provided with a temporal resolution of 3 h and a 9 km spatial resolution. Both L4 data sets (SSM and RZSM v6.0; Reichle et al., 2021), available from the website of the National Snow and Ice Data Center (NSIDC), are used in our analysis. To evaluate all products at the same daily scale, the SMAP L4 products are resampled to daily data by taking the average of all observations for 1 d (eight observations per day for a 3 h temporal resolution).

2.2.3 ESA CCI

The ESA CCI SM data set (Gruber et al., 2019; Dorigo et al., 2017) is provided as part of ESA's Climate Change Initiative (CCI). The ESA CCI SM product is based on harmonizing and merging SM retrievals from multiple satellites into a combined daily product. Three different data sets are provided, namely an active-microwave-only-based product, a passive-microwave-only-based product and a combined active and passive SM product.

We select the combined active and passive SSM product (v7.1) for our analysis. It provides daily SM observations, with a spatial resolution of 0.25° and is available from the ESA data archive. This product includes SM retrievals from active satellites, such as the Active Microwave Instrument Wind Scatterometer (AMI-WS) European Remote Sensing satellites ERS 1 and ERS 2 Wind Scatterometer Mode (SCAT) and MetOp-A and MetOp-B Advanced Scatterometer (ASCAT), and from passive satellites, such as the Nimbus-7 Scanning Multichannel Microwave Radiometer (SMMR), Defense Meteorological Satellite Program (DMSP) Special Sensor Microwave/Imager (SSM/I), the Tropical Rainfall Measuring Mission's (TRMM) Microwave Imager (TMI), Aqua Advanced Microwave Scanning Radiometer for Earth Observation Satellite (AMSR-E), Coriolis/WindSat, SMOS, GCOM AMSR2, and SMAP. Overall, this product covers SM data from 1978 to the present. It should be noted that tropical rainforest areas are completely masked out because of the strong signal scattering in the microwave observations caused by vegetation (Ulaby and Long, 2014).

3 Data processing

A comparison between satellite gravimetry and the SM products is carried out on grid cell level; therefore, the SM products are harmonized to the same $1^\circ \times 1^\circ$ geographical grid used in Eq. (1) to compute TWS from the GRACE and GRACE-FO data. Downsampling was performed using a first-order conservative remapping function, which leads to a lower spatial resolution for the various SM data sets. Despite a remaining difference in the spatial signal content between the frequency-limited TWS and the gridded SM data, no further downsampling was performed in order to preserve the characteristics of the SM time series.

The linear trend of the time series is removed before examining the agreement between SM and TWS. To isolate submonthly variations, a third-order Butterworth high-pass filter with a cutoff frequency of 30 d is applied in the forward and backward directions (to avoid a phase shift). This filter conserves the phase but removes signals with periods longer than 30 d which dominate the time series. The computation of the high-pass filtered signal is presented in further detail in Appendix B.

Since a direct comparison of the absolute values of SM and TWS is not possible due to the different integration depths and units of the respective data sets, we analyze their relationship using Pearson's pairwise correlation coefficient ρ_{xy}. Possible time lags between TWS and SM are determined using a cross-correlation analysis, which indicates the time shift for which two signals best agree with each other. Appendix A1 provides further information on these metrics. The data gaps in the TWS data set (see Sect. 2.1) were also excluded from the SM time series prior to comparison. No further temporal masking, e.g., based on quality flags, was performed for the SM data.

3.1 Spatial mask

The type of land cover can lead to limitations for observing SM. In densely vegetated areas such as tropical rainforests, the observed emissivity by passive satellites or the backscattered energy by active satellites is primarily caused by the vegetation (Ulaby and Long, 2014; Owe et al., 2001). In deserts, the SM signal may be unreliable, as the variability in the water in the upper soil is low (Dorigo et al., 2010). The problem of reduced sensitivity in deserts also accounts for the satellite gravimetry observations from GRACE and GRACE-FO, as their signal-to-noise ratio is low, and the noise floor of GRACE strongly dominates the time series. Other surface characteristics that limit the measurements of satellite SM are snow cover and frozen soil, since the dielectric constant of snow and frozen water varies significantly from the one of liquid water (Wagner, 1998).

Therefore, three spatial masks have been defined to identify problematic regions for observing SM. These are dense vegetation, regions with snow and frozen ground throughout large parts of the year, and areas with low SM (e.g., deserts), as seen in Fig. 2. To indicate dense vegetation, in our study we use the tropical rainforest mask that is also applied in the ESA CCI data set. Also, for regions with a large fraction of snow cover and frozen soil, the same method used for the ESA CCI mask is applied. It uses soil temperature (T_S) and snow water equivalent (SWE) estimates from the Global Land Data Assimilation System Noah (GLDAS Noah) to flag satellite observations that were taken under the conditions of frozen soil ($T_S < 0\,^\circ$C) and snow cover (SWE > 0 mm; Gruber et al., 2019). Grid cells in which more than 40 % of all observations are influenced by these conditions were included in the mask. We classify dry (desert) regions based on the SM signal variability, i.e., the root mean square (rms) of the daily SM time series in each grid cell. As a threshold value for low variability, we use twice the mean rms of a test region in the Sahara desert, where no major day-to-day SM variations can be expected. To define the mask with this criterion, we used the SMOS L3 data product. Using the other SM data products led to very similar results. In some regions, the low SM variability mask overlaps with the snow cover and frozen ground mask. The low SM variability areas are excluded from further analyses because no discernible signals of both SM and TWS can be expected. As we want to use the maximum of the available information of both data sets for the first analysis of this kind performed in the present study, values in the region of the other two masks (dense vegetation and snow cover and frozen ground) are considered in the analyses but will be discussed with care to recognize the limitations of SM retrieval.

4 Results

4.1 Time series comparison for an example location

The comparison of time series between TWS from ITSG-Grace2018 and SM from various products is first shown for one exemplary grid cell. We chose one cell, with marked short-term and seasonal SM variations, close to the city of Kota (25° N, 75° E), located in the southeast of the Indian state of Rajasthan and characterized by a hot semi-arid climate, with a monsoon season from July to September. The location of this grid cell is indicated in the maps in Fig. 4 (blue circle). Figure 3 (top) shows daily TWS in this grid cell in comparison to SSM derived from satellite observations only. While TWS exhibits a comparatively smooth behavior for short timescales and a dominant seasonal signal, the SSM time series are of considerably higher variability at short timescales. One reason is the noise of the satellite SM observations themselves (e.g., Karthikeyan et al., 2017). On the other hand, this variability can partly represent a real signal, as near-surface SM exhibits quick wetting and drying dynamics from individual precipitation events and from subsequent evaporation. In contrast, the much larger integra-

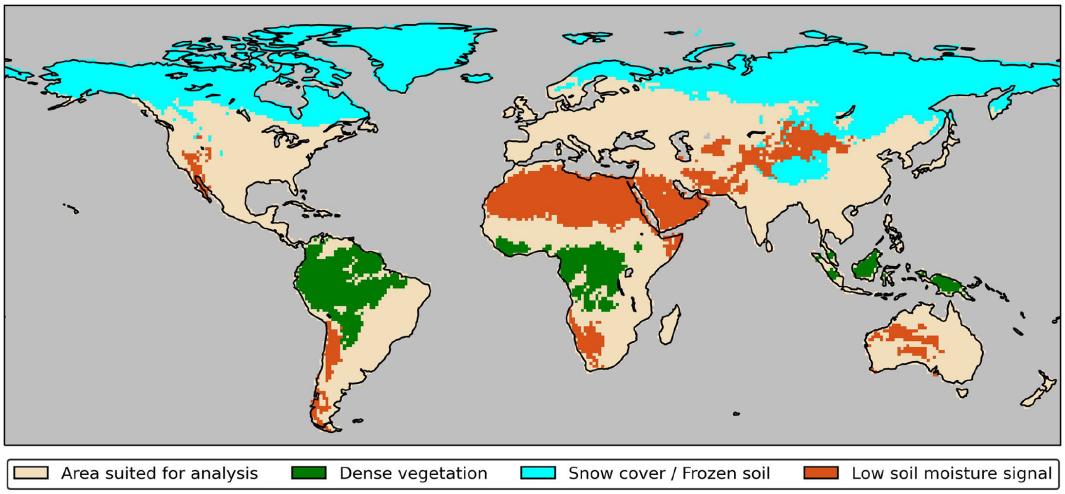

Figure 2. Spatial masks applied in this study for low SM variability (red), dense vegetation (green), and snow cover and frozen ground (blue). In the other areas (beige; here denoted as the area suited for analysis), reasonable satellite-based SM signals can be expected.

tion depth of the GRACE observations down to groundwater results in integral water storage with much slower dynamics. Furthermore, it has to be noted that, for an integration depth of the SSM products of a few centimeters, the overall amplitudes of SM experience a change of the order of 40 vol. % (shown in Fig. 3) that corresponds to water storage changes that are 1 order of magnitude smaller than those of the GRACE-based TWS. An investigation into whether the fast-changing surface signals can also be detected in the GRACE data will be pursued in Sect. 4.3 for high-pass filtered time series. Comparing the time series of the three SSM products for this particular location, SMAP L3 and the multi-satellite combination product ESA CCI time series appear less noisy than the SMOS L3 time series, which is in good agreement with findings of, e.g., Montzka et al. (2017), Cui et al. (2017), Xu and Frey (2021), and Kim et al. (2021).

While there is a general correspondence in the dynamics of TWS and SSM regarding the dominating seasonal signal (strong rise in water storage and SM during the monsoon season followed by a quick decline), a time shift can be identified between both quantities. The seasonal maxima and minima of the GRACE time series occur approximately 1–2 months later than those of SSM. This can again be attributed to the slower and delayed water storage change in the deeper layers seen by GRACE, in which a change from dry to wet conditions (or vice versa) takes much longer to evolve than in the layers close to the surface. In addition to the main seasonal maximum, a minor secondary maximum can be identified each year in the period from November to January in the SSM time series, and it is particularly well visible in the SMAP L3 data (yellow line). For the TWS data, minor peaks or a less steep TWS recession can be observed during this period, although a more general statement is hindered by the gaps in the TWS time series. Further discussion on this feature follows in the next paragraph.

Figure 3 (middle) compares the TWS time series and the L4 SM products. For SMAP, both the surface (SSM) and the root zone (RZSM) products are the result of the data assimilation procedure described in Sect. 2.2.2. The SMAP L4 RZSM time series has a smaller variability compared to the SSM data at both short-term and at seasonal timescales. This is also the case for the L4 RZSM product of SMOS, in which the seasonal variability is dampened even more strongly. The secondary maximum in November–January obvious in the L3 products is still visible in the L4 RZSM data set of SMOS, since the physical extrapolation of the SSM data into deeper layers is applied for the SMOS L4 product. In contrast, the assimilation applied to SMAP L4 removes this second seasonal maximum for both the SSM and the RZSM data sets. This indicates that the signal seen in the direct satellite SM data is not represented by the forcing data of the underlying model (i.e., precipitation) and thus fades out in the L4 SMAP product. This shows how strongly SMAP L4 is influenced by the underlying model and the climate data used as model forcing. The secondary SM peak might thus be caused by extensive irrigation after the end of the monsoon season. The results corroborate a possible deficiency of the SMAP L4 product (i.e., that it is mainly driven by precipitation input in the data assimilation framework and thus does not represent the impact of irrigation). The combination of (near-surface) soil moisture products and TWS observations may thus shed light on how human activities and irrigation practices in particular translate into water storage changes in deeper soil zones. While the focus of this study is on shorter-term storage changes, overlapping trend signals in the unsaturated zone and in the groundwater that may be caused by these activities may be difficult to disentangle. However,

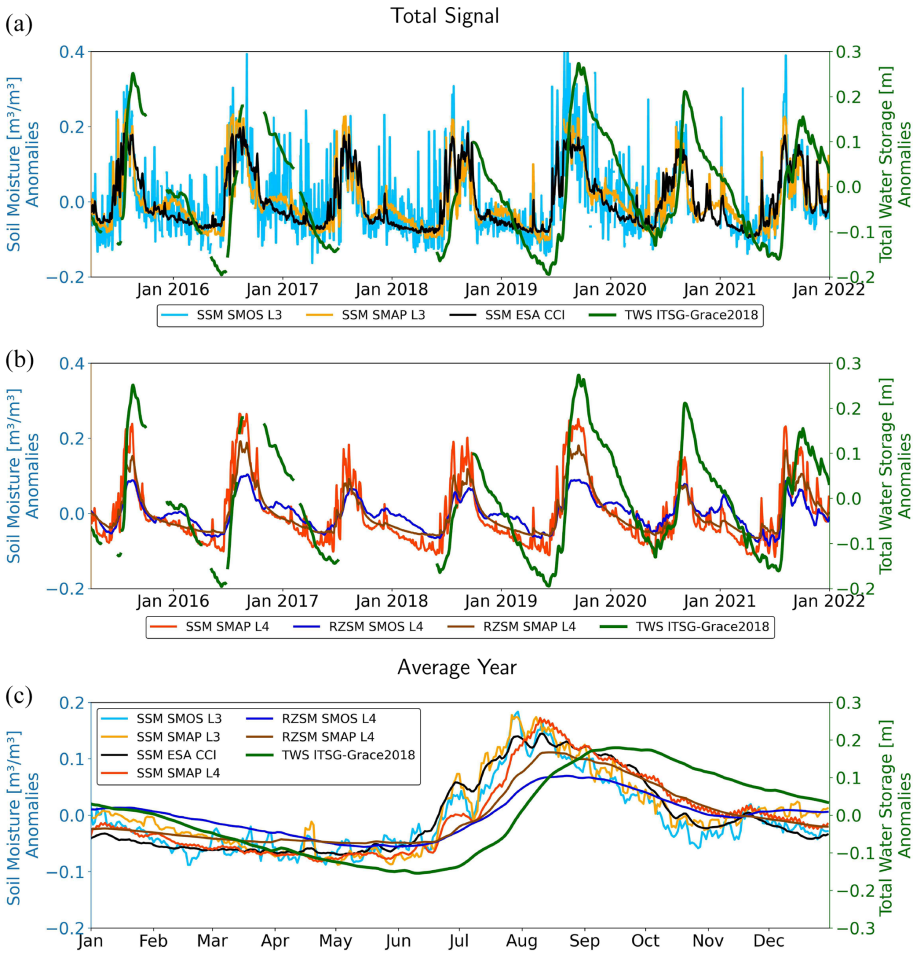

Figure 3. Time series of TWS from ITSG-Grace2018 and satellite SM for an exemplary grid cell around Kota, Rajasthan, in India (25° N, 75° E). Linear trend components have been subtracted from all time series. **(a)** TWS ITSG-Grace2018 vs. SSM from SMOS L3, SMAP L3, and ESA CCI. **(b)** TWS ITSG-Grace2018 vs. SSM from SMAP L4 and RZSM from SMOS L4 and SMAP L4. **(c)** Time series of the average year between TWS and all SM products.

a detailed analysis of this particular phenomenon is beyond the scope of this study.

The described characteristics of the different products are also confirmed when investigating the average year (i.e., the mean value for each day of the year shown in Fig. 3 at the bottom). Even though the short overlapping time span does not allow for the computation of a stable climatology, the increase in the seasonal signal with SM during the monsoon phase between July and September can clearly be identified. The SSM products exhibit a larger seasonal amplitude than the dampened RZSM counterparts. Furthermore, the time shift between SSM and TWS is generally larger than for the RZSM products. Here it can be concluded that the dynamics of RZSM are closer to the variability in the integral TWS signal that represents the entire water column, even though the RZSM data still miss the even slower processes in deeper soil layers and in groundwater.

4.2 Global analysis

The correspondence of the daily time series of TWS from ITSG-Grace2018 with the various SM products is analyzed globally for each 1° continental grid cell and displayed as global maps of the correlation coefficient in Fig. 4. Desert areas, according to the definition provided in Sect. 3.1, are excluded, as the GRACE signal is dominated by noise in these regions, and no reasonable comparison is possible. Additionally, Fig. 5 shows the cumulative distribution functions (CDFs) of cell-based correlation values, both globally and separately, for the major land cover types shown in Fig. 2.

The global patterns of regions with comparably large correlations between GRACE TWS and SM are similar for all SM products. These regions are particularly found in humid climate zones and in seasonally dry climates (parts of tropical South America, Southeast Asia, southeastern USA, northern Australia, and the outer tropics in Africa). The absolute correlation values differ markedly between the SM products.

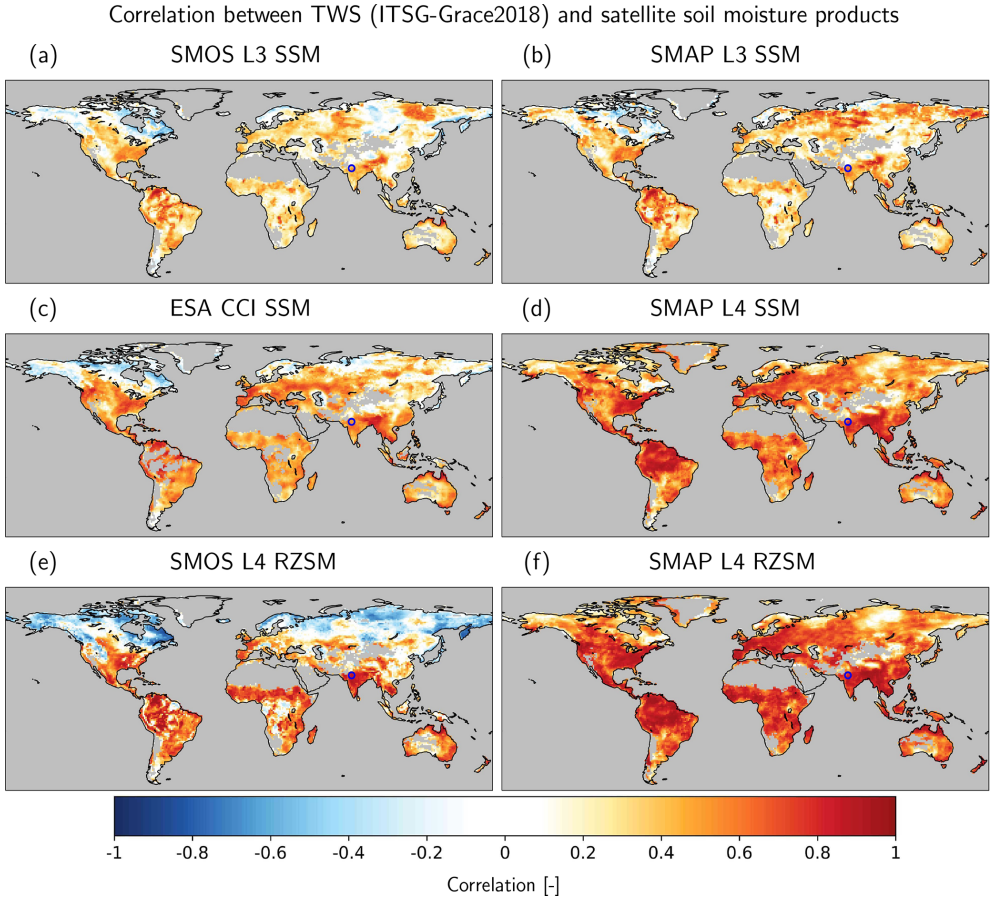

Figure 4. Comparison of the correlation coefficient between all SM products and ITSG-Grace2018. Desert regions are masked out due to low water variability. In all maps, the location of the exemplary time series in India (see Fig. 3) is marked with a blue circle.

The smallest correlations are found for the satellite-only L3 SSM data products (Fig. 4a–c). While maximum values in individual grid cells can reach up to 0.92 (SMOS) and 0.93 (SMAP), the median values amount to 0.23 (SMOS) and 0.27 (SMAP) only. SMOS L3 SSM has negative correlations (Fig. 5), particularly in the northern latitudes that are at least partly influenced by snow cover and frozen ground (Fig. 5c), and has fewer large positive correlations in grid cells that are potentially well suited for SM remote sensing (i.e., that are not influenced by snow, ice, or dense vegetation; Fig. 5b). The latter might be attributed to a larger noise level in the SMOS than in the SMAP time series. The combination data product ESA CCI (black curve in Fig. 5b) generally shows larger correlation values than both the single mission products (except in the northern latitudes), particularly in South America, Africa, and Australia (Fig. 4c). Please note that the masking of, e.g., rainforest areas in the CCI product leads to an overall smaller number of grid cells for the comparison than for SMOS or SMAP. The overall larger correlation of ESA CCI implies that the ensemble product weighs down the spurious contributions of individual data sets. Nevertheless, the interpretation needs to be done with caution, as TWS cannot be directly taken as a benchmark for SSM, and the limitations of the GRACE data product outlined in Sect. 2.1 might additionally hamper the comparison.

The effect of using a land surface model with data assimilation for generating the SMAP L4 SSM product is a strong increase in the correspondence of the temporal dynamics of this SM data set with GRACE-based TWS (Fig. 4d). The CDF in Fig. 5a (red line) reveals the most common correlation values in the range of 0.4–0.7, with a median of 0.52. This increase in the correlation for the L4 SSM data indicates that constraining the SM dynamics by a deterministic modeling approach and by independently observed forcing data, such as precipitation rates and air temperature, leads to a model-dominated product with considerably less noise than the L3 SSM product. For the L4 RZSM products of both SMOS and SMAP, their larger integration depth leads to another increase in the agreement with TWS compared to the respective surface products (Fig. 4e, f). This again indicates that reflecting the slower and delayed water transport processes in deeper soil layers in the L4 RZSM products causes their dynamics to be more similar to the integrative GRACE-based TWS, in particular with respect to the tem-

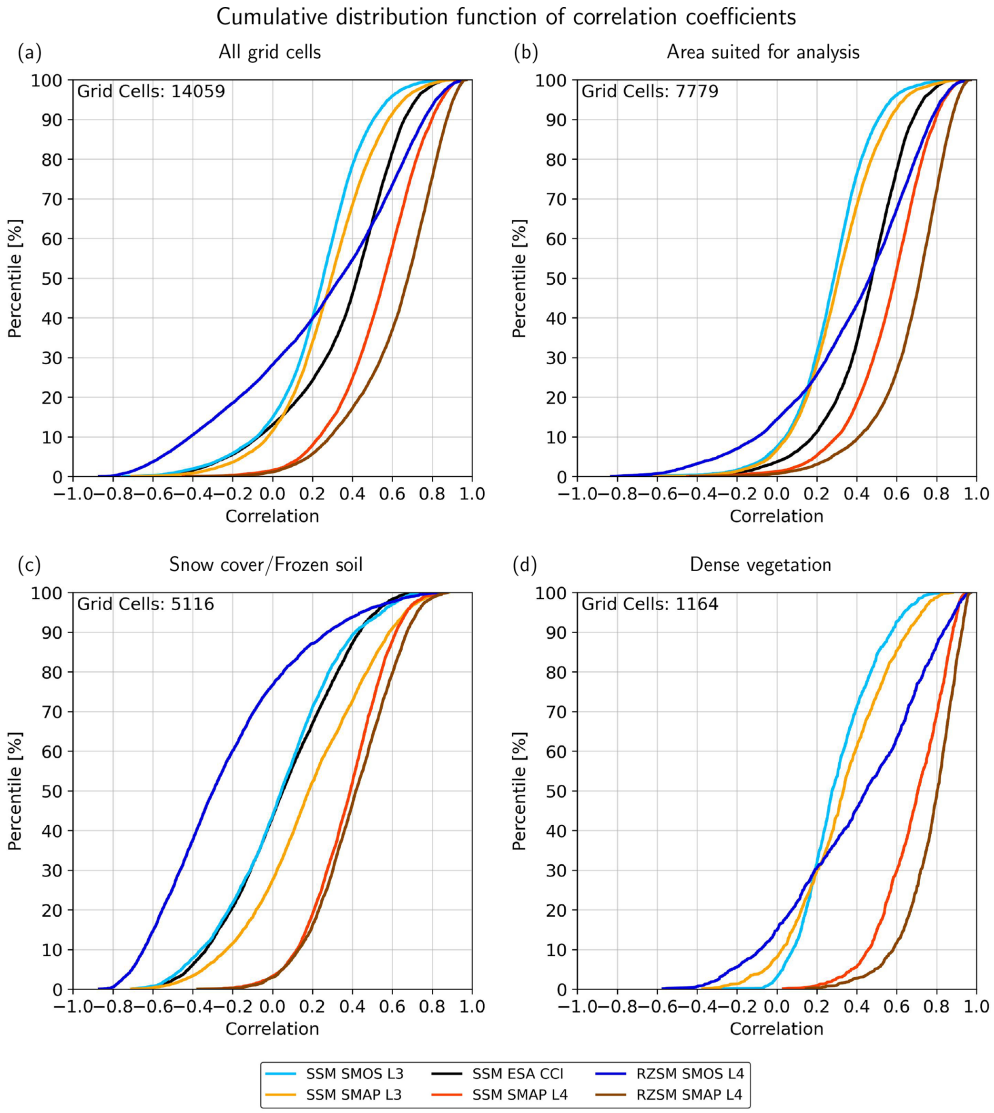

Figure 5. Cumulative distribution functions (CDFs) of cell-based correlation values. **(a)** Showing the CDFs of all grid cells globally. **(b, c, d)** Showing the grid cells for the major land cover types, as defined in Fig. 2. In the upper left corner, the number of grid cells used for the creation of the individual CDFs is shown.

poral phase (also see the time shift analysis below). This applies in particular to the grid cells that are reasonably suited for satellite-based SM monitoring for which the CDFs are shifted strongly to higher correlation values compared to the L3 data, with the most common values of around 0.7 (SMOS) and 0.8 (SMAP; Fig. 5b). In contrast, for SMOS L4 RZSM in high northern latitudes, correlations with TWS become even more negative than for SMOS L3 SSM (see the time shift analysis below). Xu et al. (2021a) have already shown that the SMAP L4 RZSM product outperforms the SMOS L4 product in terms of agreement with in situ measurements from the International Soil Moisture Network, particularly in the Northern Hemisphere.

The different integration volumes and the different processes acting on SM and TWS cause a time shift between their respective dynamics (e.g., Fig. 3). We use a cross-correlation analysis (see Appendix A1) for each grid cell to investigate the time shift on a global scale. Regarding the maps in Fig. 6, a negative time shift (blue colored grid cells) indicates a delay of the GRACE signal; i.e., the maximum of the dominant seasonal signal of TWS occurs later in the year than the maximum of SM. In the Arctic regions, mostly positive shifts (in some cases more than +120 d) are seen, in particular for the two SMOS products (see also the CDFs in Fig. 7). Snow accumulation leads to an increase and a maximum of TWS during the winter season, whereas the maximum of SM is reached during the melting season several

months later, resulting in a delay of SM versus TWS. This effect becomes even more pronounced when the further delay by SM storage in deeper layers is considered in the L4 root zone products of SMAP and, in particular, SMOS. Negative correlation coefficients of TWS and SM time series are a consequence of the inverse seasonal dynamics of the two storage terms (Fig. 5). The least positive time shifts in the northern latitude regions are visible in the ESA CCI data set, which already masks out the data in the time series when observations were taken under the conditions of frozen soil and snow cover (see Sect. 3.1). Positive time shifts are also seen in some tropical forest regions (e.g., the Amazon and Congo rainforests), where the dense vegetation cover hampers the SM retrieval. This is particularly evident in the SSM L3 products (SMOS and SMAP) and persists in the SMOS RZSM, while the data assimilation introduced for SMOS L4 strongly reduces this effect. The positive time shifts can thus be attributed to artifacts in the SM data rather than to a hydrological signal.

In grid cells that are neither influenced by snow cover nor by dense vegetation (Fig. 7b), the time shifts are primarily negative, indicating the delayed dynamics of TWS compared to SM. For the majority of the products, the time shifts are negative and can reach up to −90 d and beyond. A comparison of the different products reveals that the time shifts decrease (i.e., become less negative) the closer the SM products conceptively resemble TWS. The three surface SM products from ESA CCI, SMAP L3, and SMOS L3 show the highest negative time shifts (up to −60 to −90 d in Fig. 6), with median values of −35 d (both ESA CCI and SMAP L3) and −32 d (SMOS L3). The time shifts are smaller for SMAP L4 (SSM; median of −17 d) and even smaller for the RZSM products, with median values of −5 d (SMAP L4 RZSM) and −13 d (SMOS L4 RZSM). This supports the assumption that adding the SM dynamics of deeper soil layers to SSM increases the resemblance to the integrated TWS signal. For SMOS L4 SM, the extrapolation into deeper soil layers even leads to a change from a negative time shift to a positive time shift (i.e., TWS dynamics preceding those of SMOS L4 RZSM) in 17 % of the land areas, e.g., in parts of South America, Asia, and Australia. This points out possible deficiencies in the depth-scaling algorithm for SMOS L4 in some regions in terms of the way that it represents the transport and storage processes from the surface to deeper soil layers with too many delays and that the rates of reduction in the water storage in the deeper layers by evapotranspiration and percolation and/or runoff may be underestimated, thus leaving too much water in the storage for a time period that is too long. While the limitations of the GRACE observations can also be expected to cause some discrepancy between the two data types, there is no known deficit in the GRACE data that may spuriously pull their dynamics to an earlier stage.

4.3 Sub-monthly variations (high-pass filtered data)

The exemplary comparison of the TWS and SM time series in Fig. 3 suggests that fast-changing SM signals might be masked in the TWS time series by the dominating slower dynamics of the deeper layers in the unsaturated zone and in groundwater. Therefore, we isolate the water storage changes on sub-monthly timescales by applying a high-pass filter (third-order Butterworth filter) with a 30 d cutoff frequency (see Appendix B for details). Exemplary high-pass filtered time series for 1.5 years of SMAP L4 RZSM and TWS from ITSG-Grace2018 are shown in Fig. 8 for the same grid cell as in Fig. 3. The overall correlation of the two time series amounts to $\rho = 0.33$, but it varies strongly with signal strength. While the GRACE time series is dominated by noise and only a very small correlation to RZSM of $\rho = 0.17$ was found in dry months (October to June) with very small high-frequency water storage fluctuations, the correlation is higher in the monsoon season (July to September) with $\rho = 0.45$. Additional high-pass filtered time series for grid cells belonging to different climate zones are presented in Appendix C.

The correlations of the high-pass filtered TWS and SM time series (Fig. 9) are considerably smaller than those of the unfiltered time series. This can be expected, as the seasonal storage variations that often cause high correlation values for the unfiltered time series are not present anymore in the filtered ones. Nevertheless, correlations of the sub-monthly signals are generally positive, with only a few grid cells showing negative correlations. Non-significant correlations are stippled in Fig. 9 (for more information on significance testing, see Appendix A2). Again, it can be observed that RZSM products have a stronger correlation with TWS than their SSM counterparts. While the numbers are very small for the SSM of SMOS L3 (maximum value of $\rho_{max} = 0.33$ and significantly positive correlations in only 26 % of land areas covered by the data product, with desert areas excluded), they are larger for SMAP L3 SSM products ($\rho_{max} = 0.37$ and 43 % significantly positive). Again, the larger noise floor of the SMOS data set most likely dominates the high-pass filtered time series. The share of grid cells with significantly positive correlations increases for the combination data product ESA CCI ($\rho_{max} = 0.38$ and 58 % significantly positive) and even more for the data-assimilated product of SMAP L4 SSM ($\rho_{max} = 0.40$ and 71 % significantly positive). The former reveals the positive effect of combining several SSM data sets, which very likely results in a reduction in the high-frequency noise, and the latter indicates the influence of the forcing data of the underlying land surface model. In particular, it can be argued that model forcing with observation-based rainfall data causes major SSM increases to be closer in time and magnitude to the water storage increases that are seen by the GRACE observations. For the root zone, the percentage of the significantly positive grid cells is still low for SMOS L4 (37 %), with only a few larger areas in west-

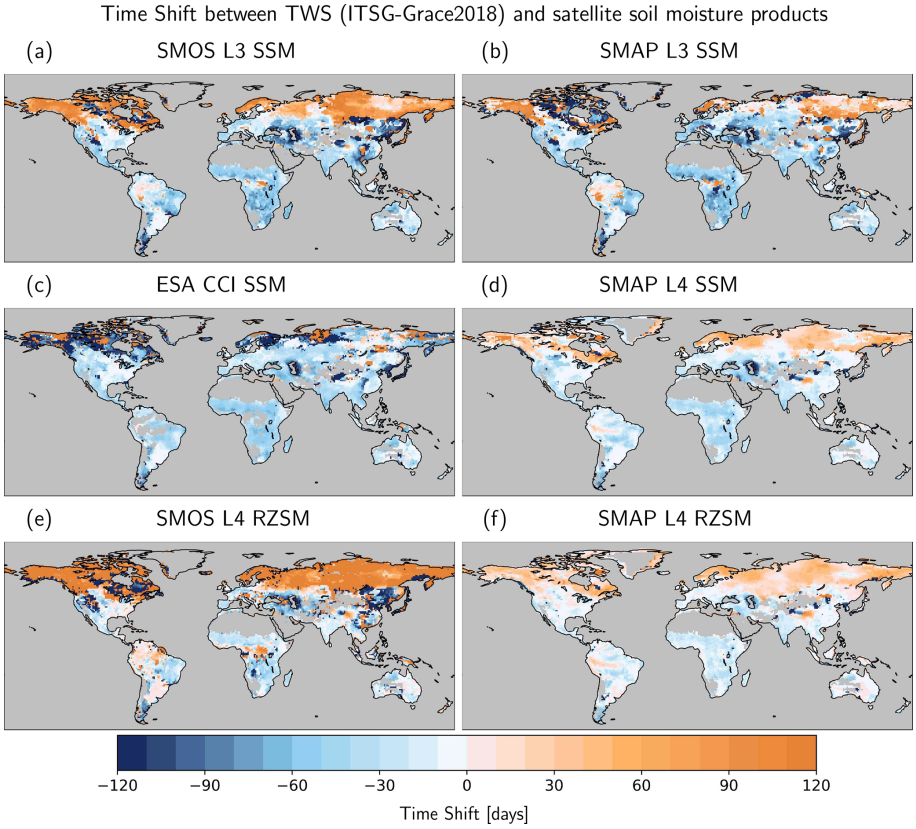

Figure 6. Time shift between SM and TWS time series per grid cell. Negative numbers imply that TWS is delayed in comparison to SM.

ern Brazil, the south of Africa, and India, but the magnitude of the correlations has increased ($\rho_{\max} = 0.50$). For SMAP L4 RZSM, the values are significantly positive in the largest parts of the continents (77 %), with exceptions only in the very high latitudes and some small spots in dry regions in Africa, Australia, and Asia. In large regions (particularly in the southeastern United States, large parts of South America's southeastern region, the Ganges–Brahmaputra basin and China, and northern Australia), the correlations are in the range of 0.5, reaching maximum values of $\rho_{\max} = 0.62$. Overall, even though correlations are rather low for the high-pass filtered signals (with the exception of SMAP L4), they are significantly positive in large parts of the continents, hinting at the fact that satellite gravimetry and SM remote sensing are sensitive to the same hydrological dynamics, even for timescales shorter than 1 month.

Finally, by computing the cross-correlation function for the high-pass filtered signals, we determine, for each grid cell, the time shift in the TWS versus the SM time series that leads to the highest correlation (Fig. 10). Time shifts larger than ± 15 d are masked out because they have no physical meaning, given that a high-pass filter of 30 d was used. The remaining regions with valid results noticeably overlap with the regions in which some correspondence of TWS and SM dynamics has already been found in the correlation analysis with an unshifted time series (Fig. 9). The time shifts found for the high-pass filtered time series are considerably smaller than those found for the full unfiltered signal. Time shifts tend to be negative, with up to -3 d for all SSM products (i.e., TWS is lagging behind SSM). For the RZSM products, however, the time shifts are less negative or close to zero (SMAP L4) or even positive (SMOS L4). The negative time shifts illustrate that GRACE observations represent the depth-integrated water storage dynamics in the subsurface that are delayed relative to SSM, even at sub-monthly timescales. This is corroborated by the observation that the time shifts mostly vanish when deeper layers are included in the SM product (SMAP L4; i.e., when the SM product becomes conceptually closer to the storage that is represented by the TWS observations). The positive time shifts for the SMOS L4 relative to TWS in most parts of the world indicate that the depth-scaling approach used for SMOS L4 may represent transport and storage processes from the surface to deeper soil layers with too much delay, which is similar to the results obtained with the full unfiltered signal. Even for the short timescales considered here with the high-pass filtered signal, some processes such as daily evapotranspiration or runoff that cause water to be removed from the storage may be underestimated.

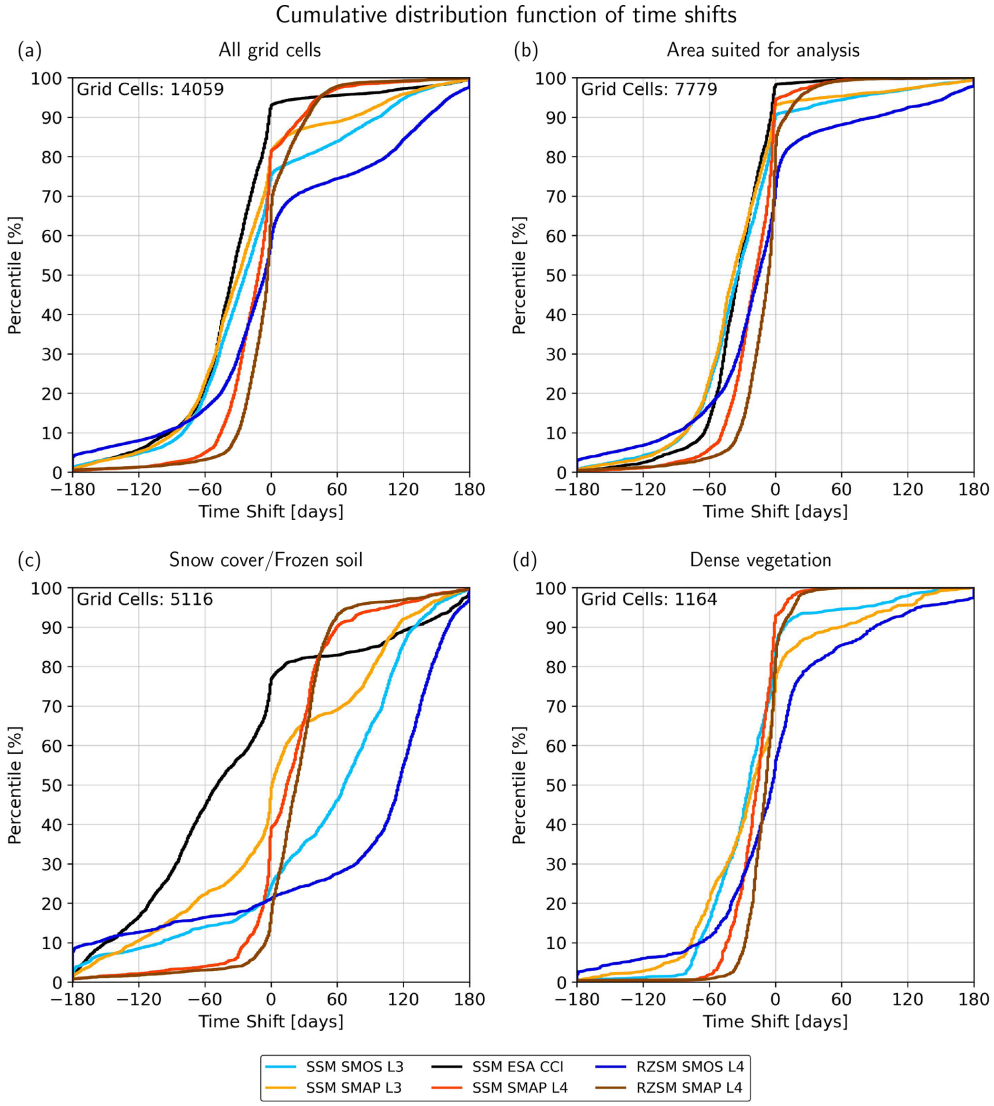

Figure 7. Cumulative distribution functions (CDFs) of the cell-based time shift. **(a)** Showing the CDFs of all grid cells globally. **(b, c, d)** Showing the CDFs for grid cells for the major land cover types which are shown in Fig. 2. In the upper left corner, the number of grid cells used for the creation of the individual CDFs is shown.

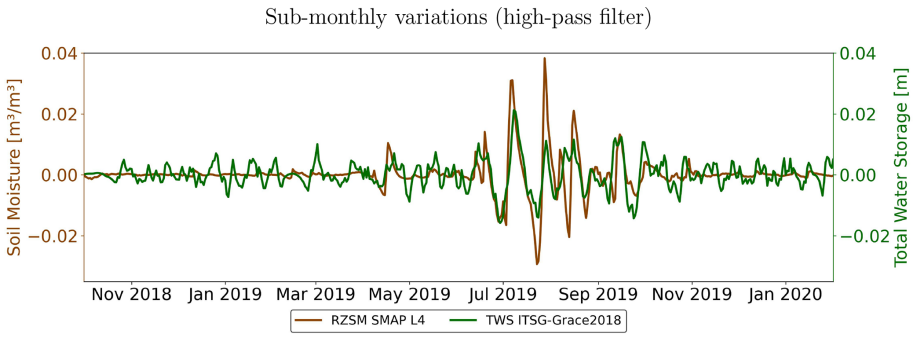

Figure 8. High-pass filtered time series of TWS from ITSG-Grace2018 and RZSM from SMAP L4 for an exemplary grid cell in India (25° N, 75° E).

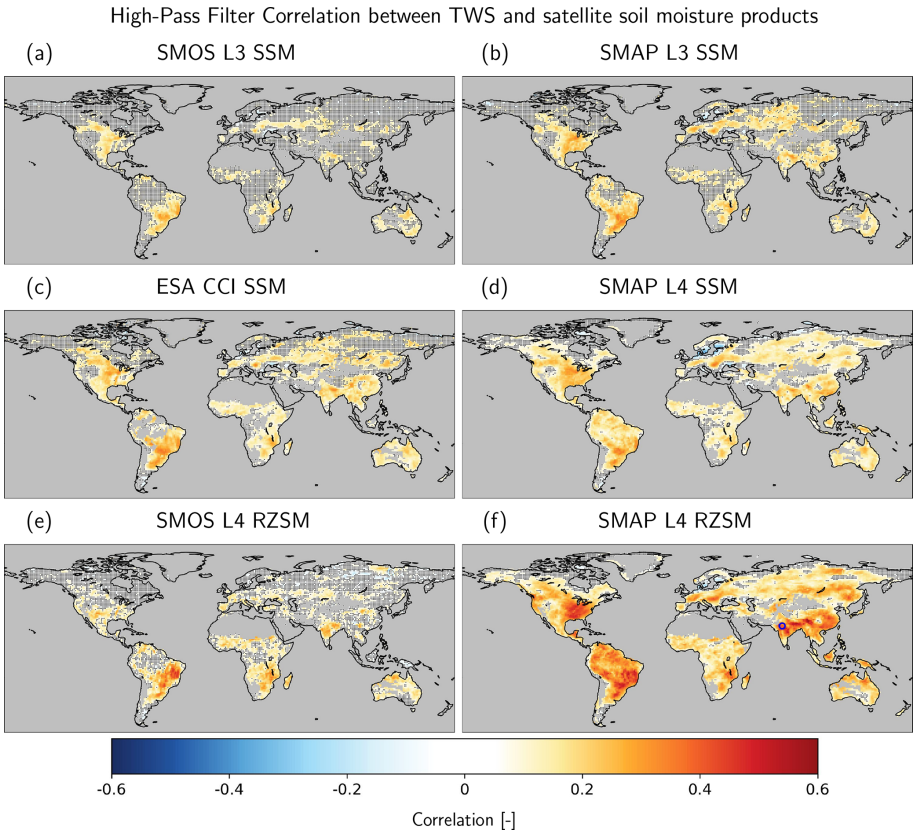

Figure 9. Correlation coefficients of high-pass filtered SM and TWS time series. Grid cells with non-significant correlations are stippled. In the lower-right map **(f)**, the location of the exemplary time series in India (see Fig. 8) is circled in blue.

5 Conclusions and outlook

In this study, we investigated the global relationship of satellite-based SM products and non-standard daily water storage observations from the GRACE and GRACE-FO satellite gravimetry missions. The SM products differ with respect to satellite data (SMAP, SMOS, or a combination of various satellites), soil depth (surface SM or root zone SM), and the degree of post-processing (L3 or L4 data products). Comparisons were carried out by correlation analyses for both the full signal and for sub-monthly variations obtained via high-pass filtering the time series with a 30 d cutoff frequency. Strong correlations between TWS and the different SM products generally occur in the same regions. These regions are mainly characterized by a seasonally wet or semi-arid climate, such as the east and south of Africa, northern parts of India, east Australia, the southeast of China, Eastern Europe, the northwest and southeast of the United States, and significant parts of South America's southeastern region. For many regions, TWS dynamics are delayed relative to the SM dynamics for both short-term variations at the scale of few days and when considering the seasonal dynamics. In particular, in cold and snow-dominated regions, low correlations between TWS and SM dynamics prevail, and the seasonal TWS dynamics are ahead of the SM dynamics.

From a hydrological point of view, both quantities (SM and TWS) actually represent different quantities regarding their spatial domain (first centimeters of soil (SSM) vs. root zone (RZSM) vs. integrated water column of all storage compartments (TWS)), their units (volumetric percentage of water in the soil vs. water mass), and their spatial and temporal variability. The observed (dis)agreements of the SM and TWS time series and the time shifts between them therefore give insights into the relationships between the different water storage compartments, including moisture variations in different soil depths. It should be noted, though, that in some regions non-hydrological effects that remain in the GRACE data (e.g., major earthquakes) or storage variations in other terrestrial water storage compartments that have not explicitly been taken into account in the present study, in particular surface waterbodies, might affect these relationships. Due to the limited spatial resolution of GRACE (i.e., 500 km for the daily gravity field models use here), such strongly localizing effects might also hamper the comparison between SM and TWS in surrounding areas due to spatial leakage, as outlined in Sect. 2.1. While both SM and TWS products are sensitive to the effects of irrigation on near-surface soil moisture,

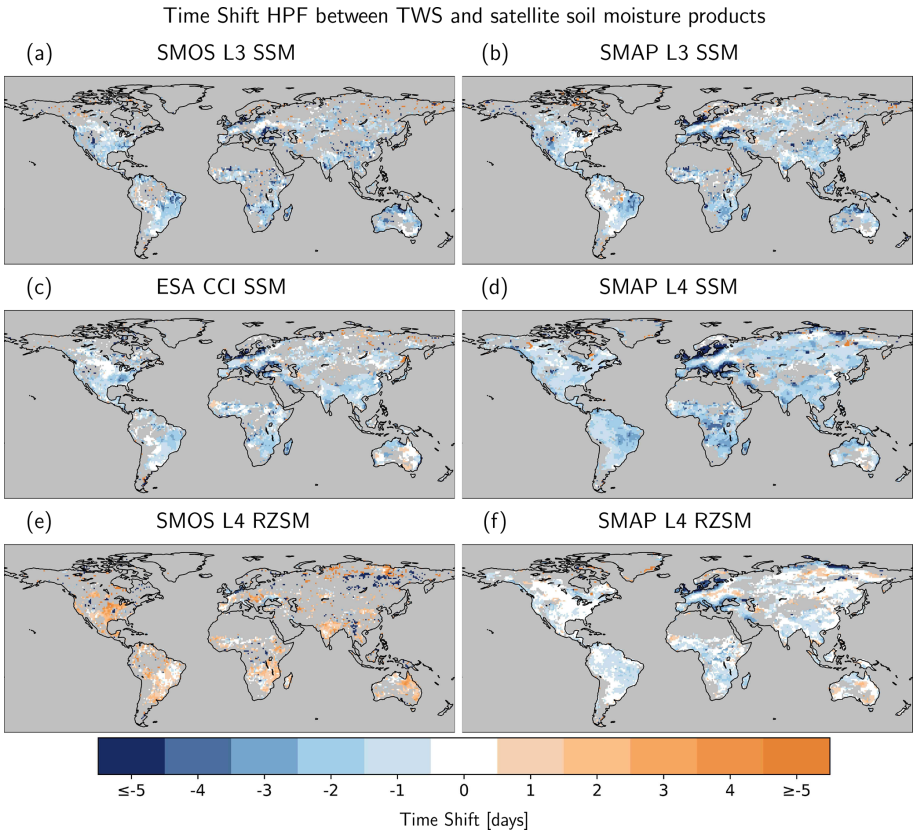

Figure 10. Time shift between high-pass filtered soil moisture and total water storage time series per grid cell. Negative numbers imply that the TWS is delayed in comparison to the SM.

GRACE-based TWS can provide additional information on the effect of such human impacts on water storage dynamics in the deeper unsaturated zone and in the groundwater, although the latter may be difficult to disentangle if it overlaps with groundwater withdrawal in the same region.

The fact that satellite gravimetry can detect high-frequency signals that are related to SM variations, at least in areas and time spans with sufficiently large short-term variability, is quite remarkable in itself and is shown for the first time in this study. While the standard products of the GRACE and GRACE-FO mission are monthly averages of water storage anomalies, the present study adds a new thematic field in which there is valuable information on the daily GRACE data that goes beyond earlier examples, e.g., floods or hydrometeorological fluxes (Gouweleeuw et al., 2018; Eicker et al., 2020).

For regions where SM plays a dominant role for TWS variations, the results indicate that satellite gravimetry can be used to identify the differences between SM products. Hydrological processes that are relevant for redistributing water vertically in the soil, particularly the percolation into deeper soil layers, can be identified as time shifts between the SM and TWS time series.

In this respect, our results give a preliminary indication that gravity-based TWS variations might have the potential to assess different methods of depth scaling (i.e., methods that are used to extrapolate surface SM variations to deeper soil layers). Such an assessment might be based on the analysis of time shifts between TWS and the depth-scaled SM time series. Assuming that the TWS signal for the region of interest and for the relevant temporal scale is dominated by SM variations, the absence of a time shift between TWS and the depth-scaled SM time series might be considered to be an indicator of a suitable depth-scaling approach. For the analyses presented here, this tends to be the case for the SMAP L4 RZSM data. In contrast, negative time shifts (i.e., SM dynamics that are ahead of those of TWS) may indicate that the delay of depth-integrated SM dynamics introduced by the depth-scaling approach is not sufficient enough. In turn, positive time shifts after depth scaling, as found here for some regions for the SMOS L4 RZSM data, may point out that the depth-scaling approach mimics the soil water redistribution processes in a way that causes a delay that is too large for the SM dynamics.

While satellite gravimetry can identify short-term SM changes in regions and time spans with large sub-seasonal storage variability, this does not work well in cases with

low signal-to-noise ratios (SNRs) of high-frequency variations. In the current study, spatial masking was applied so that desert areas were completely excluded from the analysis, and some other regions (frozen ground and dense vegetation) were discussed separately from the areas that are not influenced by either effect. Nevertheless, there are still many areas worldwide where the SNR is high in certain periods, e.g., during the rain season but low in other time periods. Therefore, an additional temporal masking and the exploration of metadata such as snow flags or indicators of low SNR is promising for an extended comparison in future.

Ongoing improvements to the GRACE/-FO data processing and future improvements in gravity field determination with the GRACE-FO laser ranging instrument measurements and with next-generation gravity missions (NGGMs), such as a constellation of two GRACE-like missions operating simultaneously at differently inclined orbits (Purkhauser et al., 2020), will give prospective increases in the temporal and spatial resolution of satellite-based TWS data in future. This can be expected to be particularly beneficial for analyzing fast-changing and rather small-scale SM variations. The present study provides the first evidence of the insights into the hydrological dynamics that can be gained from a combination of TWS and SM remote sensing data.

Appendix A: Metrics

A1 Correlation and cross-correlation

Suitable metrics are required to compare the time series of soil moisture (SM) and terrestrial water storage (TWS) for each continental grid cell. Since a direct comparison of the absolute values of the two variables is not possible due to the different integration depths and units, we analyze their relationship using Pearson's pairwise correlation coefficient ρ_{xy}, which is defined as the covariance of two variables (x, y) divided by the product of their standard deviations:

$$\rho_{xy} = \frac{\sum_{t=1}^{T} (x_t - \overline{x})(y_t - \overline{y})}{\sqrt{\sum_{t=1}^{T} (x_t - \overline{x})^2} \sqrt{\sum_{t=1}^{T} (y_t - \overline{y})^2}}. \tag{A1}$$

The summation is performed over all daily time steps t of the available time series with a length of T days.

Possible time lags between the TWS and SM time series are determined using cross-correlation analysis, which identifies the time shift k for which the two time series show maximum correlation. The concept of cross-correlation is shown in Eqs. (A2) and (A3), according to Box et al. (1994), in which first the covariance c_{xy} between the two time series x_t and y_t for a given time lag k is calculated as follows:

$$c_{xy}(k) = \begin{cases} \frac{1}{T} \sum_{t=1}^{T-k} (x_t - \overline{x})(y_{t+k} - \overline{y}) & \text{for } k = 0, 1, 2, \ldots n \\ \frac{1}{T} \sum_{t=1}^{T+k} (y_t - \overline{y})(x_{t-k} - \overline{x}) & \text{for } k = 0, -1, -2, \ldots -n, \end{cases} \tag{A2}$$

where $\overline{x}$ and $\overline{y}$ denote the mean values of the time series, and t indicates the respective point in time. We use $n = 180$ in our analysis, resulting in a total of 360 different covariances for each grid cell ($k = -180$ to 180; ± 6 months). From the covariance, the cross-correlation r is computed as follows:

$$r_{xy}(k) = \frac{c_{xy}(k)}{s_x s_y}, \tag{A3}$$

where s_x and s_y denote the standard deviations of the time series. The time lag between SM and TWS is the value of k for which the maximum cross-correlations is obtained.

A2 Significance test

To identify grid cells with significant correlations between different time series, we use hypothesis testing, with the null hypothesis H_0 stating that the correlation is not significantly different from zero and the alternative hypothesis H_A assuming a non-zero correlation.

$$\begin{aligned} H_0 &: p = 0 \\ H_A &: p \neq 0 \end{aligned} \tag{A4}$$

A statistical test is carried out by computing the test variable T, which is distributed with $n - 2$ degrees of freedom, according to Student's t distribution.

$$T = \frac{|\rho| \sqrt{n-2}}{\sqrt{1 - p^2}} \sim t_{n-2} \tag{A5}$$

In Eq. (A5), n is the total number of days with both TWS and SM observations for the respective grid cell. The test assumes uncorrelated observations from 1 d to the next, which, however, is not strictly the case for the time series at hand. An autocorrelation analysis was carried out for a large number of exemplary grid cells to determine a mean correlation length of 3 d for surface and 5 d for root zone products. Consequently, the degree of freedom was adjusted to $n/3 - 2$ (SSM) or $n/5 - 2$ (RZSM). For the significance test, we chose a significance level of $\alpha = 0.05$ and calculated the corresponding quantiles $K = F_t^{-1}(\alpha, n/3 - 2)$ (SSM) or $K = F_t^{-1}(\alpha, n/5 - 2)$ (RZSM). If $T \leq K$, the null hypothesis cannot be rejected, and the correlation is assumed to be insignificant. If $T > K$, then it is reasonable to assume that the alternative hypothesis is correct and that the correlation deviates considerably from zero.

Appendix B: Derivation of sub-monthly signals using a Butterworth high-pass filter

In this section, we demonstrate the computation of the high-pass filtered signals for the exemplary grid cell around Kota, India (also shown in Sect. 4.3 of the main text). Figure B1 shows the TWS from ITSG-Grace2018 (green lines) and RZSM from SMAP L4 (brown lines) over a 15-month period (October 2018 to December 2019). The Butterworth high-pass filter, with a cutoff frequency of 30 d, was applied to remove signals with periods longer than 30 d and thus to isolate sub-monthly fluctuations. The darker green and brown colors illustrate the high-pass filtered signal for both variables. Additionally, the corresponding low-pass filtered signals (i.e., containing signals with periods longer than 30 d) are added as dotted lines. Summing up the high-pass filtered signal and the low-pass filtered signal again results in the original full signal (shown in the respective brighter colors). It can clearly be seen that the high-pass filtered time series capture the fast variations present in the original time series. These time series are the same as those displayed in Fig. 8.

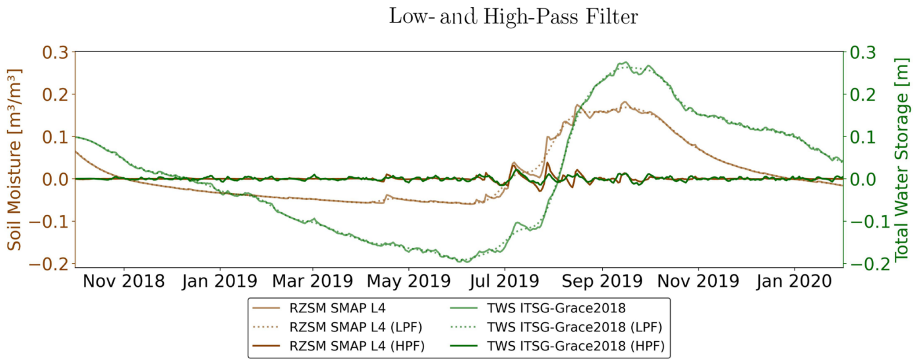

Figure B1. Sub-monthly signals using a Butterworth high-pass filter (HPF), together with the full and the low-pass filtered (LPF) time series, which are shown here for TWS from GRACE and root zone soil moisture (RZSM) from SMAP.

Appendix C: Other examples of high-pass filtered time series

In addition to the high-pass filtered signal computed for the example grid cell in Kota, India, as shown before, Fig. C1 displays the high-pass filtered signals for SM from SMAP L4 RZSM and TWS from ITSG-Grace2018 in some other geographical locations of different aridity. These places were chosen to illustrate the dynamics of the two variables under different environmental conditions and signal characteristics. Figure C1a is for a location in the northwest of the state of Arkansas in the United States. The climate is humid and subtropical, with a hot summer and no specific dry season. Accordingly, the time series show fast fluctuations and a high correspondence of SM and TWS throughout the year, with a correlation of $\rho = 0.43$. At a location in Hungary (Fig. C1b), with a humid and continental climate with warm summers, rain occurs throughout the year, while snow occurs during the winter months. The high-pass filtered SM and TWS time series show a correlation of $\rho = 0.31$ at this location. The time series of Fig. C1c are for a location north of the Kalahari Desert in Botswana. The climate there is semi-arid and mostly dry throughout the year, but there is a wet period, with strong rainfall events during the summer. These events are clearly visible in both TWS and SM time series, with good correspondence, while no correlation and largely noise in the TWS data are visible during the dry period. At this location, the correlation over the entire time period is low, with $\rho = 0.11$, but it is higher when only the precipitation period is considered, with $\rho = 0.23$.

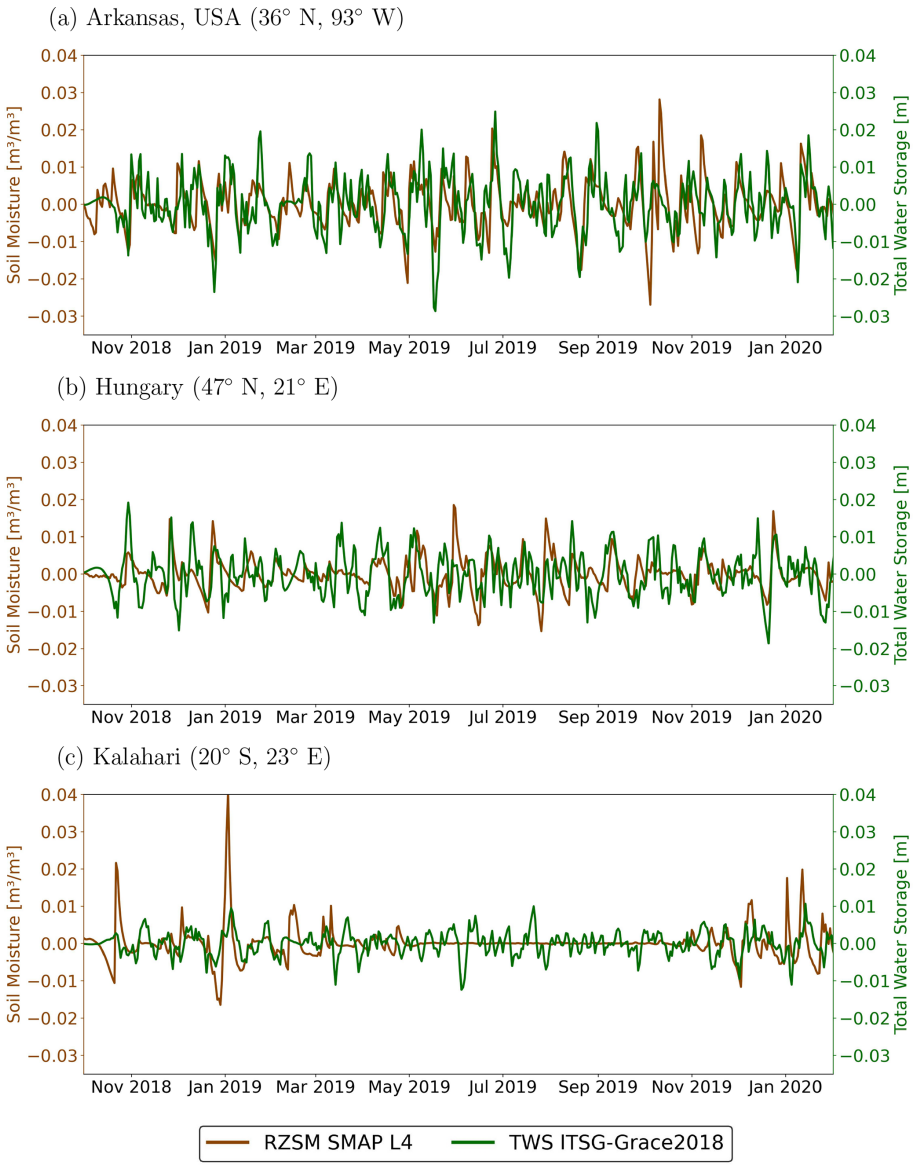

Figure C1. High-pass filtered time series for grid cells in different climatic conditions.

Data availability. The daily GRACE data products of ITSG-Grace2018 are publicly available from TU Graz (https://doi.org/10.5880/ICGEM.2018.003, Mayer-Gürr et al., 2018). The ESA CCI soil moisture product can be downloaded from the ESA's Climate Change Initiative (CCI) web page (https://doi.org/10.5285/ea3eb0714dc6402b905fe9f7ee50dbbc, Dorigo et al., 2023). Soil moisture products (Level 3 and Level 4) from the ESA's SMOS mission are made available by the Centre Aval de Traitement des Données SMOS (CATDS; https://doi.org/10.12770/9cef422f-ed3f-4090-9556-b2e895ba2ca8, CATDS, 2022a; https://doi.org/10.12770/316e77af-cb72-4312-96a3-3011cc5068d4, CATDS, 2022b). Soil moisture products (Level 3 and Level 4) from NASA's SMAP mission are provided by the National Snow and Ice Data Center (NSIDC; https://doi.org/10.5067/OMHVSRGFX38O, O'Neill et al., 2021; https://doi.org/10.5067/08S1A6811J0U, Reichle et al., 2021).

Author contributions. Conceptualization: DB and AE. Methodology: DB, AE, and LJ. Data curation and visualization: DB. Software: DB and LJ. Investigation: all authors. Funding acquisition: AE. Writing and review and editing of the original draft: all authors.

Competing interests. The contact author has declared that none of the authors has any competing interests.

Disclaimer. Publisher's note: Copernicus Publications remains neutral with regard to jurisdictional claims in published maps and institutional affiliations.

Review statement. This paper was edited by Markus Hrachowitz and reviewed by two anonymous referees.

References

Abelen, S.: Signals of Weather Extremes in Soil Moisture and Terrestrial Water Storage from Multi-Sensor Earth Observations and Hydrological Modeling, PhD Thesis, Technische Universität München, München, https://nbn-resolving.de/urn/resolver.pl?urn:nbn:de:bvb:91-diss-20160627-1295206-1-4 (last access: 23 June 2023), 2016.

Abelen, S., Seitz, F., Abarca-del Rio, R., and Güntner, A.: Droughts and Floods in the La Plata Basin in Soil Moisture Data and GRACE, Remote Sensing, 7, 7324–7349, https://doi.org/10.3390/rs70607324, 2015.

Al Bitar, A. and Mahmoodi, A.: Algorithm Theoretical Basis Document (ATBD) for the SMOS Level 4 Root Zone Soil Moisture, v30_01, Zenodo, https://doi.org/10.5281/ZENODO.4298572, 2020.

Al Bitar, A., Kerr, Y., Merlin, O., Cabot, F., and Wigneron, J.-P.: Global drought index from SMOS soil moisture, in: IEEE International Geoscience and Remote Sensing Symposium, IGARSS 2013. Melbourne, Australia, 21–26 July 2013, 2013.

Al Bitar, A., Mialon, A., Kerr, Y. H., Cabot, F., Richaume, P., Jacquette, E., Quesney, A., Mahmoodi, A., Tarot, S., Parrens, M., Al-Yaari, A., Pellarin, T., Rodriguez-Fernandez, N., and Wigneron, J.-P.: The global SMOS Level 3 daily soil moisture and brightness temperature maps, Earth System Science Data, 9, 293–315, https://doi.org/10.5194/essd-9-293-2017, 2017.

Bauer-Marschallinger, B., Paulik, C., Hochstöger, S., Mistelbauer, T., Modanesi, S., Ciabatta, L., Massari, C., Brocca, L., and Wagner, W.: Soil Moisture from Fusion of Scatterometer and SAR: Closing the Scale Gap with Temporal Filtering, Remote Sensing, 10, 1030, https://doi.org/10.3390/rs10071030, 2018.

Baur, O., Kuhn, M., and Featherstone, W.: GRACE-derived ice-mass variations over Greenland by accounting for leakage effects, J. Geophys. Res.-Sol. Ea., 114, B06407, https://doi.org/10.1029/2008JB006239, 2009.

Bergmann, I. and Dobslaw, H.: Short-term transport variability of the Antarctic Circumpolar Current from satellite gravity observations, J. Geophys. Res.-Oceans, 117, C05044, https://doi.org/10.1029/2012JC007872, 2012.

Bonin, J. A. and Chambers, D. P.: Evaluation of high-frequency oceanographic signal in GRACE data: Implications for de-aliasing, Geophys. Res. Lett., 38, L17608, https://doi.org/10.1029/2011GL048881, 2011.

Box, G., Jenkins, G., and Reinsel, G.: Time Series Analysis: Forecasting and Control, vol. 3, Prentice Hall, New Jersey, USA, ISBN 9780130607744, 1994.

Camps, A., Park, H., Pablos, M., Foti, G., Gommenginger, C. P., Liu, P.-W., and Judge, J.: Sensitivity of GNSS-R Spaceborne Observations to Soil Moisture and Vegetation, IEEE J. Sel. Top. Appl., 9, 4730–4742, https://doi.org/10.1109/JSTARS.2016.2588467, 2016.

Carranza, C. D. U., van der Ploeg, M. J., and Torfs, P. J. J. F.: Using lagged dependence to identify (de)coupled surface and subsurface soil moisture values, Hydrol. Earth Syst. Sci., 22, 2255–2267, https://doi.org/10.5194/hess-22-2255-2018, 2018.

CATDS: CATDS-PDC L3SM Filtered – 1 day global map of soil moisture values from SMOS satellite, CATDS (CNES, IFREMER, CESBIO) [data set], https://doi.org/10.12770/9cef422f-ed3f-4090-9556-b2e895ba2ca8, 2022a.

CATDS: CATDS-PDC L4SM RZSM – 1 day global map of root zone soil moisture values from SMOS satellite, CATDS (CNES, IFREMER, CESBIO) [data set], https://doi.org/10.12770/316e77af-cb72-4312-96a3-3011cc5068d4, 2022b.

Cheng, M. and Ries, J.: The unexpected signal in GRACE estimates of C_{20}, J. Geodesy, 91, 897–914, https://doi.org/10.1007/s00190-016-0995-5, 2017.

Chew, C. C. and Small, E. E.: Soil Moisture Sensing Using Spaceborne GNSS Reflections: Comparison of CYGNSS Reflectivity to SMAP Soil Moisture, Geophys. Res. Lett., 45, 4049–4057, https://doi.org/10.1029/2018GL077905, 2018.

Cui, C., Xu, J., Zeng, J., Chen, K.-S., Bai, X., Lu, H., Chen, Q., and Zhao, T.: Soil Moisture Mapping from Satellites: An Intercomparison of SMAP, SMOS, FY3B, AMSR2, and ESA CCI over Two Dense Network Regions at Different Spatial Scales, Remote Sensing, 10, 33, https://doi.org/10.3390/rs10010033, 2017.

De Lannoy, G. J. M. and Reichle, R. H.: Global Assimilation of Multiangle and Multipolarization SMOS Brightness Temperature Observations into the GEOS-5 Catchment Land Surface Model for Soil Moisture Estimation, J. Hydrometeorol., 17, 669–691, https://doi.org/10.1175/JHM-D-15-0037.1, 2016.

Dobslaw, H., Bergmann-Wolf, I., Dill, R., Poropat, L., Thomas, M., Dahle, C., Esselborn, S., König, R., and Flechtner, F.: A new high-resolution model of non-tidal atmosphere and ocean mass variability for de-aliasing of satellite gravity observations: AOD1B RL06, Geophys. J. Int., 211, 263–269, https://doi.org/10.1093/gji/ggx302, 2017.

Dorigo, W., Wagner, W., Albergel, C., Albrecht, F., Balsamo, G., Brocca, L., Chung, D., Ertl, M., Forkel, M., Gruber, A., Haas, E., Hamer, P. D., Hirschi, M., Ikonen, J., de Jeu, R., Kidd, R., Lahoz, W., Liu, Y. Y., Miralles, D., Mistelbauer, T., Nicolai-Shaw, N., Parinussa, R., Pratola, C., Reimer, C., van der Schalie, R., Seneviratne, S. I., Smolander, T., and Lecomte, P.: ESA CCI Soil Moisture for improved Earth system understanding: State-of-the art and future directions, Remote Sens. Environ., 203, 185–215, https://doi.org/10.1016/j.rse.2017.07.001, 2017.

Dorigo, W., Dietrich, S., Aires, F., Brocca, L., Carter, S., Cretaux, J.-F., Dunkerley, D., Enomoto, H., Forsberg, R., Güntner, A., Hegglin, M. I., Hollmann, R., Hurst, D. F., Johannessen, J. A., Kummerow, C., Lee, T., Luojus, K., Looser, U., Miralles, D. G., Pellet, V., Recknagel, T., Vargas, C. R., Schneider, U., Schoeneich, P., Schröder, M., Tapper, N., Vuglinsky, V., Wagner, W., Yu, L., Zappa, L., Zemp, M., and Aich, V.: Closing the Water Cycle from Observations across Scales: Where Do We Stand?, B. Am. Meteorol. Soc., 102, E1897–E1935, https://doi.org/10.1175/BAMS-D-19-0316.1, 2021a.

Dorigo, W., Himmelbauer, I., Aberer, D., Schremmer, L., Petrakovic, I., Zappa, L., Preimesberger, W., Xaver, A., Annor, F.,

Ardö, J., Baldocchi, D., Bitelli, M., Blöschl, G., Bogena, H., Brocca, L., Calvet, J.-C., Camarero, J. J., Capello, G., Choi, M., Cosh, M. C., van de Giesen, N., Hajdu, I., Ikonen, J., Jensen, K. H., Kanniah, K. D., de Kat, I., Kirchengast, G., Kumar Rai, P., Kyrouac, J., Larson, K., Liu, S., Loew, A., Moghaddam, M., Martínez Fernández, J., Mattar Bader, C., Morbidelli, R., Musial, J. P., Osenga, E., Palecki, M. A., Pellarin, T., Petropoulos, G. P., Pfeil, I., Powers, J., Robock, A., Rüdiger, C., Rummel, U., Strobel, M., Su, Z., Sullivan, R., Tagesson, T., Varlagin, A., Vreugdenhil, M., Walker, J., Wen, J., Wenger, F., Wigneron, J. P., Woods, M., Yang, K., Zeng, Y., Zhang, X., Zreda, M., Dietrich, S., Gruber, A., van Oevelen, P., Wagner, W., Scipal, K., Drusch, M., and Sabia, R.: The International Soil Moisture Network: serving Earth system science for over a decade, Hydrol. Earth Syst. Sci., 25, 5749–5804, https://doi.org/10.5194/hess-25-5749-2021, 2021b.

Dorigo, W. A., Scipal, K., Parinussa, R. M., Liu, Y. Y., Wagner, W., de Jeu, R. A. M., and Naeimi, V.: Error characterisation of global active and passive microwave soil moisture datasets, Hydrol. Earth Syst. Sci., 14, 2605–2616, https://doi.org/10.5194/hess-14-2605-2010, 2010.

Dorigo, W., Preimesberger, W., Moesinger, L., Pasik, A., Scanlon, T., Hahn, S., Van der Schalie, R., Van der Vliet, M., De Jeu, R., Kidd, R., Rodriguez-Fernandez, N., and Hirschi, M.: ESA Soil Moisture Climate Change Initiative (Soil_Moisture_cci): Version 07.1 data collection, NERC EDS Centre for Environmental Data Analysis [data set], https://doi.org/10.5285/ea3eb0714dc6402b905fe9f7ee50dbbc, 2023.

Eicker, A., Jensen, L., Wöhnke, V., Dobslaw, H., Kvas, A., Mayer-Gürr, T., and Dill, R.: Daily GRACE satellite data evaluate short-term hydro-meteorological fluxes from global atmospheric reanalyses, Sci. Rep., 10, 4504, https://doi.org/10.1038/s41598-020-61166-0, 2020.

Entekhabi, D., Njoku, E. G., O'Neill, P. E., Kellogg, K. H., Crow, W. T., Edelstein, W. N., Entin, J. K., Goodman, S. D., Jackson, T. J., Johnson, J., Kimball, J., Piepmeier, J. R., Koster, R. D., Martin, N., McDonald, K. C., Moghaddam, M., Moran, S., Reichle, R., Shi, J. C., Spencer, M. W., Thurman, S. W., Tsang, L., and Van Zyl, J.: The Soil Moisture Active Passive (SMAP) Mission, P. IEEE, 98, 704–716, https://doi.org/10.1109/JPROC.2010.2043918, 2010.

Entekhabi, D., Yueh, S., O'Neill, P. E., Kellogg, K. H., Allen, A., Bindlish, R., Brown, M., Chan, S., Colliander, A., Crow, W. T., Das, N., De Lannoy, G., Dunbar, R. S., Edelstein, W. N., Entin, J. K., Escobar, V., Goodman, S. D., Jackson, T. J., Jai, B., Johnson, J., Kim, E., Kim, S., Kimball, J., Koster, R. D., Leon, A., McDonald, K. C., Moghaddam, M., Mohammed, P., Moran, S., Njoku, E. G., Piepmeier, J. R., Reichle, R., Rogez, F., Shi, J., Spencer, M. W., Thurman, S. W., Tsang, L., Van Zyl, J., Weiss, B., and West, R.: SMAP Handbook: Soil Moisture Active Passive: Mapping Soil Moistureand Freeze/Thaw from Space, Pasadena, USA, https://asf.alaska.edu/wp-content/uploads/2019/03/smap_handbook.pdf (last access: 23 June 2023), 2014.

Escorihuela, M., Chanzy, A., Wigneron, J., and Kerr, Y.: Effective soil moisture sampling depth of L-band radiometry: A case study, Remote Sens. Environ., 114, 995–1001, https://doi.org/10.1016/j.rse.2009.12.011, 2010.

Gouweleeuw, B. T., Kvas, A., Gruber, C., Gain, A. K., Mayer-Gürr, T., Flechtner, F., and Güntner, A.: Daily GRACE gravity field solutions track major flood events in the Ganges–Brahmaputra Delta, Hydrol. Earth Syst. Sci., 22, 2867–2880, https://doi.org/10.5194/hess-22-2867-2018, 2018.

Gruber, A., Scanlon, T., van der Schalie, R., Wagner, W., and Dorigo, W.: Evolution of the ESA CCI Soil Moisture climate data records and their underlying merging methodology, Earth Syst. Sci. Data, 11, 717–739, https://doi.org/10.5194/essd-11-717-2019, 2019.

Güntner, A., Stuck, J., Werth, S., Döll, P., Verzano, K., and Merz, B.: A global analysis of temporal and spatial variations in continental water storage, Water Resour. Res., 43, W05416, https://doi.org/10.1029/2006WR005247, 2007.

Güntner, A., Reich, M., Mikolaj, M., Creutzfeldt, B., Schroeder, S., and Wziontek, H.: Landscape-scale water balance monitoring with an iGrav superconducting gravimeter in a field enclosure, Hydrol. Earth Syst. Sci., 21, 3167–3182, https://doi.org/10.5194/hess-21-3167-2017, 2017.

H SAF: Scatterometer Root Zone Soil Moisture (RZSM) Data Record 10km resolution – Multimission, EUMETSAT SAF on Support to Operational Hydrology and Water Management [data set], https://doi.org/10.15770/EUM_SAF_H_0008, 2020.

Karthikeyan, L., Pan, M., Wanders, N., Kumar, D. N., and Wood, E. F.: Four decades of microwave satellite soil moisture observations: Part 2. Product validation and inter-satellite comparisons, Adv. Water Resour., 109, 236–252, https://doi.org/10.1016/j.advwatres.2017.09.010, 2017.

Kerr, Y. H., Waldteufel, P., Wigneron, J.-P., Delwart, S., Cabot, F., Boutin, J., Escorihuela, M. J., Font, J., Reul, N., Gruhier, C., Juglea, S. E., Drinkwater, M. R., Hahne, A., Martín-Neira, M., and Mecklenburg, S.: The SMOS Mission: New Tool for Monitoring Key Elements of the Global Water Cycle, P. IEEE, 98, 666–687, https://doi.org/10.1109/JPROC.2010.2043032, 2010.

Kim, H. and Lakshmi, V.: Use of Cyclone Global Navigation Satellite System (CyGNSS) Observations for Estimation of Soil Moisture, Geophys. Res. Lett., 45, 8272–8282, https://doi.org/10.1029/2018GL078923, 2018.

Kim, S., Dong, J., and Sharma, A.: A Triple Collocation-Based Comparison of Three L-Band Soil Moisture Datasets, SMAP, SMOS-IC, and SMOS, Over Varied Climates and Land Covers, Frontiers in Water, 3, 693172, https://doi.org/10.3389/frwa.2021.693172, 2021.

Kurtenbach, E., Eicker, A., Mayer-Gürr, T., Holschneider, M., Hayn, M., Fuhrmann, M., and Kusche, J.: Improved daily GRACE gravity field solutions using a Kalman smoother, J. Geodyn., 59–60, 39–48, https://doi.org/10.1016/j.jog.2012.02.006, 2012.

Kvas, A., Behzadpour, S., Ellmer, M., Klinger, B., Strasser, S., Zehentner, N., and Mayer-Gürr, T.: ITSG-Grace2018: Overview and Evaluation of a New GRACE-Only Gravity Field Time Series, J. Geophys. Res.-Sol. Ea., 124, 9332–9344, https://doi.org/10.1029/2019JB017415, 2019.

Lambeck, K.: Geophysical geodesy: the slow deformations of the earth Lambeck, Oxford [England], Clarendon Press, New York, Oxford University Press, ISBN 9780198544371, 1988.

Landerer, F. W., Flechtner, F. M., Save, H., Webb, F. H., Bandikova, T., Bertiger, W. I., Bettadpur, S. V., Byun, S. H., Dahle, C., Dobslaw, H., Fahnestock, E., Harvey, N., Kang, Z., Kruizinga, G.

L. H., Loomis, B. D., McCullough, C., Murböck, M., Nagel, P., Paik, M., Pie, N., Poole, S., Strekalov, D., Tamisiea, M. E., Wang, F., Watkins, M. M., Wen, H., Wiese, D. N., and Yuan, D.: Extending the Global Mass Change Data Record: GRACE Follow-On Instrument and Science Data Performance, Geophys. Res. Lett., 47, e2020GL088306, https://doi.org/10.1029/2020GL088306, 2020.

Lei, F., Crow, W., Shen, H., Parinussa, R., and Holmes, T.: The Impact of Local Acquisition Time on the Accuracy of Microwave Surface Soil Moisture Retrievals over the Contiguous United States, Remote Sensing, 7, 13448–13465, https://doi.org/10.3390/rs71013448, 2015.

Longuevergne, L., Wilson, C. R., Scanlon, B. R., and Crétaux, J. F.: GRACE water storage estimates for the Middle East and other regions with significant reservoir and lake storage, Hydrol. Earth Syst. Sci., 17, 4817–4830, https://doi.org/10.5194/hess-17-4817-2013, 2013.

Mayer-Gürr, T., Behzadpour, S., Ellmer, M., Kvas, A., Klinger, B., Strasser, S., and Zehentner, N.: ITSG-Grace2018 – Monthly, Daily and Static Gravity Field Solutions from GRACE, GFZ Data Services [data set], https://doi.org/10.5880/ICGEM.2018.003, 2018.

Mayer-Gürr, T., Behzadpour, S., Eicker, A., Ellmer, M., Koch, B., Krauss, S., Pock, C., Rieser, D., Strasser, S., Süsser-Rechberger, B., Zehentner, N., and Kvas, A.: GROOPS: A software toolkit for gravity field recovery and GNSS processing, Comput. Geosci., 155, 104864, https://doi.org/10.1016/j.cageo.2021.104864, 2021.

Montzka, C., Bogena, H., Zreda, M., Monerris, A., Morrison, R., Muddu, S., and Vereecken, H.: Validation of Spaceborne and Modelled Surface Soil Moisture Products with Cosmic-Ray Neutron Probes, Remote Sensing, 9, 103, https://doi.org/10.3390/rs9020103, 2017.

O'Neill, P. E., Chan, S., Njoku, E. G., Jackson, T., Bindlish, R., and Chaubell, M. J.: SMAP L3 Radiometer Global Daily 36 km EASE-Grid Soil Moisture, Version 8, NASA National Snow and Ice Data Center Distributed Active Archive Center [data set], https://doi.org/10.5067/OMHVSRGFX38O, 2021.

Owe, M., de Jeu, R., and Walker, J.: A methodology for surface soil moisture and vegetation optical depth retrieval using the microwave polarization difference index, IEEE T. Geosci. Remote S., 39, 1643–1654, https://doi.org/10.1109/36.942542, 2001.

Owe, M., de Jeu, R., and Holmes, T.: Multisensor historical climatology of satellite-derived global land surface moisture, J. Geophys. Res.-Sol. Ea., 113, 687, https://doi.org/10.1029/2007JF000769, 2008.

Peltier, W. R., Argus, D. F., and Drummond, R.: Comment on "An Assessment of the ICE-6G_C (VM5a) Glacial Isostatic Adjustment Model" by Purcell et al., J. Geophys. Res.-Sol. Ea., 123, 2019–2028, https://doi.org/10.1002/2016JB013844, 2017.

Purkhauser, A. F., Siemes, C., and Pail, R.: Consistent quantification of the impact of key mission design parameters on the performance of next-generation gravity missions, Geophys. J. Int., 221, 1190–1210, https://doi.org/10.1093/gji/ggaa070, 2020.

Reichle, R., De Lannoy, G., Koster, R., Crow, W., Kimball, J., and Liu, Q.: SMAP L4 Global 3-hourly 9 km EASE-Grid Surface and Root Zone Soil Moisture Geophysical Data, Version 6, NASA National Snow and Ice Data Center Distributed Active Archive Center [data set], https://doi.org/10.5067/08S1A6811J0U, 2021.

Robinson, D. A., Campbell, C. S., Hopmans, J. W., Hornbuckle, B. K., Jones, S. B., Knight, R., Ogden, F., Selker, J., and Wendroth, O.: Soil Moisture Measurement for Ecological and Hydrological Watershed-Scale Observatories: A Review, Vadose Zone J., 7, 358, https://doi.org/10.2136/vzj2007.0143, 2008.

Sadeghi, M., Babaeian, E., Tuller, M., and Jones, S. B.: The optical trapezoid model: A novel approach to remote sensing of soil moisture applied to Sentinel-2 and Landsat-8 observations, Remote Sens. Environ., 198, 52–68, https://doi.org/10.1016/j.rse.2017.05.041, 2017.

Schmeer, M., Schmidt, M., Bosch, W., and Seitz, F.: Separation of mass signals within GRACE monthly gravity field models by means of empirical orthogonal functions, J. Geodyn., 59–60, 124–132, https://doi.org/10.1016/j.jog.2012.03.001, 2012.

Shiklomanov, I. A.: World fresh water resources, in: Water in Crisis: A Guide to the Word's Fresh Water Resources, edited by: Gleick, P. H., Oxford University Press, New York, USA, ISBN 9780195076288, 1993.

Sun, Y., Riva, R., and Ditmar, P.: Optimizing estimates of annual variations and trends in geocenter motion and J2 from a combination of GRACE data and geophysical models, J. Geophys. Res.-Sol. Ea., 121, 8352–8370, https://doi.org/10.1002/2016JB013073, 2016.

Swenson, S., Chambers, D., and Wahr, J.: Estimating geocenter variations from a combination of GRACE and ocean model output, J. Geophys. Res.-Sol. Ea., 113, B08410, https://doi.org/10.1029/2007JB005338, 2008.

Tangdamrongsub, N., Han, S.-C., Yeo, I.-Y., Dong, J., Steele-Dunne, S. C., Willgoose, G., and Walker, J. P.: Multivariate data assimilation of GRACE, SMOS, SMAP measurements for improved regional soil moisture and groundwater storage estimates, Adv. Water Resour., 135, 103477, https://doi.org/10.1016/j.advwatres.2019.103477, 2020.

Tapley, B. D., Bettadpur, S., Watkins, M., and Reigber, C.: The gravity recovery and climate experiment: Mission overview and early results, Geophys. Res. Lett., 31, L09607, https://doi.org/10.1029/2004GL019920, 2004.

Tian, S., Renzullo, L. J., van Dijk, A. I. J. M., Tregoning, P., and Walker, J. P.: Global joint assimilation of GRACE and SMOS for improved estimation of root-zone soil moisture and vegetation response, Hydrol. Earth Syst. Sci., 23, 1067–1081, https://doi.org/10.5194/hess-23-1067-2019, 2019.

Ulaby, F. T. and Long, D. G.: Microwave radar and radiometric remote sensing, The University of Michigan Press, Ann Arbor, ISBN 9780472119356, 2014.

Wagner, W.: Soil moisture retrieval from ERS scatterometer data, in: Geowissenschaftliche Mitteilungen: Vol. 49, Veröffentlichung des Institutes für Photogrammetrie und Fernerkundung, Inst. für Photogrammetrie u. Fernerkundung d. Techn. Univ., https://resolver.obvsg.at/urn:nbn:at:at-ubtuw:3-619 (last access: 23 June 2023), 1998.

Xiong, J., Guo, S., Abhishek, Li, J., and Yin, J.: A Novel Standardized Drought and Flood Potential Index Based on Reconstructed Daily GRACE Data, J. Hydrometeorol., 23, 1419–1438, https://doi.org/10.1175/JHM-D-22-0011.1, 2022.

Xu, L., Chen, N., Zhang, X., Moradkhani, H., Zhang, C., and Hu, C.: In-situ and triple-collocation based evaluations of eight global root zone soil moisture products, Remote Sens. Environ., 254, 112248, https://doi.org/10.1016/j.rse.2020.112248, 2021a.

Xu, X. and Frey, S.: Validation of SMOS, SMAP, and ESA CCI Soil Moisture Over a Humid Region, IEEE J. Sel. Top. Appl., 14, 10784–10793, https://doi.org/10.1109/JSTARS.2021.3122068, 2021.

Xu, Z.-g., Wu, Z.-y., He, H., Guo, X., and Zhang, Y.-l.: Comparison of soil moisture at different depths for drought monitoring based on improved soil moisture anomaly percentage index, Water Sci. Eng., 14, 171–183, https://doi.org/10.1016/j.wse.2021.08.008, 2021b.

Zhang, N., Quiring, S., Ochsner, T., and Ford, T.: Comparison of Three Methods for Vertical Extrapolation of Soil Moisture in Oklahoma, Vadose Zone J., 16, vzj2017.04.0085, https://doi.org/10.2136/vzj2017.04.0085, 2017.

A.2. Revisiting Sub-Surface Drought Cascades With Daily Satellite Observations of Soil Moisture and Terrestrial Water Storage

Reference

Blank, D., Eicker, A., Reager, J. T., and Güntner, A. (2025). Revisiting sub-surface drought cascades with daily satellite observations of soil moisture and terrestrial water storage. Water Resources Research, 61, e2024WR039321.
https://doi.org/10.1029/2024WR039321

Abstract

The increasing frequency, intensity, and duration of extreme heat and drought events in a warming climate make it crucial to understand the relationship between surface and subsurface water storage dynamics during these events. Changes in water storage can be studied globally using satellite observations. Microwave remote sensing observes the upper few centimeters of the soil, while satellite gravimetry detects changes in the entire column of terrestrial water storage. We use daily data of the Gravity Recovery and Climate Experiment (GRACE) and GRACE Follow-On (GRACE-FO), satellite-based surface soil moisture data and root zone products from Soil Moisture Ocean Salinity, Soil Moisture Active Passive, and European Space Agency Climate Change Initiative on a harmonized 1° global grid to study the evolution of water storage deficits across different soil layers. The joint analysis of the three types of data provides valuable insight into the hydrological dynamics in different soil depths and subsurface water storage compartments. To identify different dynamics, we compute the rate of change from de-seasonalized water storage anomaly time series to assess how quickly the system accumulates storage deficits during drought conditions and recovers from them for different integration depths in the subsurface. The results indicate characteristic patterns of the temporal dynamics of drought recovery with fast fluctuations and short recovery times for surface soil moisture, a prolonged behavior in the root-zone, and an even slower response in the entire water column. This highlights that the cascading propagation of drought dynamics from the surface to the subsurface can be quantified by remote sensing data with daily resolution at the global scale.

Declaration of own contribution

Table 2: Contribution to Paper No. 2.

Involved in	**Estimated contribution**
Ideas and conceptual design	90%
Computation and results	100%
Analysis and interpretation	90%
Manuscript, figures and tables	90%
Total	92.5%

Confirmation of Co-Authors

I hereby confirm the correctness of the declaration of the contribution of **Daniel Blank** for Paper No. 2 in Table 2:

Annette Eicker	Date
John T. Reager	Date
Andreas Güntner	Date

Check for updates

AGU ADVANCING EARTH AND SPACE SCIENCES

Water Resources Research®

RESEARCH ARTICLE
10.1029/2024WR039321

Revisiting Sub-Surface Drought Cascades With Daily Satellite Observations of Soil Moisture and Terrestrial Water Storage

Daniel Blank[1], **Annette Eicker**[1], **John T. Reager**[2], **and Andreas Güntner**[3,4]

[1]HafenCity University Hamburg, Hamburg, Germany, [2]Jet Propulsion Laboratory, California Institute of Technology, Pasadena, CA, USA, [3]Helmholtz Centre Potsdam GFZ German Research Centre for Geosciences, Potsdam, Germany, [4]Institute of Environmental Sciences and Geography, University of Potsdam, Potsdam, Germany

Key Points:

- Satellite soil moisture and terrestrial water storage illustrate the propagation and recovery of water deficits in the sub-surface
- Daily water storage data from satellite gravimetry are valuable for quantifying drying and re-wetting rates
- The results reveal the cascading effect of drought dynamics from the surface through the root zone to the entire sub-surface storage

Supporting Information:

Supporting Information may be found in the online version of this article.

Correspondence to:

D. Blank,
daniel.blank@hcu-hamburg.de

Citation:

Blank, D., Eicker, A., Reager, J. T., & Güntner, A. (2025). Revisiting sub-surface drought cascades with daily satellite observations of soil moisture and terrestrial water storage. *Water Resources Research*, *61*, e2024WR039321. https://doi.org/10.1029/2024WR039321

Received 30 OCT 2024
Accepted 25 JUL 2025

Author Contributions:

Conceptualization: Daniel Blank, Annette Eicker, John T. Reager, Andreas Güntner
Formal analysis: Daniel Blank
Methodology: Daniel Blank, Annette Eicker
Project administration: Annette Eicker
Software: Daniel Blank
Supervision: Annette Eicker
Visualization: Daniel Blank
Writing – original draft: Daniel Blank, Annette Eicker, Andreas Güntner
Writing – review & editing: Daniel Blank, Annette Eicker, John T. Reager, Andreas Güntner

© 2025. The Author(s).
This is an open access article under the terms of the Creative Commons Attribution License, which permits use, distribution and reproduction in any medium, provided the original work is properly cited.

Abstract The increasing frequency, intensity, and duration of extreme heat and drought events in a warming climate make it crucial to understand the relationship between surface and subsurface water storage dynamics during these events. Changes in water storage can be studied globally using satellite observations. Microwave remote sensing observes the upper few centimeters of the soil, while satellite gravimetry detects changes in the entire column of terrestrial water storage. We use daily data of the Gravity Recovery and Climate Experiment (GRACE) and GRACE Follow-On (GRACE-FO), satellite-based surface soil moisture data and root zone products from Soil Moisture Ocean Salinity, Soil Moisture Active Passive, and European Space Agency Climate Change Initiative on a harmonized 1° global grid to study the evolution of water storage deficits across different soil layers. The joint analysis of the three types of data provides valuable insight into the hydrological dynamics in different soil depths and subsurface water storage compartments. To identify different dynamics, we compute the rate of change from de-seasonalized water storage anomaly time series to assess how quickly the system accumulates storage deficits during drought conditions and recovers from them for different integration depths in the subsurface. The results indicate characteristic patterns of the temporal dynamics of drought recovery with fast fluctuations and short recovery times for surface soil moisture, a prolonged behavior in the root-zone, and an even slower response in the entire water column. This highlights that the cascading propagation of drought dynamics from the surface to the subsurface can be quantified by remote sensing data with daily resolution at the global scale.

1. Introduction

In a warming climate, the frequency, intensity, and duration of extreme heat and drought events are expected to increase (Seneviratne et al., 2021). Therefore, it is more important than ever to comprehend the relationship between surface and subsurface water dynamics during extreme events and their evolution. Droughts, characterized by prolonged periods of significantly low precipitation and high temperatures, pose a substantial environmental challenge with widespread consequences. In an ecosystem, the lack of sufficient water not only reduces the available water for human needs but also has major ecological effects, stressing and depleting plant and animal life. There are four different types of drought based on their length, severity, and effects: meteorological, agricultural, hydrological, and socio-economic drought (Crocetti et al., 2020; Mishra & Singh, 2010; Wilhite & Glantz, 1985). The first three types pertain to the physical aspects of the phenomenon, whereas the socio-economic drought is linked to the societal impacts. To focus on the physical aspects, a meteorological drought is defined as a prolonged lack of precipitation, an agricultural drought as a persistent insufficiency in soil moisture availability, and a hydrological drought as a continuous deficit in streamflow or groundwater storage.

All these three types of droughts are connected, and by using ground data from Illinois on precipitation, soil moisture, shallow groundwater levels, and streamflow, Changnon (1987) developed one of the first frameworks for evaluating the evolution of droughts across variables. The theoretical drought cascade originally defined in that study delineates the initiation of drought signals in the atmosphere, resulting in a meteorological drought. Afterward, these signals are delayed in sequence, affecting runoff, soil moisture, streamflow, and groundwater. An important feature that this theory suggests is that the time series of the drought signals get dampened and delayed as they move down the cascade from meteorology to subsurface variables (i.e., from precipitation to groundwater). The conceptual explanation of drought propagation and recovery has been confirmed in other research, for example, by Peters et al. (2006), who examined groundwater drought processes in the Pang

19447973, 2025, 8, Downloaded from https://agupubs.onlinelibrary.wiley.com/doi/10.1029/2024WR039321, Wiley Online Library on [23/10/2025]. See the Terms and Conditions (https://onlinelibrary.wiley.com/terms-and-conditions) on Wiley Online Library for rules of use; OA articles are governed by the applicable Creative Commons License

catchment (United Kingdom) through simulated groundwater patterns and by Van Loon (2015), who used hydrological models to analyze droughts in four distinct types of European river basins. Closely linked to drought propagation and recovery and the role of water storage on the Earth's climate system is the concept of soil moisture memory, that is, the mechanisms with which soils preserve the information on storage anomalies over time, including its depth-dependence (Rahmati et al., 2024).

Existing studies have shown the cascading effects of droughts across larger regions and multiple events, primarily through ground observations (Bae et al., 2019; Barker et al., 2016; Bhardwaj et al., 2020; Huang et al., 2017; Oertel et al., 2018; Tijdeman et al., 2018). The integration of remote sensing data has emerged as a valuable tool for understanding large-scale drought phenomena on a global scale (AghaKouchak et al., 2015). Although studies so far have been rare, utilizing remote sensing data to analyze drought propagation and recovery across variables could be advantageous in characterizing cascading effects over large domains Farahmand et al. (2021) employ satellite observations to characterize cascade phenomena in four major United States (US) drought case studies, whereas Rossi et al. (2023) focuses on characterizing major drought events and their propagation in three Brazilian regions. Entekhabi (2023) use remote sensing data and in situ observations to study the drought cascade and its characteristics over the continental US. A feature that all of these studies have in common is that they use monthly terrestrial water storage (TWS) data from the GRACE/GRACE-FO satellite gravimetry mission to represent the hydrological drought component.

Due to the fact that any redistribution of water mass on or above the Earth's surface leads to variations of the Earth's gravity field, satellite gravimetry can relate changes in the gravitational acceleration acting on a satellite to variations in TWS on and underneath the Earth's surface but cannot distinguish between water mass changes in individual water compartments (e.g., soil moisture, snow cover, groundwater, surface water). The twin satellite mission GRACE (Tapley et al., 2004), and its successor mission GRACE-FO (Landerer et al., 2020) have been observing gravity field changes since 2002. However, the temporal resolution of standard GRACE data for 1 month is too low to record any fast water mass changes and restricts the temporal resolution of the drought propagation analysis to a monthly range. Recent developments in GRACE data processing (Kvas et al., 2019) have enabled the computation of daily gravity fields with increased accuracy. Such daily gravity data were successfully used in various studies (Bergmann & Dobslaw, 2012; Bonin & Chambers, 2011; Eicker et al., 2020; Gouweleeuw et al., 2018; Xiong et al., 2022). Blank et al. (2023) have shown that TWS signal content is related to soil moisture variations seen in remote-sensing soil moisture products, albeit with temporal delay. They used cross-correlation analysis for the determination of time shifts between time series from which only the linear trend was removed. It was the first study in which GRACE data with a higher than monthly resolution were compared with soil moisture data.

Using daily data from TWS from GRACE/GRACE-FO appears particularly promising for a more detailed and comprehensive analysis of the dynamics of drought cascades but has not been used for this specific purpose yet. The daily resolution can capture rapid changes and short-term fluctuations in the water storage variables, offering a more comprehensive understanding of the cascading effects and enabling the identification and analysis of short-term drought events that might be overlooked when using monthly data. In addition to TWS data from GRACE, this study integrates remotely-sensed soil moisture data for an assessment of surface soil moisture (SSM) conditions that predominantly represent agricultural drought. Additionally, including root zone soil moisture (RZSM) to soil depths of up to 1 m offers insights into deeper soil layers. The main goal of this study is to use remote sensing for investigating how drought affects water storage in the subsurface across different layers, from the top layer to the root zone and finally to the whole water column of TWS, including the deeper unsaturated zone and the groundwater. By exploring these different integration depths, the study seeks to add comprehensive insights into the sub-surface components of the drought cascade, that is, how drought propagates and recovers with depth and, thus, into the overall hydrological response to prolonged water deficits. Although the physical phenomenon of drought cascades including terrestrial water storage data from satellite gravimetry has exemplarily been analyzed before (see references above), our investigation differs from these previous studies with respect to (a) the methodology, (b) the global extent of the analyses, (c) the specific soil moisture data sets, and (d) the higher observation-based temporal resolution of daily GRACE data.

The paper is structured as follows: Section 2 describes the satellite data products used for the quantification of soil moisture (SM) and total water storage (TWS). Section 3 discusses data processing and limitations of the data sets. In Section 4, the methodology and the corresponding results for calculating the recovery times of droughts are

19447973, 2025, 8, Downloaded from https://agupubs.onlinelibrary.wiley.com/doi/10.1029/2024WR039321, Wiley Online Library on [23/10/2025]. See the Terms and Conditions (https://onlinelibrary.wiley.com/terms-and-conditions) on Wiley Online Library for rules of use; OA articles are governed by the applicable Creative Commons License

explained in detail. Starting with the calculation of seasonal anomalies from each time series, we can identify periods of storage deficit when water storage is below normal levels. The variability observed during these drought periods is then utilized to estimate the probable recovery times as a measure to characterize drought behavior. Results are first presented for an exemplary time series to illustrate the subsequent steps of the approach and afterward extended to the global scale.

2. Data Sets

2.1. GRACE and GRACE-FO Data

Daily gravity field solutions were computed from GRACE and GRACE-FO observations as part of the ITSG-Grace2018 gravity field time series (Kvas et al., 2019) in the form of spherical harmonic coefficients up to degree $n = 40$ (corresponding to a spatial resolution of 500 km) to examine rapid, short-term fluctuations in terrestrial water storage (TWS) and its anomalies. In contrast to the conventional monthly solutions, the restricted satellite ground track coverage within a single day does not support a robust global gravity field inversion. Therefore, to address this limitation, the daily gravity solutions from ITSG-Grace2018 are generated within the framework of a Kalman smoothing approach (similar to Kurtenbach et al. (2012)), which integrates statistical information on the expected evolution of the gravity field over time into its process model. As a trade-off, the daily gravity field data that result from this approach are not entirely standalone solutions. Instead, they display a certain level of correlation with neighboring time steps.

In the process of data handling, temporally high-frequency mass fluctuations attributed to tides (ocean, Earth and pole tides), along with non-tidal variations in atmospheric and oceanic mass, are removed by subtracting the output of geophysical background models from the observations (de-aliasing, Dobslaw et al. (2017)). Following this step, additional post-processing measures are taken: Geocenter motion is addressed by incorporating the degree-1 harmonic coefficients provided by Sun et al. (2016) on the basis of Swenson et al. (2008). The c_{20} coefficient is replaced with a time series derived from Satellite Laser Ranging (Cheng & Ries, 2017), and the influence of glacial isostatic adjustment (GIA) is removed by the ICE6G-D model (Peltier et al., 2017). No extra spatial filtering is needed, because the Kalman smoother effectively suppresses spatially correlated noise. Subsequent to these data processing procedures, the resulting gravity field models are presumed to predominantly represent variations in water mass both above and below the Earth's surface. The gravity field solutions can then be converted into equivalent water heights across a global geographical grid according to

$$TWS(\lambda,\vartheta) = \frac{M}{4\pi R^2 \rho_w} \sum_{n=1}^{n_{\max}} \sum_{m=-n}^{n} \frac{(2n+1)}{\left(1+k'_n\right)} c_{nm}\, \Upsilon(\lambda,\vartheta) \tag{1}$$

where λ and ϑ symbolize the spherical coordinates, M and R are the mass and the radius of the Earth, ρ_w is the density of water $\left(\frac{1000\text{kg}}{m^3}\right)$, k'_n denote the Load Love Numbers (Lambeck, 1988), c_{nm} are the spherical harmonic coefficients of the gravitational potential, and $\Upsilon(\lambda,\vartheta)$ are the surface spherical harmonic functions. The degree and order of the spherical harmonic functions are denoted by n and m.

While the Kalman smoother output ensures a continuous daily time series during the mission time period, we selectively excluded days with insufficient GRACE observations from our analysis. Specifically, we omitted days with observation counts falling below 10,000 observations per day, as given on the ITSG-Grace2018 product website. During these days, the daily solutions primarily rely on the Kalman filter's process model, resulting in a tendency toward an a-priori mean trend and an annual signal. The calculation of GRACE TWS data was conducted using the Gravity Recovery Object Oriented Programming System (GROOPS; Mayer-Gürr et al., 2021).

2.2. Soil Moisture Data Sets

Microwave remote sensing is a method used to detect soil moisture in the uppermost soil layer by leveraging changes in the soil's dielectric constant associated with varying water content. Active microwave sensors transmit electromagnetic pulses to the Earth and measure the backscattered energy from the Earth's surface, while passive microwave sensors capture naturally emitted radiation from the Earth's soil, represented as brightness temperature (Robinson et al., 2008). Both techniques rely on the dielectric constant of the soil, influencing observed parameters such as backscattered energy and brightness temperature, enabling the measurement of soil moisture.

19447973, 2025, 8, Downloaded from https://agupubs.onlinelibrary.wiley.com/doi/10.1029/2024WR039321, Wiley Online Library on [23/10/2025]. See the Terms and Conditions (https://onlinelibrary.wiley.com/terms-and-conditions) on Wiley Online Library for rules of use; OA articles are governed by the applicable Creative Commons License

In this study, satellite-derived surface soil moisture products from the missions Soil Moisture Ocean Salinity (SMOS; Kerr et al. (2010)), Soil Moisture Active Passive (SMAP; Entekhabi et al., 2010), and the multi-satellite combination data product from the European Space Agency Climate Change Initiative (ESA CCI; Dorigo et al., 2017; Gruber et al., 2019; Preimesberger et al., 2021) are used, as well as root-zone soil moisture products from SMOS and SMAP. Both SMOS and SMAP provide Level 3 (L3) and Level 4 (L4) data, with L3 referring to original satellite observations acquired over a 24-hr period given as a multi-orbit global map of retrieved soil moisture, and L4 relating to post-processed data products. The way of post-processing differs among the two satellite missions. The study uses an early morning overpass for L3 satellite soil moisture products, reducing temperature differences between soil surface and vegetation canopy, and reducing thermal differences within a pixel, resulting in reduced errors and improved reliability (Entekhabi et al., 2014; Lei et al., 2015; Owe et al., 2008).

ESA's SMOS satellite mission, launched in 2009, is used to observe soil moisture using an L-band radiometer. Here we use the daily L3 surface soil moisture (SSM) data and the L4 root zone soil moisture data from the Centre Aval de Traitement des Données SMOS (CATDS). The data is provided in a global grid with a spatial resolution of 25 km × 25 km (CATDS, 2022a, 2022b). The CATDS L4 root zone soil moisture (RZSM) product is generated by propagating the L3 surface soil moisture data set (representing the uppermost 0–5 cm of the soil) into the underlying soil down to a depth of 1 m by using an exponential filter, based on a modified formulation of a recursive exponential filter while considering soil properties and an optional implementation of transpiration (Al Bitar & Mahmoodi, 2020). In this way, the SMOS L4 RZSM data set used in this study represents the water storage within an integration depth of 1 m.

NASA launched the SMAP satellite in January 2015 to observe surface soil moisture with an L-band active radar and passive radiometer. In this study, L3 and L4 products from SMAP are used. The daily L3 data (v9.0; O'Neill et al., 2023) contain all surface soil moisture retrievals for an entire day mapped to a global grid with a spatial resolution of 36 km. The L4 (surface and root zone soil moisture, v7.0; Reichle et al., 2022) products are derived by assimilating SMAP surface brightness temperature observations into the Goddard Earth Observing Model System (GEOS-5, v5) catchment land surface model, which gives estimates for the surface soil moisture as well as the root zone, provided with a temporal resolution of 3 hr and a 9 km spatial resolution. Similar to the SMOS products, the integration depth of SMAP L3 and L4 SSM data is 0–5 cm, while the L4 RZSM product represents a soil depth of 1 m.

The ESA CCI surface soil moisture data set is provided as part of ESA's Climate Change Initiative, based on harmonizing and merging soil moisture retrievals from multiple satellite missions into a combined daily product. The combined active and passive surface soil moisture product (v8.1; Dorigo et al., 2023) is selected for analysis in this study, providing daily surface soil moisture observations (0–5 cm depth) with a spatial resolution of 0.25° and is available from the ESA data archive. It should be noted that tropical rainforest areas are completely masked out because of the strong signal scattering in the microwave observations caused by vegetation (Ulaby & Long, 2014).

It is important to note that both the L3 and L4 data are not purely based on satellite observations. The L3 soil moisture products from SMAP and SMOS are directly derived from the satellite data but are influenced by ancillary data that constrain the soil moisture retrieval process, for example, vegetation indices or land surface temperature. In contrast, the L4 soil moisture product from SMAP is generated through a data assimilation framework that integrates satellite soil moisture observations into a land surface model in combination with precipitation and other climate forcing variables. Therefore, the SMAP L4 product largely depends on the model and its input data.

3. Data Pre-Processing and Limitations

3.1. Data Harmonization

In this study, the analysis is carried out on a global grid cell level, therefore, all data sets are harmonized to the same 1° × 1° geographical grid. The various soil moisture data sets, which have finer native resolutions, were downsampled using a first-order conservative remapping algorithm that preserves integrated quantities such as mass or volume. For the GRACE data it should be noted that the actual spatial resolution is even lower than 1° as the data are derived from a spherical harmonic representation that is truncated at degree and order $n = 40$ and

19447973, 2025, 8, Downloaded from https://agupubs.onlinelibrary.wiley.com/doi/10.1029/2024WR039321, Wiley Online Library on [23/10/2025]. See the Terms and Conditions (https://onlinelibrary.wiley.com/terms-and-conditions) on Wiley Online Library for rules of use; OA articles are governed by the applicable Creative Commons License

exhibits spatial dependencies between the grid cells up to a range of about 500 km for daily data (Kvas et al., 2019). Thus, the $1° \times 1°$ resolution used here represents a compromise between the higher resolution of the soil moisture products and the lower resolution of GRACE. To evaluate the potential impact of the spatial resolution, we transformed the soil moisture products into the same spherical harmonics representation and truncation as the GRACE data to mimic their resolution before re-gridding to $1° \times 1°$. The effect on the results is discussed in Section 4.4.

For a reasonable temporal overlap of all data sets, we used the time period from April 2015 (start of the SMAP mission) to December 2022 for our study, excluding the time span between the end of the mission GRACE (August 2017) and the start of the successor mission GRACE-FO (July 2018). The SMOS and SMAP missions have a maximum revisiting time of 3 days, resulting in temporal gaps in the SMOS, SMAP, and ESA CCI data. For gap filling, linear interpolation is applied, and a 3-day moving average is calculated afterward to reduce noise. Linear interpolation was only carried out for gaps lasting up to a maximum of 3 days, while gaps exceeding this duration remain unfilled, persist in the time series and were not considered for further analyses. Although this method guarantees data set continuity, the smoothing effect of the linear interpolation may cause a minor delay in representing quick changes, especially during recovery phases. Further details on the effect of the linear interpolation on the results is provided in Section 4.4. Periods with data gaps in the TWS data set (see Section 2.1) were excluded from the analyses.

3.2. De-Seasonalized and Standardized Signal

In this study, droughts are considered as periods with a water storage deficit relative to the regular climatological conditions. Therefore, residuals were computed by removing the mean, the trend, and seasonal cycle from the time series by best fitting the following equation to each soil moisture or TWS time series:

$$f(t) = a + b \cdot t + c \cdot \cos(\omega t) + d \cdot \sin(\omega t) + e \cdot \cos(2\omega t) + f \cdot \sin(2\omega t) \tag{2}$$

with parameters for the mean (a), linear trend (b), and annual and semi-annual cycles (c, d, e, f).

After removing the mean, trend and annual signal from the complete signal, a de-seasonalized signal, denoted as $D_{y,d}$ at any year y and day d, remains. Given the different units of the observations (volumetric soil moisture and equivalent water heights) and the varying integration depths of water content (SSM: 0–5 cm, RZSM: 0–1 m, TWS: all storage compartments, no depth limit), the de-seasonalized signal is standardized by dividing it by its standard deviation, resulting in the unit-less z-score time series $\mathrm{SD}_{y,d}$.

$$\mathrm{SD}_{y,d} = \frac{D_{y,d}}{\sigma_d} \tag{3}$$

The degree of correlation (generally higher for root-zone products) and the percentage value of signal sign agreements (at least above 50% for most grid cells across all soil moisture products) between the standardized signals from GRACE and the soil moisture products are presented globally in the Figures S1–S4 in Supporting Information S1.

The baseline statistics (mean, trend, and seasonal cycle) were computed using the maximum length of the overlapping observational time span available for all data sets, covering the period from 2015 to 2022. The limited length of the data record is a known constraint in satellite-based analysis. While this duration allows for the identification of relative anomalies within the observed window, it does not represent long-term climatological conditions in the conventional sense (i.e., multi-decadal climate normals). Therefore, the derived anomalies should be interpreted as deviations from the average conditions prevailing during this specific observational period, rather than as deviations from the long-term climatology.

One limitation of the de-trending approach is the potential removal of long-term groundwater storage changes which can play an important role in the persistence of hydrological droughts in the deeper sub-surface. Previous studies have demonstrated that groundwater variability operates on decadal to multi-decadal timescales and is modulated by hydrogeological and topographic factors (Barros et al., 2017; Fan, 2015). This is a recognized limitation when using relatively short time series as in our study, and it should be considered when interpreting the results.

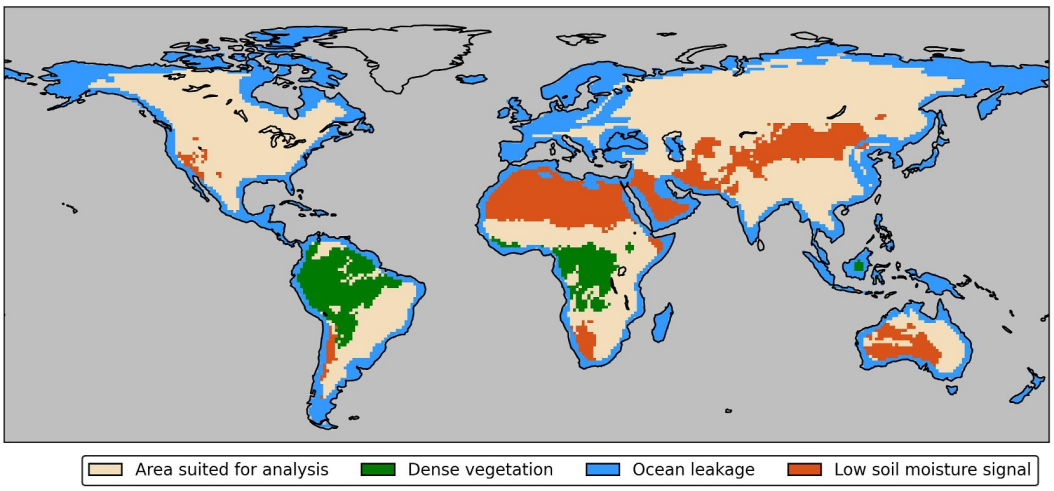

Figure 1. Spatial masks applied to exclude regions low soil moisture variability (brown), dense vegetation (green) and ocean leakage (blue) from the analysis; other areas (beige) are considered to be suited for analysis.

3.3. Spatial Limitations and Masking

The land cover type has an impact on the ability to observe soil moisture by microwave remote sensing techniques. Therefore, we apply spatial masking to exclude adversely affected regions from the analysis, see Figure 1. In densely vegetated areas, such as tropical rain forests, the vegetation has a significant impact on passive or active microwave signals (Owe et al., 2001; Ulaby & Long, 2014). While the ESA CCI data set mask out observations in rain forest regions, the other products include these regions in their data sets. For consistency in our analysis, we mask out these regions. In deserts, the soil moisture signal may be unreliable due to low variability in water content in the upper soil layers (Dorigo et al., 2010). Also for satellite gravimetry observations from GRACE and GRACE-FO, the signal-to-noise ratio is low and the noise floor strongly dominates the time series in dry areas. To classify dry (desert) regions, we rely on the soil moisture signal variability, that is, the root mean square (RMS) of the daily time series in each grid cell. We set a low variability threshold of twice the mean RMS of a test region in the Sahara desert, which has minimal day-to-day soil moisture variations. To define the mask using this criterion, we used the SMOS L3 data product. Other SSM data products yielded similar results. Furthermore, snow cover and frozen soil prevent satellites from measuring soil moisture because the dielectric constant of snow and frozen water is very different from that of liquid water (Wagner, 1998). Regions with snow and frozen ground throughout large parts of the year were not spatially masked out, but we excluded the affected days from the analysis. To this end, soil temperature (T_S) and snow water equivalent (SWE) estimates of the Global Land Data Assimilation System NOAH (GLDAS NOAH) were used. Observations taken under the conditions of frozen soil ($T_S < 0$°C) and snow cover (SWE > 0 mm) according to the simulation results were excluded. A similar approach is used by ESA CCI (Gruber et al., 2019).

The GRACE TWS data used in this study has spatial limitations that are also relevant to our analysis. The primary limitation is the coarse spatial resolution, which results in the non-independence of TWS grid cell values from neighboring cells. This lack of independence can lead to leakage effects (Longuevergne et al., 2013), which are particularly relevant in coastal areas so that oceanic and terrestrial mass changes cannot be separated unambiguously. A more comprehensive discussion and a map highlighting continental areas affected by ocean leakage can be found in Eicker et al. (2020) (Figure S4 in Supporting Information S1). We used this map in our study to mask out areas that are largely affected by ocean leakage. GRACE-derived TWS also encompasses storage variations in other compartments than soil moisture and groundwater, for example, glaciers or surface water bodies, which are not directly of interest for the present study. For an identification of such regions including their effect on neighboring cells by leakage, we refer to Jensen et al. (2020) (Figure S2 in Supporting Information S1) but do not explicitly exclude such areas from our analyses.

19447973, 2025, 8, Downloaded from https://agupubs.onlinelibrary.wiley.com/doi/10.1029/2024WR039321, Wiley Online Library on [23/10/2025]. See the Terms and Conditions (https://onlinelibrary.wiley.com/terms-and-conditions) on Wiley Online Library for rules of use; OA articles are governed by the applicable Creative Commons License

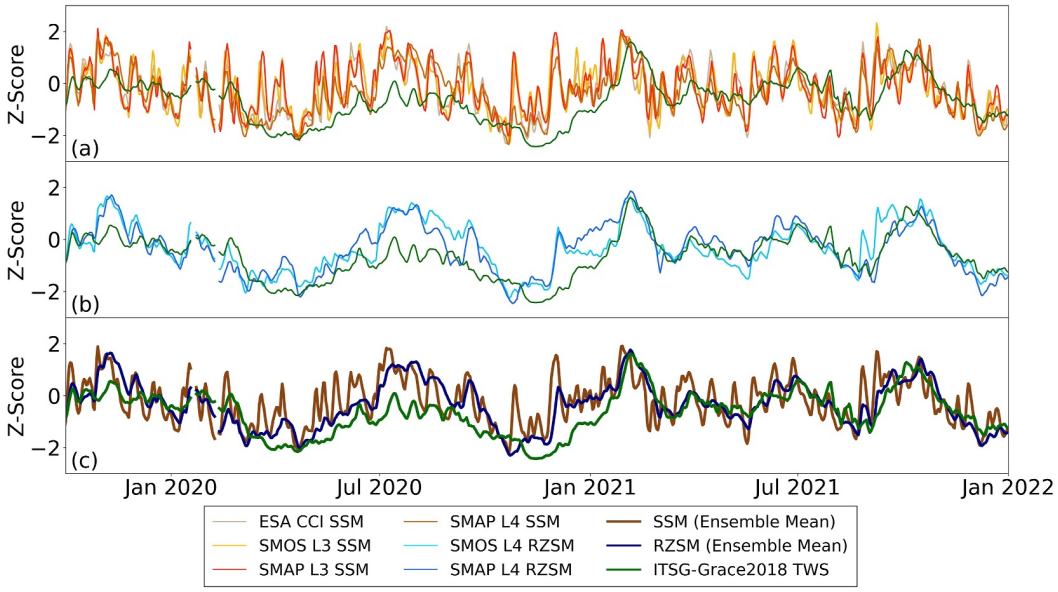

Figure 2. De-seasonalized time series for an example grid cell in the south of Brazil (29°S, 54°W). (a) Surface soil moisture (SSM) of ESA CCI, SMOS L3, SMAP L3, SMAP L4, and TWS from GRACE. (b) Root zone soil moisture (RZSM) of SMOS L4, SMAP L4, and TWS data from GRACE. (c) Ensemble mean of all SSM data sets (light brown) and RZSM data sets (dark blue) and TWS from GRACE. The individual time series are plotted as well, with a smaller line width.

4. Methods and Results

In the following, the methodology for investigating drought dynamics is described step by step and each calculation step is directly illustrated by results for one exemplary grid cell (Sections 4.1 to 4.3). Afterward, the methodology is extended to the global scale (Section 4.4).

4.1. Quantifying Water Storage Deficits

The standardized de-seasonalized signals for all products are illustrated in Figure 2 for an exemplary grid cell (29° S, 54° W) in the Brazilian state of Rio Grande do Sul, located in the south of Brazil within the Rio de la Plata river basin. This region experienced severe droughts from 2019 to 2022, as detailed in the European Commission report by Naumann et al. (2023). It is evident that the surface soil moisture data from SMOS L3, SMAP L3, ESA CCI and SMAP L4 exhibit fast dynamics with marked fluctuations of the soil water content and with quick recoveries from below-average moisture conditions (Figure 2a). In comparison, the storage fluctuations are smaller in the root zone time series from SMOS L4 and SMAP L4 (Figure 2b) and are further dampened in the entire water column time series of TWS from GRACE. Not only are fluctuations dampened when considering larger integration depths, but also the tendency toward more long-lasting water deficit conditions with a larger soil depth is evident, in particular for the recovery period between July 2020 and January 2021. With larger integration depths, also the onset and the gradual storage loss of storage deficit periods over time is dampened and delayed. While there are some differences between the individual data sets, the ensemble mean of all SSM data sets (light brown) and of all RZSM data sets (dark blue), along with TWS, clearly illustrates the distinct dynamics of water storage for the different integration depths (Figure 2c). Additional examples of time series for other grid cells worldwide are shown in Supporting Information S1. Figures S5 and S6 show results of the drought in New South Wales, Australia in 2019 (Bureau of Meteorology, 2019; Nguyen et al., 2021). Figures S7 and S8 in Supporting Information S1 show results of the drought in the Mekong river basin from 2019 to 2021 (Keovilignavong et al., 2023; Mekong River Commission, 2022). These are in line with the general results of depth dependencies of storage dynamics as presented here for the example of southern Brazil.

As mentioned before, to analyze the dynamics of droughts, we take a broad definition of water storage droughts in this study by considering all negative values of the standardized de-seasonalized water storage time series per grid cell, referred to herein as storage deficit. Furthermore, instead of focusing on a limited number of specific drought occurrences, we take a comprehensive approach that includes all occurrences of storage deficits, even in cases

19447973, 2025, 8, Downloaded from https://agupubs.onlinelibrary.wiley.com/doi/10.1029/2024WR039321, Wiley Online Library on [23/10/2025]. See the Terms and Conditions (https://onlinelibrary.wiley.com/terms-and-conditions) on Wiley Online Library for rules of use; OA articles are governed by the applicable Creative Commons License

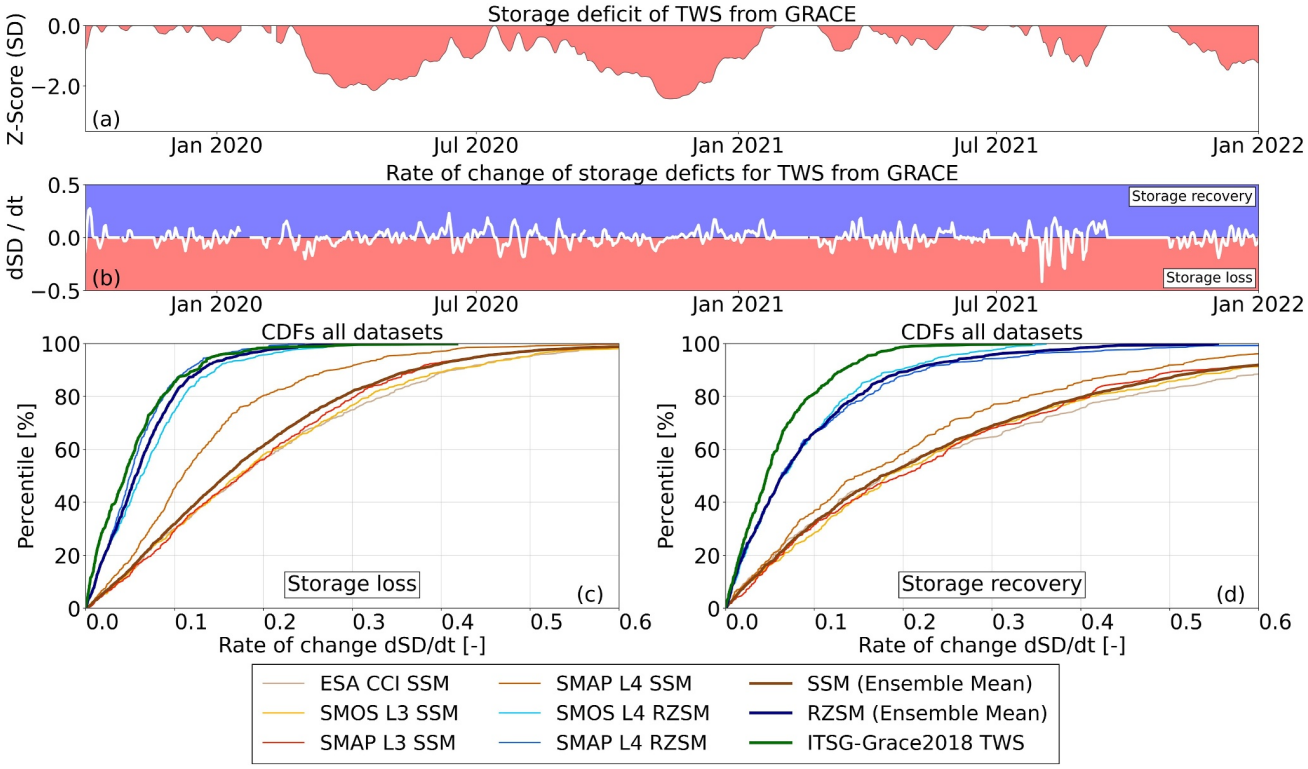

Figure 3. (a) Time series of TWS storage deficit for the exemplary grid cell in the south of Brazil (29°S, 54°W). (b) TWS rate of change time series (dSD/dt). (c) Cumulative distribution function (CDF) of storage loss rate of change values for all data sets. (d) CDF of storage recovery rate of change values for all data sets.

where the duration of a particular deficit in the time series is quite short. The metric used to quantify the storage deficits is based on a statistical method proposed by Thomas et al. (2014). The temporal evolution of storage deficits, encompassing storage loss and recovery over time, is determined by estimating the time derivative of the storage deficit dSD/dt. The computation is performed using the backward difference method:

$$\frac{dSD}{dt}(t) = SD_t - SD_{t-1} \tag{4}$$

To illustrate the method, we again show the results for the exemplary grid cell in Brazil. In Figure 3a, the storage deficit of TWS from GRACE/GRACE-FO during the drought period from 2019 onward is displayed, corresponding to the negative values of the green curve in Figure 2. The time derivative of the storage deficit describes the rate of change in the storage compartment over time (the rate of change here represents the change of the standardized unit-less values of the z-score SD per day). In the visual representation, values in the red area indicate storage loss (negative changes), while values in the blue area represent storage recovery (positive changes). A straight line around zero or gaps indicate that there was no storage deficit during that time.

For the further analyses, we assume that the entire rate of change (dSD/dt) time series of a grid cell represents the typical range of values during storage deficits. An empirical cumulative distribution function (CDF) of the rate of change time series is used to characterize the dynamics of droughts. The CDFs of all data sets are categorized into storage loss (Figure 3c) and storage recovery values (Figure 3d) because the number of loss and recovery time steps can be different and in order to distinguish between storage recovery and loss dynamics. It is important to note that storage loss values are typically negative. However, for visualization purposes, the absolute values are considered to make them more easily comparable to the positive values of storage recovery. The more to the right the values are, the faster the rate of change is during deficits. Upon closer examination of the CDFs of the storage recovery values (bottom right figure), it is evident that the recovery rates of SSM are the fastest, RZSM recovers more slowly from storage deficits, and the slowest rate of change are observed for TWS from GRACE. This indicates that the recovery time from droughts is much faster in the upper layers compared to the recovery of the

19447973, 2025, 8, Downloaded from https://agupubs.onlinelibrary.wiley.com/doi/10.1029/2024WR039321, Wiley Online Library on [23/10/2025]. See the Terms and Conditions (https://onlinelibrary.wiley.com/terms-and-conditions) on Wiley Online Library for rules of use; OA articles are governed by the applicable Creative Commons License

19447973, 2025, 8, Downloaded from https://agupubs.onlinelibrary.wiley.com/doi/10.1029/2024WR039321, Wiley Online Library on [23/10/2025]. See the Terms and Conditions (https://onlinelibrary.wiley.com/terms-and-conditions) on Wiley Online Library for rules of use; OA articles are governed by the applicable Creative Commons License

entire water column from the surface to the subsurface. When looking at the rate of change values during storage loss periods (bottom left figure), we observe a similar pattern, but the difference is that both SMAP Level 4 products (SSM and RZSM) in this case are slower than the other surface soil moisture or root zone data. The SMAP Level 4 RZSM is even very close to the dynamics of storage loss from TWS. These different characteristics of the SMAP L4 water deficit change rates may be due to the particular properties of the hydrological model into which the observations are assimilated, such as model structure or model equations that govern the redistribution of water in the soil column, including losses by evapotranspiration or percolation. Also, the results may indicate that during the assimilation process, a rather small weight is given to the observations, as seen in particular by the large differences between SMAP L3 SSM observations and SMAP L4 SSM after assimilation.

Furthermore, Figure 3 shows that the dynamics of storage loss tend to be slower than the storage change rates during recovery periods. However, it should be noted that these results relate to one specific grid cell only and may vary in other locations, see Section 4.4.

4.2. CDF Ratios Between Data Sets

Going beyond the visual comparison of the CDFs (Figures 3c and 3d) for quantifying the CDF differences in a comprehensive global analysis, one approach is to select specific percentile values for comparison. To include the entire spectrum of CDF differences, we calculate the ratio of a range of percentiles (from the 1st to the 99th percentile) between TWS and the different soil moisture data sets. When dividing the percentile value of a soil moisture data set by the same percentile value of the TWS change rate, values greater than 1 indicate that the percentile of the soil moisture data set recovers faster than TWS, while a value below 1 indicates that TWS changes are faster. The larger the ratio, the faster the soil moisture data set recovers from storage deficits compared to TWS. It should be noted that this comparison of CDFs in terms of ratios is only possible when all data are standardized.

For the example of the 50th percentile of storage recovery, the ratios between surface soil moisture and TWS are 3.3–4.3 (SMOS L3 = 3.9, SMAP L3 = 4.3, SMAP L4 = 3.3, and ESA CCI = 4.0), while the ratios between RZSM and TWS are smaller with 1.3 (SMOS L4) to 1.4 (SMAP L4). For most data sets, the CDF ratios for storage loss are similar to those for storage recovery (SMOS L3 = 3.8, SMAP L3 = 3.9, ESA CCI = 3.9, SMOS L4 = 1.4), with the exception of both SMAP L4 data sets that result in considerably smaller ratios (SSM/TWS = 2.5, RZSM/TWS = 1.1).

For storage recovery, the mean value of all ratio values are very similar from the 10th and 90th percentiles ($\overline{x}_r$, step of 1%, in total 80 values) leads to ratios in a similar range than for the 50th percentile, with values between 3.3 and 4.2 for the surface soil moisture data sets (SMOS L3 ($\overline{x}_r = 4.1$), SMAP L3 ($\overline{x}_r = 4.0$), SMAP L4 ($\overline{x}_r = 3.3$, and ESA CCI $\overline{x}_r = 3.8$). The mean ratio for the root zone data is again significantly lower (SMOS L4: $\overline{x}_r = 1.4$; SMAP L4 $\overline{x}_r = 1.4$). The mean ratios for the storage loss CDF on the other hand, are slightly higher for ESA CCI ($\overline{x}_r = 4.5$), SMOS L3 ($\overline{x}_r = 4.4$), SMAP L3 ($\overline{x}_r = 4.5$), and SMOS L4 ($\overline{x}_r = 1.5$)), while they are lower for the two data assimilated SMAP L4 data sets (surface $\overline{x}_r = 3.0$, root zone $\overline{x}_r = 1.1$).

4.3. Recovery Time From Storage Deficit

As another approach to compare the different storage data sets, we estimate the median drought recovery time ($RT_{y,d}$) for any daily storage deficit ($SD_{y,d}i$) by

$$RT_{y,d} = \frac{|SD_{y,d}|}{r_{50}}. \tag{5}$$

where r_{50} is the 50th percentile (median) of the storage change CDF of the respective data set. Using this approach allows for estimating a probabilistic recovery time for each day within a storage deficit period assuming a linear recovery from the day of the deficit. It is, of course, important to mention that real-world conditions may not follow such a linear pattern. However, the approach provides a first-order idea of the expected duration of a drought to be used for the comparison of the different storage data sets and of regional differences. Figure 4 illustrates the recovery times RT for the example grid cell in southern Brazil. While the maximum z-score of the storage deficit is quite similar for all data sets with values of about −2.0 (see Figure 2), the recovery time is scaled by the 50th percentile rate of change, which is different for each data set. Consequently, we observe that the

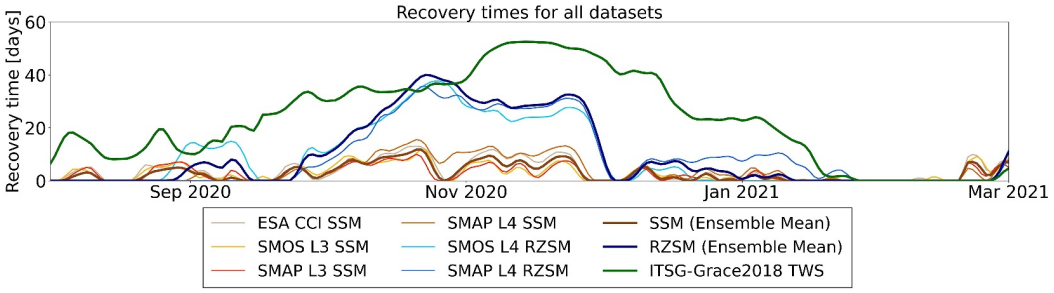

Figure 4. Time series of expected recovery times when considering the 50th percentile of storage recovery rates from the CDFs in Figure 3d for an exemplary grid cell in the south of Brazil: 29°S, 54°W.

recovery times for surface soil moisture data are much faster compared to the data sets of root zone soil moisture and even faster than the TWS data from GRACE. These patterns are corroborated by the mean $\bar{x}$ and maximum x_{max} of these recovery times for the entire time series in Table 1 (Figure 4 displays just a shorter snapshot). We can observe this effect again and see faster recovery times in the surface layer ($\bar{x} \sim 4$ d and $x_{max} \sim 10$–15 d), which are prolonged in the deeper layers ($\bar{x} \sim 12$ d and $x_{max} \sim 36$ d in the root zone, and $\bar{x} \sim 17$ d and $x_{max} \sim 52$ d in the TWS). Additionally, recovery time ratios are calculated between the soil moisture data sets and TWS. The ratios are similar to those calculated from the CDFs (Section 4.2) for the SMAP L4 and SMOS L4 data, while for the SMOS L3, SMAP L3, and ESA CCI data set, the ratios are slightly higher. An added advantage of utilizing recovery times as a metric is that there is no need to standardize the data in advance. Comparisons and calculations can be conducted solely based on the anomaly signal.

4.4. Global Analysis

So far, the analysis approach was illustrated on the basis of only one exemplary grid cell and shall now be extended to the global scale. The global maps in Figure 5 show the average recovery times from storage deficit following Equation 5 on the 1° continental grid. The analysis excluded regions affected by desert conditions (where noise dominates the signal) and ocean leakage (where ocean signal corrupt TWS data from GRACE/GRACE-FO). For the remaining grid cells, the global cumulative distribution functions (CDF) of the cell-based recovery time values are depicted in Figure 7a. Both the maps and the CDFs make it evident that also on the global scale the mean recovery time is substantially shorter for the four SSM products than for RZSM and TWS, typically in the range of 5 and 10 days with a global median value of the ensemble mean map of 6.4 days. The data assimilated SMAP L4 SSM data shows slightly higher recovery times, with some regions exceeding 10 days. In contrast, RZSM exhibits longer recovery times related to deeper and longer travel times of infiltrating water and the larger storage volume to be filled compared to SSM, with a median value of the ensemble mean map of 14.0 days. Noticeable differences are observed between the SMOS and SMAP root zone data sets, particularly in rain forests and northern latitude regions. The longer recovery times for the SMAP L4 root zone product are particularly evident. TWS generally has the longest recovery times. The global median value of all grid cells is

Table 1
Average and Maximum Recovery Times for the Different Surface Soil Moisture (SSM), Root-Zone Soil Moisture (RZSM) Products, and for TWS

Data set	$\bar{x}$ [days]	x_{max} [days]	Ratio $\bar{x}$ [−]	Ratio x_{max} [−]
ESA CCI SSM	3.8	13.1	4.5	4.0
SMOS L3 SSM	3.5	11.8	4.9	4.5
SMAP L3 SSM	3.3	10.8	5.2	4.9
SMAP L4 SSM	4.8	15.5	3.5	3.4
SMOS L4 RZSM	12.5	37.7	1.3	1.4
SMAP L4 RZSM	12.0	35.7	1.4	1.5
ITSG-Grace2018 TWS	17.1	52.6	–	–

Note. Additionally, the ratios of the soil moisture recovery times w.r.t to TWS are shown.

19447973, 2025, 8, Downloaded from https://agupubs.onlinelibrary.wiley.com/doi/10.1029/2024WR039321, Wiley Online Library on [23/10/2025]. See the Terms and Conditions (https://onlinelibrary.wiley.com/terms-and-conditions) on Wiley Online Library for rules of use; OA articles are governed by the applicable Creative Commons License

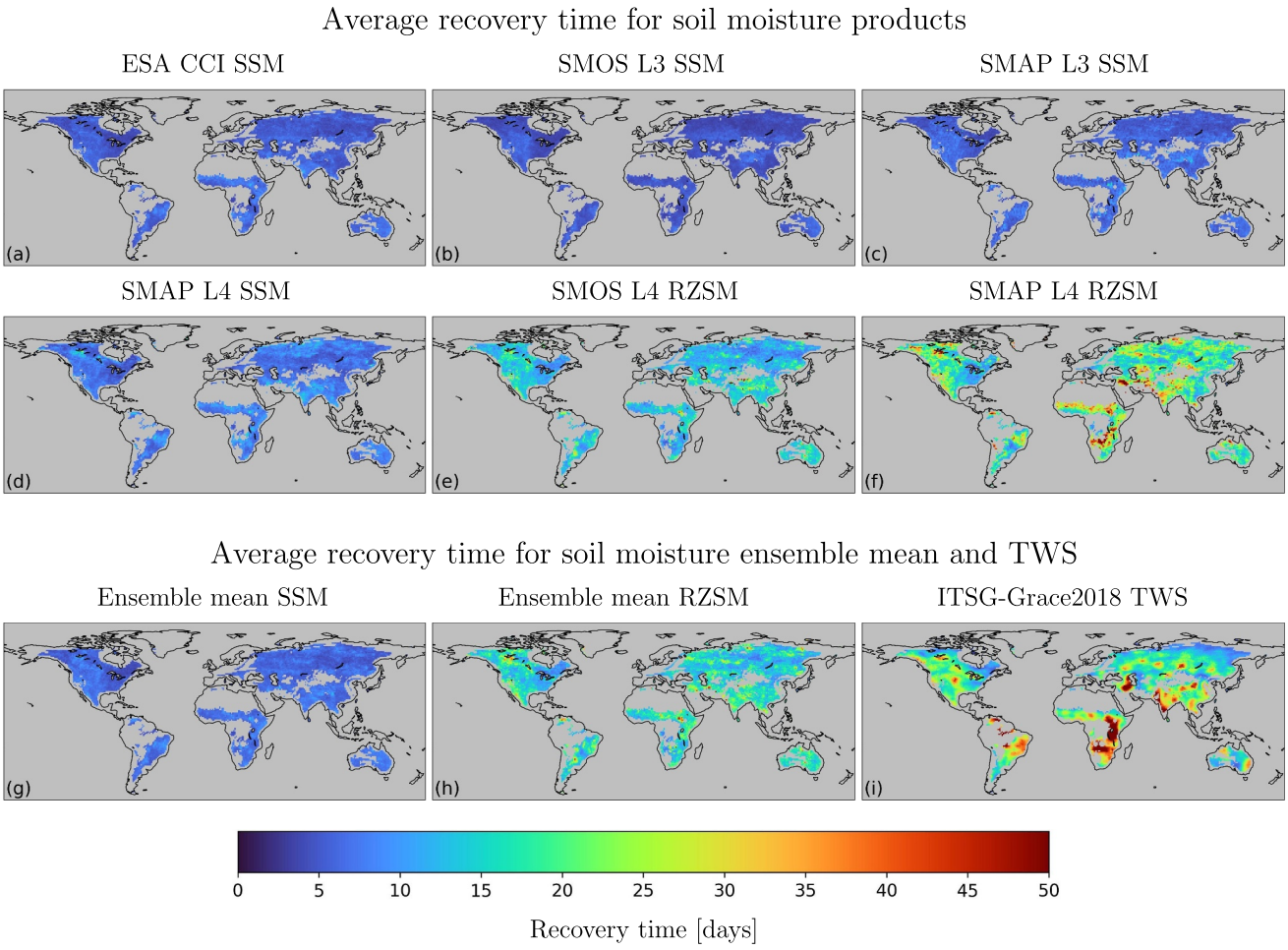

Figure 5. Average recovery times for storage deficits (04.2015–12.2022) computed for each grid cell assuming the 50th percentile of the daily rate of storage increase during deficit periods. Maps (a–d) surface soil moisture products; maps (e) and (f) root zone soil moisture products; maps (g) and (h) ensemble mean of SSM and RZSM; (i) TWS.

21.0 days. Regions with the longest recovery times include southern and eastern Africa, India, and the Tigris-Euphrates river system southwest of the Caspian Sea, but other regions, such as the eastern regions of Brazil and Australia, show significant differences in recovery times between TWS and RZSM. There are some regions, where the recovery times of SMAP L4 RZSM are even longer than those of TWS, particularly in parts of the northern latitude regions of Canada and Russia and in arid regions south of the Sahara.

We would like to recall the fact that data gaps in the SSM time series were filled by linear interpolation (see Section 3.1). To evaluate the effect of linear interpolation, we performed a simulation based on SMAP L4 SSM product as a reference, which shows similar short-periodic variability as the other SSM products, but does not contain data gaps. We then artificially introduced the same gaps present in the other SSM products (SMOS L3, SMAP L3, ESA CCI) into the SMAP L4 SSM data set and applied our gap-filling procedure and subsequent estimation of the recovery times. For ESA CCI with only a few data gaps, there is hardly any difference in the results. For SMOS and SMAP L3 data gaps our findings indicate that linear interpolation does introduce minor differences. The smoothing effect of linear interpolation results in a slightly slower recovery process, as expected, due to reduction of inherent variability. While for individual grid cells this can amount to about 2–3 days of recovery time, the average delay is around one day. This implies that the CDFs of the recovery times for these SSM data sets in Figure 7 would be slightly further to the left in case of no data gaps, resulting in a slightly stronger difference between recovery times of SSM and RZSM. However, the overall patterns and qualitative conclusions remain unaffected by the linear interpolation.

19447973, 2025, 8, Downloaded from https://agupubs.onlinelibrary.wiley.com/doi/10.1029/2024WR039321, Wiley Online Library on [23/10/2025]. See the Terms and Conditions (https://onlinelibrary.wiley.com/terms-and-conditions) on Wiley Online Library for rules of use; OA articles are governed by the applicable Creative Commons License

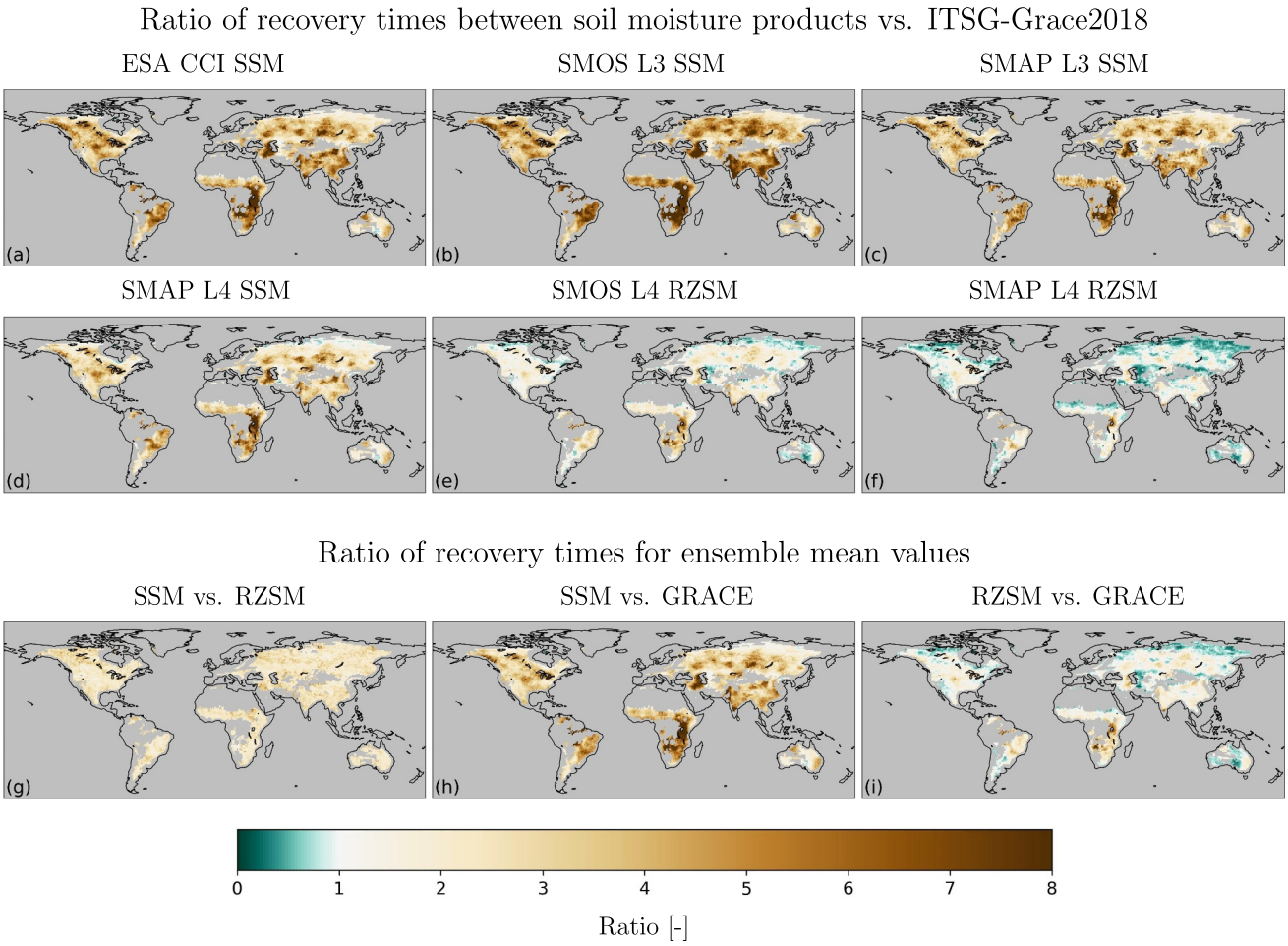

Figure 6. Global maps of the ratios of recovery times between TWS and the respective soil moisture products. Maps (a–d): surface soil moisture products; maps (e) and (f): root zone soil moisture products; maps (g–i) ensemble mean ratios: (g) SSM and RZSM, (h) SSM and TWS, and (i) RZSM and TWS. Values above 1 (depicted in brownish color) indicate faster storage recovery for the soil moisture product, while values below 1 (shown in greenish color) suggest faster storage recovery for TWS.

As mentioned in Section 3.1, another potential limitation of the performed analysis is the different native spatial resolution of the soil moisture and TWS data sets. To address this, we additionally computed recovery times after converting the soil moisture data sets into a spherical harmonics representation up to degree $n = 40$ (approximately 500 km) matching the spatial resolution of the GRACE data. The results are shown in Figures S9 and S10 in Supporting Information S1. For surface soil moisture products, the recovery times computed from this harmonized resolution showed negligible differences to the original $1° \times 1°$ grid. For root-zone soil moisture, particularly for SMAP L4 RZSM, shorter recovery times were observed after harmonization (see Figure S9 in Supporting Information S1). This can also be seen when comparing the CDFs of the recovery times (Figure S10 in Supporting Information S1), in which the CDF of the spherical harmonic result for SMAP L4 RZSM is further to the left and thus further apart from the TWS line compared to the corresponding result shown in Figure 7. This means that when aligning the spatial resolution between TWS and soil moisture data, the differences between TWS and RZSM recovery times become even more pronounced. However, the qualitative conclusion of our study, that is the relative order of the CDFs, is not influenced by the choice of the spatial resolution suggesting that the spatial smoothing inherent in GRACE data does not bias our findings. Therefore, we retain the $1° \times 1°$ resolution for soil moisture data as a practical compromise between their finer native resolutions and the coarser effective resolution of GRACE-based TWS, while avoiding additional unnecessary smoothing of the soil moisture signals.

Along the lines of the numbers provided in Table 1, we again established TWS as the reference and computed the ratios of average recovery times for each soil moisture product relative to TWS for each investigated grid cell (Figures 6a–6f). In addition to the ratios of the individual soil moisture products, also the ratios of the two

19447973, 2025, 8, Downloaded from https://agupubs.onlinelibrary.wiley.com/doi/10.1029/2024WR039321, Wiley Online Library on [23/10/2025]. See the Terms and Conditions (https://onlinelibrary.wiley.com/terms-and-conditions) on Wiley Online Library for rules of use; OA articles are governed by the applicable Creative Commons License

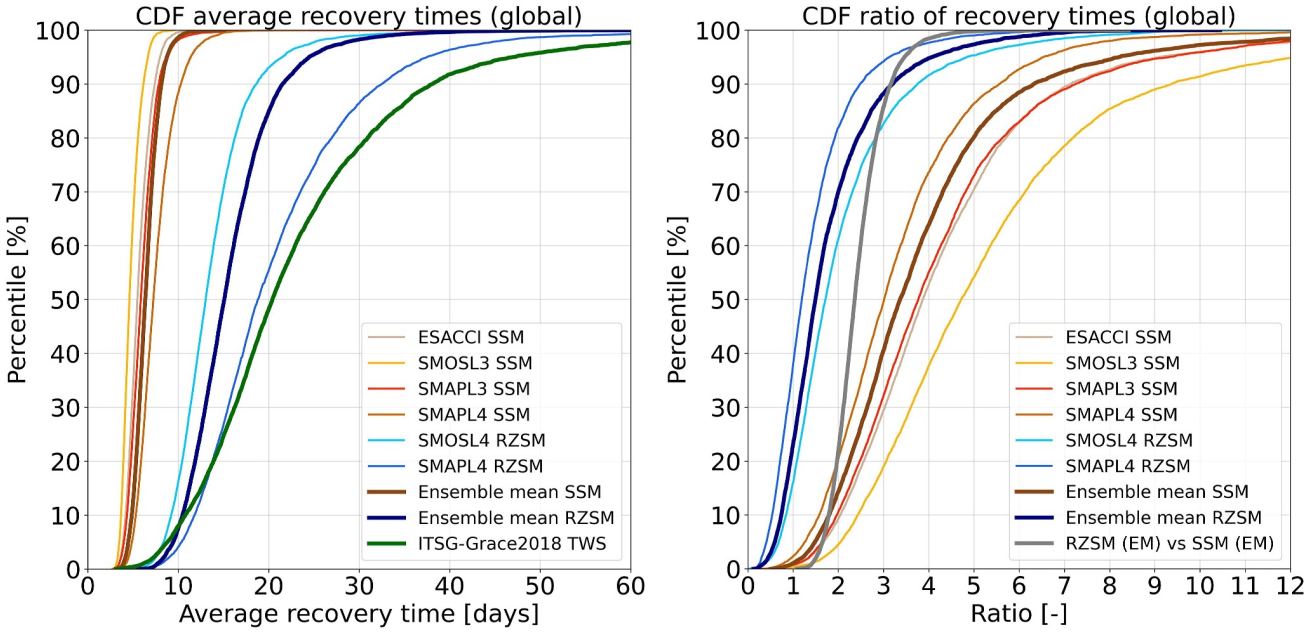

Figure 7. (a) Cumulative distribution functions (CDF) of cell-based mean recovery time values. Recovery times are calculated by the 50th percentile of the rate of change values, describing the storage recovery during water deficit periods. (b) Cumulative distribution functions (CDF) of cell-based ratios between TWS from GRACE and the respective soil moisture product. Both CDFs are restricted to grid cells defined as "area suited for analysis" in Figure 1.

ensemble means of SSM and RZSM with respect to TWS are plotted (h and i) and the ratio of the SSM ensemble mean with respect to the ensemble mean of the RZSM products (g). Corresponding CDFs of the cell-based ratio values are presented in Figure 7b with the fat brown and green lines representing the ensemble means of SSM and RZSM. Ratio values exceeding 1 indicate faster storage recovery for the respective soil moisture product, whereas values below 1 suggest faster storage recovery for TWS. In general, all surface soil moisture products exhibit ratios substantially above 1, with the majority (CDF range between percentiles from 20% to 80%) falling between a ratio of 2 and 6. This is also confirmed by the results of the respective ensemble mean (Figure 6h, median grid value equal to 3.1). Notably, the ratios between SMOS L3 SSM and TWS are higher compared to the other SSM products, which could partly be attributed to a higher noise level in the data set resulting in faster fluctuations of the time series and thus spuriously shorter recovery times. The ratios of SMAP L3 SSM and ESA CCI are about the same, but the SMAP L4 SSM product has smaller ratios. The RZSM ratios are notably smaller than SSM ratios, with the majority falling in the range of 1–3, with a median value of 1.5. Additionally, a higher fraction of values below 1 is observed for RZSM, indicating slower recovery than TWS. While for SMOS L4 RZSM this applies to approximately 15% of all grid cells, for SMAP L4 RZSM, 35%–40% of all grid cells exhibit ratios smaller than 1. As indicated above, these values are primarily located in the northern latitudes or in arid regions such as the Sahel region, large parts of Australia, the southwestern United States, and Central Asia. Overall, in other regions, the SMOS L4 RZSM ratios are slightly higher than SMAP L4 RZSM ratios, suggesting that differences in the methods used to generate the root zone data may play a role in the variability of the storage recovery. The ratio of the SSM versus the RZSM recovery times (Figure 6g, median grid value of 2.4) confirms the slower dynamics of RZSM. While these ratios offer a convenient and intuitive way to express the relative differences in recovery dynamics between variables and to illustrate spatial patterns of hydrological dynamics, they should be interpreted with caution. Each ratio represents the division of two quantities that are both subject to considerable uncertainties due to data resolution and processing techniques. Consequently, these uncertainties are propagated and accumulated in the ratios at the grid cell level.

5. Discussion and Conclusions

The results shown here demonstrate that satellite products with daily resolution, particularly satellite gravimetry from GRACE/GRACE-FO and satellite soil moisture data, can quantify the dynamics of drought cascades across the entire depth of the water column to comprehensively analyze sub-surface drought propagation processes.

19447973, 2025, 8, Downloaded from https://agupubs.onlinelibrary.wiley.com/doi/10.1029/2024WR039321, Wiley Online Library on [23/10/2025]. See the Terms and Conditions (https://onlinelibrary.wiley.com/terms-and-conditions) on Wiley Online Library for rules of use; OA articles are governed by the applicable Creative Commons License

19447973, 2025, 8, Downloaded from https://agupubs.onlinelibrary.wiley.com/doi/10.1029/2024WR039321, Wiley Online Library on [23/10/2025]. See the Terms and Conditions (https://onlinelibrary.wiley.com/terms-and-conditions) on Wiley Online Library for rules of use; OA articles are governed by the applicable Creative Commons License

Understanding these dynamics is crucial for effective water resource management and mitigating the impacts of droughts. Overall, the concept of drought propagation and recovery across different soil depths can well be recognized in the results.

Through a detailed examination of storage deficits and recovery times across various integration depths in the subsurface, from surface soil moisture to the entire water column represented by TWS, this study reveals differences in drought dynamics. The findings indicate that surface soil moisture exhibits faster evolution and recovery times compared to deeper soil layers and TWS, suggesting that near-surface soil moisture data could provide valuable insights for the early detection and monitoring of droughts. Moreover, the comparison of recovery times and ratios between different soil moisture products and TWS highlights the importance of considering different integration depths below the surface in drought monitoring and prediction. While TWS data from GRACE provide valuable information on the longer lasting features of hydrological droughts, surface soil moisture and root-zone soil moisture data offer more rapid and localized insights on meteorological and agricultural droughts, particularly during the early stages of drought events.

The results presented here show recovery times that are on average around 1.6 times longer (median value of recovery time ratios shown in Figure 6i) for TWS compared to RZSM. Similar relations of drought dynamics can be found, for example, in Farahmand et al. (2021), who conclude an average drought duration of 18.5 months for modeled SM including SSM and RZSM versus 27.5 months for TWS for four major US drought case studies, albeit with large variations among the different drought events. Time series shown in Rossi et al. (2023) allow an estimation of the duration of individual drought events of, for example 14 months (sub-surface SM) versus 21 months (TWS) for a drought event in Cerrado, Brazil. This is also well within the range of our findings on the recovery times from water storage deficits. In Entekhabi (2023), the delay and dampening effects of soil moisture and terrestrial water storage are analyzed for the continental United States, see Figure 5 of their manuscript. These dampening effects may be related to our rate of change values, as both reflect the reduced variability in deeper soil layers. However, a direct one-to-one comparison remains challenging due to the differing physical interpretations and sensitivities of the respective variables. The results from Entekhabi (2023) indicate that SMAP soil moisture data is dampened by approximately 25%–30%, while GRACE TWS experiences a stronger dampening effect of up to 80% relative to meteorological drought signals derived from precipitation. This corresponds to a ratio between SMAP and GRACE of approximately 0.31–0.37. Similarly, in our analysis, the average recovery time for the United States is around 6 days for SMAP L3 SSM and 20 days for GRACE TWS, resulting in a ratio of approximately 0.30. Despite the differences in methodologies, this could suggest that our findings align well with the observed dampening effect reported in Entekhabi (2023).

In our results, SMAP L4 RZSM exhibits slower rates of change and longer recovery times than TWS in some regions. This is a conceptually unexpected result at the first glance. For areas where soil moisture and groundwater are the dominant storage compartments, such as south of the Sahara, this might be attributed to the too slowly reacting soil water dynamics in the SMAP assimilation model. Other affected regions are in the northern latitudes. Here the temporal masking of the soil moisture products during frozen soil conditions leads to inconsistencies with the time coverage of the TWS time series, which may influence the results. In the overlapping time spans in the summer months, time series of SMAP L4 RZSM show a substantially smoother behavior and less temporal variability compared to TWS, which is in contrast to the findings in other regions. For these high latitude regions, Reichle et al. (2023, Figure 29c) show very small RZSM observation increments in the SMAP L4 data assimilation scheme as indicated by the temporal standard deviation of these increments. This means that in these regions, the satellite observations provide only minimal corrections to the model forecast of RZSM. Thus, the too slow RZSM dynamics compared to TWS are driven almost entirely by the underlying hydrological model. The discussion above and the results of our study in general suggest the potential of the remote sensing data sets with different integration depths to help in evaluating or even improving the infiltration and percolation schemes of hydrological models. Also, the data might be of use for tuning empirical model parameters such as those of exponential filters or other transfer functions that are used for the depth-extrapolation of SSM to RZSM (e.g., Rasche et al., 2024).

The results show that recovery time increases with deeper sub-surface integration depths. While the global spatial distribution of recovery times (Figure 5) for the soil moisture products is rather homogeneous, there are marked spatial variations of recovery times when considering TWS. For the soil moisture products, a uniform depth is assumed globally (5 cm for SSM and 1 m for RZSM), leading to a comparatively homogeneous behavior

19447973, 2025, 8, Downloaded from https://agupubs.onlinelibrary.wiley.com/doi/10.1029/2024WR039321, Wiley Online Library on [23/10/2025]. See the Terms and Conditions (https://onlinelibrary.wiley.com/terms-and-conditions) on Wiley Online Library for rules of use; OA articles are governed by the applicable Creative Commons License

everywhere which is dominated by vertical water transport processes. For TWS, in contrast, the hydrologically active zone, in which relevant magnitudes of water storage change can occur, may differ considerably between regions depending, for example, on the depth to bedrock or the thickness of unconsolidated sediments. Another aspect are heterogeneous groundwater dynamics governed by the regional hydrogeology and associated lateral groundwater transport. These factors cause the recovery times to vary spatially much more markedly. To further explore the spatial variability of recovery times and their potential drivers, we performed a first-order qualitative analysis by comparing the CDFs of recovery times for zones of different environmental characteristics based on global data sets of topography (NOAA National Centers for Environmental Information, 2022), vegetation-based land cover (Friedl & Sulla-Menashe, 2022), Köppen-Geiger climate zones (Kottek et al., 2006), and soil clay fraction data from GLDAS (Rodell et al. (2004) as derived from global soil data sets from Reynolds et al. (2000)). The corresponding figures are shown in Figures S11–S14 in Supporting Information S1. However, identifying causality for the spatial patterns of recovery times from this comparison is inherently difficult due to the spatial co-occurrence of many environmental factors that may affect the actual hydrological processes in a complex way. Some tendencies that emerged from this analysis are the following: Recovery times tend to be shorter in lowland regions than in higher elevation zones particularly for TWS and root-zone soil moisture, possibly due to the convergence of lateral water flow in the lowlands. As an example of differences between vegetation types, grasslands generally exhibited longer recovery times than savannas, suggesting a role of larger rooting depth and soil structure with higher macro-porosity in savannas due to a higher tree coverage. The latter, in turn, may favor the faster water transport into larger depths and thus a quicker storage recovery after dry periods in savanna regions. Climate zones showed distinct signatures, with equatorial regions displaying slower recovery, while warm temperate zones recovered more quickly. Furthermore, with respect to soil properties, here soil texture, higher clay fractions are associated with slower recovery times at the global scale, possibly due to lower infiltration capacities and retarded vertical water transport in soils with higher clay content. It should be stressed again that these are preliminary results of a first-order univariate analysis and a much more elaborated multi-factorial study is needed in future work to disentangle the complex interplay of various environmental factors on the subsurface storage dynamics and recovery rates.

Further research should also focus on improving the integration of satellite gravimetry and soil moisture data to enhance the accuracy and reliability of drought monitoring systems. Joint assimilation of surface soil moisture and TWS into hydrological models has already proven very valuable (Tangdamrongsub et al., 2020) and holds further potential in improving the simulation of water storage in the subsurface due to the distinct sensitivity of the two data types to water storage dynamics in different soil depths.

Furthermore, continued advancements in satellite remote sensing and data analysis techniques offer great potential for enhancing our understanding of drought dynamics and improving drought management strategies. Ongoing improvements to the GRACE/-FO data processing and next-generation gravity missions such as the MAGIC constellation of two GRACE-like missions operating simultaneously at differently inclined orbits (Daras et al., 2023), give prospect to an increase of the temporal and spatial resolution of satellite-based TWS data in the future. Also, the growing record of satellite soil moisture products provides a constantly increasing length of overlapping time series. This, in turn, will allow for extending the analyses to longer drought durations and a larger number of events, ultimately leading to more robust results.

The global scope of study at hand exploits the advantage that satellite data are mostly available with global coverage. In future studies, the potential of the data sets can be enhanced with regional analyses that may also include in situ observations with different soil depths or with different integration depths such as networks of terrestrial gravimetry, Cosmic Ray Neutron sensors or other in situ soil moisture measurements.

Data Availability Statement

The daily GRACE and GRACE-FO data products of ITSG-Grace2018 are publicly available from TU Graz (Mayer-Gürr et al., 2018):

https://ftp.tugraz.at/outgoing/ITSG/GRACE/ITSG-Grace2018/daily_kalman/daily_n40/

https://ftp.tugraz.at/outgoing/ITSG/GRACE/ITSG-Grace_operational/daily_kalman/daily_n40/

The ESA CCI soil moisture product can be downloaded from the ESA's Climate Change Initiative (CCI) web page (Dorigo et al., 2023):

http://catalogue.ceda.ac.uk/uuid/ff890589c21f4033803aa550f52c980c

Soil moisture products (Level 3 and Level 4) from the ESA's SMOS mission are made available by the Centre Aval de Traitement des Données SMOS (CATDS, 2022a, 2022b):

https://doi.org/10.12770/9cef422f-ed3f-4090-9556-b2e895ba2ca8

https://doi.org/10.12770/316e77af-cb72-4312-96a3-3011cc5068d4

Soil moisture products (Level 3 and Level 4) from NASA's SMAP mission are provided by the National Snow and Ice Data Center (NSIDC; O'Neill et al., 2023; Reichle et al., 2022):

https://doi.org/10.5067/4XXOGX0OOW1S and https://doi.org/10.5067/EVKPQZ4AFC4D.

Acknowledgments
A portion of this work was conducted at the Jet Propulsion Laboratory, California Institute of Technology, under contract with NASA. The authors would like to thank the editors for handling the manuscript and three anonymous reviewer for their constructive feedback. Open Access funding enabled and organized by Projekt DEAL.

References

AghaKouchak, A., Farahmand, A., Melton, F. S., Teixeira, J., Anderson, M. C., Wardlow, B. D., & Hain, C. R. (2015). Remote sensing of drought: Progress, challenges and opportunities. *Reviews of Geophysics*, *53*(2), 452–480. https://doi.org/10.1002/2014RG000456

Al Bitar, A., & Mahmoodi, A. (2020). *Algorithm theoretical basis document (ATBD) for the SMOS level 4 root zone soil moisture*. (Tech. Rep.). Zenodo. https://doi.org/10.5281/ZENODO.4298572

Bae, H., Ji, H., Lim, Y.-J., Ryu, Y., Kim, M.-H., & Kim, B.-J. (2019). Characteristics of drought propagation in South Korea: Relationship between meteorological, agricultural, and hydrological droughts. *Natural Hazards*, *99*(1), 1–16. https://doi.org/10.1007/s11069-019-03676-3

Barker, L. J., Hannaford, J., Chiverton, A., & Svensson, C. (2016). From meteorological to hydrological drought using standardised indicators. *Hydrology and Earth System Sciences*, *20*(6), 2483–2505. https://doi.org/10.5194/hess-20-2483-2016

Barros, A. P., Hodes, J. L., & Arulraj, M. (2017). Decadal climate variability and the spatial organization of deep hydrological drought. *Environmental Research Letters*, *12*(10), 104005. https://doi.org/10.1088/1748-9326/aa81de

Bergmann, I., & Dobslaw, H. (2012). Short-term transport variability of the Antarctic Circumpolar Current from satellite gravity observations. *Journal of Geophysical Research*, *117*(C5), C05044. https://doi.org/10.1029/2012JC007872

Bhardwaj, K., Shah, D., Aadhar, S., & Mishra, V. (2020). Propagation of meteorological to hydrological droughts in India. *Journal of Geophysical Research: Atmospheres*, *125*(22), e2020JD033455. https://doi.org/10.1029/2020JD033455

Blank, D., Eicker, A., Jensen, L., & Güntner, A. (2023). A global analysis of water storage variations from remotely sensed soil moisture and daily satellite gravimetry. *Hydrology and Earth System Sciences*, *27*(13), 2413–2435. https://doi.org/10.5194/hess-27-2413-2023

Bonin, J. A., & Chambers, D. P. (2011). Evaluation of high-frequency oceanographic signal in GRACE data: Implications for de-aliasing. *Geophysical Research Letters*, *38*(17), L17608. https://doi.org/10.1029/2011GL048881

Bureau of Meteorology. (2019). Special climate statement 72 - Dangerous bushfire weather in spring 2019. Retrieved from http://www.bom.gov.au/climate/current/statements/scs72.pdf

CATDS. (2022a). *CATDS-PDC L3SM filtered - 1 day global map of soil moisture values from SMOS satellite*. CATDS (CNES, IFREMER, CESBIO). https://doi.org/10.12770/9CEF422F-ED3F-4090-9556-B2E895BA2CA8

CATDS. (2022b). *CATDS-PDC L4SM RZSM - 1 day global map of root zone soil moisture values from SMOS satellite*. CATDS (CNES, IFREMER, CESBIO). https://doi.org/10.12770/316E77AF-CB72-4312-96A3-3011CC5068D4

Changnon, S. A. (1987). *Detecting drought conditions in Illinois*. Illinois State Water Survey. Circular No. 169.

Cheng, M., & Ries, J. (2017). The unexpected signal in GRACE estimates of C_{20. *Journal of Geodesy*, *91*(8), 897–914. https://doi.org/10.1007/s00190-016-0995-5

Crocetti, L., Forkel, M., Fischer, M., Jurečka, F., Grlj, A., Salentinig, A., et al. (2020). Earth observation for agricultural drought monitoring in the Pannonian Basin (southeastern Europe): Current state and future directions. *Regional Environmental Change*, *20*(4), 123. https://doi.org/10.1007/s10113-020-01710-w

Daras, I., March, G., Pail, R., Hughes, C., Braitenberg, C., Güntner, A., et al. (2023). *Mass-change and geosciences international constellation (MAGIC) expected impact on science and applications. Geophysical Journal International, ggad472*. Oxford University Press. https://doi.org/10.1093/gji/ggad472

Dobslaw, H., Bergmann-Wolf, I., Dill, R., Poropat, L., Thomas, M., Dahle, C., et al. (2017). A new high-resolution model of non-tidal atmosphere and ocean mass variability for de-aliasing of satellite gravity observations: AOD1B RL06. *Geophysical Journal International*, *211*(1), 263–269. https://doi.org/10.1093/gji/ggx302

Dorigo, W., Preimesberger, W., Hahn, S., van der Schalie, R., de Jeu, R., Kidd, R., et al. (2023). *ESA soil moisture climate change initiative (Soil_moisture_cci): Version 08.1 data collection*. NERC EDS Centre for Environmental Data Analysis. Retrieved from http://catalogue.ceda.ac.uk/uuid/ff890589c21f4033803aa550f52c980c

Dorigo, W., Scipal, K., Parinussa, R. M., Liu, Y. Y., Wagner, W., de Jeu, R. A. M., & Naeimi, V. (2010). Error characterisation of global active and passive microwave soil moisture datasets. *Hydrology and Earth System Sciences*, *14*(12), 2605–2616. https://doi.org/10.5194/hess-14-2605-2010

Dorigo, W., Wagner, W., Albergel, C., Albrecht, F., Balsamo, G., Brocca, L., et al. (2017). ESA CCI soil moisture for improved Earth system understanding: State-of-the art and future directions. *Remote Sensing of Environment*, *203*, 185–215. https://doi.org/10.1016/j.rse.2017.07.001

Eicker, A., Jensen, L., Wöhnke, V., Dobslaw, H., Kvas, A., Mayer-Gürr, T., & Dill, R. (2020). Daily GRACE satellite data evaluate short-term hydro-meteorological fluxes from global atmospheric reanalyses. *Scientific Reports*, *10*(1), 4504. https://doi.org/10.1038/s41598-020-61166-0

Entekhabi, D. (2023). Propagation in the drought cascade: Observational analysis over the continental US. *Water Resources Research*, *59*(9), e2022WR032608. https://doi.org/10.1029/2022WR032608

Entekhabi, D., Njoku, E. G., O'Neill, P. E., Kellogg, K. H., Crow, W. T., Edelstein, W. N., et al. (2010). The soil moisture active passive (SMAP) mission. *Proceedings of the IEEE*, *98*(5), 704–716. https://doi.org/10.1109/JPROC.2010.2043918

19447973, 2025, 8, Downloaded from https://agupubs.onlinelibrary.wiley.com/doi/10.1029/2024WR039321, Wiley Online Library on [23/10/2025]. See the Terms and Conditions (https://onlinelibrary.wiley.com/terms-and-conditions) on Wiley Online Library for rules of use; OA articles are governed by the applicable Creative Commons License

Entekhabi, D., Yueh, S., O'Neill, P. E., Kellogg, K. H., Allen, A., Bindlish, R., et al. (2014). *SMAP handbook–soil moisture active passive: Mapping soil moisture and freeze/thaw from space*. JPL Publication. Retrieved from https://asf.alaska.edu/wp-content/uploads/2019/03/smap_handbook.pdf

Fan, Y. (2015). Groundwater in the Earth's critical zone: Relevance to large-scale patterns and processes. *Water Resources Research*, *51*(5), 3052–3069. https://doi.org/10.1002/2015WR017037

Farahmand, A., Reager, J. T., & Madani, N. (2021). Drought cascade in the terrestrial water cycle: Evidence from remote sensing. *Geophysical Research Letters*, *48*(14), e2021GL093482. https://doi.org/10.1029/2021GL093482

Friedl, M., & Sulla-Menashe, D. (2022). *MODIS/Terra+Aqua land cover type yearly L3 global 0.05Deg CMG V061*. NASA EOSDIS Land Processes Distributed Active Archive Center. https://doi.org/10.5067/MODIS/MCD12C1.061

Gouweleeuw, B. T., Kvas, A., Gruber, C., Gain, A. K., Mayer-Gürr, T., Flechtner, F., & Güntner, A. (2018). Daily GRACE gravity field solutions track major flood events in the Ganges–Brahmaputra Delta. *Hydrology and Earth System Sciences*, *22*(5), 2867–2880. https://doi.org/10.5194/hess-22-2867-2018

Gruber, A., Scanlon, T., van der Schalie, R., Wagner, W., & Dorigo, W. (2019). Evolution of the ESA CCI soil moisture climate data records and their underlying merging methodology. *Earth System Science Data*, *11*(2), 717–739. https://doi.org/10.5194/ESSD-11-717-2019

Huang, S., Li, P., Huang, Q., Leng, G., Hou, B., & Ma, L. (2017). The propagation from meteorological to hydrological drought and its potential influence factors. *Journal of Hydrology*, *547*, 184–195. https://doi.org/10.1016/j.jhydrol.2017.01.041

Jensen, L., Eicker, A., Stacke, T., & Dobslaw, H. (2020). Predictive skill assessment for land water storage in CMIP5 decadal hindcasts by a global reconstruction of GRACE satellite data. *Journal of Climate*, *33*(21), 9497–9509. https://doi.org/10.1175/JCLI-D-20-0042.1

Keovilignavong, O., Nguyen, T. H., & Hirsch, P. (2023). Reviewing the causes of Mekong drought before and during 2019–20. *International Journal of Water Resources Development*, *39*(1), 155–175. https://doi.org/10.1080/07900627.2021.1967112

Kerr, Y. H., Waldteufel, P., Wigneron, J.-P., Delwart, S., Cabot, F., Boutin, J., et al. (2010). The SMOS mission: New tool for monitoring key elements of the global water cycle. *Proceedings of the IEEE*, *98*(5), 666–687. https://doi.org/10.1109/JPROC.2010.2043032

Kottek, M., Grieser, J., Beck, C., Rudolf, B., & Rubel, F. (2006). World map of the Köppen-Geiger climate classification updated. *Meteorologische Zeitschrift*, *15*(3), 259–263. https://doi.org/10.1127/0941-2948/2006/0130

Kurtenbach, E., Eicker, A., Mayer-Gürr, T., Holschneider, M., Hayn, M., Fuhrmann, M., & Kusche, J. (2012). Improved daily GRACE gravity field solutions using a Kalman smoother. *Journal of Geodynamics*, *59–60*, 39–48. https://doi.org/10.1016/j.jog.2012.02.006

Kvas, A., Behzadpour, S., Ellmer, M., Klinger, B., Strasser, S., Zehentner, N., & Mayer-Gürr, T. (2019). ITSG-Grace2018: Overview and evaluation of a new GRACE-only gravity field time series. *Journal of Geophysical Research: Solid Earth*, *124*(8), 9332–9344. https://doi.org/10.1029/2019JB017415

Lambeck, K. (1988). *Geophysical geodesy: The slow deformations of the Earth*. Clarendon Press ; Oxford University Press.

Landerer, F. W., Flechtner, F. M., Save, H., Webb, F. H., Bandikova, T., Bertiger, W. I., et al. (2020). Extending the global mass change data record: GRACE follow-on instrument and science data performance. *Geophysical Research Letters*, *47*(12), e2020GL088306. https://doi.org/10.1029/2020GL088306

Lei, F., Crow, W., Shen, H., Parinussa, R., & Holmes, T. (2015). The impact of local acquisition time on the accuracy of microwave surface soil moisture retrievals over the contiguous United States. *Remote Sensing*, *7*(10), 13448–13465. https://doi.org/10.3390/rs71013448

Longuevergne, L., Wilson, C. R., Scanlon, B. R., & Crétaux, J. F. (2013). GRACE water storage estimates for the Middle East and other regions with significant reservoir and lake storage. *Hydrology and Earth System Sciences*, *17*(12), 4817–4830. https://doi.org/10.5194/hess-17-4817-2013

Mayer-Gürr, T., Behzadpour, S., Eicker, A., Ellmer, M., Koch, B., Krauss, S., et al. (2021). GROOPS: A software toolkit for gravity field recovery and GNSS processing. *Computers & Geosciences*, *155*, 104864. https://doi.org/10.1016/j.cageo.2021.104864

Mayer-Gürr, T., Behzadpur, S., Ellmer, M., Kvas, A., Klinger, B., Strasser, S., & Zehentner, N. (2018). ITSG-Grace2018 - Monthly, daily and static gravity field solutions from GRACE. *GFZ Data Services*. https://doi.org/10.5880/ICGEM.2018.003

Mekong River Commission. (2022). Mekong low flow and drought conditions in 2019-2021. Retrieved from https://www.mrcmekong.org/wp-content/uploads/2024/08/LowFlowReport20192021-1-1.pdf

Mishra, A. K., & Singh, V. P. (2010). A review of drought concepts. *Journal of Hydrology*, *391*(1–2), 202–216. https://doi.org/10.1016/j.jhydrol.2010.07.012

Naumann, G., Podesta, G., Marengo, J., Luterbacher, J., Bavera, D., Acosta Navarro, J., et al. (2023). Extreme and long-term drought in the La Plata Basin: event evolution and impact assessment until September 2022. (KJ-NA-31-381-EN-N (online)). https://doi.org/10.2760/62557

Nguyen, H., Wheeler, M. C., Hendon, H. H., Lim, E.-P., & Otkin, J. A. (2021). The 2019 flash droughts in subtropical eastern Australia and their association with large-scale climate drivers. *Weather and Climate Extremes*, *32*, 100321. https://doi.org/10.1016/j.wace.2021.100321

NOAA National Centers for Environmental Information. (2022). *ETOPO 2022 15 arc-second global relief model*. NOAA National Centers for Environmental Information. https://doi.org/10.25921/FD45-GT74

Oertel, M., Meza, F., Gironás, J., A. Scott, C., Rojas, F., & Pineda-Pablos, N. (2018). Drought propagation in semi-arid River Basins in Latin America: Lessons from Mexico to the Southern Cone. *Water*, *10*(11), 1564. https://doi.org/10.3390/w10111564

O'Neill, P. E., Peggy, E., Chan, S., Njoku, E., Jackson, T., Bindlish, R., & Chaubell, M. (2023). *SMAP L3 radiometer global daily 36 km EASE-grid soil moisture, version 9*. NASA National Snow and Ice Data Center Distributed Active Archive Center. https://doi.org/10.5067/4XXOGX0OOW1S

Owe, M., de Jeu, R., & Holmes, T. (2008). Multisensor historical climatology of satellite-derived global land surface moisture. *Journal of Geophysical Research*, *113*(F1), 687. https://doi.org/10.1029/2007JF000769

Owe, M., de Jeu, R., & Walker, J. (2001). A methodology for surface soil moisture and vegetation optical depth retrieval using the microwave polarization difference index. *IEEE Transactions on Geoscience and Remote Sensing*, *39*(8), 1643–1654. https://doi.org/10.1109/36.942542

Peltier, W. R., Argus, D. F., & Drummond, R. (2017). Comment on "An assessment of the ICE-6G_c (VM5a) glacial isostatic adjustment model" by Purcell et al. *Journal of Geophysical Research: Solid Earth*, *123*(2), 2019–2028. https://doi.org/10.1002/2016JB013844

Peters, E., Bier, G., Van Lanen, H., & Torfs, P. (2006). Propagation and spatial distribution of drought in a groundwater catchment. *Journal of Hydrology*, *321*(1–4), 257–275. https://doi.org/10.1016/j.jhydrol.2005.08.004

Preimesberger, W., Scanlon, T., Su, C.-H., Gruber, A., & Dorigo, W. (2021). Homogenization of structural breaks in the global ESA CCI soil moisture multisatellite climate data record. *IEEE Transactions on Geoscience and Remote Sensing*, *59*(4), 2845–2862. https://doi.org/10.1109/TGRS.2020.3012896

Rahmati, M., Amelung, W., Brogi, C., Dari, J., Flammini, A., Bogena, H., et al. (2024). Soil moisture memory: State-of-the-art and the way forward. *Reviews of Geophysics*, *62*(2), e2023RG000828. https://doi.org/10.1029/2023RG000828

Rasche, D., Blume, T., & Güntner, A. (2024). Depth extrapolation of field-scale soil moisture time series derived with cosmic-ray neutron sensing (CRNS) using the soil moisture analytical relationship (SMAR) model. *SOIL*, *10*(2), 655–677. https://doi.org/10.5194/soil-10-655-2024

19447973, 2025, 8, Downloaded from https://agupubs.onlinelibrary.wiley.com/doi/10.1029/2024WR039321, Wiley Online Library on [23/10/2025]. See the Terms and Conditions (https://onlinelibrary.wiley.com/terms-and-conditions) on Wiley Online Library for rules of use; OA articles are governed by the applicable Creative Commons License

Reichle, R., De Lannoy, G., Koster, R., Crow, W., Kimball, J., Liu, Q., & Bechtold, M. (2022). *SMAP L4 global 3-hourly 9 km EASE-grid surface and root zone soil moisture. Geophysical data, version 7*. NASA National Snow and Ice Data Center Distributed Active Archive Center. https://doi.org/10.5067/EVKPQZ4AFC4D

Reichle, R., Liu, Q., Ardizzone, J. V., Bechtold, M., Crow, W. T., De Lannoy, G., et al. (2023). Soil moisture active passive (SMAP) project assessment report for version 7 of the L4_sm data product. Retrieved from https://nsidc.org/sites/default/files/documents/technical-reference/smap_l4v7_sm_assessmtreport.pdf

Reynolds, C. A., Jackson, T. J., & Rawls, W. J. (2000). Estimating soil water-holding capacities by linking the food and agriculture organization soil map of the world with global pedon databases and continuous pedotransfer functions. *Water Resources Research*, *36*(12), 3653–3662. https://doi.org/10.1029/2000WR900130

Robinson, D. A., Campbell, C. S., Hopmans, J. W., Hornbuckle, B. K., Jones, S. B., Knight, R., et al. (2008). Soil moisture measurement for ecological and hydrological watershed-scale observatories: A review. *Vadose Zone Journal*, *7*(1), 358–389. https://doi.org/10.2136/vzj2007.0143

Rodell, M., Houser, P. R., Jambor, U., Gottschalck, J., Mitchell, K., Meng, C.-J., et al. (2004). The global land data assimilation system. *Bulletin of the American Meteorological Society*, *85*(3), 381–394. https://doi.org/10.1175/BAMS-85-3-381

Rossi, J. B., Ruhoff, A., Fleischmann, A. S., & Laipelt, L. (2023). Drought propagation in Brazilian biomes revealed by remote sensing. *Remote Sensing*, *15*(2), 454. https://doi.org/10.3390/rs15020454

Seneviratne, S. I., Zhang, X., Adnan, M., Badi, W., Dereczynski, C., Di Luca, A., et al. (Eds.), Climate change 2021: The physical science basis. Contribution of working group I to the sixth assessment report of the intergovernmental panel on climate change (pp. 1513–1766). Cambridge University Press. https://doi.org/10.1017/9781009157896.013

Sun, Y., Riva, R., & Ditmar, P. (2016). Optimizing estimates of annual variations and trends in geocenter motion and J2 from a combination of GRACE data and geophysical models. *Journal of Geophysical Research: Solid Earth*, *121*(11), 8352–8370. https://doi.org/10.1002/2016JB013073

Swenson, S., Chambers, D., & Wahr, J. (2008). Estimating geocenter variations from a combination of GRACE and ocean model output: Estimating geocenter variations. *Journal of Geophysical Research*, *113*(B8), B08410. https://doi.org/10.1029/2007JB005338

Tangdamrongsub, N., Han, S.-C., Yeo, I.-Y., Dong, J., Steele-Dunne, S. C., Willgoose, G., & Walker, J. P. (2020). Multivariate data assimilation of GRACE, SMOS, SMAP measurements for improved regional soil moisture and groundwater storage estimates. *Advances in Water Resources*, *135*, 103477. https://doi.org/10.1016/j.advwatres.2019.103477

Tapley, B. D., Bettadpur, S., Watkins, M., & Reigber, C. (2004). The gravity recovery and climate experiment: Mission overview and early results. *Geophysical Research Letters*, *31*(9), L09607. https://doi.org/10.1029/2004GL019920

Thomas, A. C., Reager, J. T., Famiglietti, J. S., & Rodell, M. (2014). A GRACE-based water storage deficit approach for hydrological drought characterization. *Geophysical Research Letters*, *41*(5), 1537–1545. https://doi.org/10.1002/2014GL059323

Tijdeman, E., Barker, L. J., Svoboda, M. D., & Stahl, K. (2018). Natural and human influences on the link between meteorological and hydrological drought indices for a large set of catchments in the contiguous United States. *Water Resources Research*, *54*(9), 6005–6023. https://doi.org/10.1029/2017WR022412

Ulaby, F. T., & Long, D. G. (2014). *Microwave radar and radiometric remote sensing*. The University of Michigan Press.

Van Loon, A. F. (2015). Hydrological drought explained. *WIREs Water*, *2*(4), 359–392. https://doi.org/10.1002/wat2.1085

Wagner, W. (1998). *Soil moisture retrieval from ERS scatterometer data (No. Heft 49)*. Wien: Veröffentlichung des Instituts für Photogrammetrie und Fernerkundung.

Wilhite, D. A., & Glantz, M. H. (1985). Understanding: The drought phenomenon: The role of definitions. *Water International*, *10*(3), 111–120. https://doi.org/10.1080/02508068508686328

Xiong, J., Guo, S., Abhishek, Li, J., & Yin, J. (2022). A novel standardized drought and flood potential index based on reconstructed daily GRACE data. *Journal of Hydrometeorology*, *23*(9), 1419–1438. https://doi.org/10.1175/JHM-D-22-0011.1

19447973, 2025, 8, Downloaded from https://agupubs.onlinelibrary.wiley.com/doi/10.1029/2024WR039321, Wiley Online Library on [23/10/2025]. See the Terms and Conditions (https://onlinelibrary.wiley.com/terms-and-conditions) on Wiley Online Library for rules of use; OA articles are governed by the applicable Creative Commons License

Supporting Information for "Revisiting sub-surface drought cascades with daily satellite observations of soil moisture and terrestrial water storage"

Daniel Blank[1], Annette Eicker[1], John T. Reager[2], Andreas Güntner[3,4]

[1]HafenCity University Hamburg, Hamburg, Germany

[2]Jet Propulsion Laboratory, California Institute of Technology, Pasadena, CA, USA

[3]Helmholtz Centre Potsdam GFZ German Research Centre for Geosciences, Potsdam, Germany

[4]University of Potsdam, Institute of Environmental Sciences and Geography, Potsdam, Germany

Contents of this file

1. Text S1
2. Figures S1 to S14

Introduction

This supporting information contains text and figures that provide additional visual context to the main text.

Text S1. Describing supporting figures S1 to S14

Figure S1 shows the Pearson correlation coefficient between ITSG-Grace2018 and the individual soil moisture products. Additionally, the correlation between the surface soil moisture and the root-zone soil moisture ensemble means is calculated (Fig. S1(g)). Figure S2 presents the corresponding cumulative distribution function of the cell-based

correlation coefficients. In general, there is good agreement between soil moisture and terrestrial water storage. The least agreement is observed for the SMOS L3 and SMAP L3 products, although more than 50% of global correlation values still exceed 0.2. The correlation coefficients for root-zone products are generally higher compared to surface soil moisture products. The highest agreement is seen for the SMAP L4 root-zone products, with more than 50% of all values above 0.5.

Figures S3 (global results) and S4 (cumulative distribution function) show the sign agreement, indicating the percentage of times the signs (positive or negative) of the z-scores from ITSG-Grace2018 match those of the individual soil moisture products. In general, for most grid cells (80%), the signs agree more than 50% of the time. The sign agreement for the root-zone products is also considerably higher compared to the surface soil moisture products. For almost all grid cells, the agreement between the ensemble means of surface soil moisture and root-zone soil moisture exceeds 70%.

Figures S5 and S6 (based on Figures 2 and 3 from the main text) show time series results for another example grid cell in New South Wales, Australia (30° S, 148° E). The region was affected by droughts from 2017 to 2019, with recovery beginning in 2020, which is also visible in the time series. The CDFs follow a similar pattern to what was observed in the main text.

Figures S7 and S8 (based on Figures 2 and 3 from the main text) show time series results for another example grid cell located in the Mekong River basin (17° S, 102° E). The region was affected by droughts from 2019 to 2021. The signals follow a similar pattern during water storage deficits, as described in the main text.

Figures S9 and S10 illustrate the influence of the spatial resolution. To investigate the

effect of smoothing and averaging, soil moisture data sets were converted into a spherical harmonics representation up to degree n = 40 (i.e. 500km) to achieve a spatial resolution consistent with the GRACE data. Figure S9 shows recovery times for ESA CCI, SMOS L3, and SMAP L4 RZSM (for the other products the change of the results is similar). The maps on the left correspond to the 1°×1° resolution used in the paper, while those on the right result from first converting to spherical harmonics up to n = 40, and then evaluating on the 1°×1° grid. Figure S10 compares the CDFs of the recovery times with and without conversion to spherical harmonics.

Figures S11 to S14 illustrate the influence of different environmental characteristics on the determination of recovery times on global datasets of topography (S11), vegetation-based land cover (S12), Köppen-Geiger climate zones (S13), and soil clay fraction (S14). For each characteristic, the left figure shows a global map of the different values and the right figure shows their influence on the CDFs of the recovery times.

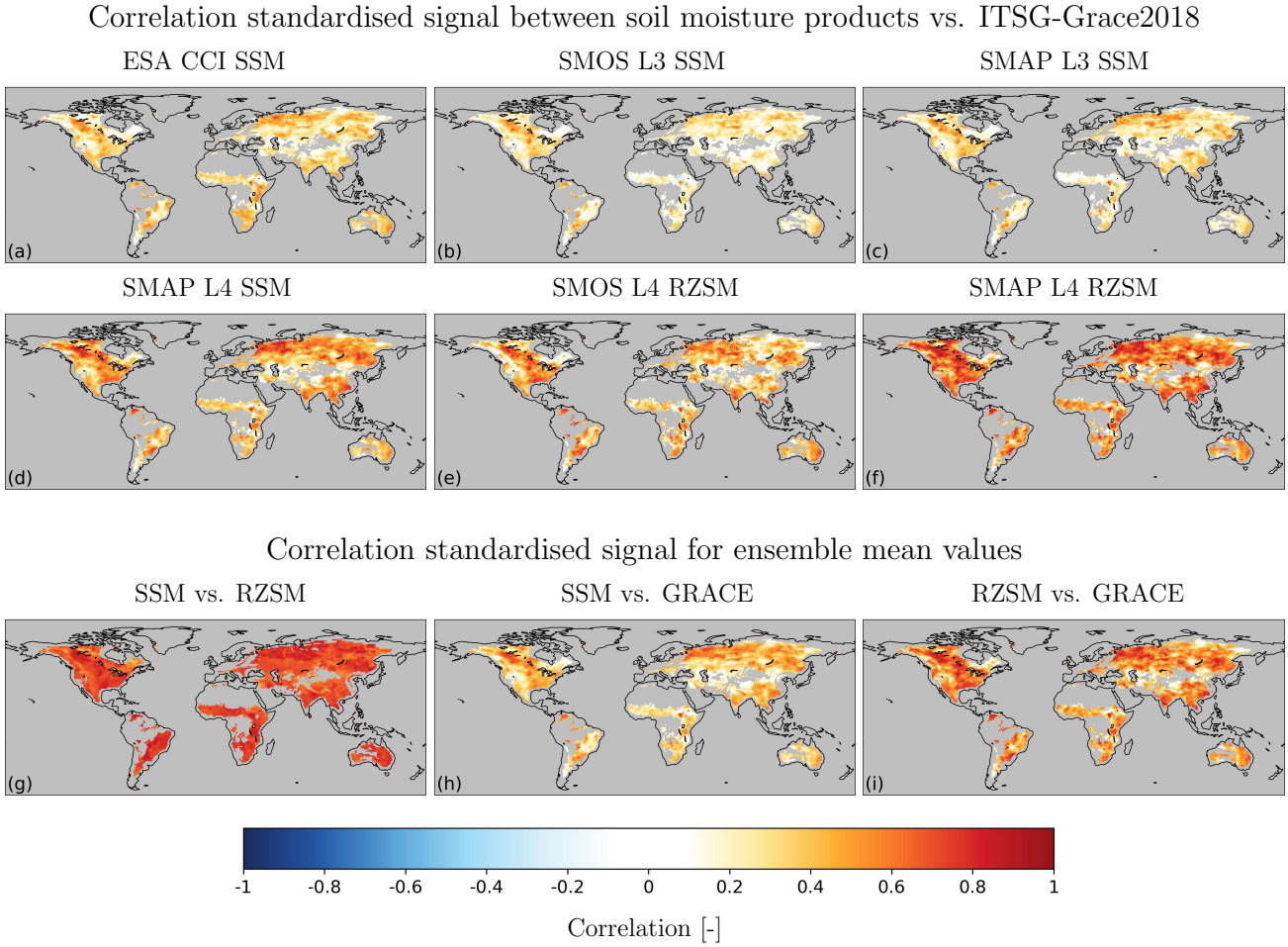

Figure S1. Global maps of correlation coefficients between the standardised signal from TWS and the corresponding soil moisture products. The correlation between the ensemble mean of surface soil moisture (SSM) and root-zone soil moisture (RZSM) is also shown in (g). The spatial mask shown in the main paper (Fig. 1) is used as well.

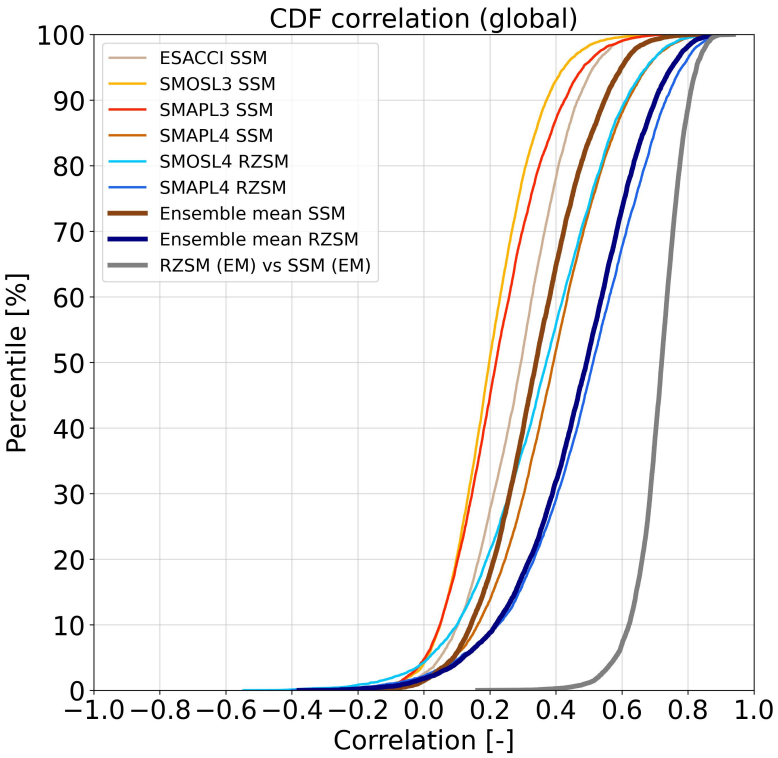

Figure S2. Cumulative distribution functions (CDF) of cell-based correlation coefficients based on global maps from Fig. S1.

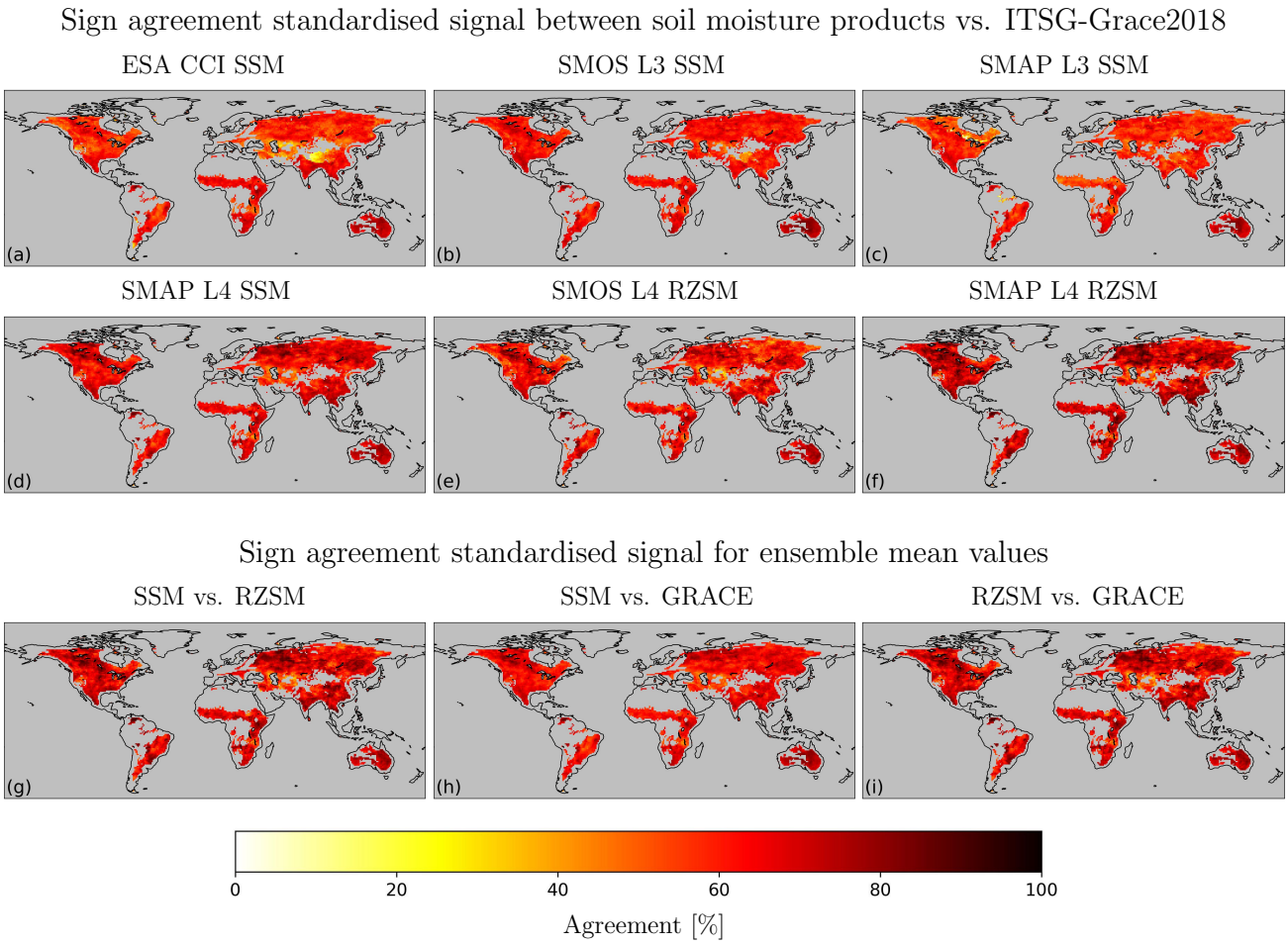

Figure S3. Global maps of sign agreement between the standardised signal from TWS and the corresponding soil moisture products. The spatial mask shown in the main paper (Fig. 1) is used as well.

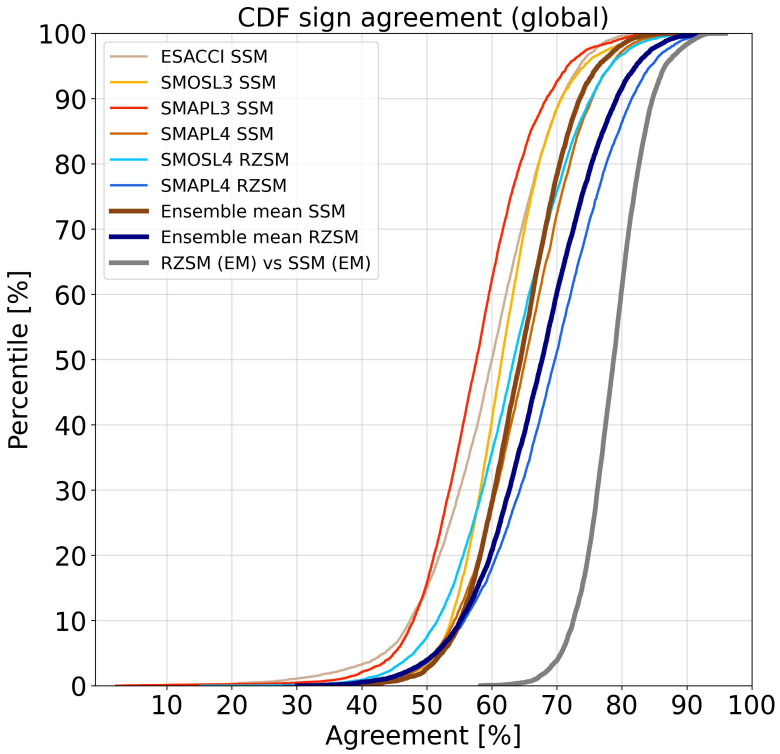

Figure S4. Cumulative distribution functions (CDF) of cell-based sign agreement based on global maps from Fig. S1.

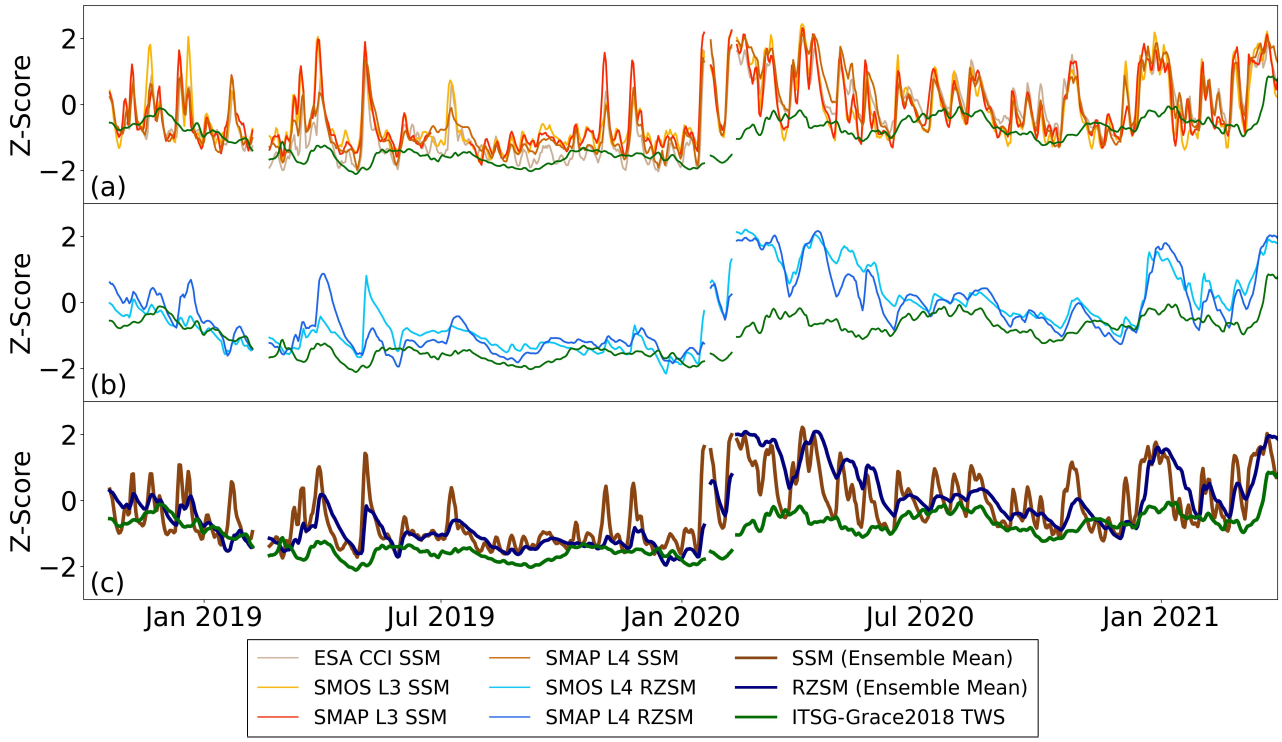

Figure S5. De-seasonalised time series for an example grid cell in in New South Wales, Australia (30° S, 148° E). (a): Surface soil moisture (SSM) of ESA CCI, SMOS L3, SMAP L3, SMAP L4, and TWS from GRACE. (b): Root zone soil moisture (RZSM) of SMOS L4, SMAP L4, and TWS data from GRACE. (c): Ensemble mean of all SSM data sets (light brown) and RZSM data sets (dark blue) and TWS from GRACE. The individual time series are plotted as well, with a smaller line width.

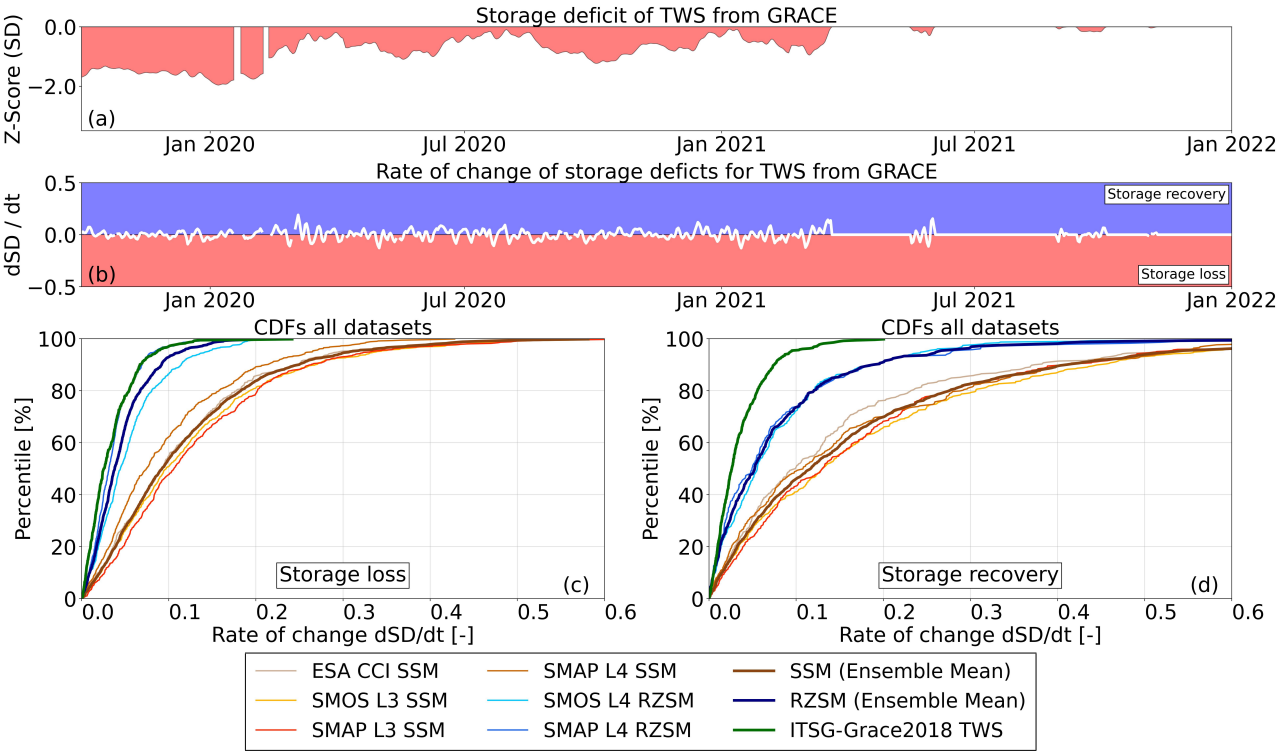

Figure S6. (a): Time series of TWS storage deficit for the exemplary grid cell in New South Wales, Australia (30° S, 148° E). (b): TWS rate of change time series (dSD/dt). (c): Cumulative distribution function (CDF) of storage loss rate of change values for all data sets. (d): CDF of storage recovery rate of change values for all data sets.

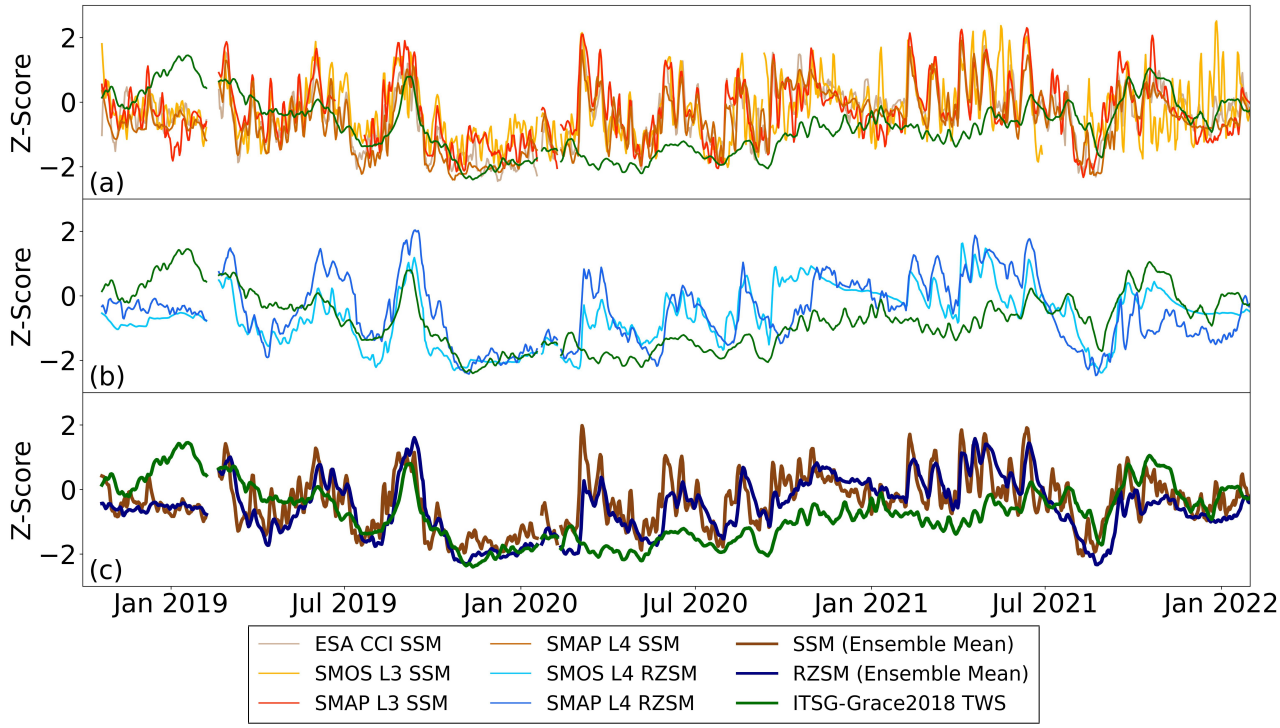

Figure S7. De-seasonalised time series for an example grid cell Mekong river basin (17° S, 102° E). (a): Surface soil moisture (SSM) of ESA CCI, SMOS L3, SMAP L3, SMAP L4, and TWS from GRACE. (b): Root zone soil moisture (RZSM) of SMOS L4, SMAP L4, and TWS data from GRACE. (c): Ensemble mean of all SSM data sets (light brown) and RZSM data sets (dark blue) and TWS from GRACE. The individual time series are plotted as well, with a smaller line width.

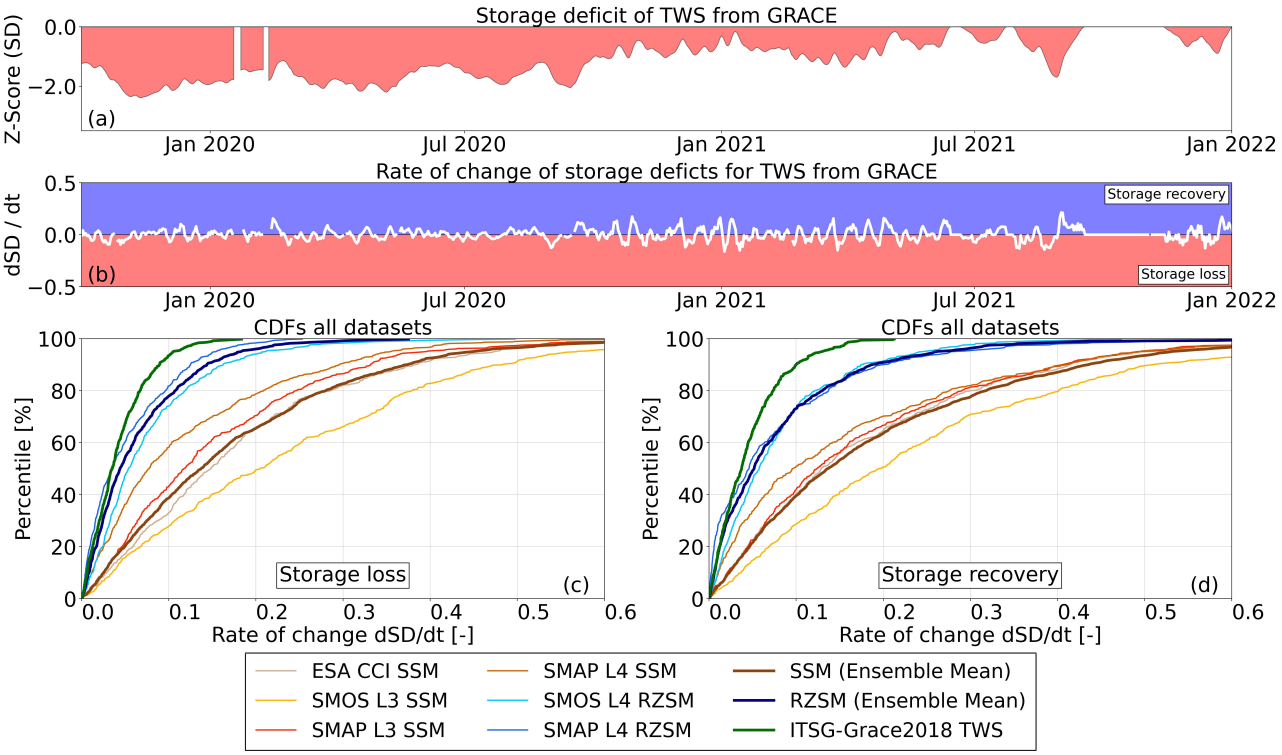

Figure S8. (a): Time series of TWS storage deficit for the exemplary grid cell in the Mekong river basin (17° S, 102° E). (b): TWS rate of change time series (dSD/dt). (c): Cumulative distribution function (CDF) of storage loss rate of change values for all data sets. (d): CDF of storage recovery rate of change values for all data sets.

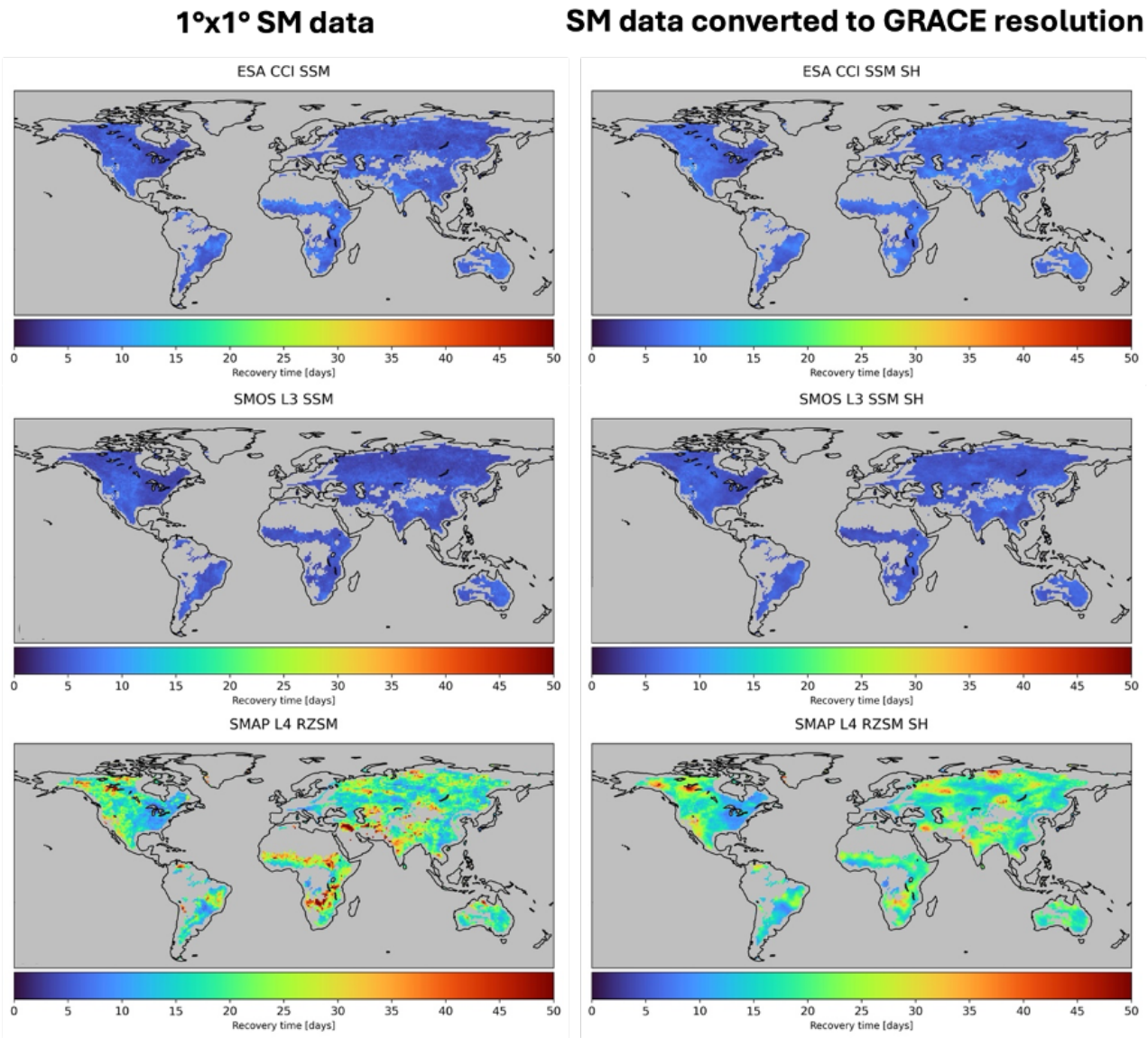

Figure S9. Comparison of the recovery time of exemplary soil moisture data derived from the harmonized 1°x1° spatial resolution (left, as used in the paper) and from SM data after aligning the spatial resolution with GRACE (left, i.e. after converting to a GRACE-like spherical harmonics representation up to degree 40 and subsequent evaluation on the 1°x1° grid).

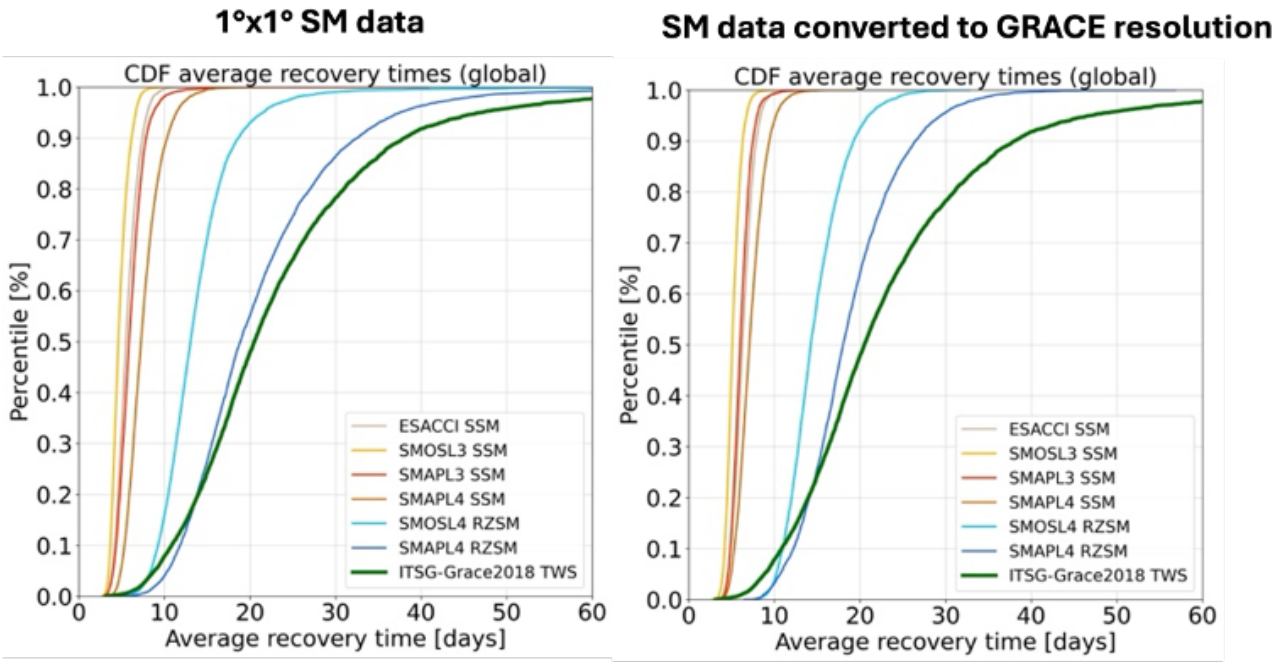

Figure S10. CDFs for average recovery time. Left: CDF for the harmonized resolution of 1° for soil moisture data which (as used in the paper. Right: results after converting to a GRACE-like spherical harmonics representation up to degree 40.

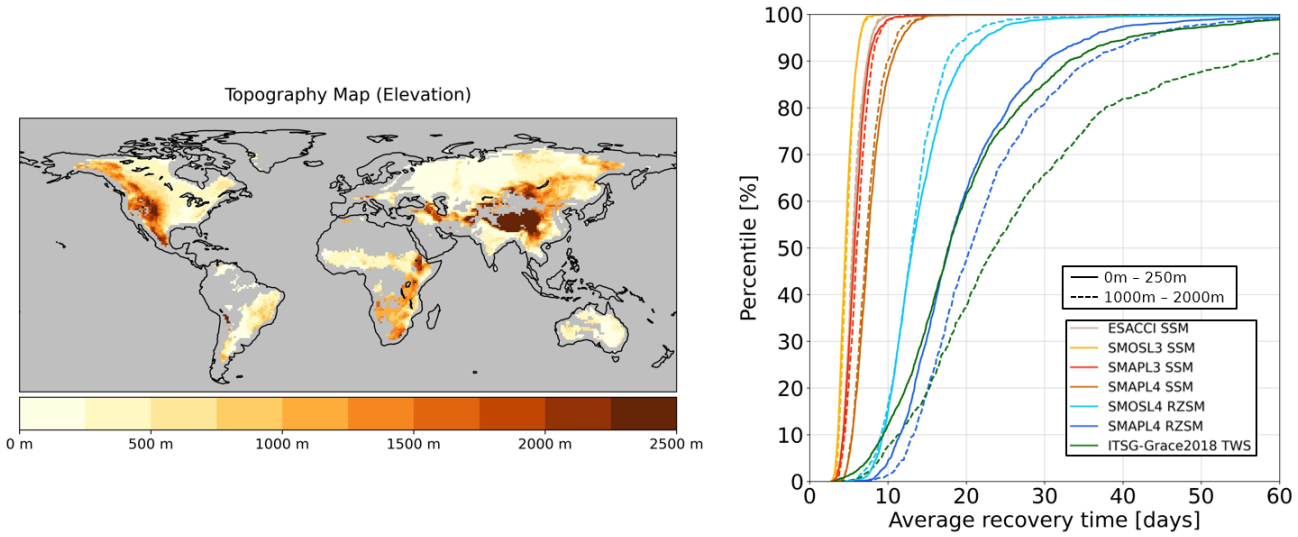

Figure S11. Topography map from NOAA ETOPO 2022 Global Relief Model (left) and CDF for average recovery times in the particular grid cells for low elevation (0–250 m; solid lines) and moderate-to-high elevation (1000–2000 m; dotted lines).

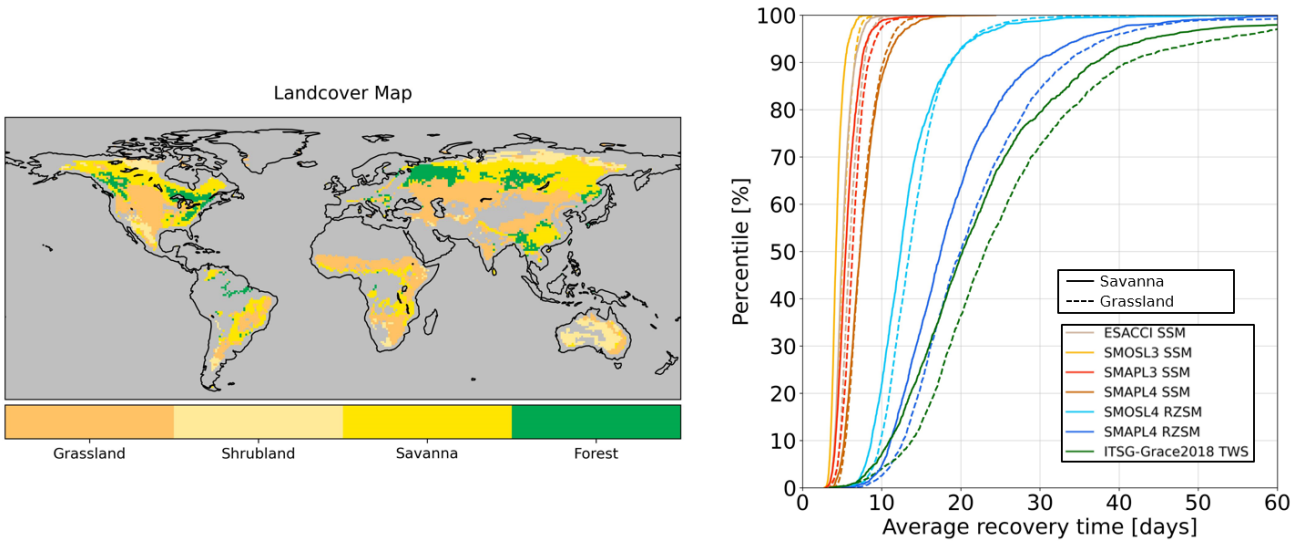

Figure S12. Landcover map from MCD12C1 MODIS Land Cover Type product (left) and CDF for average recovery times in the particular grid cells for Savannas (solid lines) and Grasslands (dashed lines).

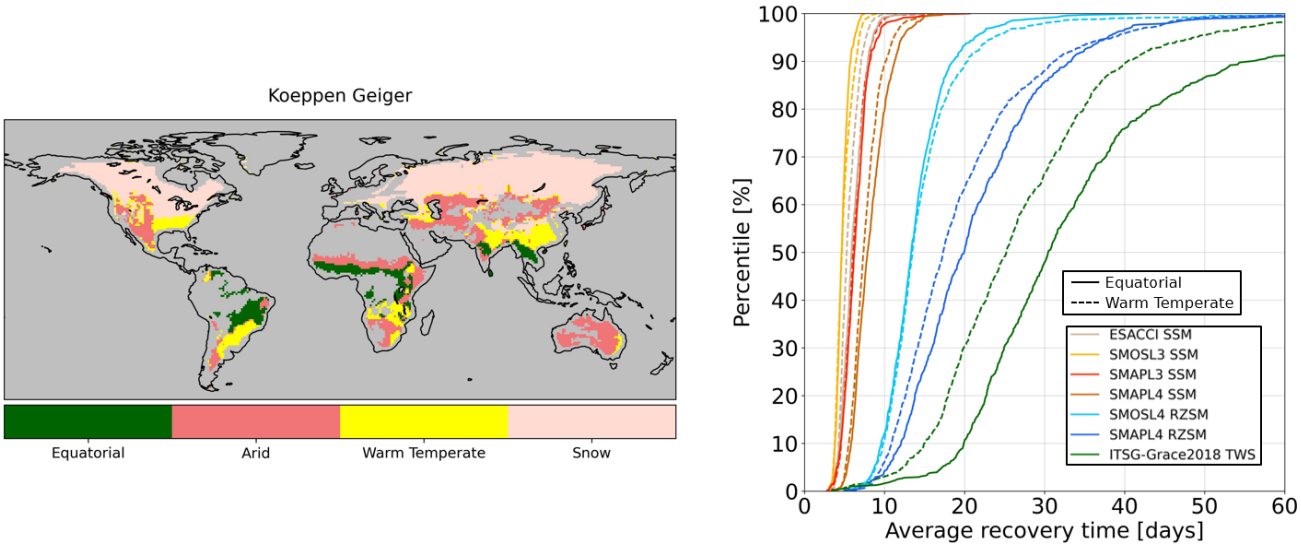

Figure S13. Climate regions map from the Köppen-Geiger global climate classification scheme (left) and CDF for average recovery times in the particular grid cells for equatorial regions (solid lines) and warm temperate regions (dashed lines).

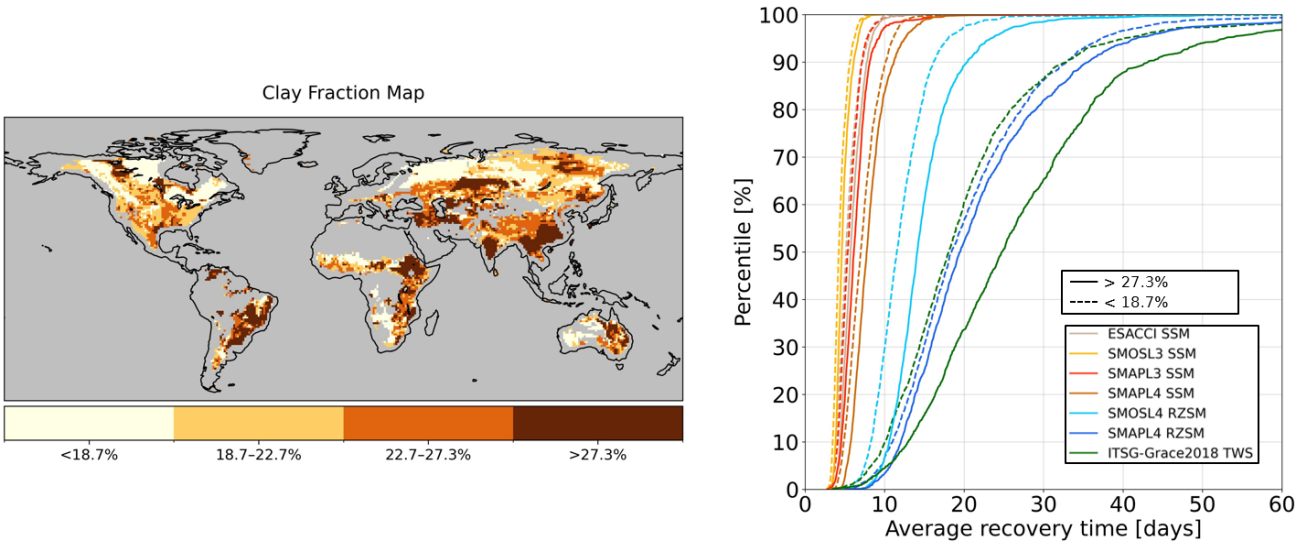

Figure S14. Clay fraction map from GLDAS soil dataset (left) and CDF for average recovery times in the particular grid cells for high clay content regions (>27.3%, solid lines) and low clay content regions (<18.7%, dashed lines).

A.3. Assessing sub-seasonal subsurface water storage dynamics using exponential filtering of ESA CCI soil moisture and daily GRACE terrestrial water storage data

Reference

Blank, D., Rasche, D., Güntner, A., Eicker, A. (2026). Assessing Sub-seasonal Subsurface Water Storage Dynamics Using Exponential Filtering of ESA CCI Soil Moisture and Daily GRACE Terrestrial Water Storage Data. In: International Association of Geodesy Symposia. Springer, Berlin, Heidelberg. https://doi.org/10.1007/1345_2026_357

Abstract

We present a global framework to infer sub-seasonal subsurface water storage dynamics from daily satellite surface soil moisture by optimizing the time constant of an exponential filter used for the depth extrapolation against GRACE and GRACE-FO terrestrial water storage (TWS) anomalies. The approach uses ESA CCI v9.1 surface and root-zone soil moisture products together with daily ITSG-Grace2018 gravity fields on a 1° global grid. For each grid cell, the time constant T of the filter is optimized to maximize the correlation between exponentially filtered soil moisture and GRACE-based TWS from which snow, surface-water, and seasonal components have been removed before. On average, the global area-weighted correlation increases from 0.19 for unfiltered surface soil moisture to 0.39 after optimization. The optimal T values decrease systematically with the depth of the soil moisture layer used as input and show physically consistent patterns related to climatic and hydrogeological controls such as aridity, soil characteristics, and depth to the groundwater table. In contrast to existing approaches that use in-situ soil moisture data to compute globally uniform T parameters, our approach allows to capture spatially varying infiltration dynamics into deeper soil layers. The resulting global T field thus provides an observation-driven proxy for subsurface storage dynamics at weekly-to-monthly time scales, offering a simple and transferable approach for linking satellite surface soil moisture to terrestrial water storage variations.

Declaration of own contribution

Table 3: Contribution to Paper No. 3.

Involved in	**Estimated contribution**
Ideas and conceptual design	85%
Computation and results	100%
Analysis and interpretation	90%
Manuscript, figures and tables	95%
Total	92.5%

Confirmation of Co-Authors

I hereby confirm the correctness of the declaration of the contribution of **Daniel Blank** for Paper No. 3 in Table 3:

Daniel Rasche	Date
Andreas Güntner	Date
Annette Eicker	Date

Assessing Sub-seasonal Subsurface Water Storage Dynamics Using Exponential Filtering of ESA CCI Soil Moisture and Daily GRACE Terrestrial Water Storage Data

Daniel Blank, Daniel Rasche, Andreas Güntner, and Annette Eicker

Abstract

We present a global framework to infer sub-seasonal subsurface water storage dynamics from daily satellite surface soil moisture by optimizing the time constant of an exponential filter used for the depth extrapolation against GRACE and GRACE-FO terrestrial water storage (TWS) anomalies. The approach uses ESA CCI v9.1 surface and root-zone soil moisture products together with daily ITSG-Grace2018 gravity fields on a 1° global grid. For each grid cell, the time constant T of the filter is optimized to maximize the correlation between exponentially filtered soil moisture and GRACE-based TWS from which snow, surface-water, and seasonal components have been removed before. On average, the global area-weighted correlation increases from 0.19 for unfiltered surface soil moisture to 0.39 after optimization. The optimal T values decrease systematically with the depth of the soil moisture layer used as input and show physically consistent patterns related to climatic and hydrogeological controls such as aridity, soil characteristics, and depth to the groundwater table. In contrast to existing approaches that use in-situ soil moisture data to compute globally uniform T parameters, our approach allows to capture spatially varying infiltration dynamics into deeper soil layers. The resulting global T field thus provides an observation-driven proxy for subsurface storage dynamics at weekly-to-monthly time scales, offering a simple and transferable approach for linking satellite surface soil moisture to terrestrial water storage variations.

Keywords

GRACE · Remote sensing · Soil moisture · Terrestrial water storage

1 Introduction

Root-zone soil moisture (RZSM) is crucial for plant water availability, regulates land–atmosphere exchanges of energy and carbon, and is central to drought and flood risk assessment. However, RZSM is difficult to observe directly at continental to global scales. In-situ networks provide valuable point measurements but are sparse and heterogeneous, while land surface models have high uncertainties through

Supplementary Information The online version contains supplementary material available at https://doi.org/10.1007/1345_2026_357.

D. Blank (✉)
HafenCity University Hamburg, Hamburg, Germany
e-mail: daniel.blank@hcu-hamburg.de

D. Rasche
GFZ Helmholtz Centre for Geosciences, Potsdam, Germany

A. Güntner
GFZ Helmholtz Centre for Geosciences, Potsdam, Germany

Institute of Environmental Sciences and Geography, University of Potsdam, Potsdam, Germany

A. Eicker
HafenCity University Hamburg, Hamburg, Germany

GFZ Helmholtz Centre for Geosciences, Potsdam, Germany

International Association of Geodesy Symposia,
https://doi.org/10.1007/1345_2026_357, © The Author(s) 2026

parametrization and forcing data. Satellite microwave observations provide consistent monitoring of surface soil moisture (SSM). However, their sensing depth is limited to the upper few centimetres of the soil. This does not match the root-zone, where water transport and storage processes shape the hydrologic response on weekly to monthly scales. The exponential filter method (Albergel et al. 2008; Wagner et al. 1999) provides a simple, globally applicable way to approximate RZSM from SSM satellite retrievals alone. The exponential filter delays and smooths the more variable SSM signal in time to approximate root-zone dynamics. The method is widely used because it delivers reasonable performance without ancillary inputs while remaining computationally efficient and straightforward to implement. To apply the filter, its single parameter, the time constant T, must be optimized. This typically requires calibration with in-situ soil moisture, monitored at a certain soil depth in the root zone. Because such observations are sparse and unevenly distributed, many applications adopt a single, globally constant T value instead (Pasik et al. 2023).

Satellite gravimetry from the Gravity Recovery and Climate Experiment (GRACE) and the GRACE-Follow-On (GRACE-FO) mission provide a complementary, integrative, and globally available view of terrestrial water storage (TWS) variations. Due to the fact that any redistribution of water mass on or above the Earth's surface causes variations in the Earth's gravity field, satellite gravimetry can link changes in the gravitational acceleration acting on a satellite to changes in TWS on and underneath the Earth's surface, representing the only globally consistent observations of these integrated storage variations. The TWS signal aggregates changes in soil moisture, groundwater, snow, ice, and surface water. In previous studies (Blank et al. 2023, 2025), we examined the relationship between SSM, RZSM, and GRACE-derived TWS at daily resolution and across multiple frequency bands (full signal, seasonal, anomalies, and sub-monthly). We found that the TWS signal is smoothed and lagged behind RZSM and even more so relative to SSM, and that the lag decreases when evaluating shorter sub-monthly time scales instead of, e.g., seasonal signals.

In this study, we develop a globally distributed optimization approach for the exponential filter time constant T. The method transforms daily SSM (from the ESA CCI data set) into an estimate of subsurface water storage dynamics. Our aim is to capture temporal dynamics and relative changes in subsurface storage. Absolute storage values cannot be provided, though. We use GRACE-based TWS as an independent large-scale constraint and focus on sub-seasonal time scales. To isolate subsurface variations, we subtract snow and surface-water from TWS so that the residual primarily reflects soil moisture and groundwater. For each grid cell, we choose T that the correlation between the exponentially filtered SSM and TWS, after removing the seasonal cycle and inter-annual variability is maximized. Deseasonalizing TWS largely removes groundwater and ice mass variations that are often dominated by seasonal variations, and preserves shorter-term signals from soil moisture dynamics. The resulting T values are analysed as an indicator of the dynamics of downward redistribution of soil moisture in the subsurface. Additionally, we apply this approach using the ESA CCI RZSM product with different integration depths (0–10, 0–40, 0–100, 0–200 cm) as the input for the estimation of the T values by calibration against TWS. In Fig. 1, the schematic of the datasets and the optimization workflow is shown. The input SSM and the four RZSM layers are each passed through an exponential filter with individual time constants T (denoted T_5, T_{10}, T_{40}, T_{100}, T_{200}) that are calibrated per grid cell against GRACE resulting in five different depth-extrapolated subsurface storage time series. With this setup, we test whether the dynamics are already captured by a certain integration depth of ESA CCI or whether deeper layers add additional subsurface storage variability.

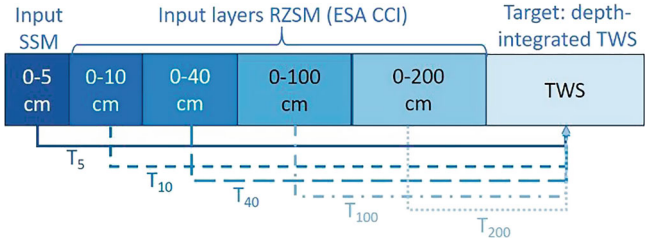

Fig. 1 Schematic of the analysis: input layers of surface SSM (0–5 cm) and ESA CCI RZSM (0–10, 0–40, 0–100, 0–200 cm) are each filtered with an exponential filter with time constant T and calibrated against the depth-integrated GRACE TWS. Please note that the blue boxes do not denote distinct separate layers but always refer to the integration depth starting from the surface

Linking SSM observations to TWS variations is conceptually challenging because TWS represents the combined variability of multiple storage compartments, including the unsaturated zone at different depths and groundwater. Transfer functions such as the exponential filter thus do not directly estimate a specific storage compartment but rather provide a simplified representation of the temporal redistribution of SSM signals into deeper storage layers. Consequently, the optimized filter parameter T reflects the combined influence of multiple subsurface transport and storage processes and related parameter such as soil hydraulic properties. In this study, RZSM refers to soil moisture integrated over a predefined soil depth, whereas subsurface storage describes the total amount of water stored below the surface in all soil layers and in groundwater.

Optimizing T per grid cell against GRACE-based TWS yields spatially varying T values that capture local subsurface storage dynamics. The same framework can be applied to alternative SSM datasets. The primary contribution of this

study therefore is a diagnostic framework that evaluates whether GRACE-TWS observations can be used to constrain spatially varying time constants in the exponential filter approach rather than to provide a new soil moisture dataset.

2 Data Sets

2.1 GRACE and GRACE-FO Data

We use daily gravity field solutions from ITSG-Grace2018 (Kvas et al. 2019), provided as spherical-harmonics coefficients truncated at degree 40 corresponding to ~500 km resolution and estimated with a Kalman-smoothing approach. We apply standard GRACE/GRACE-FO post-processing by addressing geocenter motion, replacing c_{20} derived from Satellite Laser Ranging, and correcting for glacial isostatic adjustment. The processed gravity field solutions are then converted to water mass variations as gridded equivalent water heights. Since we use daily data, we selectively excluded days with insufficient GRACE observations (below 10,000) from our analysis.

Because GRACE TWS includes surface water and snow, we remove these components to isolate subsurface storage (soil moisture and groundwater). We use monthly surface-water and snow-water storage from G3P (Güntner et al. 2024), interpolate them to daily resolution, and subtract the resulting time series from TWS before further analysis. The interpolation to daily resolution is performed using a piecewise cubic Hermite interpolating polynomial to match the temporal sampling of the GRACE data. This temporal downscaling represents an approximation, as possible sub-monthly variability of these storage components cannot be resolved. Removing surface and snow water prevents their dynamics from biasing the results and ensures that the GRACE constraint reflects the subsurface storages we aim to capture with the exponential filter.

2.2 Soil Moisture Data

Soil moisture is the water content in the vadose zone of the subsurface and governs infiltration, evapotranspiration, groundwater recharge and land-atmosphere coupling. Microwave remote sensing infers near-surface soil moisture from changes in the soil's dielectric constant: active sensors use backscatter, while passive sensors use brightness temperature retrievals. The sensing depth is about 0–5 cm.

We use the ESA CCI COMBINED (active + passive; v9.1; Dorigo et al. 2017; Gruber et al. 2019; Preimesberger et al. 2021) SSM product, a harmonized multi-mission daily record at 0.25° representing volumetric soil moisture in the 0–5 cm layer. The dataset applies quality flags and masks dense tropical rainforest where retrievals are unreliable. Additionally, days are flagged in which the soil temperature is below 0 °C and the snow water equivalent is bigger than 0 mm representing snow and frozen soil conditions.

In addition to the ESA CCI SSM, we use the ESA CCI RZSM product (Stradiotti and Preimesberger 2024; v9.1), which is derived from the COMBINED SSM dataset via an exponential filter. The filter's temporal length T parameter is optimized using a large set of in-situ soil moisture time series (Pasik et al. 2023) and applied as depth dependent spatially uniform T value for all global grid cells. The product provides soil moisture in three discrete layers (0–10, 10–40, 40–100 cm). Additionally we derived a 100–200 cm layer using the same methodology of Pasik et al. (2023). Implementation details of this 100–200 cm layer are provided in the Supplementary Material (Sect. 1). To derive the soil moisture over the different integration depths of 0–10, 0–40, 0–100 and 0–200 cm, we calculate thickness-weighted averages of the contributing layers.

For clarity, each discrete layer (0–10, 10–40, 40–100, 100–200 cm) uses a single global T value specific to that layer depth. As a result, an integrated depth estimate combines multiple discrete layers and therefore multiple T values. For example, the 0–40 cm product averages the 0–10 and 10–40 cm layers, and the 0–200 cm averages all four layers.

3 Data Pre-processing and Limitations

3.1 Data Harmonization

All datasets are harmonized to a global 1° × 1° grid. The higher resolution ESA CCI product is aggregated to this grid using first-order conservative remapping. GRACE's effective resolution is coarser than 1°, because daily gravity fields are truncated spherical-harmonics solutions with spatial dependence over ~500 km; thus 1° × 1° is a compromise between the resolution of soil moisture and GRACE data and signals of neighbouring GRACE grid cells remain strongly correlated. We analyze the time period of January 2003–December 2022, excluding the GRACE/GRACE-FO gap (August 2017–June 2018). The ESA CCI record contains occasional short gaps which were filled by linear interpolation for gaps smaller than 3 days.

3.2 Signal Decomposition

We focus on the sub-seasonal component of TWS and soil moisture variability. First, a linear trend from all datasets. Next, the seasonal cycle as a day-of-year climatology over

the common 20-years period and subtract it to obtain an anomaly signal. To separate the sub-seasonal variability of the anomaly signal, we apply a Butterworth high-pass filter with a 365-day cut-off frequency (Butterworth 1930).

3.3 Spatial Limitations and Masking

We mask regions where microwave soil-moisture retrievals or GRACE data are unreliable. Dense tropical forests contaminate active/passive signals, but ESA CCI already masks these areas. Arid deserts show negligible SSM variability and low GRACE signal-to-noise-ratio. We exclude such pixels via low RMS variability in daily SSM, using a conservative threshold derived from a Sahara reference. Snow and frozen soil also bias SSM retrievals, thus while we do not mask these regions permanently we exclude days flagged as frozen or snow-covered (see Sect. 2.2). This results in a consistent analysis domain in which both SSM and TWS are informative for the scope of this study (see Blank et al. 2023; Fig. 1 for a spatial map displaying this domain).

4 Methodology

4.1 Exponential Filter

The exponential filter method (Wagner et al. 1999) treats soil moisture as a two-layer water balance model in which infiltration is the only exchange between the surface layer and the subsurface reservoir. The flux is assumed proportional to the moisture difference between SSM and RZSM. In the classical formulation, the exponential filter is used to estimate RZSM from SSM observations using the standard recursive formulation of the exponential filter method (Albergel et al. 2008; Pasik et al. 2023):

$$\boldsymbol{RZSM_t = RZSM_{t-1} + K_t\,(SSM_t - RZSM_{t-1})} \quad (1)$$

$$\boldsymbol{K_t = \frac{K_{t-1}}{K_{t-1} + e^{\frac{\Delta t}{T}}}}. \quad (2)$$

where t_n and t_{n-1} denote the current and previous timestamp (days), Δt is their difference, and K_t (ranges from 0 to 1) is the gain term. The new RZSM is thus a weighted average of the latest SSM observation and the previous estimate. The only unknown parameter of this equation is T (temporal length in days). It defines the weighting, with a larger T resulting in a smaller K_t, related to a stronger smoothing and greater time delay. A smaller T implies less smoothing and a closer resemblance to SSM. When no preceding estimates are available (initial values), the exponential filter calculation is started with $K_0 = 1$ and $RZSM_{t0} = SSM_{t0}$. In this study, we use the same recursive formulation of the exponential filter but calibrate the filter parameter T against GRACE-based TWS in order to represent the temporal dynamics of integrated subsurface storage. The variable RZSM in Eq. (1) therefore represents the exponentially filtered subsurface storage and should not be interpreted as a direct estimate of RZSM.

Temporal variability is smaller in the root zone than at the surface, so the time constant T and thus the inherent smoothing generally increases with deeper soil depth (e.g. Wagner et al. 1999; Paulik et al. 2014). The optimal T can depend on several environmental factors (e.g. soil properties, vegetation or climatic variables). Alternative transfer-function approaches exist, including statistical methods and semi-physical models such as SMAR (e.g., Manfreda et al. 2014; Zhang et al. 2017). We use the exponential filter due to its simplicity and single calibration parameter, while acknowledging that it represents a simplified approximation of subsurface processes.

4.2 T-Parameter Optimization

To estimate RZSM, T is commonly calibrated against in-situ soil moisture at the target depth. Hereby a set of T values (e.g., 1–100 days) is tested and the value that maximizes a skill metric, typically correlation coefficient or Nash Sutcliffe efficiency, is selected. The ESA CCI RZSM dataset defines a single, globally constant T for each of its four defined depth layers (see Sect. 2.2). In contrast, we optimize T without relying on in-situ depth references. Instead, we apply GRACE-derived TWS (with surface- and snow-water removed) as an independent large-scale constraint, which does not assume a globally constant behaviour but can account for regionally different characteristics. For each grid cell, we choose T to maximize the correlation between the exponentially filtered ESA CCI SSM or RZSM and TWS over a range of 0–100 days. This yields a spatially varying T value map tailored to local conditions. Because GRACE TWS and ESA CCI soil moisture are expressed in different units, the optimization focuses on reproducing temporal variability rather than absolute magnitude, and therefore relies on the correlation coefficient as the performance metric.

In principle, SSM could be calibrated with the full GRACE TWS signal (including the seasonal cycle). However, the exponential filter acts as a low-pass filter. Thus, optimizing T with the full signal would therefore be dominated by seasonality and lead to larger T values. We therefore calibrate on the sub-seasonal component (trend, seasonal, and interannual signal removed) so that the optimization targets weekly–to–monthly dynamics and reduces the influence of seasonality.

Many RZSM products blend multiple depth layers and weigh them with depth to retain higher frequency signals. In

our setting, the effective sensing depth of GRACE is covering the entire relevant depth domain. Instead of specifying layer weights, we infer a single locally optimized T parameter that focuses on the higher-frequency part. This GRACE-based constraint allows T to reflect locally effective storage depths that can be deeper than the commonly assumed 0–200 cm.

5 Results

5.1 Time Series Results for an Example Location

We first illustrate the optimization for the example of a single grid cell near Kota, Rajasthan (25° N, 75° E) in India, a hot semi-arid region with a monsoon season from July to September. Figure 2a summarizes the optimization. For a set of T values ranging from 0 to 100 days we filter SSM (T_5 see Fig. 1) and compute the correlation with TWS. The correlation rises quickly from about 0.30 (initial value), peaks with 0.66 at $T = 22$ days, and then declines again for larger T because the resulting time series becomes too strongly smoothed. This pattern illustrates the transition from short-term SSM variability to the slower storage dynamics sensed by GRACE that include the deeper subsurface. Figure 2b shows the sub-seasonal anomalies from January 2007 to January 2011 (as a visual excerpt, all metrics are computed over the full 20-year period). The ESA CCI SSM time series is more variable and slightly shifted in time relative to GRACE-based TWS. Applying the exponential filter with the optimized $T = 22$ days dampens the high frequent fluctuations and introduces a modest delay, yielding a much closer visual agreement with TWS. Accordingly, the time lag between the time series computed by a cross correlation analysis shifts from about +10 days before filtering (SSM leading TWS) to 0 days after optimization. We observe a marked decrease in temporal variability due to the dampening caused by the exponential filtering. The root-mean square (RMS) variability of the signal drops from 3% for the original SSM to 1.2% for the filtered SSM, a reduction of about 60%.

5.2 Global Results

The framework is then applied on a global scale. As described in Sect. 3.3, desert and rainforest regions are excluded from the analysis. For the remaining grid cells, we evaluate the correlations at the sub-seasonal time scale between GRACE TWS and the unfiltered ESA CCI SSM product (Fig. 3a), with a global area weighted mean of 0.19 and a maximum value of 0.57. After depth extrapolation of SSM (T_5 see Fig. 1) with the exponential filter using GRACE TWS as the constraint the correlations increase to a global area weighted mean of 0.39 with the maximum value reaching 0.80 (Fig. 3b). The CDF of the correlations in Fig. 3c confirms this improvement, with the optimized ESA CCI series in orange consistently exceeding the original ESA CCI series in blue. The correlation gains are widespread and are particularly pronounced in the south-eastern United States, northern Australia, south-eastern South America or in the eastern regions of Africa. In snow-covered or seasonally frozen regions, improvements are less visible.

For comparison, we also computed correlations between GRACE and the original ESA CCI RZSM product integrated to 0 to 200 cm (without depth extrapolation against GRACE; shown in Supplementary Information Sect. 2). The area weighted mean correlation is 0.38 and the maximum value reaches 0.80. The corresponding CDF closely matches that of the our optimally filtered SSM, indicating a similar skill at sub-seasonal time scales.

In Fig. 3d, we map the optimal T values for ESA CCI SSM (T_5) optimized against TWS, which leads to the

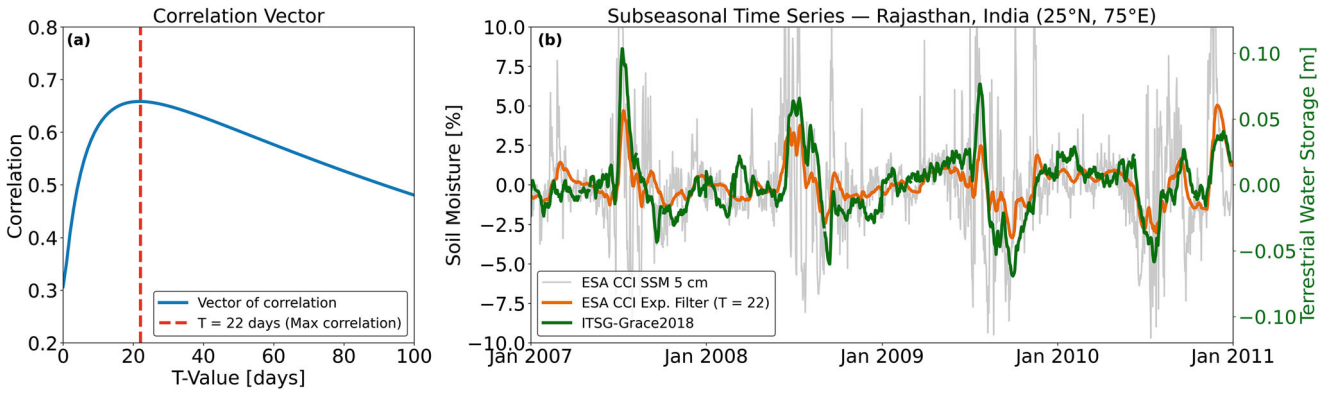

Fig. 2 (**a**) Optimization of T visualized as the correlation between filtered SSM and TWS. The red dashed line marks the maximum at $T = 22$ days. (**b**) Sub-seasonal time series for a grid cell located in Rajasthan, India (25° N, 75° E, January 2007–January 2011). Shown are ESA CCI SSM (grey), exponentially filtered SSM with $T = 22$ days (orange) and GRACE based-TWS (green)

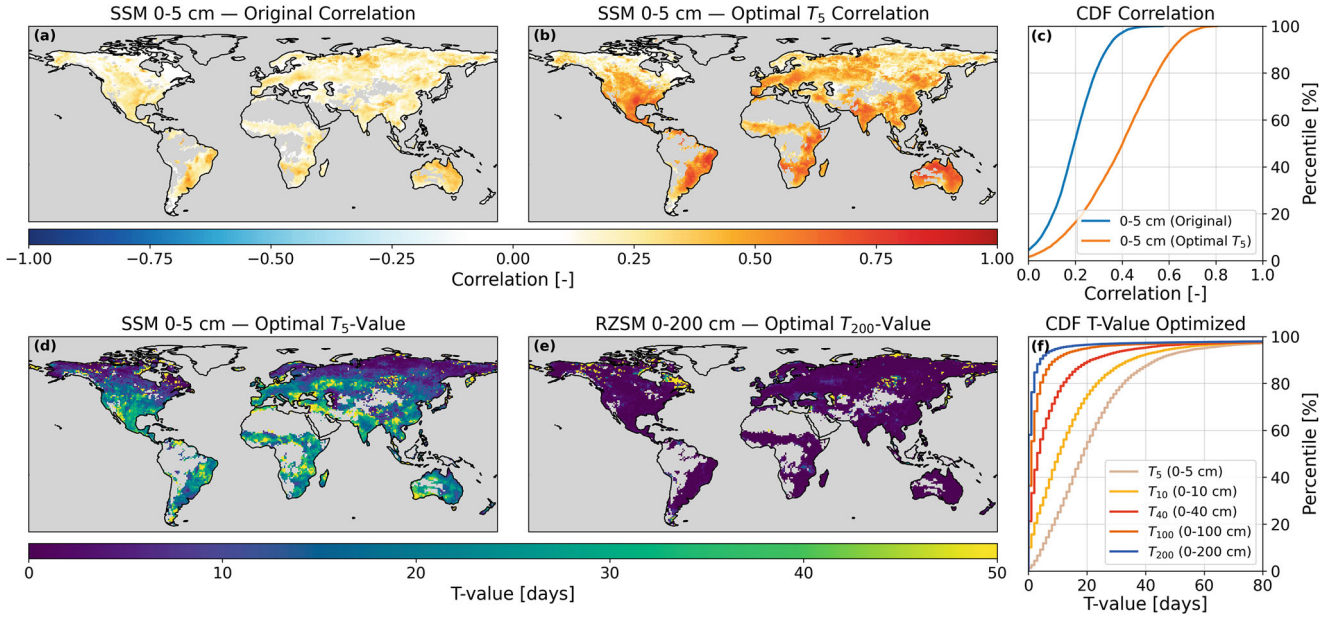

Fig. 3 Global correlation between ESA CCI SSM (0–5 cm) and GRACE based TWS before (**a**) and after (**b**) applying the exponential filter with cell-specific optimized *T*. (**c**) Area-weighted CDF of the correlations corresponding to (**b**). Panels (**d**) and (**e**) map the optimized *T* values using SSM 0–5 cm (T_5) and RZSM 0–200 cm (T_{200}) as input layers. (**f**) Summarizes *T* distributions as CDF for all soil depths (0–5, 0–10, 0–40, 0–100, 0–200 cm) and the maps for the intermediate layers are provided in the Supplementary Information

improved correlations seen in Fig. 3b. The area-weighted global mean for the *T* value is around 24 days and the median is 16 days. Larger *T* values occur across more arid regions like central and western Australia, north-eastern Brazil, the Middle East, central Asia, and the western United States. Smaller *T* values are more common in humid landscapes, such as parts of Europe, the eastern United States, and the La Plata Basin. Larger *T* values indicate stronger smoothing related to longer travel times in drier and/or deeper unsaturated soil profiles and thus longer effective memory, while smaller *T* values indicate a quicker vertical transport and thus a faster response of the integrative TWS signal.

In Fig. 3e, the optimized *T* value map using RZSM 0–200 cm as input (T_{200}) shows values that are much smaller than for SSM. The area weighted global mean *T* is about 5 days, the median is 0 days, and roughly 58% of grid cells have a value of 0 days. A *T* value of zero means the unfiltered RZSM time series already correlates best with TWS at sub-seasonal scales, so additional exponential filtering does not improve the fit. This indicates that the 0–200 cm ESA CCI product already captures much of the TWS variability at sub-monthly time scales. However, about 42% of grid cells still benefit from filtering, which hints at relevant storage dynamics below the 200 cm layer in these regions. As shown in the Supplementary Information, the correlation gain for the 0–200 cm layer is comparably small with the area-weighted global mean increasing to 0.385, which is only about a 0.5% improvement over the input data. However, regional gains can be substantial, with the correlations for individual grid cells increasing by up to 0.30.

Figure 3f summarizes the CDF of optimized *T* for each input depth (T_5, T_{10}, T_{40}, T_{100}, T_{200}; maps for 0–10, 0–40, and 0–100 cm are provided in Supplementary Material Sect. 3). *T* decreases systematically with the integration depth of the input data because the deeper slower soil moisture dynamics of deeper layers are already captured for input data with larger integration depths. The area-weighted global mean values are 17 days for T_{10}, 11 days for T_{40}, and 7 days for T_{100}. The *T* values for 5 and 200 cm are described above.

A sensitivity analysis based on independent sub-periods shows that while absolute *T* values can vary for different time periods, the overall distributions, relative relationships and spatial patterns remain consistent (see Supplementary Material, Fig. 4). Additionally, the removal of snow and surface water has only a minor impact on the global distribution of *T*, despite the expected regional differences.

5.3 Linking *T* to Physical Properties

To relate the optimized *T* values (T_5 from calibrating ESA CCI SSM against GRACE TWS) to physical controls, we classify grid cells by different properties that may influence the subsurface vertical water transport dynamics (here, the water table depth (WTD), the clay fraction representing an important soil property, and the average SSM over a 20-year period as an indicator of climatological aridity)

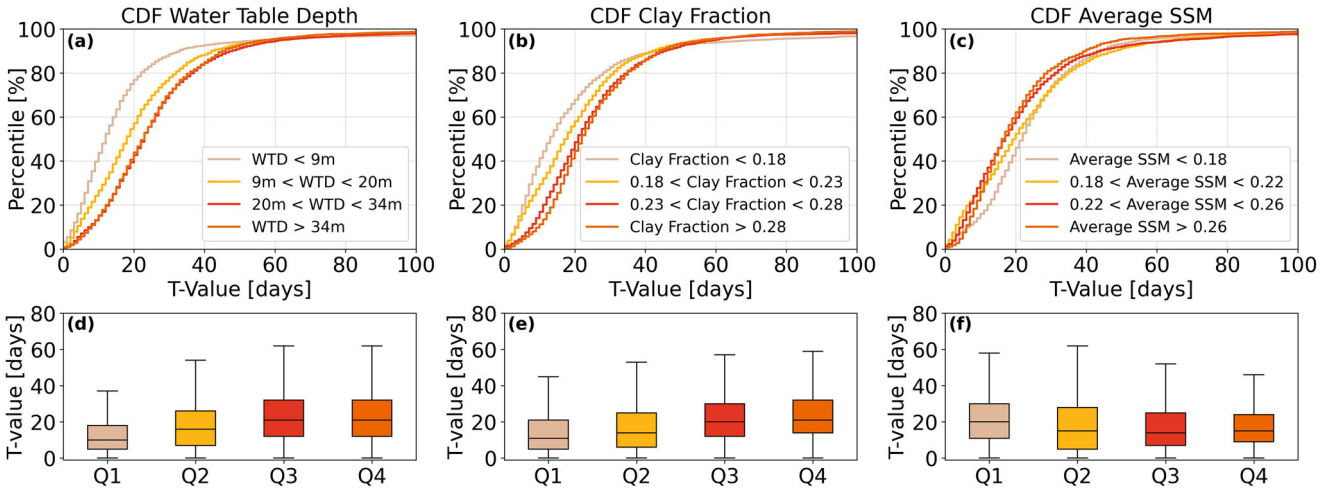

Fig. 4 Global grid cell CDFs of T-values by physical property: (**a**) water table depth (WTD), (**b**) clay fraction, and (**c**) average SSM. For each property, grid cells are split into four equal quantile bins (Q1-Q4). Panels (**d–f**) show boxplots of the same T-values grouped by the same classes as in (**a–c**). Colours are consistent between the CDF curves and the boxplots

and compare the resulting T distributions. For each property, we group the grid cells into four equal bins (Q1-Q4) and show both the CDFs and the matching boxplots (Fig. 4a–f, respectively). These CDF relationships should be read as global tendencies rather than strict causal relationships, as the spatial co-occurrence of different environmental factors influences hydrological processes in a complex way.

For groundwater table depth, the CDFs in Fig. 4a and the boxplot in Fig. 4d show a clear tendency in which shallower water Tables (Q1) are associated with short T values (faster response), and T increases with water table depth. Median T is about 10 days for Q1, 16 days for Q2, and 21 days for both Q3 and Q4. The similarity between Q3 and Q4 suggest diminishing sensitivity once the groundwater table is sufficiently deep. A plausible interpretation is that deeper groundwater tables are an expression of thicker unsaturated zones with more storage capacity. Thus, response dynamics stretch out over longer timescales, while for shallow water tables the entire subsurface water storage system adjusts faster to surface forcing, yielding shorter T. In regions with strong lateral groundwater dynamics or anthropogenic abstraction, the optimized time constants may also reflect processes that are partially decoupled from SSM dynamics, which can introduce an uncertainty in the interpretation of T.

As another physical control we used the soil clay fraction from GLDAS (Rodell et al. 2004), shown in Fig. 4b, e. The CDFs and boxplots again indicate a clear relationship between T and clay content. Cells with low clay content tend to have a short T, and T increases with clay content. Median T is 11 days for Q1, 14 days for Q2, 20 days for Q3, and 21 days for Q4. This pattern is consistent with soil-physical expectations. A higher clay content causes slower water flow velocities in the soil and slows the vertical redistribution of water. This is generally in line with findings on the optimal T correlating with soil properties in previous studies (Wang et al. 2017; Bouaziz et al. 2020).

Finally, we use the long-term average SSM as a proxy of general climatology-driven aridity or humidity of a certain region. The values are computed from the ESA CCI 5 cm product averaged over the full 20-year record with trend and seasonality retained. The goal is to test whether T differs between drier and wetter locations (Fig. 4c, f). Unlike WTD and clay fraction, there is a less obvious relationship between T and aridity. Median T values by quartile are 20 days for Q1, 15 days for Q2, 14 days for Q3, and 15 days for Q4. Q2 shows the largest spread, with both higher and lower T values, while Q3 and Q4 are quite similar. Considering the overall difference between Q1 and Q4, drier regions tend to have larger T values then humid regions, consistent with expectations of slower flow dynamics in more arid regions.

5.4 Best Layer Correlation with GRACE

In the previous analyses, we estimated for each grid cell five different T values (T_5, T_{10}, T_{40}, T_{100}, T_{200}) by optimizing against GRACE TWS using the five ESA CCI SSM and RZSM input layers that represent soil moisture from the surface to a certain depth. Applying these T values, we could compute five depth-extrapolated subsurface storage time series that each represent the water content in the full soil column. For each grid cell we then selected the input layer for which the resulting depth-extrapolated time series achieved the highest correlation with the GRACE TWS observations (Fig. 5). For this evaluation, we also included the original ESA CCI 0–200 cm RZSM product that has not been further depth-extrapolated to TWS, i.e., the deepest

root-zone product provided by ESA (shown in black in Fig. 5). The results show that when using the shallowest ESA CCI 0–5 cm layer as input for the exponential filter, the highest correlation with GRACE TWS is found in about 27% of the investigated land area (beige colour). Other input layers produce the best correlations in 15% (0–20 cm input layer, orange), 9% (0–40 cm input layer, purple), 20% (0–100 cm input layer, green), and 15% (0–200 cm input layer, blue) of the global land area. The original 0–200 cm ESA CCI RSZM product performs best in comparison to GRACE TWS in 14% of the land area (black cells in Fig. 5), particularly in regions of North America.

For discussing these results, it has to be considered that the overall six calculation methods compared here contain to a different degree (1) one or more depth-varying but globally constant T values as used in the ESA CCI input data sets, and (2) spatially varying T values derived in our approach by optimizing against GRACE TWS data. The ESA CCI data sets use individual (but globally constant) T values for each discrete soil layer they represent, which may allow for a more detailed representation of depth-dependent subsurface soil moisture dynamics. The ESA CCI RZSM 0–200 cm data, for example, is influenced by four individual T values, one for each layer. Our GRACE-based optimization, on the other hand, results in only one T value that governs the extrapolation from the lower boundary of the respective ESA CCI input layer down to the entire soil profile as represented by TWS. This T value, in turn, varies with each grid cell and thus allows for representing regional differences. Thus, the deeper the ESA CCI input layer introduced into the GRACE-based exponential filter, the more the results are influenced by the spatially uniform but depth-dependent information of the CCI product. For shallower input layers, the spatial sensitivity of the grid-based T value estimates gains more influence. When using the ESA CCI 0–40 cm layer as input layer for our TWS optimization, for instance, two globally constant (but depth-dependent) T values of the ESA CCI data set are used (5–10, 10–40 cm) to extrapolate from SSM (0–5 cm) into the root zone and, additionally, T_{40} for the additional extrapolation from 40 cm down to the full soil column (TWS), optimized individually per grid cell.

In regions where shallower input layers provide better results (Fig. 5), the regional adaption of the T values against the spatially varying grid-based GRACE information has a beneficial influence on the fit to the TWS observations. This applies to large areas in high northern latitudes in cold and snow-dominated climates. As seen in Fig. 3d, these regions tend to have smaller T values, indicating TWS dynamics to be close to the high-frequency near-surface soil moisture water dynamics. It can be argued that these dynamics can be better represented by the spatially-distributed optimization approach presented here than by the globally constant T values of ESA CCI. The latter tend to perform well in the many parts of the southern hemisphere where the 0–100 cm layer turns out to be the optimal input to the TWS-based T estimation, as well as for several coherent patterns worldwide where the ESA CCI 0–200 cm layer is the optimal input. For both cases, the improvement by the additional spatially distributed depth-extrapolation with T_{100} or T_{200}, respectively, suggests the importance of even deeper storage dynamics for the sub-seasonal variability. The best performance of the original 0–200 cm ESA CCI RSZM product without further depth-extrapolation against GRACE particularly in regions of North America. This might be related to the fact that the globally uniform ESA CCI T values have primarily been derived from in-situ soil moisture data measured in the

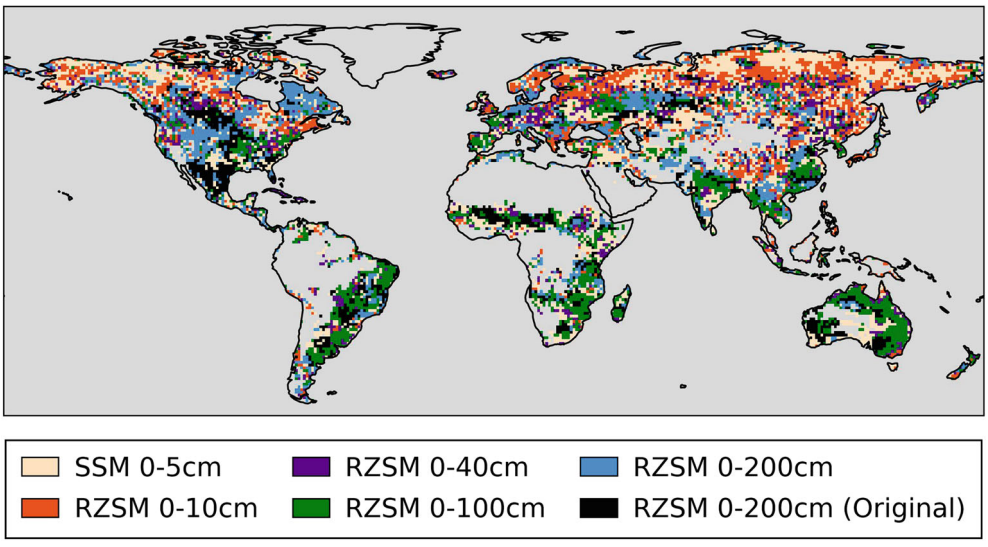

Fig. 5 Depth of the ESA CCI SSM or RZSM data set that performs best when used as input for the depth-extrapolation with an exponential filter for GRACE-based TWS

United States and therefore reflect soil properties, climate, and vegetation typical of that region rather than conditions elsewhere.

6 Conclusions and Outlook

We introduced a global, spatially distributed approach to infer sub-seasonal subsurface water storage dynamics from remotely sensed SSM by calibrating the exponential filter time constant T against GRACE- and GRACE-FO–derived terrestrial water storage anomalies. The method provides an observation-driven estimate of root-zone memory and damping behaviour without requiring in-situ calibration data. By optimizing the exponential filter per grid cell, correlations between surface soil moisture and GRACE-based storage improved in the global mean from 0.19 (max: 0.57) to 0.39 (max: 0.80) demonstrating that a simple one-parameter filter can effectively bridge the gap between surface and subsurface hydrologic variability at sub-monthly time scales.

The resulting subsurface storage time series show a similar quality (in terms of agreement with the GRACE TWS time series) as the original 0–200 cm RZSM product provided by ESA CCI. While the ESA CCI product results from a more sophisticated depth-dependent extrapolation scheme, its globally uniform T values derived from a limited number of in-situ stations lead to a good agreement particularly in regions were in-situ data are available. However, in 86% of the land area, our signals derived either directly from the SSM or from different RZSM data shows a better correlation with GRACE TWS than the deepest extrapolated ESA product. This implies most likely a combination of two effects: (1) spatially varying subsurface dynamics are important to consider and (2) relevant water storage variability occurs also below the 0–200 cm layer in many regions.

The first effect is additionally supported by the fact that the resulting global field of optimal time constants reflects meaningful spatial patterns that are consistent with physiographic factors: longer time constants occur in arid regions and areas with deep water tables, and shorter constants in humid environments or shallow groundwater settings. The decrease of optimal T with the increasing integration soil depth of the input data indicates that the exponential filter captures physically plausible vertical differences of the storage dynamics. These results suggest that GRACE data can serve as a large-scale constraint to generalize the calibration of approaches for the depth-extrapolation of near-surface soil moisture, beyond the limits of ground observations.

Our framework offers a lightweight, transferable tool for deriving regionally adaptive subsurface storage dynamics from satellite-based surface soil moisture records. It can be directly applied to other sensors or merged soil moisture products and eventually extended to assess storage dynamics at seasonal and interannual scales. Limitations arise from GRACE's coarse spatial resolution, residual contributions of mass variations of surface water and snow, and the assumption of a single effective storage layer.

Future work should refine the physical interpretation of the time constant, explore multi-parameter formulations that better represent deep groundwater and spatial variations, and integrate this approach into land-surface data assimilation systems. Ongoing improvements to the GRACE/-FO data processing and next-generation gravity missions such as the MAGIC constellation of two GRACE-like missions operating simultaneously at differently inclined orbits (Daras et al. 2024) give prospect to an increase of the temporal and spatial resolution of satellite-based TWS data in the future. This can be expected to refine the approach presented here.

Competing Interests The author(s) has no competing interests to declare that are relevant to the content of this manuscript.

References

Albergel C, Rüdiger C, Pellarin T, Calvet J-C, Fritz N, Froissard F, Suquia D, Petitpa A, Piguet B, Martin E (2008) From near-surface to root-zone soil moisture using an exponential filter: an assessment of the method based on in-situ observations and model simulations. Hydrol Earth Syst Sci 12:1323–1337. https://doi.org/10.5194/hess-12-1323-2008

Blank D, Eicker A, Jensen L, Güntner A (2023) A global analysis of water storage variations from remotely sensed soil moisture and daily satellite gravimetry. Hydrol Earth Syst Sci 27:2413–2435. https://doi.org/10.5194/hess-27-2413-2023

Blank D, Eicker A, Reager JT, Güntner A (2025) Revisiting sub-surface drought cascades with daily satellite observations of soil moisture and terrestrial water storage. Water Resour Res 61:e2024WR039321. https://doi.org/10.1029/2024WR039321

Bouaziz LJE, Steele-Dunne SC, Schellekens J, Weerts AH, Stam J, Sprokkereef E, Winsemius HHC, Savenije HHG, Hrachowitz M (2020) Improved understanding of the link between catchment-scale vegetation accessible storage and satellite-derived soil water index. Water Resour Res 56:e2019WR026365. https://doi.org/10.1029/2019WR026365

Butterworth S (1930) On the theory of filter amplifiers. Exp Wireless Wireless Eng 7:536–541

Daras I, March G, Pail R, Hughes CW, Braitenberg C, Güntner A, Eicker A, Wouters B, Heller-Kaikov B, Pivetta T, Pastorutti A (2024) Mass-change and geosciences international constellation (MAGIC) expected impact on science and applications. Geophys J Int 236:1288–1308. https://doi.org/10.1093/gji/ggad472

Dorigo W, Wagner W, Albergel C, Albrecht F, Balsamo G, Brocca L, Chung D, Ertl M, Forkel M, Gruber A, Haas E, Hamer PD, Hirschi M, Ikonen J, De Jeu R, Kidd R, Lahoz W, Liu YY, Miralles D, Mistelbauer T, Nicolai-Shaw N, Parinussa R, Pratola C, Reimer C, Van Der Schalie R, Seneviratne SI, Smolander T, Lecomte P (2017) ESA CCI soil moisture for improved Earth system understanding: state-of-the art and future directions. Remote Sens Environ 203:185–215. https://doi.org/10.1016/j.rse.2017.07.001

Gruber A, Scanlon T, Van Der Schalie R, Wagner W, Dorigo W (2019) Evolution of the ESA CCI Soil Moisture climate data records and their underlying merging methodology. Earth Syst Sci Data 11:717–739. https://doi.org/10.5194/essd-11-717-2019

Güntner A, Sharifi E, Haas J, Boergens E, Dahle C, Dobslaw H, Dorigo W, Dussailant I, Flechtner F, Jäggi A, Kosmale M, Luojus K, Mayer-Gürr T, Meyer U, Preimesberger W, Ruz Vargas C, Zemp M (2024) Global Gravity-based Groundwater Product (G3P). https://doi.org/10.5880/G3P.2024.001

Kvas A, Behzadpour S, Ellmer M, Klinger B, Strasser S, Zehentner N, Mayer-Gürr T (2019) ITSG-Grace2018: overview and evaluation of a new GRACE-only gravity field time series. J Geophys Res Solid Earth 124:9332–9344. https://doi.org/10.1029/2019JB017415

Manfreda S, Brocca L, Moramarco T, Melone F, Sheffield J (2014) A physically based approach for the estimation of root-zone soil moisture from surface measurements. Hydrol Earth Syst Sci 18:1199–1212. https://doi.org/10.5194/hess-18-1199-2014

Pasik A, Gruber A, Preimesberger W, De Santis D, Dorigo W (2023) Uncertainty estimation for a new exponential-filter-based long-term root-zone soil moisture dataset from Copernicus Climate Change Service (C3S) surface observations. Geosci Model Dev 16:4957–4976. https://doi.org/10.5194/gmd-16-4957-2023

Paulik C, Dorigo W, Wagner W, Kidd R (2014) Validation of the ASCAT soil water index using in situ data from the international soil moisture network. Int J Appl Earth Obs Geoinf 30:1–8. https://doi.org/10.1016/j.jag.2014.01.007

Preimesberger W, Scanlon T, Su C-H, Gruber A, Dorigo W (2021) Homogenization of structural breaks in the global ESA CCI soil moisture multisatellite climate data record. IEEE Trans Geosci Remote Sensing 59:2845–2862. https://doi.org/10.1109/TGRS.2020.3012896

Rodell M, Houser PR, Jambor U, Gottschalck J, Mitchell K, Meng C-J, Arsenault K, Cosgrove B, Radakovich J, Bosilovich M, Entin JK, Walker JP, Lohmann D, Toll D (2004) The global land data assimilation system. Bull Amer Meteor Soc 85:381–394. https://doi.org/10.1175/BAMS-85-3-381

Stradiotti P, Preimesberger W (2024) ESA CCI SM RZSM long-term climate record of root-zone soil moisture from merged multi-satellite observations. https://doi.org/10.48436/V8CWJ-JK556

Wagner W, Lemoine G, Rott H (1999) A method for estimating soil moisture from ERS scatterometer and soil data. Remote Sens Environ 70:191–207. https://doi.org/10.1016/S0034-4257(99)00036-X

Wang T, Franz TE, You J, Shulski MD, Ray C (2017) Evaluating controls of soil properties and climatic conditions on the use of an exponential filter for converting near surface to root zone soil moisture contents. J Hydrol 548:683–696. https://doi.org/10.1016/j.jhydrol.2017.03.055

Zhang N, Quiring S, Ochsner T, Ford T (2017) Comparison of three methods for vertical extrapolation of soil moisture in Oklahoma. Vadose Zone J 16:1–19. https://doi.org/10.2136/vzj2017.04.0085

Open Access This chapter is licensed under the terms of the Creative Commons Attribution 4.0 International License (http://creativecommons.org/licenses/by/4.0/), which permits use, sharing, adaptation, distribution and reproduction in any medium or format, as long as you give appropriate credit to the original author(s) and the source, provide a link to the Creative Commons license and indicate if changes were made.

The images or other third party material in this chapter are included in the chapter's Creative Commons license, unless indicated otherwise in a credit line to the material. If material is not included in the chapter's Creative Commons license and your intended use is not permitted by statutory regulation or exceeds the permitted use, you will need to obtain permission directly from the copyright holder.



Supplementary Information for:

Assessing sub-seasonal subsurface water storage dynamics using exponential filtering of ESA CCI soil moisture and daily GRACE terrestrial water storage data

Daniel Blank,
HafenCity University Hamburg, Hamburg, ORCID

Daniel Rasche,
GFZ Helmholtz Centre for Geosciences, Potsdam, ORCID

Andreas Güntner,
GFZ Helmholtz Centre for Geosciences, Potsdam
Institute of Environmental Sciences and Geography, University of Potsdam, Potsdam

Annette Eicker,
HafenCity University Hamburg, Hamburg
GFZ Helmholtz Centre for Geosciences, Potsdam

1 Implementation of 100-200 cm Layer

We extend the ESA CCI COMBINED RZSM dataset with an additional 100–200 cm layer. The native product includes 0–10, 10–40, and 40–100 cm layers. Depth specific T values reported by Pasik et al. (2023) are used to exponentially filter the SSM for each grid cell, applying the same T value for all cells within a given layer. Since Pasik et al. (2023) also provide a T value for 100–200 cm, we implement that layer in the same way and include it in our analysis.

To validate the implementation, we use the ESA CCI PASSIVE-only RZSM product, which is derived from passive sensors only and provides estimates for all four layers, including the 100–200 cm layer. We apply the same globally depth-dependent T values to the PASSIVE SSM and confirm our exponentially filtered 100–200 cm time series by comparison with the native PASSIVE 100–200 cm layer.

Having confirmed methodological consistency within the PASSIVE dataset, we then apply the same settings to the COMBINED SSM product, which merges active and passive observations and is the primary dataset used in our analysis.

2 Global Correlation

Fig. 1a shows the correlation between GRACE TWS and the unfiltered ESA CCI RZSM 0-200 cm product, with a global area weighted mean of 0.38 and a maximum value of 0.80. After depth extrapolation of the 0-200 cm (T_{200}) with the exponential filter using GRACE TWS as the constraint the correlations increase to a global area weighted mean of 0.385 with the maximum value reaching 0.80 (Fig. 1b). The corresponding CDF (Fig. 1c) closely matches that of the original 0-200 cm, indicating a similar skill at sub-seasonal time scales and small improvements.

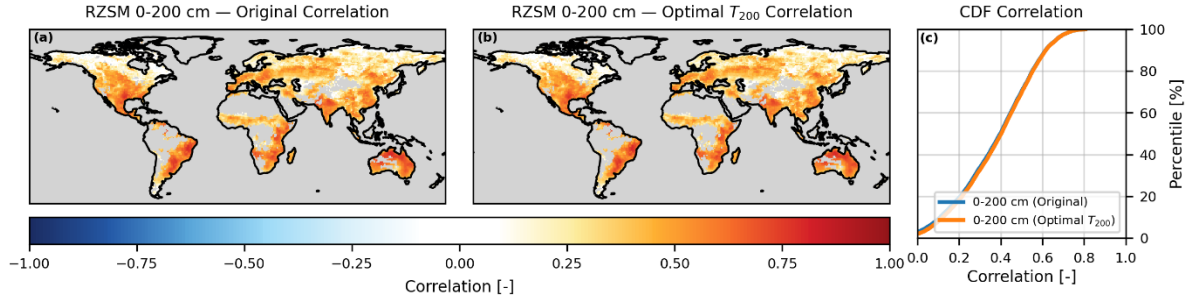

Fig. 1 Global correlation between ESA CCI RZSM (0-200 cm) and GRACE-based TWS before (a) and after (b) applying the exponential filter with cell wise optimized T_{200}. (c) shows the area weighted CDF of the correlations corresponding to (a) and (b).

3 Global T-value maps

Fig. 2a-c show global maps of the optimized T-values for the RZSM 0-10, 0-40cm, and 0-100 cm input layers. The results for the 0-5 and 0-200 cm layer are shown in the main text (Fig 3d-e) and the corresponding CDFs for all layers are given in the main text Fig 3f.

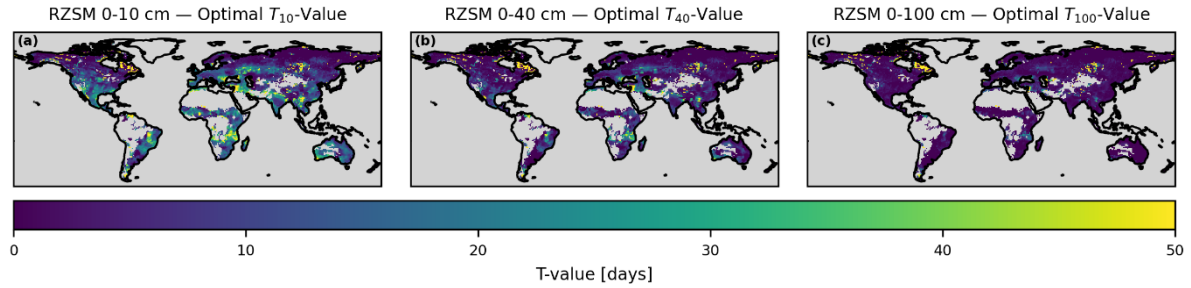

Fig. 2 Global map of the optimized T values using (a) RZSM 0-10 (T_{10}), (b) 0-40 (T_{40}), and (c) 0-100 cm (T_{100}) as input for the GRACE-based exponential filter.

4 T-Value for different periods

Fig. 3 shows the CDFs of the optimized T-values for the ESA CCI SSM 0-5 cm for three different periods. The left panel shows the complete time span, the middle panel the first half from 01.2003 – 12.2012, and the right panel the second half from 01.2013 - 12.2022. We find that absolute T values differ across sub-periods, with larger values in the later period. This indicates that the optimized parameter is sensitive to the temporal characteristics of the input data and may reflect changes in climate conditions, data characteristics, or signal variability. However, despite these differences in magnitude, the main spatial patterns and the overall distribution of T remain consistent across all periods.

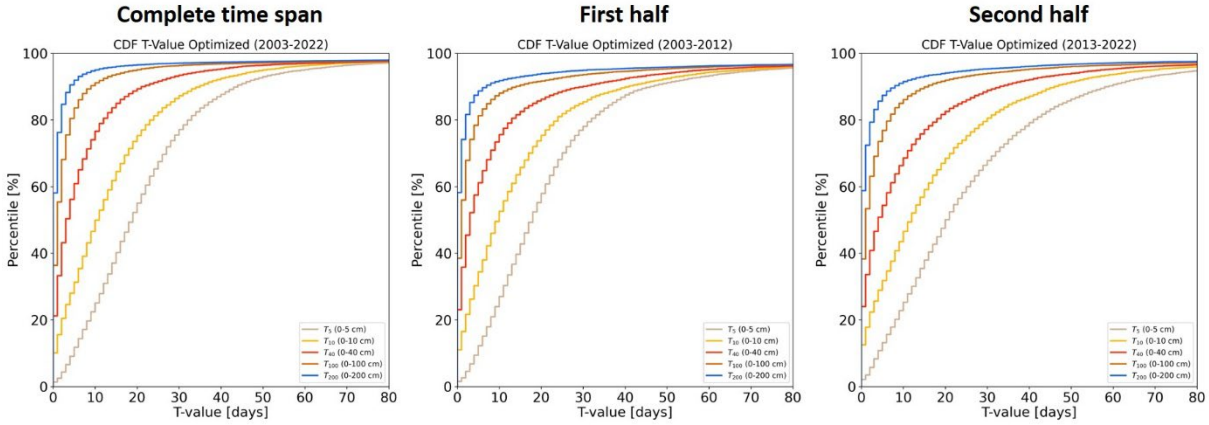

Fig. 3: Comparison of cumulative distribution functions (CDFs) of the optimized time constant T for different soil depths (0–5 cm to 0–200 cm) over the full period (2003–2022), the first sub-period (2003–2012), and the second sub-period (2013–2022).

References

Pasik, A., Gruber, A., Preimesberger, W., De Santis, D., Dorigo, W., 2023. Uncertainty estimation for a new exponential-filter-based long-term root-zone soil moisture dataset from Copernicus Climate Change Service (C3S) surface observations. Geosci. Model Dev. 16, 4957–4976. https://doi.org/10.5194/gmd-16-4957-2023